UNIVERSITY OF CALIFORNIA

Los Angeles

# An Electrophysiological Model of Gap-Junction Mediated Cortical Spreading Depression Including Osmotic Volume Changes

A dissertation submitted in partial satisfaction of the requirements for the degree Doctor of Philosophy in Biomathematics

by

Bruce Edward Shapiro

2000

The dissertation of Bruce Edward Shapiro is approved.

Andrew Charles

Sung-Cheng Huang

Elliot Landaw

Carol Newton, Committee Chair

University of California, Los Angeles

2000

To Merril

# CONTENTS

# LIST OF FIGURES

# LIST OF TABLES

# ACKNOWLEDGEMENTS

I could not have completed this work without the influence and generous assistance of many individuals. The following paragraphs make some attempt to acknowledge and thank at least some of them.

Carol Newton has taught, mentored, cajoled, criticized and lauded me time and again for the past seven years. She was the first person I met in the UCLA biomathematics department. Sometime in 1993 I telephoned her to ask just what biomathematics was. She invited me to “sit in” during a few lectures or courses and also suggested that I meet with James Sneyd to talk about applying to the masters program. After I had accomplished these weighty tasks she promptly “roped” me into the Ph.D. program. I think she is trying to do the same thing to my son Micah; she always has a gift for him whenever she returns from her latest jaunt.

James Sneyd also encouraged me right from the start. He allowed me to take his deterministic modeling class as an extension student while I decided whether or not I really wanted to apply to this department, all the while telling me that I should really apply to the applied mathematics program instead, since I looked so old, tired, and lazy that I would probably never finish, and because applied math was so much easier than biomathematics. He then resigned from the department and moved to the other side of the world (first to New Zealand, then to Michigan, and then back to New Zealand). Such geographic encumbrances mean very little in this new age of global electronic communication. I promptly started mailing him papers, first by snail mail,

and later, electronically. I informed him that he had no choice but to mentor me for life since he had made the mistake of allowing me into his class, and I began to barrage him with email asking mysterious questions about modeling. He never failed – even once – to respond promptly and very politely with many useful suggestions about how to proceed with my research. Even those times when I accused him of making mistakes in his book.

Hong Qian taught me how to do biophysical modeling. What began as a simple class assignment developed into a productive collaboration. A poster presentation and the publication of three papers having absolutely nothing whatever to do with my dissertation research were the result of this collaboration. He then left UCLA and moved to Seattle.

Julian Cook helped me get started on spreading depression research, once he understood that I really wasn't all that interested in slime molds. After I explained to him just what spreading depression is, he actually became quite interested, and helped me formulate the problem in a useful manner. Although he kept mumbling a lot about spatial pattern formation the whole time (none of which I ever understood). He then quit UCLA and moved to parts unknown.

Andy Charles has helped me to understand some of the intricacies of calcium waves, calcium imaging and migraine headaches.

Elliott Landaw, in his dual roles of educator and department chairman, has been a constant source of useful advice and encouragement.

Bill Holmes showed me that it was possible to graduate in biomathematics from Carol's department with a specialization in neuroscience.

After I had decided to model spreading depression as my dissertation project, George Somjen suggested studying the effect of neuronal gap junctions on spreading depression.

Nobody could possibly navigate the maze of UCLA administrivia without the help of the departmental student affairs administrators. The fact that there have been so many SAAs during my time at UCLA is probably an indicator that I have been here too long. Laura Biswas, Carolyn Myers, Li Hong, and David Tomita have always had the right form to fill out at the right time, knew who to give it too, and knew all the deadlines.

The faculty and students in the UCLA inter-departmental neuroscience program were unanimously supportive. The students accepted me as one of their own, even though I didn't actually get my hands wet, and the faculty repeatedly expressed the opinion that I would fill a vital role in their field as a mathematical biologist. Suzie Vader, the neuroscience program coordinator, was particularly helpful in understanding and explaining program requirements, scheduling classes, and coordinated comprehensive examinations. And we had a lot of fun showing each other our latest Swatches.

The Jet Propulsion Laboratory of the California Institute of Technology moved massive quantities of money into the coffers of various moving companies

and travel agencies to relocate me to California in 1990. If this momentous event had not occurred I might not have discovered the UCLA biomathematics program three years later. JPL engineers, by and large, are stereotypical techno-nerds. As a result very few of them ever understood or accepted my somewhat perplexing (to them) decision to study biology. The other members of the TOPEX/Poseidon Navigation Team, including Ray Frauenholz, Ram Bhat, and Bob Leavitt, all supported me through the early years of bizarre work hours while I attended classes across town. Especially when they weren't off at a bridge game or playing pool and drinking beer.

My son Micah David was born just a few weeks before I started in the biomath program. I naively gave myself until he started kindergarten to finish. It just didn't seem reasonable that two of us should be in school at the same time. Little did I know what I was getting myself into. He is now in the first grade. He has never known a father who was not a student, and since he has been in school for as long as he can remember, it seems perfectly natural to him that daddy should also be in school. And he (almost) always lets me use his computer to do my research.

My wife Merril has made all of the difference in both my life and in my graduate program. She encouraged my career exploration, allowed me to enter a tedious graduate program, never said a discouraging word about school, and has put up with my bizarre idiosyncrasies for years. Without her constant love and encouragement I could not have completed this dissertation, which is dedicated to her.

*Pro-FORTRAN* is a trademark of Absoft Corporation, Rochester Hills, MI.

*Apple* and *iMac* are trademarks of Apple Compter, Inc., Cupertino, CA.

*Excel* is a trademark of Microsoft Corporation, Redmond, WA.

*Mathematica* is a trademark of Wolfram Research, Inc., Champaign, IL.

This research was supported by the National Institutes of Health via a systems and integrative biology training grant from the National Institute of General Medical Sciences.

# VITA

| | |
|---|---|
| 1977 | B. S., Mathematics, Magna cum Laude<br>University of Maryland, College Park, Maryland |
| 1978 | B. S., Physics, with Honors in Physics<br>University of Maryland, College Park, Maryland |
| 1980 | M. S., Applied Physics, Electrical Engineering Minor<br>Cornell University, Ithaca, New York |
| 1982 – 1989 | Systems Engineer, Ford Aerospace Corporation |
| 1985 | B. S., Computer Science<br>University of Maryland, College Park, Maryland |
| 1987 | M. S., Computer Science<br>Johns Hopkins University, Baltimore, Maryland |
| 1989 – 1990 | Computer Scientist, Computer Sciences Corporation |
| 1990 – 2000 | Member of the Technical Staff, Jet Propulsion Laboratory<br>California Institute of Technology |
| 1991 | Married Merril Ann Simon |
| 1993 | Birth of Micah David Shapiro |
| 1995 | M. S., Biomathematics<br>University of California, Los Angeles |
| 1997 – 2000 | Systems and Integrative Biology Training Grant,<br>National Institute of General Medical Sciences |
| 1999 - 2000 | Part Time Faculty, Department of Mathematics<br>California State University, Northridge |

## PUBLICATIONS AND PRESENTATIONS


Bhat RS, Shapiro BE, Frauenholz RB (1993) TOPEX/Poseidon Orbit Acquisition Maneuver Sequence. Advances in the Astronautical Sciences, Volume 85 (Univelt: San Diego).

Bhat RS, Shapiro BE, Frauenholz RB, Leavitt RK (1998) TOPEX/Poseidon Orbit Maintenance for the First Five Years. Advances in the Astronautical Sciences, Volume 100 (Univelt: San Diego).

Frauenholz RB, Bhat RS, Shapiro BE, Leavitt RK (1998) The TOPEX/Poseidon Operational Orbit. Journal of Spacecraft and Rockets, 35:212-224.

Frauenholz RB, Hamilton TW, Shapiro BE, Bhat RS (1993) The Role of Anomalous Satellite Fixed Accelerations in TOPEX/Poseidon Orbit Maintenance. Advances in the Astronautical Sciences, Volume 85 (Univelt: San Diego).

Frauenholz RB, Shapiro BE (1991) The Role of Predicted Solar Activity in the TOPEX/Poseidon Orbit Maintenance Maneuver Design. Advances in the Astronautical Sciences, Volume 76 (Univelt: San Diego).

Qian H, Shapiro BE (1999) Graphical Method for Force Analysis: Macromolecular Mechanics with Atomic Force Microscopy. Proteins: Structure, Function, and Genetics, 37:576-581.

Shapiro BE (1988) The GEOSAT Orbit Adjust. Journal of the Astronautical Sciences, 36:407-424.

Shapiro BE (1996) Phase Plane Analysis and Frozen Orbit for TOPEX/Poseidon. Advances in the Astronautical Sciences, Volume 91 (Univelt: San Diego).

Shapiro BE (1997) Hysteresis in Atomic Force Microscopy. Poster presented at the annual meeting of the Society for Mathematical Biology, Raleigh, North Carolina.

Shapiro BE (1999) Leão's Spreading Depression and Gap Junctions: An Electrodiffusion Model of the DC-Voltage Shift, Ionic Movement, and Osmotic Volume Changes. Society of Neuroscience Abstracts, 25:128.6.

Shapiro BE, Bhat RS (1993) GTARG - The TOPEX/Poseidon Ground Track Maintenance Maneuver Targeting Program. Paper presented at the 1993 AIAA Aerospace Design Conference, Irvine, California.

Shapiro BE, Bhat RS (1994) The Use of Anomalous Satellite Fixed Forces to Control the TOPEX/Poseidon Ground Track. Advances in the Astronautical Sciences, Volume 87 (Univelt: San Diego).

Shapiro BE, Pino A (1988) Maintenance of an Exact Repeat Ground Track - The GEOSAT ERM. Proceedings of the AIAA/AAS Astrodynamics Specialists Conference.

Shapiro BE, Qian H (1997) A Quantitative Analysis of Single Protein-Ligand Complex Separation with the Atomic Force Microscope. Biophysical Chemistry, 67:211-219.

Shapiro BE, Qian H (1998) Hysteresis in Force Probe Microscopy: A Dynamical Systems Perspective. Journal of Theoretical Biology, 194:551-559.

ABSTRACT OF THE DISSERTATION

An Electrophysiological Model

of Gap-Junction Mediated Cortical Spreading Depression

Including Osmotic Volume Changes

by

Bruce Edward Shapiro

Doctor of Philosophy in Biomathematics

University of California, Los Angeles, 2000

Professor Carol Newton, Chair

A model of gap-junction mediated spreading depression (SD) is presented. Ionic movement through a neuronal syncytium of gap junction connected cells is modeled electrodiffusively. The usual reaction-diffusion approach is used extracellularly. Standard biophysical models of sixteen different membrane currents and ion pumps are included. Osmotic pressure gradients are countered by water flow across the cellular membrane that causes volumetric changes. The predicted wave speed, wave magnitude, and waveform shape depend on the combination and quantity of NMDA receptors, voltage gated $K^+$-channels, and K(Ca) channels present in the

tissue. There are threshold NMDA, delayed rectifier, and BK-channel conductances. Below threshold SD cannot be induced. Above threshold wave speed is a continuously increasing function of conductance. Wave magnitude increases with the delayed-rectifier and BK conductance, and decreases (above threshold) with increasing NMDA conductance. The SK (K(Ca)) and A-type channels are predicted to be inhibitory, with cutoff (maximum) rather than threshold (minimum) conductances. The predicted wave speed increases when glial cells are blocked. The predicted extracellular $K^+$ concentration increases to ≈25 to ≈50 mM. Extracellular $Na^+$ and $Cl^-$ fall by ≈80% to ≈90% and $Ca^{++}$ falls by >95%. The simulated wave speed ranges from ≈2 to ≈18 mm/min over the range of parameters tested. Interstitial space is predicted to fall by ≈20% to ≈50%. Preventing cell expansion prevents wave initiation and propagation. Preventing $K^+$ passage through gap junctions prevents wave propagation except at high membrane conductances that are near or beyond the physiological range. The cytoplasmic diffusion of other species has less effect, and extracellular diffusion has almost no effect on wave propagation in the model. These results are consonant with recent findings that gap junction poisons block SD and support the theory that ionic diffusion via gap junctions is an important mechanism underlying SD.

# CHAPTER 1

# INTRODUCTION

The phenomenon of spreading depression (SD) was first reported and characterized over half a century ago by Aristides Leão (1944a, 1944b, 1944c, 1947, 1951). The name originated from electroencephalographic (EEG) observations of a wave-like, slowly moving depression of electrical activity in the cerebral cortex. It has since been discovered that spreading depression consists of a wave of membrane depolarization (a "DC voltage shift") and ionic concentration changes lasting for up to two minutes at any given point and traveling at a speed between three and twelve millimeters per minute (Kraig and Nicholson, 1978). Wave passage is typically accompanied by a period of increased blood flow and is followed by a prolonged period of vasodilation (Lauritzen and others, 1982). Spreading depression is widely believed to be one of the electrophysiological processes involved in migraine headaches (Lauritzen, 1985). It has also been observed to accompany cerebral ischemia, hypoxia, and concussion. There is even some evidence that exposure to spreading depression induces a subsequent tolerance against ischemic cell damage (Yanamoto and others, 1998). Furthermore, an approaching wave of spreading depression is usually preceded by seemingly random bursts of electrical activity.

These electrical bursts, referred to as prodromal spikes, or AC voltage shifts, resemble epileptic discharges. For this reason spreading depression has also been used as an animal model of epilepsy (Bures, Buresová and Krívánek, 1974).

There is no generally accepted theory explaining spreading depression. Previously published models (Grafstein, in Bures, Buresová and Krívánek, 1974; Reshodko and Bures, 1975; Tuckwell and Miura, 1978; Tuckwell, 1980, 1981; Tuckwell and Hermansen, 1981; Reggia and Montgomery, 1994, 1996; Tepley and Wisesinghe, 1996; Revett and others, 1998; Ruppin and others, 1999) do not provide a mechanism to explain why gap junction poisons prevent spreading depression (Somjen and others, 1992; Martins-Ferreira and Ribeiro, 1995; Nedergaard, Cooper and Goldman, 1995; Largo and others, 1997; Brand, Fernandes de Lima and Hanke, 1998). It had been previously suggested that neuroglia, which are widely connected by gap junctions, might provide a substrate for SD wave propagation (Gardner-Medwin, 1981). However, it has also been demonstrated that the application of glial poisons does not prevent spreading depression (Largo and others, 1996, 1997; Largo, Ibarz and Herreras, 1997). Hence it is unlikely that the required gap junctions are glial. Furthermore, the previous models do not explain the inconsistent effects of $Ca^{++}$ removal and/or calcium channel antagonists (Ramos, 1975; Somjen and others, 1990; Young, Aitken and Somjen, 1991; Jing, Aitken and Somjen, 1991, 1993; Hada and others, 1996; Basarsky and others, 1998). Finally, no previous model has described the nearly 50% reduction in interstitial volume that occurs during spreading

depression (Kraig and Nicholson, 1978; Jing, Aitken and Somjen, 1994). This dissertation addresses all of these observations.

A novel model of spreading depression will be presented in the following chapters. This model differs from previous ones in that it incorporates the effects of (a) gap junctions between neurons, (b) intracellular (cytoplasmic) voltage gradients, and (c) osmotically induced volume changes. The earlier biophysical models have all been based on the assumption that spreading depression propagates as a diffusional potassium wave through extracellular space. Because intracellular space was believed to be compartmentalized into separate neurons, concentration changes within the individual cells were treated as purely local phenomena in these models. Information was propagated only through membrane currents and extracellular diffusion.

A different approach is taken in the model presented in this dissertation. Neurons are assumed to be interconnected by gap junctions. Ions are allowed to propagate through an intracellular continuum formed by the resulting neuronal syncytium. Through the remainder of this dissertation the term “cytoplasmic” is taken to refer to this continuum of cells, and does not refer to the space within a single neuron. It can be distinguished from the terms “extracellular” or “interstitial” space, which are used interchangeably to describe the widely connected space between cells. The model presented here is based on ionic movements through bulk neural tissue composed of these “cytoplasmic” and “interstitial” spaces. In this context, it is not meaningful to refer to the space within a single neuron, but rather to

refer to the “cytoplasmic” or “extracellular” space at a particular location described by its spatial coordinates. The concept of “intercellular” communication or the “intercellular” propagation of waves is not distinguishable, in this context, from propagation within the “cytoplasmic” continuum. While it will be conceded that such propagation through gap junctions requires the “intercellular” movement of ions between cells, to avoid any confusion the terms “intracellular” and “intercellular” will be avoided in the remainder of this dissertation.

Because of the large ionic movements that occur during spreading depression, neither the cable equation nor standard compartmental models can be used to describe ionic concentration changes. Both of these approaches are derived based on the assumption that all concentration changes are small with respect to their resting values (Keener and Sneyd, 1998). Furthermore, a simple system of reaction-diffusion equations coupled by membrane currents is also insufficient. This is because voltage gradients develop along the length of dendritic processes during SD. To alleviate this difficulty electric fields as described by the Nernst-Planck equation are incorporated directly into the derivation of the diffusion equation. The resulting “electrodiffusion” equation is similar in form to standard reaction-diffusion equations but has an extra term that takes the voltage gradients into account. The electrodiffusive approach has been previously shown to be equivalent to the cable approach in the limit of small ionic variations (Qian and Sejnowski, 1989). In the model that will be developed and studied in the following chapters, ions are allowed to move between the neuronal

syncytium and interstitial space via the standard array of ion channels and pumps. Cytoplasmic ionic movements are also caused by the extra electrodiffusive term. These ionic movements, coupled with large membrane fluxes of sodium and chloride, may then lead to an osmotic imbalance. This imbalance is countered (in the model) by the flow of water into or out of cells. This causes cells to either expand or contract. These cellular volume changes are spatially limited by the surrounding parenchyma (expansion) and intracellular organelles (contraction).

This dissertation presents a mathematical formulation of this model of cortical spreading depression, its implementation as a FORTRAN computer program, and the results of numerical simulations (program executions) used to evaluate the model. These simulations predict that spreading depression – or at least a variety of spreading depression-like phenomena – can be described in terms of dendritic and somatic physiology. In particular, it is predicted that rather than having a single cause, these phenomena are supported by a variety of mechanisms. These mechanisms include ionic movement through gap junctions, osmotically induced volume changes, and ionic movement through membrane channels.

The simulations predict that membrane currents fall into three classes: those that facilitate wave propagation, those that impede or inhibit wave propagation, and those that appear to have no effect on spreading depression. The predicted propagation velocity and predicted waveform shape depend on the combination and quantity of membrane channels present in the tissue. Facilitating currents include $K^+$

curents through n-methyl-d-aspartate receptor (NMDA-R) gated channels (referred to as NMDA-channels in the remainder of this dissertation), the delayed rectifying (DR) voltage-gated $K^+$ channels (VGKC), and the large conductance (BK) $Ca^{++}$-activated $K^+$ channels (K(Ca)). Consequently the partial or complete block of spreading depression by NMDA-R antagonists (Hernandez-Caceres and others, 1987; Lauritzen and others, 1988; Marrannes and others, 1988; Amemori and Bures, 1990; Lauritzen and Hansen, 1992; McLachlan, 1992; Nellgard and Wieloch, 1992), Magnesium ($Mg^{++}$) ions (Van Harreveld, 1984; Lauritzen and others, 1988) and tetraethylammonium (TEA) ions (Scheller, Tegtmeir and Schlue, 1998) can be explained. The presence of voltage-gated calcium channel (VGCC) antagonists or the removal of extracellular calcium will inhibit spreading depression only if the appropriate combination of ionic conductances is present.

Other predictions that will be presented suggest that some neuronal membrane currents could impede or prevent the propagation of spreading depression. These currents include those associated with both the A-type (KA) voltage gated potassium channel (VGKC) and the small conductance (SK) K(Ca) channel. These predictions are consistent with observations of spontaneous spreading depression following application of 4-AP (a KA channel blocker) (Psarropoulou and Avoli, 1993; Avoli and others, 1996) and seizures induced by apamin (an SK channel blocker) (McCown and Breese, 1990). The model also predicts that intracellular (cytoplasmic) calcium waves will be generated by all classes of SD, a prediction that is also consistent with

recent observations (Kraig and Kunkler, 1997; Kunkler and Kraig, 1998; Basarsky and others, 1998).

Furthermore, the model predicts that poisoning gap junctions (e.g., by reducing the intracellular diffusion coefficient to zero) will inhibit spreading depression. The existence of wave initiation and propagation in the simulations is independent of the presence of either sodium or chlorine channels; however, for complete recovery (in this model) the presence of both is required, and they can affect waveform shape. The model that will be presented in the following chapters also predicts large neuronal volume changes, and that these volume changes are integral to wave propagation. These predicted volume changes are consistent with observations.

Chapter 2 (Background) provides a survey of the published literature, and summarizes the clinical and biological significance of spreading depression. This includes a survey of experimental findings in a wide variety of species, experimental protocols, and a description of the nature of the SD wave as it passes through cortical tissue. Previously published mathematical models of spreading depression are also summarized and evaluated. Chapter 3 (Methods) presents the model and its mathematical formulation. All novel equations are derived, while equations drawn from earlier sources (e.g., ion channels and membrane pumps) are provided for reference. Chapter 4 (Results) presents the results of the simulations, and measures the model's successes and failures against the experimental evidence. This chapter

also evaluates the robustness of the model, by exploring the effects of parametric variation across applicable physiological ranges. Chapter 5 (Discussion) summarizes the dissertation and restates key results and predictions. Concerns and questions about biological validity are explored here and possible future extensions of this research are proposed. A glossary of frequently used technical terms (mathematical, biological, and clinical) is provided in the appendix.

# CHAPTER 2

# BACKGROUND

This chapter reviews the literature that has been published regarding spreading depression. A number of comprehensive reviews (Marshall, 1959; Ochs, 1962; Leão, 1972; Somjen and others, 1992; Bures, Buresová and Krívánèk, 1984) and at least one book (Bures, Buresová and Krívánèk, 1974) have been previously written on this subject. Because of the large amount of material published regarding spreading depression since it was first reported in 1944, this review focuses on the more recent literature. The reader is referred to the above-cited references for a review of the earlier literature. An overview of this material is provided in this and the following pages preceding section 2.1. Because of the more general nature of this overview than that of the remainder of this chapter, specific citations to the research literature are deferred until the more detailed presentation.

In the context of this literature survey, a neuro-protective hypothesis of spreading depression will be presented. In this theory, spreading depression results from a combination of mechanisms that occur in response to the loss of cellular homeostasis. All of the stimuli that have been observed to cause spreading depression (mechanical, electrical, chemical) will also lead to neural injury if presented in

sufficient magnitude. Sudden increases in the interstitial potassium concentration or the cytoplasmic sodium or chlorine concentrations, similar to those observed during spreading depression, or a hypoxic inhibition of metabolic activity, could also cause cell damage. A cascade of cytoplasmic signals, starting with neuronal calcium entry, and eventually leading to the production of the proteins that are required for cellular repair and/or re-growth, could be the response to this injury. This production of regenerative proteins in response to neural trauma could be the evolutionary advantage that is provided by spreading depression. The propagating potassium increase that is characteristic of SD would, in this theory, be the mechanism by which the neuro-protective signal is propagated to the surrounding tissue. The consequent membrane depolarization could also be interpreted as a way of preventing further cell damage. Depolarization makes the membrane highly permeable to the usual inorganic ions of biological significance: potassium, sodium, chlorine and calcium. As these species approach their equilibrium concentrations, the driving forces for additional currents disappear and these membrane currents are neutralized. In fact, if the membrane voltage is clamped to a nonzero level, cells will die; otherwise, if the membrane potential is allowed to float, the cells recover. This is presumably because the membrane resistance goes to zero and extremely large currents are required to maintain the voltage clamp (this observation, and this aspect of the theory was suggested by Istvan Mody). It is not the goal of this dissertation to prove or disprove this particular theory of spreading depression. Indeed, the goal is to model the significance of gap junctions, cytoplasmic diffusion, and osmotic forces in spreading

depression. Presenting this theory provides a useful mechanism (in my opinion) of integrating and interpreting the material in the remainder of this chapter.

Spreading depression, as it was first reported by the Brazilian physiologist Aristides Leão over half a century ago (Leão, 1944a,b), consists of a slowly moving depression of electrical activity in the cortex as measured with the electroencephalogram (EEG). This progressive front of EEG depression is accompanied by a "slow

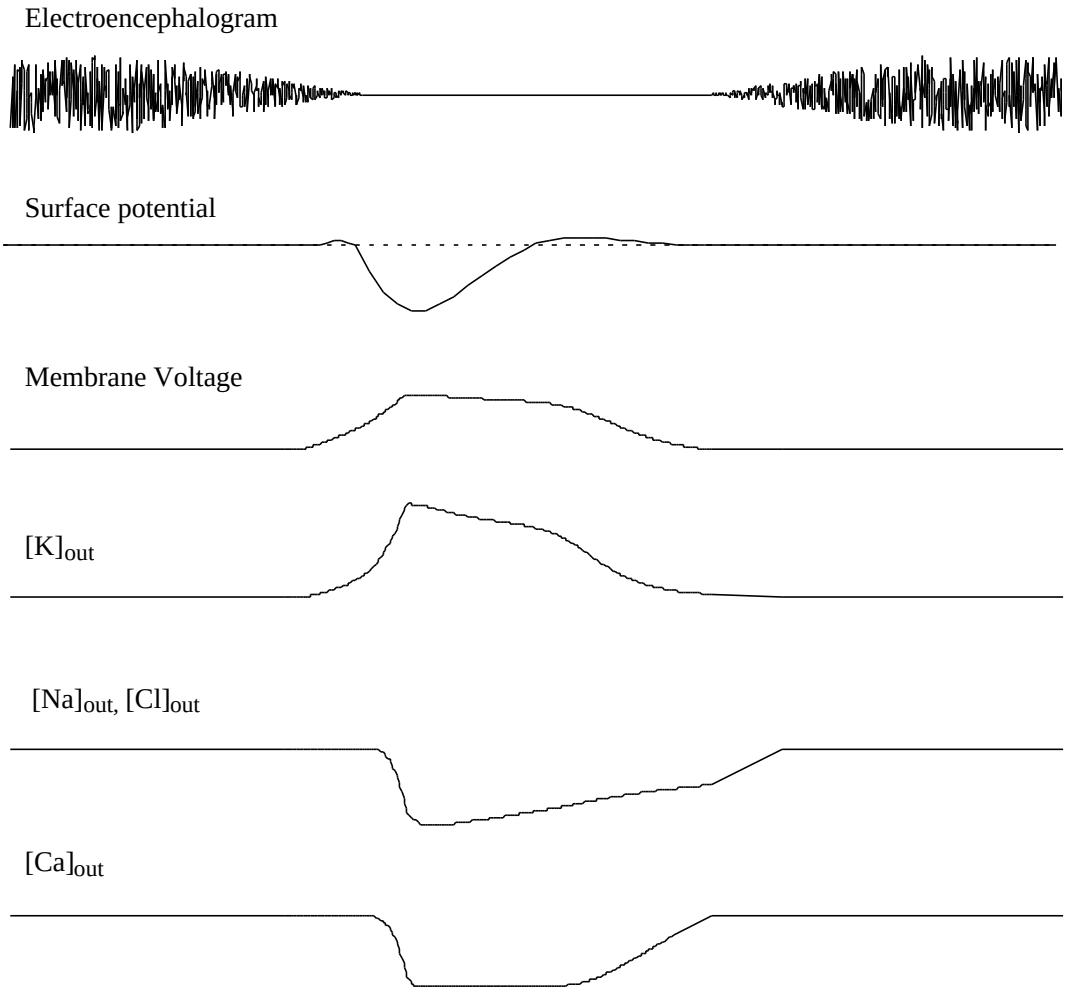


Figure 2.1. Illustration of voltage and ionic changes during passage of SD wave observed at a fixed point as a function of time (not to scale).

potential change" (SPC) seen at the cortical surface. The SPC consists of a negative voltage shift (a "surface-negative wave") of 5 to 15 mV in amplitude and up to ≈30 seconds duration, followed by a smaller, but longer-duration (up to two minutes) positive voltage shift (a "surface-positive wave"). Sometimes a short surface-positive wave is also seen to pass just prior to the initial negative voltage shift. Bursts of voltage spikes ("population spikes") always precede the wave front, but completely disappear with the arrival of the surface-negative wave, during which there is a complete EEG silence.

It is now known that the potential shifts are due to a propagating synchronized membrane depolarization of the neuronal population. Microscopically, the membranes of each neuron are (sometimes) initially hyperpolarized. This is followed by a prolonged depolarization and the cessation of all synaptic and cellular electrical activity. Wave passage is typically accompanied by a wave of hyperemia (increased blood flow), elevated extracellular potassium concentration, reduced extracellular sodium and chlorine concentrations (Figure 2.1), and a nearly complete disappearance of extracellular calcium. Following this, there is a prolonged oligemic phase (a deficiency in blood volume).

The wave speed typically ranges from two to twelve mm/minute, although slower waves have been reported, and propagates across the cortical surface more or less uniformly in all directions. There is some anisotropy due to morphological (e.g. cytoarchitectural changes) and anatomical variation (e.g. sulci). No detailed

quantitative studies of this anisotropy have been published. Electrophysiological observations are usually only based on a small number (three to five) electrodes placed at various distances from the stimulation. The SD wave will usually stop at large sulci (e.g., the central sulcus) or at the transition between cytoarchitecturally different regions

Spreading depression is not restricted to either the cerebral cortex or to mammals. It has been observed throughout the CNS, *e.g.*, in the cerebellum, retina, hippocampus, amygdala, caudate, thalamus, and spinal cord, and in a wide variety of species, ranging from fish to amphibians, birds, and insects. It has been observed in the brains of both anaesthetized and freely moving animals as well as in tissue slice preparations. Lissencephalic (less convoluted) cortex is significantly more susceptible to spreading depression than is convoluted cortex. Thus it is much easier to induce in the rat brain or rabbit brain than in the cat brain or monkey brain. *In vitro* preparations that have been studied in the most detail are those that are devoid of convolution: hippocampus (usually rat) and retina (usually chicken).

Spreading depression propagates in all directions from the point of stimulation through gray matter. However, since cortical gray matter forms a relatively thin layer about the surface of the brain, over long time periods (*i.e.*, seconds or minutes) wave propagation is essentially parallel to the gross cortical surface. The wave also propagates perpendicularly to the surface but only through gray matter and stops when it arrives at white matter.

Spreading depression has been implicated or theorized to occur in many clinical situations. It is widely believed to be an electrophysiological process involved in migraine auras. SD has also been observed in the ischemic penumbra (the area adjacent to and surrounding the ischemic region), and prior exposure of tissue to SD limits infarct growth following neural injury. Spreading depression almost always occurs following a mechanical stimulation sufficient to induce concussion, and probably has a neuro-protective effect, as noted above. Because population spikes preceding wave passage resemble epileptic discharge, spreading depression has been used as an animal model of epilepsy. There may even be a functional relationship between SD and epilepsy, although the nature of such a relationship, if it exists, is probably complex. While spreading depression typically will not propagate into a seizure zone, chemicals that induce seizures (such as picrotoxin) tend to increase the likelihood of spontaneous SD when they are administered at sub-convulsive doses. The similarity between some migraine symptoms and epilepsy has also been noted (e.g., the prodromal hallucinations and propagating wave front). More recent observations are consistent with hippocampal SD being involved in transient global amnesia (TGA). A generalized "spreading depression syndrome" has even been hypothesized to describe a variety of post-traumatic symptoms that have been observed to follow head injury, particularly in pre-teen age children. Finally, since spreading depression itself does not appear to cause any tissue damage and the brain (usually) recovers completely following wave passage, it has been widely used in animal studies to produce a "functional decorticozation" or to selectively "turn off"

various brain organs. SD has also been suggested as a potential tool for functional/anatomical localization during neurosurgery.

We now turn to a more detailed description of recent research regarding the phenomenon of spreading depression, citing the appropriate literature as we proceed. A wide variety of relevant observations have been reported. Rather than just presenting the salient facts needed to support the model developed in Chapter 3 ("Methods") and tested in Chapter 4 ("Results"), an attempt is also made in this chapter to integrate this mass of observational data. At times, the facts seem quite disparate and conflicting. It has not been possible to completely reconcile all of this data into a unified, cogent theory, although various conjectures have been made in the literature. This attempt to integrate the data has allowed the mathematical model to be tested against the widest possible range of biological data. This mass of data presented also tends to support the neuroprotective hypothesis discussed above. Thus this review is substantially longer that it would be if its only goal were to provide the background for the mathematical model presented in following chapters. Section 2.1 describes how spreading depression has been induced, and section 2.2 examines the events that have been observed to occur during spreading depression. The use of modern techniques to observe SD is discussed in section 2.3. This is followed in section 2.4 with an investigation of the clinical significance of spreading depression. Finally, previously published mathematical models of spreading depression are described in section 2.5.

## 2.1. INDUCTION OF SPREADING DEPRESSION

This section describes *where* spreading depression has been observed and *how* it has been *provoked*. SD has been observed in a wide variety of species, both *in vitro* and *in vivo* (Table 2.1, section 2.1.1), and has been induced in a variety of gray matter substrates (*e.g.*, cortex, hippocampus, cerebellum, and retina; section 2.1.2). Spreading depression has been induced electrically (section 2.1.3), mechanically (section 2.1.4), chemically (section 2.1.5), by intense neuronal activity (section 2.1.6) or by hypoxia (reducing the oxygen level, section 2.1.7). A discussion of *what* occurs (section 2.2), *how* it is *observed* (section 2.3), *why* it may be of clinical relevance (section 2.4), and *how* it has been previously *modeled* (section 2.5) is deferred to the following sections.

Table 2.1. Species and organs in which spreading depression has been observed. SD has not been observed in every organ listed in every species listed. The list is representative and not inclusive. For details, see sections 2.1.1 and 2.1.2.

| Species | | Organ |
|---|---|---|
| alligator | marmoset | cortex |
| carp | monkey | retina |
| cat | pigeon | hippocampus |
| catfish | rabbit | cerebellum |
| chicken | rat | thalamus |
| cockroach | skate | caudate/striatum |
| frog | toad | reticular formation |
| gerbil | turtle | hypothalamus |
| human | | spinal ganglia |
| | | amygdala |

### 2.1.1. Species in which Spreading Depression has been Observed

The first observations were in rabbit cerebral cortex (Leão, 1944a,b), which is still a popular preparation (see, for example, Megirian and Bures, 1970; Higashida and others, 1971; Higashida, Mitarai and Watanabe, 1974; Haglund and Schwartzkroin, 1984; Busija and Meng, 1993; Colonna and others, 1994a, 1997). Other preparations that have been studied include the chicken retina (Ookawa and Bures, 1969; Martins-Ferreira and de Oliveira Castro, 1966, 1971; Martins-Ferreira and others, 1974; Cherkin and Van Harreveld, 1978; de Azeredo and Martins-Ferreira, 1979; Ferreira-Filho and Martins-Ferreira, 1982; Gorelova and Bures, 1983; do Carmo and Martins-Ferreira, 1984, 1988; de Oliveira Castro, Martins-Ferreira and Gardino, 1985; Martins-Ferreira and do Carmo, 1987; Chebabo, do Carmo and Martins-Ferreira, 1988; de Azeredo, 1991; Drejer and others, 1989; Marrocos and Martins-Ferreira, 1990; Chebabo and do Carmo, 1991; Chebabo, do Carmo and Martins-Ferreira, 1993; Martins-Ferreira, Ribeiro and do Carmo, 1993; Sheardown, 1993; Fernandes de Lima and others, 1993; Fujimoto and Yanase, 1994; Fernandes de Lima and Hanke, 1996; Dahlem and Muller, 1997; Maranhao-Filho and others, 1997; Brand, Fernandes de Lima and Hanke, 1998); rat hippocampus (Herraras and Somjen, 1993a, 1993b, 1993c); rat cortex (Latour and others, 1994); and cat cortex (Goldensohn, Escueta and Runk, 1967; Pieri and others, 1973; Sugaya, Takato and Noda, 1975; Blank and

Kirshner, 1977; Nicholson and others, 1977, 1978; Goadsby, 1992; Goadsby, Kaube and Hoskin, 1992; Piper and Lambert, 1996; Kaube and Goadsby, 1994; Goadsby, Adner and Edvinsson, 1996; Fujimoto and Yanase, 1994; Andersson, 1995; Conteras, Destexhe and Steriade, 1997). The chicken retina is a particularly useful preparation because recurrent waves of spreading depression can be induced for several hours. Cellular volume changes induce optical reflectance and/or transmittance changes that are more observable in this substrate than in other preparations because of the relative transparency of the retina. Furthermore, the chicken retina is avascular so SD can be observed independently of the vascular changes that occur in other preparations (Fernandes de Lima and others, 1993). Spreading depression has also been reported in carp retina (Higashida, Sakakibara and Mitarai, 1977; Fujimoto and Yanase, 1994); catfish cerebellum (the catfish is the teleost *Corydoras aneus*) (Kraig and Nicholson, 1978); pigeon forebrain (Boiko and Buresh, 1981); gerbil cortex (Mayevsky, 1978; Mayevsky, Lebourdais and Chance, 1980; Guedes and do Carmo, 1980; Mayevsky, Zarchin and Friedli, 1982; Evans and Smith, 1987; Haselgrove and others, 1990; de Azeredo and Peret, 1992); toad and frog retina and spinal cord (*rana catesbeiana, rana ridibunda, rana pipiens, salienta anura*) (Mori, Miller and Tomita, 1976; Ferreira-Filho and Martins-Ferreira, 1982; Fujimoto and Tomita, 1986; Fujimoto and Yanase, 1994); monkey cortex (van Harreveld, Stamm and Christensen, 1956; Rebert, 1970); marmoset (Marshall, 1959 ); alligator (Martins Ferreira and Leão, 1958); turtle cerebellum (Rice and Nicholson, 1987); skate cerebellum (the elasmobranches *raja erinacea* and *raja ocellata*) (Young, 1980; Rice and Nicholson, 1988); and cockroach

ganglia (Rounds, 1967, 1968) (propagation was not observed in the cockroach, only the electrophysiological phenomena).

### 2.1.2. NEURAL SUBSTRATES

Spreading depression has also been observed in numerous sub-cortical structures as well as in the cerebral and cerebellar cortices and the hippocampus. It has been observed in the thalamus (Aquino Cias and others, 1966a, 1996b; Buresová, Fifkova and Bures, 1966; Balinska, Buresová and Fifkova, 1967; Bures and Buresová, 1981; Albe-Fessard and others, 1984); the striatum (Bures and Hartman, 1967; Bures, Hartmann and Lukyanova, 1967; Albe-Fessard and others, 1984); the olfactory bulb (Amemori, Gorelova and Bures, 1987; Amemori and Bures, 1988); the caudate nucleus (de Luca and Bures, 1977; Bures and Buresová, 1981; Kasser and others, 1988; Amemori and Bures, 1990); the amygdala (Bures and Buresová, 1981); the reticular formation (Bures and Buresová, 1981); the zona incerta (Bures and Buresová, 1981); the hypothalamus (Bures and Buresová, 1981); and spinal ganglia (Somjen and Czeh, 1989; Czeh and Somjen, 1990; Streit, Ferreira Filho and Martins-Ferreira, 1995). There are some differences in the properties of wave propagation (*e.g.*, different wave speeds) in different brain organs (Amemori and Bures, 1986). Though it is somewhat unusual, waves of SD can even cross the cytoarchitectural boundaries between brain organs. For example, subcortical spreading depression may spread from the brain stem to the cortex (de Luca and Bures, 1977), while cortical SD can penetrate through the amygdala and into the caudate without stopping and return back to the cortical induction point (Vinogradova, Koroleva and Bures, 1991). Similarly, reentrant waves can occur in the retina. Self-sustained repetitive circular waves

(Fernandes de Lima and Hanke, 1996) or spiral waves (Dahlem and Muller, 1997; Gorelova and Bures, 1983) that can be induced to reverberate around a mechanical obstacle (Shibata and Bures, 1975). Furthermore, retinal waves can be observed optically. Changes in cell volume cause different light scattering profiles as the wave passes (Martins-Ferreira and de Oliveria Castro, 1966).

### 2.1.3. Electrical Stimulation

Spreading depression can be induced electrically by either direct current or pulse train stimulation, via either implanted or surface electrodes. The electrodes may be either cathodal or anodal (Marrannes and others, 1988; Martin, Warner and Todd, 1994). Direct current (DC) stimulation has usually been preferred because convulsive activity can sometimes be induced by alternating current (AC) stimulation. This could complicate the experiments. The early experimenters induced spreading depression with a one-second to ten-second tetanus at frequencies from ≈10 Hz to ≈50 Hz, and also by one second DC stimulations at ≈0.1 mA to ≈3 mA (Leão, 1944a, Leão and Morrison, 1945; Marshall, 1950; Grafstein, 1956 a, b). Others have reported that a train of electrical pulses at ≈10 Hz and 0.1 to 0.3 msec duration applied to the surface is sufficient (Kraig, Ferreira-Filho and Nicholson, 1983; Koroleva, Oitzl and Bures, 1985).

### 2.1.4. MECHANICAL STIMULATION

A wide range of mechanical stimuli ranging from gently stroking the cortex to striking tissue with a blunt instrument will induce SD. For example, pricking the gray matter with a needle (Lambert and Michalicek, 1994) or minor brain injury (Rogatsky and others, 1996) will induce spreading depression. The very acts of inserting electrodes, applying drugs, or exposing the cortex to air are sufficient, as are cardiac and respiratory pulsations against broken bone or electrodes (Marshall, 1959). Zachar and Zacharová (1961) quantified the threshold for mechanical stimulation by dropping rods of varying weights from various heights on the exposed dura. They found that there are inverse relationships between (a) stimulation threshold and area and (b) stimulation threshold and displacement of the cortical surface by the stimulation. There is a minimum threshold energy of ≈400 ergs/mm$^2$ for rods over 1 mm in diameter, so long as the cortical surface is displaced by at least 1 mm. The stimulation threshold for concussion (≈$10^5$ erg/mm$^2$, Bures, Buresová and Krívánek, 1974) significantly exceeds this threshold. This suggests that concussion might usually be accompanied by spreading depression, although clinical verification of this conclusion has not been published. Focused ultrasonic irradiation of the exposed cortex at 800 kHz in live animals will also induce spreading depression; the threshold duration decreases by increasing the temperature (Ueda, Bures and Fischer, 1977). However, since histological examination of these animals after the experiment indicated the existence of a central coagulation lesion surrounded by edema, the SD might not have

been due to the ultrasonic radiation but, rather, to subsequent ischemic damage, trauma or hypoxia.

### 2.1.5. Chemical Stimulation

Numerous chemicals have been used to initiate spreading depression. These include both organic and inorganic ions and various metabolic inhibitors, as summarized in Table 2.2. In most cases, the chemical either directly induces massive depolarization, or causes a breakdown of cellular homeostasis that then induces a depolarization and massive potassium release. This potassium release is presumably the imminent cause of the subsequent spreading depression. The most common protocol in this class is the use of KCl. Application is via continuous perfusion, dialysis, or topical application, such as by laying wet tissue paper on the cortical surface. The stimulation threshold has been reported to be as low as 8 mM (Leão and Morrison, 1945; Bures, 1956; Marshall, 1959; van Harrevald, 1959; Martins-Ferreira, Ribeiro and do Carmo, 1993). Sodium and lithium salts are ineffective, while rubidium and ammonium chloride are effective (Bures, Buresová and Krívánek, 1974).

Depolarizing amino acids such as glutamate, aspartate, asparagine, NMDA and homocysteic acid are also frequently used to stimulate spreading depression (Bures, 1956; Marshall, 1959; Van Harrevald, 1959; Curtis, Phillis and Watkins, 1960; Curtis and Watkins, 1963; Leão, 1947a). Proline has a "dual" effect – it has both an antagonist and agonistic effect. At lower concentrations, l-proline prevents SD (Cherkin and Van Harreveld, 1978; Van Harrevald, Cherkin and Davis, 1980)

probably by inhibiting glutamate release. At higher concentrations proline can promote spreading depression (Van Harreveld and Reuter, 1981), possibly by activation of the glycine receptor.

Acetylcholine (Ach), prostigmine (an acetylcholenesterase), nicotine and cytisine (a nicotinic agonist) will all elicit SD. Ach-induced spreading depression can be blocked by cholinergic antagonists such as d-tubocurarine (curare, a poison that is extracted from plants of the *menispermaceae* family, acts primarily on neuromuscular nicotinic receptors, but appears to have some effect on some nicotinic receptors in the brain), atropine (a muscarinic antagonist), or mecamylamine (a nicotinic agonist) (Rodrigues and Martins-Ferreira, 1980; Sheardown, 1997). Spreading depression induced by the GABA-A receptor blocker picrotoxin (which will induce seizures at higher doses) has been prevented by application of carbachol (carbamylcholine, an Ach agonist) (Sutor and Hablitz, 1989).

Enhancement of spreading depression has reportedly been induced by the dopaminergic D1-receptor agonist SKF 38393. Similarly, the dopamine D2-receptor agonist quinpirole has been observed to block SD (de Azeredo and Ribeiro, 1992). The D1-receptor stimulates adenylyl cyclase activity, while the D2-receptor is coupled to adenylyl cyclase inhibition. Apomorphine (a non-selective D1/D2 agonist), on the other hand, apparently does not effect SD (Amorim and others, 1988).

Table 2.2. Chemicals that affect spreading depression. See text for more details.

| | Facilitates SD | Hinders SD | No effect |
|---|---|---|---|
| Salts | KCl<br>RbCl<br>$NH_4Cl$ | | NaCl<br>LiCl |
| Amino Acids | glutamate<br>aspartate<br>NMDA<br>asparagine<br>homocysteic acid<br>proline (at high concentrations) | proline (at low concentrations) | |
| Cholinergic modulators | acetylcholine<br>prostigmine<br>nicotine<br>cytisine | curare<br>atropine<br>mecamylamine<br>carbachol | |
| GABA modulators | picrotoxin | | |
| Dopaminergic modulators | D1 agonist | D2 agonist | apomorphine |
| Serotonergic modulators | | d-fen<br>sumatriptan | |
| Opiods | DAME<br>met-enkephalin<br>leu-enkephalin | naloxine<br>4AP | |
| Metabolic inhibitors | NaCN<br>NaF<br>2,4-DNP<br>$NaN_3$<br>$CH_3COOH$<br>$NH_42SO_4$<br>ouabain<br>veratrine<br>theophylline<br>ethanol | tetrodotoxin (spikes)<br>dipyridamole<br>NBI<br>octanol<br>heptanol | tetrodotoxin (DC Voltage shift)<br>conotoxins |
| Anaesthetic | | benzocaine<br>lidocaine<br>halothane<br>urethane + chloralose<br>thionembutal<br>isoflurane | alpha-chloralose |

Serotonin (5HT) appears to have an inhibitory effect on spreading depression. The serotonin reuptake blocker d-fenfluramine will slow or completely block a wave of SD (Cabral-Filho, Trindade-Filho and Guedes, 1995). Blocking 5HT reuptake increases its interstitial concentration, thereby prolonging its availability in the synaptic cleft. The 5HT1D-transporter agonist sumatriptan blocks SD in a dose dependent manner (Maranhao-Filho and others, 1997). Sumatriptan is also an anti-migraine agent.

Various opiods will also induce spreading depression. For example, d-ala-2-met-enkephalinamide (DAME), met-enkephalin, and leu-enkephalin have all induced SD (Sprik and others, 1981; Oitzl and Huston, 1984; Oitzl, Koroleva and Bures, 1985). This effect has been blocked by naloxine, a non-selective opiod antagonist, and reversed by the application of 4-aminopyridine (4AP), which blocks some types of voltage gated potassium channels. Oitzl argues that DAME exerts an inhibitory effect on cortical neurons and that the induction of SD by DAME is due to the early blockade of inhibitory neurons in superficial cortical layers.

Metabolic inhibitors and poisons such as NaCN, NaF, 2,4-DNP, $NaN_3$, $CH_2COOH$, strophanthin, NA2SO3, $HgCl_2$, $NH_42SO_4$, ouabain and veratrine will also induce SD (Bures, 1956; Aquino-Cais and Bures, 1967; Marshall, 1959; Bures, Buresová and Krívánek, 1974; Martins-Ferreira, Ribeiro and do Carmo, 1993). These agents probably induce SD via a loss of homeostasis. For example, ouabain poisons

the Na/K membrane pump. This leads to a slow leakage of potassium from the cell into the interstitial space. As extracellular potassium accumulates, a membrane depolarization develops. A wave of SD may be induced when a threshold potassium concentration is exceeded. Tetrodotoxin (TTX, a sodium channel blocker) has no effect on wave propagation but does block the prodromal spikes. Conotoxins (N-type Ca-channel blockers) appear to have no effect on spreading depression (Sheardown, 1993). Dipyridamole (DPR) and nitrobenzylthioinosine (NBI), adenosine transport (uptake) inhibitors, partially block $K^+$ induced SD. Theophylline, a non-selective adenosine receptor antagonist, increases the susceptibility to spreading depression (Kaku, Hada and Hayashi, 1994; Hada and others, 1996). Octanol and heptanol, which poison gap junctions, have both been used to prevent SD (Martins-Ferreira and Ribeiro, 1995; Nedergaard, Cooper and Goldman, 1995; Largo and others, 1997; Brand, Fernandes de Lima and Hanke, 1998). Ethanol increases the susceptibility to SD and increases wave speed (Guedes and Frade, 1993). Hypothetical points of action for ethanol are adenosine transport inhibition and GABA-mediated $Cl^-$ channel enhancement (De Lorey and Olsen, 1992).

The choice of anaesthetic is of both experimental and clinical significance, as some appear to completely prevent spreading depression, while others seem to have only a marginal (or no) blocking effect. Since there are some indications that when spreading depression occurs in an ischemic zone the subsequent histological damage is more extensive, it would be preferable to avoid SD during neurosurgery. In the

laboratory, if agents that block spreading depression are used to anesthetize animals, it will be more difficult (or impossible) to observe SD. Benzocaine and lidocaine produce dose dependent blockage of SD (Chebabo, do Carmo and Martins-Ferreira, 1993). Urethane plus chloralose, thionembutal or isoflurane will slow the speed of the SD wave but will not completely prevent it (Guedes and Barreto, 1992; Verhaegen, Todd and Warner, 1992). Halothane, in sufficient doses, has been reported to completely block SD (Saito and others, 1995, 1997), while alpha-chloralose does not appear to have any blocking effect (Saito and others, 1995).

### 2.1.6. NEURONAL STIMULATION

Intense neuronal activity has also been reported to induce spreading depression. This was first suggested when spreading depression in the contralateral hemisphere followed tetanic callosal stimulation (Leão 1944a, Leão and Morrison, 1945). In subsequent experiments tetanic stimulation was followed by spreading depression in regions remote from the stimulation point (Van Harrevald and Stamm, 1953, 1954). It is not known why these remote events of spreading depression took place. In general, however, electrical stimulation is not usually followed by spreading depression in remote regions (Bures, Buresová and Krívánèk, 1974). This phenomenon has not been discussed in the more recent literature.

### 2.1.7. HYPOXIC INDUCTION

Spreading depression has been observed following a reduction in the oxygen level of the perfusing solution (Balestrino, Aitken and Somjen, 1989; Aitken and others, 1991; Czeh, Aitken and Somjen, 1992, 1993; Young and Somjen, 1992; Hershkowitz, Katchman and Veregge, 1993; Jing, Aitken and Somjen, 1994; Turner, Aitken and Somjen, 1995). Spontaneous seizures are also possible in hypoxic tissue (Kawasaki, Traynelis and Dingledine, 1990). Hypoxia can lead to a loss of synaptic function (Young, Aitken and Somjen, 1991), a lowering of the resting potential (Davis, Janigro and Schwarzkroin, 1986), a reduction of membrane resistance (Czeh, Aitken and Somjen, 1992), increase in the holding current (Czeh, Aitken and Somjen, 1992, 1993), and the failure of synaptic transmission (Czeh and Somjen, 1990; Young and Somjen, 1992). The likelihood of the recovery of synaptic transmission decreases with the duration of hypoxia (Balestrino, Aitken and Somjen, 1989). Hypoxia most commonly occurs clinically in connection with ischemic stroke or other neural injury. Thus it seems possible that spreading depression would occur naturally in connection with these events. The possible relationships between spreading depression and hypoxia will be discussed in section 2.4.1 (“Trauma”). Epilepsy and seizures will be discussed in section 2.4.3.

## 2.2. NEUROPHYSIOLOGICAL OBSERVATIONS

The previous section described *how* and *where* spreading depression has been observed. This section focuses on *what* occurs during spreading depression. Because of the large amount of material, it is presented in a "bottom-up" sequence, starting at the molecular level, proceeding to physiological processes that occur at the cellular level, and continuing to organ- and systems- level observations. Both the effects of these processes and/or materials on spreading depression and the effect of spreading depression on these processes are presented as it becomes relevant to the discussion. At the most microscopic level, the significance of various inorganic ions is presented in section 2.2.1. This is followed in section 2.2.2 by a discussion of neurotransmitters and amino acids that affect spreading depression or whose levels of expression have been observed to change during SD. Changes in protein production observed during spreading depression are discussed in section 2.2.3. Glutamatergic receptors are discussed in section 2.2.4 and voltage- and calcium-gated ion channels are discussed in section 2.2.5. Several recent reports indicate that poisoning neuronal gap junctions will prevent spreading depression. These are discussed in section 2.2.6. While the interaction between SD and metabolic activity is still not well understood a great deal of material has been published on the subject. An attempt to integrate this material is provided by section 2.2.7. Glial cells were at one time thought to provide the primary substrate for the propagation of spreading depression. More recently it has been

reported that metabolic poisons that specifically inhibit glial cells do not prevent spreading depression. These results are discussed in section 2.2.8. Circulatory changes are discussed in section 2.2.9 and changes in cellular volume observed during SD are presented in section 2.2.10.

### 2.2.1. INORGANIC IONS

Along with the DC-Voltage shift, a travelling wave of high interstitial $[K^+]_{out}$ is one of the defining characteristics of spreading depression. This potassium wave always occurs during SD, regardless of the mechanism of stimulation. Furthermore, a perfusion (*in vitro*) or dialysis (*in vivo)* of a high $K^+$ solution will almost invariably be followed by SD. Thus high interstitial levels of $K^+$ appear to be both necessary for the propagation of and sufficient to induce spreading depression. During spreading depression, the extracellular potassium concentration will typically increase from its resting level of ≈3 mM/l to ≈30 to ≈60 mM/l in two to three seconds. Besides potassium, spreading depression is always accompanied by a significant reduction of the levels of extracellular sodium and chlorine, and a nearly complete loss of extracellular calcium (Kraig and Nicholson, 1978; Hansen and Olsen, 1980) as illustrated in Figure 2.1.

Prodromal population spikes (voltage spikes which that are synchronized among a neuronal population and precede the DC-voltage shift) usually herald an approaching wave of spreading depression. These spikes are synchronized at all levels of gray matter. The synchronizing mechanism remains unknown. The interstitial $K^+$ wave and DC potential shift follow the voltage spikes, and appear to occur simultaneously (Herreras and others, 1994). This suggests that neither changes in the extracellular $K^+$ concentration nor the voltage depolarization are the

imminent mechanism of wave propagation. The spike bursts themselves are not part of the mechanism, because they are completely suppressed by TTX, a $Na^+$ channel blocker, without impeding the slow potential change or potassium wave. When a wave of SD passes through a region that is locally perfused with TTX, the spikes disappear, and then reappear as before when the wave leaves the perfused region. Thus the spikes would appear to be caused by sodium currents.

Barium ions are known to block the muscarinic potassium channel, the inward rectifying potassium channel and the small-conductance calcium sensitive (SK) potassium channel (Johnston and Wu, 1995). A perfusion of $Ba^{++}$ at micromolar concentrations will usually also elicit spreading depression. Increasing the $Ba^{++}$ concentration subsequently reduces the speed of (and eventually completely blocks) SD wave propagation in retinal preparations (Fernandes de Lima and others, 1993; Fernandes de Lima, Goldermann and Hanke, 1994; Ribeiro and Martins-Ferreira, 1994; Brand, Fernandes de Lima and Hanke, 1998). Finally SD has been induced in the presence of voltage-gated $K^+$ channel blockers such as 4-AP (which blocks the A-channel) and TEA (which blocks the delayed rectifier and the BK-channel) (Avoli and others, 1996). Thus $K^+$ currents and elevated extracellular $K^+$ levels would be appear to be sufficient but not necessary for the induction of spreading depression.

The reduction of extracellular calcium is significant, with reductions to less than 10% of the resting concentration typically reported. Levels as low as 0.08 mM have been reported (Nicholson and others, 1977, 1978; Hansen and Olsen, 1980).

This is a substantially greater reduction than the maximum loss of 20% seen during neuronal activity, such as the repeated stimulation of the parallel fiber – Purkinje cell circuit (Nicholson and others, 1977, 1978). The calcium may move into neuronal and glial cells and induce a cascade of signals, eventually leading to protein production (my own conjecture, based on the evidence presented below in section 2.2.3, "Molecular Genetics"). Evidence indicates that the passage into brain cells is mediated by voltage gated channels (Osuga and others, 1997; Sheardown, 1997) and not via glutamate channels (Young and Somjen, 1992).

The traveling depression of calcium concentration is accompanied by a cytoplasmic calcium wave (Fernandes de Lima, Goldermann and Hanke, 1994; Kraig and Kunkler, 1997; Kunkler and Kraig, 1997; Basarsky and others, 1998). Two waves have been observed in hippocampal slices: a fast calcium wave that moves along the pyramidal cell layers ahead of the SD wave, and a slow, more isotropic calcium wave moving at the same speed as the SD wave. The slow wave precedes the DC voltage shift by several seconds. Both calcium waves can be abolished by heptanol, which also prevents spreading depression (Kunkler and Kraig, 1998) or removing extracellular calcium from the medium (Basarsky and others, 1998). The mechanism for propagation of these calcium waves is not known. It is likely that the slow wave corresponds to the propagating cellular uptake of calcium. Glial cells appear to be at least partly involved in these calcium waves (Fernandes de Lima, Goldermann and Hanke, 1994; Basarsky and others, 1998).

The role of interstitial calcium in the propagation of spreading depression is not clear. Some evidence indicates a facilitating role, while other evidence would indicate an inhibitory role. Some experimenters have been able to induce SD in calcium-free or low calcium media (Ramos, 1975; Snow, Taylor and Dudek, 1983) but the susceptibility to SD appears to be reduced (Hada and others, 1996). In hippocampal SD, recovery may be faster in a calcium-deprived bath (Jing, Aitken and Somjen, 1991). Young, Aitken and Somjen (1991) have reported that SD will sometimes occur earlier in low calcium media than when a normal Ringer's solution is used for the bath. The wave speed of retinal SD is an increasing function of calcium concentration in the bath (Ramos, 1975; do Carmo and Martins-Ferreira, 1988; Fernandes de Lima and others, 1993). Basarsky and others (1998) have reported, on the other hand, that the slope of SD onset (optical transmittance) is smaller and the rise time to maximum signal is longer in a calcium-deprived bath.

It is difficult to reconcile these reports. Hippocampal spreading depression is not prevented by blocking voltage gated calcium channels with divalent cations such as $Ni^{++}$ or $Co^{++}$ (Jing, Aitken and Somjen, 1993). Thus while calcium may not be necessary for the propagation of SD in all types of tissue, these observations suggest that the presence of calcium may increase a tissue's susceptibility to SD, and that any factors that increase the membrane permeability of calcium are likely to augment SD. They may be of clinical interest. Cyclandelate, a calcium channel antagonist, has been used to treat some forms of migraine (Siniatchkin, Gerber and Vein, 1998). Whether

such agents work because they prevent or partially block spreading depression remains to be seen.

Hypotonic exposure to either sodium or chlorine or their complete removal can also trigger SD (Haglund and Schwartzkroin, 1984; Chebabo and others, 1995a). The reduction of chloride in the perfusing solution causes a logarithmic increase in the wave speed (Marrocos and Martins-Ferreira, 1990). A combination of gastric washing (which has been correlated with decreased CSF NaCl levels) and intra-muscular administration of 3-beta-aminoethylpyrazole increased the susceptibility of rabbits to spreading depression, and also intensified spreading depression associated epileptiform activity. These effects were abolished by the injection of sodium chloride, but were intensified by sodium isethionate (which replaced the $Na^+$ but not the $Cl^-$) (Guedes and do Carmo, 1980). Together with the observations that both serum and CSF $Na^+$ and $Cl^-$ levels are significantly reduced by gastric washing, these results suggest that a chlorine deficiency (when it is present) could play a significant role in spreading depression. This would not be too surprising given that the resting potential for most cells is very close to the reversal potential for chlorine. Hence the presence of chlorine ions may have a stabilizing effect on the tissue (thereby reducing the susceptibility to SD), and removing chlorine may have a destabilizing influence (increasing the susceptibility to SD).

Reducing the extracellular concentration of magnesium ions ($Mg^{++}$) has also been reported to induce spreading depression (Mody, Lambert and Heinemann, 1987; Avoli and others, 1991). Similarly, increasing the magnesium concentration has been reported to prevent SD (van Harreveld, 1984; Lauritzen and others, 1988; Rodrigues and others, 1988). These results suggest that NMDA-receptor-gated currents could play a facilitatory role in spreading depression, since $Mg^{++}$ normally blocks NMDA-channels. It is generally believed that this block is removed and the channels activated only when the membrane is depolarized. NMDA-channels also require a neurotransmitter (presumably glutamate) for activation. This subject is discussed in more detail in section 2.2.4 ("Glutamate Receptors").

### 2.2.2. Amino Acids and Neurotransmitters

It is likely that many neurotransmitters play modulatory roles in spreading depression. Although spreading depression only propagates through gray matter, and stops at the boundary of white matter regions, gray matter is thoroughly innervated with axonal endings and arborizations. As a wave of depolarization passes through a region of tissue, some quantity of neurotransmitter is likely to be released before the interstitial calcium is completely removed by whatever mechanisms are involved in SD. This neurotransmitter is likely to interact with the receptors on the dendritic tree and further modulate the membrane voltage. Whether this effect is causative or purely modulatory remains to be determined.

Glutamate is the most common excitatory neurotransmitter in the mammalian CNS, and a perfusion of glutamate has been used to induce spreading depression. Observations suggest that this effect is mediated primarily by the NMDA receptor, although other glutamate receptors can play a role. Waves of SD can be completely blocked by either $Mg^{++}$ or NMDA channel blockers such as MK-801, as well as by blocking the glycine-binding site of NMDA receptors. $Mg^{++}$ is believed to block the pore of NMDA-channels except during depolarization. This subject is discussed (and detailed citations are presented) in section 2.2.4 (“Glutamate Receptors).

That acetylcholine (Ach) is released during spreading depression comes as no surprise because of the presence of Ach mediated synapses throughout the CNS. Acetylcholine has also been reported to induce spreading depression (Rodrigues and Martins-Ferreira, 1980; Sheardown, 1997). Ach induced SD is blocked by the competitive receptor blocker d-tubocurarine (curare) or by atropine (Rodrigues and Martins-Ferreira, 1980). Lower concentrations of these toxins reduced the wave speed without completely suppressing the wave. Retinal spreading depression has been induced by nicotine, and has been blocked by the nicotinic cholinergic receptor antagonist mecamylamine (Sheardown, 1997), but not by the snake neurotoxin alpha-bungarotoxin. This suggests a facilitatory role for acetylcholine that is mediated by the alpha-bungarotoxin insensitive nicotinic acetylcholine receptor subtype. However, the effect of Ach may be indirect, via its depolarizing influence, since blocking NMDA sensitive glutamate channels has also been reported to prevent Ach-induced spreading depression in these same experiments (Sheardown, 1997). Other experiments suggest that Ach may have a stabilizing effect, since the cholinergic agonist carbachol (carbamylcholine) has been reported to prevent picrotoxin-induced SD (Sutor and Hablitz, 1989). Picrotoxin is a GABA-receptor blocker that induces spreading depression at low dosages and induces seizures at higher dosages (Hablitz and Heinemann, 1989; Sutor and Hablitz, 1989; McLachlan, 1992).

The catecholamines are neurotransmitters and modulators that are derived from the amino acid tyrosine, and include dopamine (DA), epinephrine and norepinephrine

(NE). They are present in many brain areas because of the wide projections from the nigrostriatal system (DA) and the locus coereleus (NE). During the passage of a wave of SD the interstitial cortical catecholamine content has been observed to increase some 60 percent above baseline (Pavlasek and others, 1993). Dopaminergic neurons are also present in the retina, where SD velocity has been observed to increase follow application of a dopamine D1-receptor agonist (SKF 38393) and to decrease following application of a D2-receptor agonist (Quinpirole) (de Azeredo and Ribeiro, 1992). The D1-receptor stimulates adenylyl cyclase activity, while the D2-receptor is coupled to adenylyl cyclase inhibition. Apomorphine (a non-selective D1/D2 agonist), on the other hand, apparently does not effect SD (Amorim and others, 1988). Striatal SD is also accompanied by dopamine release (Moghaddam and others, 1987) and is enhanced by sufficiently high levels of glutamate and inhibited by APH (an NMDA antagonist) (Moghaddam and others, 1990). In the nucleus accumbens DA release and a DC-voltage shift that may be due to spreading depression are observed to follow application of the glutamatergic agonists NMDA or AMPA (α-amino-3-hydroxy-5-methyl-4-isoxalone propionic acid) (Svensson and others, 1994). There is no evidence to indicate that catecholamine activity is anything but modulatory (as opposed to causative) in spreading depression.

Serotonin (5-hydroxytryptamine, 5HT) seems to have an inhibitory effect on spreading depression. This, too, is not surprising, given that as a neuromodulator, serotonin tends to be inhibitory and reduces the excitability of neurons. Blocking

serotonin reuptake increases the interstitial 5HT concentration. One blocking agent, d-fen (d-fenfluramine) has been reported to slow or block spreading depression (Cabral-Filho, Trindade-Filho and Guedes, 1995). The serotonergic agonist CPP (3-((+-)-2-carboxypiperazin-4-yl)-propyl-1-phosphonic acid) has been observed to delay the onset of, and to speed recovery from spreading depression (Jing, Aitken and Somjen, 1991; Herreras and Somjen, 1993a). The 5HT1D-transporter agonist sumatriptan blocks SD in a dose dependent manner (Maranhao-Filho and others, 1997). Sumatriptan is also an anti-migraine medication, but that effect may be coincidental, since 5HT is also a potent vasodilator that is impermeable to the blood-brain barrier. Sumatriptan does appear to have a direct neuronal effect though, since the experiments of Maranhao-Filho and others (1997) were done in (avascular) retinal preparations.

In addition to the biogenic amines (e.g., the catecholamines and serotonin) the levels of various other amino acids also increase during spreading depression. Increases in the release of gamma-aminobutyric acid (GABA), glutamine, glutamate, aspartate, taurine, glycine, serine, alanine and arginine have been observed to accompany SD (Clark and Collins, 1976; Fabricius, Jensen and Lauritzen, 1993; Davies and others, 1995; Kaku, Hadu and Hayashi, 1994; Hada and others, 1996). On the other hand, the level of histidine decreases (Fabricius, Jensen and Lauritzen, 1993). Increased plasma glutamate levels and decreased histidine levels have also been observed in migraine-with-aura patients (Ferrari and others, 1990). Glutamic acid and aspartic acid levels have been reported to decrease during migraines (Castillo and

others, 1994). Glutamine and l-proline both appear to block spreading depression (Cherkin and Van Harreveld, 1978; Van Harrevald, Cherkin and Davis, 1980; Maranhao-Filho and Leão, 1991). L-proline actually has a "dual effect," as it tends to block spreading depression at lower levels, probably by inhibiting glutamate release, and to promote it at higher concentrations (Van Harreveld and Reuter, 1981).

### 2.2.3. MOLECULAR GENETICS

Many of the events that occur during spreading depression might also be interpreted as signals of cellular damage. A rise in extracellular potassium could indicate a membrane puncture, for example, and the resulting depolarization and large influx of calcium could set off a cascade of second messengers. It would therefore not be a surprise if some of the signals transduced were to lead to protein synthesis. In particular, one might anticipate the production of proteins that are normally associated with cell growth, repair and the removal of dead tissue, and the induction of reactive gliosis. This is, in fact, what seems to happen. Increases in the synthesis of growth factors, neurotrophins, heat shock proteins, protein kinases and other signaling factors have all been observed (Kelley and Steward, 1997). The following paragraphs discuss the proteins whose induction has been observed following spreading depression. There is some indication that overall protein production subsequently declines following repeated waves of spreading depression, possibly as sources of amino acids are exhausted (Mies, 1993).

The neurotrophin family of proteins is involved intimately with the survival of nervous tissue. Their presence (or absence) affects a cell's ultimate fate through selective apoptosis, the proliferation of neuronal precursors, cell differentiation, enzyme synthesis, synapse regulation, neuronal growth and branching, stress-tolerance and injury response. Its members include neural growth factor (NGF); brain derived

neurotrophic factor (BDNF), and neurotrophin-3, -4, -5, and -6 (NT-3, NT-4, NT-5, and NT-6). They act through a set of tyrosine kinase receptors (TRK), TRK-A (primarily for NGF), TRK-B (primarily for NT-4/5 and BDNF), TRK-C (primarily for NT-3), and also bind to a receptor known as p75. NGF appears to be involved in the survival of peripheral sympathetic neurons, in hematopoiesis, and in immune response; BDNF and NT-4 in sensory neurons and sensorimotor development; NT-3 in progenitor neurons and neurons involved in proprioception. All neurotrophins have an effect on synapse activity and plasticity. Neurotrophin induction may be somewhat delayed and long lasting. Kokaia and others (1993) saw no indication of the upregulation of NGF or NT-3 or the receptors TRK-B or TRK-C following spreading depression. Herrera and others (1993), on the other hand, reported a strong induction of NGF mRNA throughout the rat cortex after KCl treatment at levels sufficient to induce spreading depression, with up to a 50-fold increase in the entorhinal cortex up to 24 hours after induction. BDNF protein levels are increased for up to three days following SD; this increase is attenuated by application of an NMDA receptor antagonist (CGS-19755) (Kokaia and others, 1993; Kawahara and others, 1997). These findings are consistent with the hypothesis that spreading depression can induce ischemic tolerance via the upregulation of NGF and BDNF. Expression of the receptor tyrosine kinases TRK-B and TRK-C appears to be unchanged during spreading depression (Kokaia and others, 1993).

Glial fibrillary acidic protein (GFAP) has been observed in the hippocampus and cortex for up to two weeks following application of high levels of extracellular potassium alone or following spreading depression, especially in reactive astrocytes (Kraig and others, 1991; Herrera and Cuello, 1992). Increased GFAP levels have been seen at points that are distant from the stimulation (Herrera and others, 1998). The maximum GFAP levels were observed after ≈24 hours in the hippocampus and after ≈4 days in the cortex. Following a seizure, GFAP expression levels have been seen to increase to as much as four-fold above normal. Following both a seizure and spreading depression, the increase was as much as ten-fold (Bonthius and others, 1994; Kelly and Steward, 1996b). GFAP expression following spreading depression has been blocked by the NMDA receptor antagonist MK-801 (Herrera and Cuello, 1992; Bonthius and Steward, 1993; Bonthius, Lothman and Steward, 1995; Herrera and others, 1998).

Calcitonin gene-related peptide (CGRP) is released from trigeminal peri-vascular sensory nerves, and is believed to contribute to vasodilation during hypotension, reactive hyperemia, seizures and spreading depression (Brian, Faraci and Heistad, 1996). The pial arteriolar dilation observed during spreading depression in the parietal cortex of cats (*in vivo*) was reduced when both the CGRP receptor agonist CGRP-(8-37) and the NO agonist NOLAG (NG-Nitro-L-Arginine) were applied simultaneously (Wahl and others, 1994). Similar results were obtained when CGRP-(8-37) was applied alone to the cortical surfaces of rabbits during SD (Colonna and

others, 1994a), and also when either L-NAME (N omega-nitro-L-arginine methyl ester) or L-NA (NG-nitro-L-arginine), two NOS inhibitors, were applied (Colonna and others, 1994b). In one clinical observation, elevated CGRP levels have been measured in humans following a migraine when samples were taken from the external jugular vein (Lance, 1991). In another clinical series, migraine with aura was induced in four susceptible patients by Xe-133 angiography (Xe-133). The clinicians did not observed any changes in CGRP levels, even though samples were taken from both the carotid artery and the jugular vein (Friberg and others, 1994). No changes in plasma CGRP levels were observed in cats (samples taken from the jugular vein) following cortical spreading depression (Piper and others, 1993).

Immediate early genes (IEG) and their associated proteins are (by definition) quickly induced following various types of neural stimulation. This class of proteins includes the leucine-zipper families of FOS and JUN; the zinc-finger proteins EGR, NURR, and the NGF (neural growth factors, discussed above) family; and the HSP (heat shock proteins) family. All of these proteins have been observed following middle cerebral artery (MCA) occlusion (via suture) in adult rats (Honkaniemi and others, 1997). This procedure induced ischemia, infarction and spreading depression. Expression of the zinc-finger proteins was greatest in the anterior cingulate and the anterior cerebral artery/MCA transition zone, and was also observed in the hippocampus. Upregulation of the NGFs was seen in the thalamus. The authors hypothesize that this protein expression may be related to spreading depression, but

they did not specifically determine whether it was due to SD or another factor involved in the injury. Outside the immediate infarct zone, the expression returned to control levels after ≈24 hours. The one exception was the thalamus where above-normal levels continued to be observed for at least 72 hours. The authors suggest that the extended presence of these proteins provides a marker for slowly dying neurons.

The FOS family (*e.g.*, C-FOS, FOS-B) are proto-oncogenes that are typically induced by trauma such as endovascular penetration, cortical infarction, transient cerebral ischemia, neurosurgery, and focal brain injury (Dragunow and others, 1990; Gass and others, 1992; Ikeda and others, 1994; Herrera and Robertson, 1996; Harada and others, 1997). This expression has been attributed to spreading depression (Dragunow and others, 1990). Neuronal C-FOS expression following SD has been observed for over six hours (Herdegen and others, 1993; Herrera and others, 1993,, 1998; Kobayashi, Harris and Welsh, 1995). Post-traumatic expression of C-FOS has been suppressed by application of the NMDA-receptor antagonists MK-801 (Gass and others, 1992; Harada and others, 1997) or ketamine (Dragunow and others, 1990). It has been partially blocked by the voltage gated calcium channel antagonist nifedipine, and by the calmodulin antagonist trifluoperazine (Dragunow and others, 1990). Similarly, the induction of FOS-B following cortical infarction has been prevented by MK-801 (Gass and others, 1992). Both FOS-B and C-FOS have been observed following spreading depression; C-FOS expression has been blocked following

spreading depression by MK-801 (Herrera and Robertson, 1990; Herdegen and others, 1993; Herrera and others, 1998).

The JUN proteins have also been seen following trauma such as endovascular penetration or cortical infarction (Gass and others, 1992; Harada and others, 1997). Like the FOS proteins, expression of the JUN proteins has also been blocked by MK-801. Three members of this family (JUN B, C-JUN and JUN D) have been observed neuronally following spreading depression (Herdegen and others, 1993). Based on these observations it seems reasonable to conjecture that induction of both the FOS-proteins and the JUN-proteins following SD occurs via an NMDA-receptor mediated process.

In a number of experiments, the levels of various heat shock proteins (HSP-27, HSP-70, and HSP-72) have been studied following endovascular penetration and ischemia-associated spreading depression. In gerbils, neither short (≈1 min duration) ischemic insults to the cortex or hippocampus, nor SD induced without ischemia, produced any detectable change in HSP-70 levels, while longer duration insults (≈2 to ≈5 min) did (Ikeda and others, 1994). In another set of experiments (Kobayashi, Harris and Welsh, 1995), SD was induced in rats by the topical application of KCl to one hemisphere for two hours; after a 24-hour recovery period, bilateral forebrain ischemia was induced for 6 minutes. After a 6-day recovery period, histopathological examination revealed that the number of necrotic neurons was significantly smaller in the hemisphere that had been pre-treated with KCl, and that expression of HSP-72 was

significantly higher in the pre-treated hemisphere. Expression of C-FOS was increased in both hemispheres. It is not clear if the “protective” effect of KCl suggested by this result is due to SD (which occurred following the KCl application) or to some other KCl-induced mechanism that is unrelated to spreading depression. When subarachnoid hemorrhage was induced by endovascular penetration in 49 rats (Harada and others, 1997), HSP-70 expression was observed widely (cortex, hippocampus, thalamus, hypothalamus, caudate, putamen) and bilaterally (in all of the mentioned organs), while C-FOS and C-JUN were induced ipsilaterally to the injury (cortex, hippocampus, dentate gyrus). Both C-FOS and C-JUN expression was prevented by MK-801 (an NMDA-receptor antagonist), but the HSP-70 expression was not. The authors conclude from this that C-FOS and C-JUN are induced by SD, while HSP-70 induction is caused by another mechanism. Finally, HSP-27 has been observed (Plumier and others, 1997) in GFAP-positive rat cortical astrocytes following KCl-induced spreading depression (in measurement taken after either 5 minute or 20 minutes duration applications of KCl). The increase, which was observed only in the ipsilateral cortex, could be blocked by systemic application of MK-801. The authors hypothesize that HSP-27 is involved in spreading depression-induced ischemic tolerance via a glia-protective function.

Other proteins that have been seen at above-normal levels following spreading depression include KROX24 (Herdegen and others, 1993), protein kinase C (PKC), NGFI-A, NGFI-B, NGFI-C, EGR-2, EGR-3, and NURR, but not CREB (Herdegen

and others, 1993; Kríváněk and Koroleva, 1996; Osten, Hrabetova and Sacktor, 1996; Honkaniemi and others, 1997). Protein kinase induction appears to be limited to the zeta-isoform; other isoforms (alpha, beta-I, beta-II, gamma, delta, epsilon and eta) appear to be down-regulated during spreading depression. The zeta-isoform of PKC, in particular, is involved in long-term potentiation (LTP) and depression (LTD); this may be why there is no memory loss during hippocampal SD (Osten, Hrabetova and Sacktor, 1996). The hippocampus is generally believed to be involved in memory formation (for a review of the processes thought to be involved in memory formation, see, for example, Kandel, Schwartz and Jessel, 1991).

### 2.2.4. GLUTAMATE RECEPTORS

Glutamate is the most common excitatory neurotransmitter in the mammalian CNS. Spreading depression has been observed following a perfusion of glutamate or the glutamatergic cation channel agonists NMDA (n-methyl-d-aspartic acid) (Drejer and others, 1989), kainic acid (a natural toxin produced by the red algae *digenea simplex*), or quisqualic acid (produced naturally in the plant seed *quisquqalis indica*) (Lauritzen and others, 1988; Drejer and others, 1987; Sheardown, 1993). These glutamate receptors are associated with non-selective cation channels that allow the passage of potassium, sodium and calcium. Activating these channels may have several effects during spreading depression. First, it allows potassium to leave the cell, contributing to the regenerative effect of the passing potassium wave. Second, it augments the voltage triggered calcium currents that lead to an increase of the neuronal calcium concentration. This increased $Ca^{++}$ concentration can contribute to cytosolic signals that are involved in protein production and the development of ischemic tolerance and recovery. Furthermore, the additional cytosolic calcium can contribute to activation of K(Ca) channels, further augmenting potassium extrusion from the cell.

The principal glutamatergic effect on spreading depression appears to be via NMDA receptors. As discussed above (section 2.2.1, “Inorganic Ions”) spreading depression has been prevented by applying the divalent cation $Mg^{++}$. Removing

magnesium from the perfusate has also been reported to induce spreading depression. The NMDA-receptor associated ion channel is normally blocked by $Mg^{++}$ at the resting membrane potential, and the channel only becomes unblocked when there is sufficient depolarization to remove the ion. The NMDA-R has thus been implicated in "long term potentiation" (LTP), a putative learning mechanism. This is because voltage-dependent $Mg^{++}$ block confers on NMDA-receptor gated channels the capability to implement the following Hebbian learning algorithm: an increase in post-synaptic activity only occurs when the membrane is already depolarized. Furthermore, there is a long list of NMDA-R blockers that reportedly increase the threshold for spreading depression at low concentrations, and which will completely block it at higher concentrations. These agents include the NMDA-R antagonists dizocilpine ((+)-5-methyl-10,11-dihydro-5H-dibenzo[a,d]cyclohepten-5,10-imine maleate, also referred to as MK-801) (Lauritzen and Hansen, 1992; Nellgard and Wieloch, 1992; Busch and others, 1996); APH (amino-7-phosphonoheptanoate) (Marrannes and others, 1988; Lauritzen and Hansen, 1992); APV (DL-2-aminophosphonovaleric acid) (Lauritzen and others, 1988; McLachlan, 1992; Footitt and Newberry, 1998); ketamine (Gorelova and others, 1987; Hernandez-Caceres and others, 1987; Marrannes and others, 1988; Amemori and Bures 1990); CGS 19755 (cis-4-phosphonomethyl-2-piperidine carboxylate)(Nellgard and Wieloch, 1992); and CGP 40116 (D-(E)-2-amino-4-methyl-5-phosphono-3-pentenoic acid) (Nellgard and Wieloch, 1992). The serotonergic agonist CPP (3-((+-)-2-carboxypiperazin-4-yl)-propyl-1-phosphonic acid), which is also an NMDA-antagonist, has been reported to

delay the onset of, and speed recovery from spreading depression, presumably due to its anti-glutamatergic effect (Jing, Aitken and Somjen, 1991; Herreras and Somjen, 1993a). CPP and DNQX (dinitroquinoxaline-2-3-dione, an AMPA-receptor antagonist), alone or together, have been reported to delay hypoxic spreading depression and decrease the magnitude of the voltage shift (Jing, Aitken and Somjen, 1993). PCP (phencyclidine), which is believed to antagonize NDMA-receptor mediated acetylcholine release, has been reported to increase the threshold and decreased its duration (Marrannes and others, 1988). Finally, spreading depression has also been prevented by specifically blocking the glycine receptor site of the NMDA channel with L-701, 324 (7-chloro-4-hydroxy-3-(3-phenoxy)phenyl-2-(1H)-quinolone) (Obrenovitch and Zilkha, 1996).

Further evidence for the involvement of NMDA channels in spreading depression is that the specific AMPA receptor blocker NBQX (2,3-dihydroxy-6-nitro-7-sulfamoylbenzo(F) quinoxaline) did not prevent cortical spreading depression in experiments in which specific NMDA-channel blockers (MK-801, APH) did prevent SD (Lauritzen and Hansen, 1992; Nellgard and Wieloch, 1992). NBQX has been reported to prevent both kainate-induced and quisqualate-induced retinal spreading depression (Sheardown, 1993). This may also be an indication of parallel or different glutamatergic mechanisms being involved in spreading depression.

Repeated treatments with the NMDA-R antagonist ketamine appears to induce a conformational change at its binding site(s) on the NMDA receptor. Repeated

applications of ketamine have been observed to induce a tolerance to the block of spreading depression by both ketamine and MK-801 (Rashidy-Pour, Motaghed-Larijani and Bures, 1995). Ketamine, MK-801, and PCP block of the NMDA-channel is voltage sensitive; block by other NMDA antagonists is not voltage dependent (except for $Mg^{++}$). This may indicate that these three agents share the same (or nearby) binding sites in the channel protein (Dingledine and McBain, 1994). Magnesium ion ($Mg^{++}$) block is voltage dependent, but is probably due to a physical blockage of the pore. PCP also binds to the sigma-receptor, which has been implicated in models of psychosis, and may partially account for its hallucinogenic effects. However, the sigma receptor is not believed to be involved in spreading depression (Barchas and others, 1994).

That spreading depression is NMDA-R dependent is consistent with the hypothesis that it is a neuro-protective reaction to cellular damage. This is supported by a number of observations. The NMDA-R antagonist MK-801 has been observed to reduce immediate early gene (IEG) expression following infarction (Gass and others, 1992) and $K^+$ application (Herrera and Robertson, 1990); to prevent COX production following spreading depression (Miettinen and others, 1997); to reduce cellular damage when spreading depression occurs in the ischemic penumbra (Gill and others, 1992); and to block GFAP mRNA upregulation following SD (Bonthius and Steward, 1993; Bonthius, Lothman and Steward, 1995). Attenuated BDNF production has been

observed following application of the NMDA antagonist CGS 19755 during spreading depression (Kokaia and others, 1993).

Finally, nitric oxide (NO) release during spreading depression is believed to be associated with the NMDA receptor (Fabricius, Akgoren and Lauritzen, 1995). NO is a known vasodilator and has been associated with the post-SD hyperperfusion. The circulatory effects of spreading depression will be discussed in more detail in a later section (2.2.9, “Circulatory Changes”).

## 2.2.5. VOLTAGE AND CALCIUM GATED ION CURRENTS

Two of the major features of spreading depression are the simultaneously propagating waves of (1) high extracellular potassium and (2) membrane depolarization. The observed membrane depolarization is consistent with that predicted by the Goldman-Hodgkin-Katz voltage equation. Phenomenologically, the voltage increases when $[K^+]_{out}$ increases, as does $V_K$ (the $K^+$ Nernst potential). Since both $V_K$ and $V_{GHK}$ are close to one another it is not known if they actually cross during passage of the wave. The simplest analogy is to say that the membrane voltage is being "pulled" towards $V_K$ as $[K^+]_{out}$ increases. This argument suggests that spreading depression is propagated via potassium currents. This appears to contradict the traditional dictum that potassium currents are hyperpolarizing and not depolarizing. However, there is no contradiction. The resting membrane potential $V_{rest}$ of most neurons is around –70 mV to –80 mV, while the Nernst potential for potassium is $V_K \approx$-100 mV (with $[K^+]_{in}$ = 130 mM and $[K^+]_{out}$ = 3 mM). Thus at rest, potassium currents will hyperpolarize the membrane potential (make it more negative) by pulling it towards $V_K$. The apparent contradiction arises because the membrane is depolarized during spreading depression. Consider the following scenario. An initial stimulus, such as a concussion or ischemic injury, damages the cell membrane. This exposes the cytoplasm to the extracellular medium. As a result, there is a sudden,

large increase in the interstitial $K^+$ concentration. This sudden increase has been "simulated" experimentally, *e.g.*, by the exogenous application of KCl (dropping wet tissue paper or the cortical surface or perfusion or dialysis via implanted electrodes). The timing of the cytoplasmic $K^+$ concentration increase at the stimulation site is not known. Measurements are typically taken at a point some distance away (say a few hundred microns to a few millimeters) to eliminate any artifacts that may be caused by the experimental process. In the simulations presented in Chapter 4 ("Results") this "sudden" increase is translated into the initial conditions of a system of partial differential equations that are subsequently integrated. An examination of this "activation" process – the injury and consequent potassium efflux – is not within the scope of this dissertation. The current study examines what may happen in response to this sudden appearance of potassium.

The theory that will be presented in the following chapters is as follows. Because the extracellular $K^+$ concentration increases, $V_K$ , the Nernst potential for potassium, increases to ≈ -25 mV (assuming $[K^+]_{in}$ = 130 mM and $[K^+]_{out}$ = 50 mM, Nicholson and others, 1978). The membrane is pulled toward the new $V_K$. This modified resting potential is depolarized with respect to the rest potential. The depolarization activates potassium currents that cause additional potassium to leave the cell. Extracellular potassium diffuses away from the point of maximum concentration, spreading the membrane depolarization. At the same time, intracellular diffusion, putatively mediated by gap junctions (testing this theory, suggested by

Somjen and others, 1992, is a primary focus of this dissertation), pushes a pulse of intracellular potassium in the same direction. Local membrane depolarization also induces $Na^+$ and $Cl^-$ influx. Both processes can cause an osmotic imbalance. This imbalance is countered by the flow of water across the cellular membrane. This can lead to either cellular swelling or cellular shrinkage. The simulations that will be presented in chapter 4 suggest that the cytpolasmic $K^+$ wave precedes the $Na^+$ and $Cl^-$ waves. As will be demonstrated in the computer simulations presented in later chapters, the net effect can induce a wave of cell swelling moving away from the stimulation point. Equivalently, interstitial space shrinks by as much as half in the simulations. This could conceivably nearly double the extracellular ionic concentrations. In this theory the process is regenerative, and propagates as a wave.

Several classes of potassium currents may be involved in different forms of spreading depression. These include currents through nonspecific cation channels that are gated by glutamate (see section 2.2.4, "Glutamate Receptors"); currents through the delayed-rectifying (DR) and A-type (KA) voltage gated potassium channels (which will be discussed in the current section); and currents through calcium gated potassium channels (BK and SK channels, which will also be discussed in this section). The results presented in the following chapters will support the conjecture that currents due to the NMDA, DR, and BK channels may facilitate SD, while currents due to the KA and the SK channel appear to inhibit SD. They do this by changing the predicted shape of the voltage waveform or by increasing or decreasing

the predicted wave magnitude or predicted wave speed. Increasing the KA and SK membrane conductances, for example, may decrease the onset slope of the voltage slope to a point where a sustained depolarization no longer occurs. Decreasing the other conductances (NMDA, DR, and BK) below certain threshold values (that are predicted in Chapter 4, "Results") may lead to a situation where the conditions for wave propagation are no longer met. In the sub-threshold environment (the quiescent physiological state) the ion pumps would then be able to maintain homeostasis and there would not be enough ionic movement to induce any significant osmotic imbalance. This hypothesis is consistent with both the computational predictions (discussed in Chapter 4) and the physiological data (presented in the present chapter) where it is available. Unfortunately, quantitative data on the dependence of waveform shape, wave speed, and wave magnitude on the various membrane conductances is extremely sparse in the literature. The qualitative physiological data are consistent with the above hypothesis and the qualitative nature of the predictions in Chapter 4.

Several voltage dependent potassium currents have been identified. Among these are the delayed rectifier ($I_{K(DR)}$), the transient ($I_{K(A)}$) potassium current, the inward rectifier ($I_{K(IR)}$), the muscarinic ($I_{K(M)}$) potassium current, several hyperpolarization activated currents, and a chlorine sensitive current (For a general review of these currents see chapter 7 of Johnson and Wu.1995). The delayed rectifier can be blocked by extracellular application of TEA (tetraethylammonium); the transient (A) current is insensitive to TEA but can be blocked by 4-AP (4-aminopyridine); and the M-current

is blocked by activation of muscarinic receptors and $Ba^{++}$. There is no evidence to indicate a role for the hyperpolarization activated, inward rectifying and chlorine sensitive currents in spreading depression. TEA has been reported to reduce the amplitude of the potassium accumulation and voltage change, and in some cases completely blocks spreading depression (Aitken and others, 1991; Scheller, Tegtmeir and Schlue, 1998). A perfusion of 4-AP will occasionally induce spreading depression (Psarropoulou and Avoli , 1993; Avoli and others, 1996).

Very little has been published on the effect of calcium activated currents (K(Ca)) on spreading depression. At least three classes of calcium-gated potassium channels (K(Ca)) have been identified in neurons (Blatz and Magleby, 1987; Sah, 1996; Vergara and others, 1998). These are classified based on their calcium and voltage sensitivity and pharmacological properties. The large conductance (BK) channel is both voltage- and calcium-dependent and can be blocked by TEA (tetraethylammonium) and CTX (charybdotoxin). The BK channel has a single channel conductance of ≈200 pS to ≈250 pS. Small conductance (SK) channels have single channel conductances of ≈4 pS to ≈20 pS, are unaffected by both TEA and CTX, and have at least two subtypes: those that can be blocked by apamin (apamin-sensitive channels) and those that cannot (apamin-insensitive channels). Other K(Ca) channels, which have intermediate single channel conductances (IK) ranging from ≈20 pS to ≈120 pS, are sensitive to both CTX and clotrimazole, and are both calcium sensitive and voltage sensitive. In several neuronal preparations the so-called "apamin sensitive" and "apamin insensitive" slow after-hyperpolarization (sAHP) currents have

been associated with the SK channels. In cerebellar Purkinje cells K(Ca) channels have been identified that activate at lower calcium concentrations than the BK channels and are sensitive to both TEA and CTX (Farley and Rudy, 1988; Reinhart, Chung, and Levitan, 1989; Groul and others, 1991). These may correspond to IK channels, or there may be two sub-populations of BK channels.

The other major ionic currents - sodium, chlorine, and calcium - are also activated as the depolarization spreads. This causes sodium to enter the cell and reduces the Nernst potential for sodium from its usual value of $V_{NA}$≈70 mV (assuming $[Na^+]_{out}$=140 mM and $[Na^+]_{in}$=10 mM) towards zero. This reduction in the sodium reversal potential is stabilizing, as it prevents the membrane from depolarizing too far. Chlorine currents appear to be passive; as the only highly permeable anion they attempt to maintain electrotonic neutrality. This leads primarily to chlorine entry into cells.

Calcium currents are also activated by membrane depolarization. The total concentrations of calcium on either side of the membrane (typically $[Ca^{++}]_{out}$ ≈ 1 mM to 2 mM and $[Ca^{++}]_{in}$ ≈ 100 nM (nanomolar)) are not large enough to have any significant effect on the membrane potential and are usually excluded from the Goldman equation. Calcium ions can play a significant role in a different manner. Calcium ions are frequently involved in the generation of intracellular signals throughout the cell (see Berridge, 1993, 1994 for reviews). These signals typically involve calcium spikes, oscillations, and waves that induce protein synthesis. The

predicted large increase in the cytoplasmic $Ca^{++}$ concentration during the passage of an SD wave should be correlated with the large numbers of neuroprotective and trophic proteins that are produced, as discussed earlier (see section 2.2.3, “Molecular Genetics”). This trophic effect could possibly be an evolutionary advantage that is provided by spreading depression in response to neural trauma. One additional effect of the calcium accumulation has already been mentioned: the activation of calcium sensitive potassium channels. This effect will augment the potassium currents induced by depolarization.

Sodium currents can be blocked by TTX (tetradotoxin, a poison that occurs naturally in *tetraodontiformes*, an order that includes the puffer fish). Application of TTX has little or no effect on the induction of spreading depression (Ramos, 1975; Tobiasz and Nicholson, 1982; Aitken and others, 1991). The lipid-soluble alkaloid veratridine, which occurs naturally in *veratrum* (the lily family) and slows inactivation of the sodium channel, has been observed to induce spreading depression (Ashton and others, 1990, 1997). The reason for this is not clear, but is probably related to the loss of homeostasis that occurs when large quantities of $Na^{+}$ ions enter the cell. Similarly, the imposition of a hypotonic NaCl state can induce spreading depression (Chebabo and others, 1995a,b) while the imposition of a hypertonic NaCl state may block spreading depression (de Araujo-Pinheiro and Martins-Ferreira, 1984). Completely removing sodium from the perfusate does not appear to affect SD (Marrocos and Martins-Ferreira, 1990) so these effects are probably more the result of a change in

chlorine concentration than of sodium. Since chlorine currents are stabilizing, the removal of extracellular chlorine should be depolarizing, while adding chlorine should be stabilizing. Hence these observations are consistent.

### 2.2.6. GAP JUNCTIONS

Some of the most interesting observations reported concerning spreading depression in the past decade indicate that gap junctions may be required for the propagation of SD. These reports suggest that spreading depression can neither be induced nor propagated in the presence of certain alcohols (e.g., heptanol and octanol) that will poison gap junctions (Nedergaard, Cooper and Goldman, 1995; Largo and others, 1997; Brand, Fernandes de Lima and Hanke, 1998). While other possible effects of these agents have not been completely ruled out (see the last paragraph of this section, below), these authors conjecture that the effect upon spreading depression is due to gap junction block. At lower concentrations of these alcohols the wave speed actually increases, and at higher concentrations there is complete block (Martins-Ferreira and Ribeiro, 1995). Following application of these gap junction blockers, the volume of infarction was smaller after middle cerebral arterial occlusion (MCAO) (Rawanduzy and others, 1997) than it typically was when the blocking agents were not applied. The speed of MCAO-induced SD waves was also reduced in these experiments. This provides additional support to the hypothesis that spreading depression, mediated via gap junctions, provides ischemic tolerance. Ischemia frequently results from neural injury. The clinical significance of spreading depression is discussed further in section 2.4.

For a long time it had been hypothesized that this gap junction mediated propagation would be glial (Gardner-Medwin, 1981; Leibowitz, 1992). However, metabolic poisons that inhibit glial activity do not block hippocampal-spreading depression (Martins-Ferreira and Ribeiro, 1995; Largo and others, 1997). Hence it has been hypothesized more recently that normally closed gap junctions between dendrites in different cells may open in response to some SD-induced stimulus such as membrane stretch (Somjen and others, 1992). However, there is no certain reason to assume *a priori* that these gap junctions are normally closed.

One must maintain some caution in interpreting these results. Neither heptanol nor octanol are entirely specific gap junctional blockers. For example, increases in the proton permeability of isolated rabbit renal membrane vesicles have been observed following application of heptanol (Ives and Verkman, 1985); this may affect the osmotic balance. Heptanol has also been reported to reduce Na/K ATPase activity in renal cortical microsomes (Kim and others, 1986) and appears to interact with the MK801 binding site of the NMDA receptor (Reynolds and Rush 1990). Both octanol and heptanol appear to modulate GABA-A currents (Mihic and Harris, 1996; Kurata and others, 1999), inhibit the nicotinic acetylcholine receptor (Wood and others 1995), and to modulate membrane $K^+$ currents (Paternostre and Pichon, 1987; Chu and Treistman, 1997). Furthermore agents used to inhibit glial activity (as discussed in the preceding paragraph) are somewhat general metabolic inhibitors and may have side effects as well (see section 2.2.8, "Neuroglia").

### 2.2.7. METABOLIC ACTIVITY

The interaction between spreading depression and metabolic activity is not well understood, and this is currently a very active area of research. Such an interaction may be inferred via changes in the activity of ATP (adenosine triphosphate) and the oxidation/reduction state of the nicotinamide adenine dinucleotide (NADH in its reduced form, $NAD^+$ in its oxidized form). This is because energy metabolism in all organisms involves the conversion of glucose to ATP via glycolysis, the citric acid cycle, and oxidative phosphorylation in mitochondria.

The oxidation/reduction state of NAD can be inferred from changes in NADH fluorescence, because oxidation causes a decrease in the fluorescence level. Changes in the NADH redox state have been correlated with the DC-voltage shift and ionic redistribution that occur during spreading depression. Mayevsky has developed a multi-probe measurement system that can simultaneously observe metabolic, ionic and electrical activity (Mayevsky and others, 1992, 1996). Parameters measured include hemoglobin oxygenation, oxygen delivery, tissue oxygen level, intra-mitochondrial redox state (via NADH fluorescence), extracellular $K^+$ and $Ca^+$ levels, bipolar surface potential and DC potential shifts. Spreading depression was first observed with this device in gerbils. In these animal observations, blood flow increased approximately 75% and oxygen extraction increased 45% as the SD wave passed.

Any vasodilation that occurs during spreading depression probably contributes to the compression of interstitial space, although there is no data in the literature that would specifically support or refute this conjecture (see also sections 2.2.9 "Circulatory Changes" and 2.2.10. "Volume Changes"). In addition to the vasodilatory effects, oscillations in NADH activity that were induced by ischemia were abolished by the spreading depression wave. Spreading depression can also be observed with a surface electrode that measures $pO_2$ levels, since the oxygen level is a good indicator of the vasoconstriction-vasodilatation responses (Mayevsky, Lebourdais and Chance, 1980). A similar device was developed for use in humans to diagnose cerebral trauma. This device measures cerebral blood flow (CBF), cerebral blood volume (CBV), intra-mitochondrial NADH redox state, extracellular $K^+$ concentration, DC potential, electrocorticography and intracranial pressure (ICP). Spreading depression was observed in one comatose patient following a traumatic injury utilizing this device. (Mayevsky and Chance, 1975; Mayevsky, Lebourdais and Chance, 1980; Mayevsky, Crowe and Mela, 1980; Mayevsky, Zarchin and Friedli, 1982; Mayevsky and Weiss, 1991; Mayevsky and others, 1992, 1996).

Changes in adenosine nucleotide levels have also been observed during spreading depression, possibly indicating a change in metabolic activity (Kaku, Hada and Hayashi, 1994). Increased ADP levels have been reported during and after SD wave passage (Lauritzen and others, 1990) while tissue ATP levels have been observed to decrease some ≈12% preceding the DC potential shift and continue to

decline to ≈54% of normal levels following wave passage (Mies and Paschen, 1984). Levels of the cyclic nucleotide cAMP have been observed to nearly double following CSD (Krívánèk, 1977). It is not known if the changes in adenosine levels are related to metabolic activity or due to the increase or decrease of adenosine dependent signals. Adenosine receptors are widely present in the CNS.

While levels of adenosine and its various nucleotides (AMP, ADP, and ATP) are certainly related to energy metabolism, neither the effect of exogenous adenosine nor the effect or significance of changes in endogenous adenosine is clear. The application of the adenosine receptor agonist theophylline has been reported to increase susceptibility to SD and to decrease the latency of its occurrence following application of high levels of potassium (Kaku, Hada and Hayashi, 1994; Hada and others, 1996). This might indicate that adenosine has an excitatory effect on SD. Alternatively, application of the combination of adenosine transport inhibitors dipyridamole (DPR) plus nitrobenzylthioinosine (NBI) reduces the susceptibility to spreading depression (Kaku, Hadu and Hayashi, 1994; Hada and others, 1996). These agents, which block the uptake of adenosine, increase the levels of extracellular adenosine concentration while decreasing the levels of SD-induced glutamate release. The effect of DPR plus NBI is blocked by application of the adenosine A1 receptor agonist DPCPX (8-cyclopentyl-1,3-dipropylxanthine). These results have been interpreted as implying that adenosine may have a neuroprotective effect against

potassium-evoked glutamate toxicity during spreading depression (Kaku, Hada and Hayashi, 1994; Hada and others, 1996).

Spreading depression also affects glucose consumption and glycolysis. A decrease in the regional plasma glucose concentration by approximately one-third has been observed following passage of the SD wave. Levels remain low even after recovery from the voltage shift and ionic redistribution, taking up to ≈10 min to return to normal. This has been attributed to the stimulation of anaerobic glycolysis and tissue acidosis (Gjedde, Hansen and Quistoff, 1981; Mies and Paschen, 1984; Csiba, Paschen and Mies, 1985; Lauritzen and others, 1990). A rise in the net cortical glucose consumption has been associated with this (Winn, Kent and Libkuman, 1975; Kocher, 1990).

Depleting the plasma glucose levels (e.g., via insulin injection) has been observed to extend the calcium transient and the duration of the DC-voltage shift. No adverse side effects, such as unusual histological damage or necrosis, was observed as a result of any signaling pathways that may have been induced by the extended calcium transient (Gido and others, 1993; Gido, Kristian and Siesjo, 1994). Spontaneous spreading depression does seem to occur more frequently in rats with depleted plasma glucose levels (Harris and others, 1984). In another series of experiments, blocking glycolysis did not appear to affect either SD initiation or wave propagation but did delay its recovery (Andersen and Marmarou, 1992).

The family of hormones known as prostaglandins, and their related compounds, the eicosanoids ($C_{20}$ compounds), have a wide range of physiological effects at nanomolar concentrations (for a review see Wolfe and Horrocks, 1994). Among their many functions are mediation of the inflammatory response, the regulation of blood pressure and blood clotting, and the production of pain and fever. The primary prostaglandin precursor is arachidonic acid (AA, 5,8,11,14-eicosatetraenoic acid) which is generated by phospholipid hydrolysis. The enzymes involved are the lipoxygenases (LIPOXes) and cyclo-oxygenases (COXes). Corticosteriods inhibit the production of AA by blocking phospholipase-A-1 ($PLA_2$), and aspirin inhibits the production of prostaglandins from arachidonic acid. Arachidonic acid levels have been observed to increase during the DC-voltage shift of spreading depression and for ≈3 minutes following the voltage shift, and then return to resting levels after another ≈5 minutes (Lauritzen and others, 1990). These authors suggest that the AA rise reflects augmented phospholipase activity during passage of the SD-wave. Cortical glucose and glycogen levels decreased by approximately half during the same period in this series of experiments. COX production is upregulated for as much as 21 days following spreading depression; in particular, COX-2 but not COX-1 has been identified in these studies. Application of an NMDA-antagonist (e.g., MK-801) and $PLA_2$ inhibitors prevented COX-2 production. While COX inhibitors did not prevent spreading depression-induced reactive gliosis when dexamethasone (a glucocorticoid), nordihydroguaiaretic acid (a lipoxygenase inhibitor), or nitroprusside

(an NO donor) were applied, the levels of microglia observed three days subsequent to spreading depression were reduced (Caggiano, Breder and Kraig, 1996; Caggiano and Kraig, 1996; Miettinen and others, 1997) (see also section 2.2.8, "Neuroglia," for a discussion of glial activity during spreading depression).

Because prostaglandins may be involved in thermoregulation, there has been some interest in the interaction between spreading depression and body temperature. Spreading depression normally has no effect on body temperature. In some experiments fevers were induced in rates by the intracerebroventricular injection of prostoglandin-E1 and *E. coli* endotoxin. After the fevers developed cotton pellets soaked with KCl were applied to the cortical surface. This induced spreading depression and the fevers abated. It is not clear if SD was involved in the mechanism for fever reduction in these experiments or if the fevers were reduced by some other effect of the KCl application. NaCl-soaked cotton (which does not induce SD) was applied to other animals, and in these instances the fevers were not reduced. In the same set of experiments, fevers induced by injection of CRH (corticotrophin-releasing hormone) were not affected by spreading depression (Monda and Pittman, 1993; Komaromi and others, 1994).

Prostaglandins may also have an effect on SD-induced vasodilation. When the nitric oxide synthase (NOS) inhibitor NG-nitro-L-arginine (L-NNA) was applied during spreading depression, the magnitude of vasodilation associated with the SD wave was reduced by over 50% (Meng and others, 1995). When indomethacin (a

prostaglandin synthesis inhibitor) was applied instead of L-NNA the level of vasodilation was nearly doubled (with respect to what is normally observed during SD) (Shibata, Leffler and Busija, 1991, 1992; Meng and others, 1995). When both indomethacin and L-NNA were applied together (inhibiting both NOS activity and prostaglandin synthesis) the same results were obtained as with indomethacin alone (Meng and others, 1995).

As with glucose, a decrease in cortical tissue pH persisting longer than the DC-voltage shift has been observed during spreading depression. The delay in the recovery of both glucose and pH levels following the recovery from the depolarization may be due to acidosis resulting from the stimulation of anaerobic glycolysis (Csiba, Paschen and Mies, 1985). Initially, intracellular pH increases. This is followed by an acid shift, and, finally, by a late alkaline rebound (Kraig, Ferreira-Filho and Nicholson, 1983; Mutch and Hansen, 1984; Somjen, 1984; Kraig and Cooper, 1987; de Azeredo, 1991). The alkaline shift has been correlated with reactive gliosis in and acid extrusion by astrocytes (Chesler and Kraig, 1989; Kraig and Jaeger, 1992). Somjen (1984) suggests that the late alkaline rebound is due to the production of carbon dioxide. The interstitial bicarbonate concentration has been seen to fall by approximately half, the interstitial ammonia concentration to nearly double, and the ammonium ion concentration to more than triple during spreading depression (Kraig and Cooper, 1987).

Dietary effects on SD are not limited to glucose and lipid consumption. Feeding rats a protein-deprived diet – the basic regional diet of poor (human) populations in northeastern Brazil – increased the animals' susceptibility to spreading depression and increased the observed speed of wave propagation (Guedes, Andrade and Cabral-Filho, 1987; Andrade, Guedes and Teodosio, 1990; Rocha de Melo and Guedes, 1997). This effect was reversed when the rats were fed casein (a protein dietary supplement). In other observations the susceptibility to spreading depression in both gerbils and rats was observed to decrease with age; feeding the animals a diet free of antioxidant vitamins C and E reversed this decrease (Guedes, Amorim and Teodosio, 1996). Rats nursed by dams fed a diet high in lead were also more susceptible to spreading depression (Riexinger, Petit and Dudek, 1986). A dietary chlorine deficiency may also play a role, as discussed above (see section 2.2.1, "Inorganic Ions"). A combination of gastric washing (which has been correlated with decreased CSF NaCl levels) and intra-muscular administration of 3-beta-aminoethylpyrazole increased the susceptibility of rabbits to spreading depression, and also intensified spreading-depression associated epileptiform activity. These effects were abolished by the injection of sodium chloride, but were intensified by sodium isethionate (Guedes and do Carmo, 1980). Finally, administration of the anti-thyroid drug PTU (propylthiouracil, which reduces thyroid secretions) significantly reduced the susceptibility of rats to spreading depression and also reduced the speed of wave propagation when SD could be stimulated. Since PTU-treated rats usually also have a

significantly reduced body weight, this effect may be metabolically related (Guedes and Pereira-da-Silva, 1993).

### 2.2.8. NEUROGLIA

Glial cells have long been known to participate in the inactivation of neurotransmitter molecules (Martin, 1995) and absorption of $K^+$ ions released by neural activity, thereby preventing persistent excitation (Kuffler and Nicholls, 1976; Newman 1995). A failure in this spatial buffering mechanism was thought to be involved in SD because glial cells are widely connected by gap junctions (Gardner Medwin, 1981; Leibowitz, 1992; Ransom, 1995). Furthermore, cytosolic $Ca^{++}$ waves are also believed to propagate through this glial syncytium of gap junction-connected cells. There are intriguing similarities between these glial $Ca^{++}$ waves and SD. Most of the stimuli that will induce SD will also induce these calcium waves (Kostyuk and Verkhrasky, 1995). This is that suggestive of a related mechanism. An increase in wave speed was observed when low concentrations of agents that poison gap junctions (heptanol or octanol) were applied. At higher concentrations, the SD wave speed decreased rather than increased, and eventually SD was completely blocked (Nedergaard, Cooper and Goldman, 1995). In other experiments where metabolic poisons that inhibit glial cells have been applied, SD was not prevented. Under these conditions SD was observed to propagate faster and last longer than when the glial cells were not poisoned (Largo and others, 1997). In some cases, repetitive waves of spreading depression have occurred after glial cells were disabled (Largo, Cuevas and Herraras, 1996; Largo and others, 1996). This may indicate that the level of susceptibility to spreading depression is higher when glia are damaged or that

induction of spreading depression may be due to glial failure in some tissue. These results suggest that spreading depression is propagated neuronally, and that glia may act to hinder rather than facilitate SD. However, some care must be taken in interpreting these results. The glial inhibitors used in these experiments, fluoroacetate and its metabolite fluorocitrate, are metabolic poisons that inhibit energy metabolism (the citric acid cycle) (Koenig and Patel, 1970; Spector and Carr, 1976; Bosakowski and Levin 1987; Rist and others 1996). Although these agents are widely accepted as glial poisons neither their cellular specificity nor the totality of their effect is completely clear. Sodium fluoroacetate is so toxic that it has been used in household rat poisons (Reigart and others 1975). Fluoroacetate has also been observed to increase glutamine and glutamate uptake in renal ammoniagenesis, to inhibit lipolysis in adipose tissue, to inhibit membrane adenylate cyclase activity, and to inhibit whole-body oxygen consumption (Taylor and others 1977; Lemieux and others 1979; Twigg and others 1986). Some of these effects may be interrelated.

Increases in reactive gliosis have been observed following spreading depression (Caggiano and Kraig, 1996). In this process, microglia are transformed into reactive glia following the passage of an SD wave. This is probably due to the elevation of interstitial potassium concentration, as a high concentration of $K^+$ is itself sufficient to induce reactive gliosis as well as spreading depression (Kraig and Jaeger, 1990). After repeated waves of hippocampal spreading depression were induced for one hour by a topical application of KCl, microglia remained activated for up to three days. This included the new production of MHC-II (major histocompatibility complex

class II) antigens (Gehrman and others, 1993). This activity was unaffected by the $PLA_2$ inhibitor mepacrine, the COX inhibitor indomethacin, or the adrenergic agonist phenylephrine (Caggiano and Kraig, 1996).

Nitric oxide (NO) is a vasodilator that is thought to be released during SD(see section 2.2.9, "Circulatory Changes"). In addition to its vasodilatory effect, NO may mediate the response to ischemic injury via reactive gliosis. Following spreading depression, NOS (nitric oxide synthase) activity is increased. Since NOS can promote hyperemia following SD, various NO and NOS blocking agents have been examined. L-NAME (NA-nitro-L-arginine methyl ester, an NOS inhibitor) has been used to prevent NOS-induced hyperemia (Goadsby, Kaube and Hoskin, 1992; Colonna and others, 1997). When L-NAME was applied during SD, an increase in reactive gliosis was observed (Caggiano and Kraig, 1998). In other experiments, treatment with L-NAME during SD induced an initial brief phase of hypoperfusion preceding the usual wave of hyperperfusion-then-hypoperfusion (Duckrow, 1993). L-NAME did not prevent the production of NOS following spreading depression in astrocytes (Caggiano and Kraig, 1998). Increasing the levels of NO by applying the NO donor nitroprusside prevented reactive gliosis following SD (Caggiano and Kraig, 1996). So either the presence of NOS or a reduction in NO may be related to reactive gliosis. Furthermore, applications of both sodium nitroprusside and phenylephrine together, or phenylephrine alone, prevents SD-induced NOS production in astrocytes (Caggiano and Kraig, 1998). This suggests that NO could be an important signaling molecule during SD, and that it induces reactive gliosis in astrocytes.

### 2.2.9. Circulatory Changes

There is a large body of data concerning changes in blood flow that have been observed during spreading depression. There is some evidence that these circulatory changes are generated by neuronal, and not parenchymal, mechanisms. However, as with much of the data regarding spreading depression, it is not completely clear which effects are caused by SD and which are caused by the same set of stimuli that induced the SD.

As a wave of spreading depression passes, the mean rCBF (regional cerebral blood flow) typically increases by approximately 75% (Mayevsky and Weiss, 1991). This wave of hyperemia is followed by a prolonged period of oligemia (reduced blood volume) lasting for some 60 to 90 minutes (Fabricius and Lauritzen, 1993). Since migraines are also associated with a wave of "spreading oligemia" the similarity is suggestive of a causative relationship between SD and migraine (Lauritzen, 1984, 1987; Lauritzen and Olesen, 1984; Lacombe and others, 1992; Lauritzen and others, 1993). Cortically, there is a pronounced period of pial arteriolar dilation. Blood flow changes following cortical spreading depression have also been observed in the deep brain organs. Mraovitch and others (1992) reported rCBF changes in the brain stem lasting for up to 90 minutes following CSD.

Blood flow changes following calcium entry into neurons may occur due to enhanced protein production (Shimazawa and others, 1995). Shibata, Leffler and

Busija (1991a) continuously perfused the cortical surface with artificial cerebrospinal fluid (aCSF) while inducing spreading depression in rabbits. This did not prevent pial arteriolar dilation, suggesting that the diffusion of vasoactive metabolites released from the parenchyma is not involved. When the rabbits inhaled 10% $CO_2$, however, all vasodilation was abolished. That this vasodilation is limited by prostanoid production as has been discussed above (see section 2.2.7, “Metabolic Activity”) (Shibata, Leffler and Busija, 1991b, 1992). The vasodilation appears to be induced in part by the release of NO and CGRP, although blocking production of these two substances will not completely inhibit vasodilation (Colonna and others, 1994a, 1994b; Wahl and others, 1994; Zhang and others, 1994). Other experiments have indicated that the peptide vasoconstrictor endothelin is not involved (Goadsby, Adner and Edvinsson, 1996).

It is widely believed that NO release can be induced by activation of NMDA receptors; that this occurs during spreading depression is very likely (Fabricius, Akgoren and Lauritzen, 1995). Following application of NO during retinal spreading depression the wave speed decreased in a concentration-and time-dependent manner. This effect was partially mimicked by applying membrane-permeable cGMP derivatives. Recovery from spreading depression also occurred more quickly (Ulmer, de Lima and Hanke, 1995). In addition to its vasodilatory effect, there is some evidence that NO (nitric oxide) may mediate the response to ischemic injury via reactive gliosis. This is discussed in more detail in section 2.2.8, "Neuroglia". These

results are compatible with the interpretation of SD as a neuro-protective signaling mechanism. In this theory, a wave of spreading depression would induce protein production and post-traumatic reactive gliosis. The need for additional nutrients would lead to the production of NO, which would subsequently increase the local blood supply by pial arteriolar dilation. As the local blood supply and nutrients are replenished there is no further need for any neuro-protective signal to continue and it is then turned off.

### 2.2.10. VOLUME CHANGES

As a wave of spreading depression passes, the extracellular space has been observed to shrink by as much as 70%. At the height of the DC-voltage shift, the total interstitial volume has been estimated to be less than 4% of the total (van Harreveld and Khattab, 1967; Hansen and Olson, 1980; Jing, Aitken and Somjen, 1994). This will be seen to be a critical observation in the present model, as the results presented in Chapter 4 will show. No combination of parameters could be found in the present model that permitted traveling waves to propagate unless this expansion was allowed.

An additional piece of evidence that may be crucial to understanding spreading depression is that potassium-induced seizures have been abolished by hyperosmotic agents that are restricted to the extracellular space, but not by membrane permeable agents. This implies that hyperosmotic suppression of electrographic seizures is associated with expansion of the extracellular space in hippocampal slices (Traynelis and Dingledine, 1989).

The application of hypertonic solutions – e.g. molar concentration of KCl - will induce spreading depression, as has already been discussed (see section 2.1.5, "Chemical Stimulation" and section 2.2.1, "Inorganic Ions"). It turns out that spreading depression has also been observed following the application of certain hypotonic solutions (Haglund and Schwartzkroin, 1984; Chebabo and others, 1995a). The higher ion concentration inside cells (compared to the concentration outside the

cells) bathed in a hypotonic solution leads to cellular swelling as water is drawn into the cell. Low levels of extracellular NaCl cause cellular swelling leading to a decrease in interstitial volume fraction of ≈25%, as well as inducing spreading depression (Chebabo and others, 1995a,b). Hada (1996) has suggested that the neurotransmitter taurine, which is normally released during spreading depression, may have an osmoregulatory function that opposes SD by inhibiting cellular swelling.

As has been discussed above (see section 2.2.9, "Circulatory Changes") SD wave passage is followed by a prolonged period of vasodilation. Such increases in blood volume could exert additional pressure on neurons and compress extracellular space leading to increased interstitial ionic concentrations. For this reason vascular effects could play a role in the propagation of SD. Unfortunately, detailed quantitative measurements of the onset time of vasodilation with respect to the ionic and voltage shifts have not been reported in the literature. Because vasodilation continues for several minutes after all other biophysical variables (e.g., voltages and concentrations) have recovered to their resting states it seems unlikely that vasodilation alone is sufficient to induce SD. However this does not rule out a role for the vasculature in some (if not all) forms of spreading depression. Because of the lack of both quantitative measurements and any evidence for such a causative role, any vasodilatory effects are purely conjectural and, as such, were deemed beyond the scope of the present dissertation, which is limited to purely neuronal (and to some

extent, glial) mechanisms. The interaction between the vasculature and neuronal tissue remains an important consideration in the further study of spreading depression.

In the model that will be presented in chapter 3, an isotonic imbalance leads to osmotic forces and the passage of water into (or out of) a cell. In the regions where cellular expansion occurs, the interstitial space contracts. As the results presented in chapter 4 will illustrate, the model predicts that this expansion may cause the cell to occupy from 20% to 50% of the previously interstitial space. This shrinkage of interstitial space causes a near-doubling of all interstitial concentrations, without any particle movement (i.e., it is a purely geometric effect). The model predicts that the osmotic imbalance results principally from two factors: NaCl entry and cytoplasmic $K^+$ diffusion. This cellular expansion provides the model with a regenerative mechanism necessary to induce a propagating wave. This theory, and its implications, will be discussed in greater detail in the remaining chapters of this dissertation.

## 2.3. MODERN OBSERVING TECHNIQUES

The original techniques for observing spreading depression were limited to the EEG and surface and implanted electrodes. This allowed observations of the depression of electroencephalographic activity – for which spreading depression was named – and the corresponding voltage shifts. Retinal spreading depression had the added advantage of inducing easily visible optical changes that were correlated with the changes in electrical activity. The development of the ion-selective microelectrode allowed experimenters to make precise measurements of the ionic redistributions that occur during spreading depression, both in the extracellular environment and within cells.

The explosion in imaging techniques in the past two decades has not been ignored in the spreading depression research community. The development of extremely sensitive magnetic field sensors such as SQUID (superconducting quantum interference device) have made it possible to observe the electrical disturbances in a non-invasive manner. Blood flow changes can be observed utilizing magnetic resonance imaging (MRI), positron emission tomography (PET), transcranial Doppler sonography (ultrasound), and optical intrinsic imaging (OIS). Simultaneously combining these techniques with traditional electrophysiological methods has allowed precise observations of both the electrical and vascular disturbances in laboratory animals.

Okada, Lauritzen and Nicholson (1988) observed slowly varying magnetic fields during the passage of an SD wave in the isolated turtle cerebellum. These signals lasted for up to ten minutes and could be measured up to four cm away from the tissue; the nature of the magnetic signal indicated that in cerebellar SD the current flow is primarily normal to the surface. Gardner-Medwin and others (1991) also observed slowly changing fields with SQUID outside the skulls of anaesthetized rabbits during cortical spreading depression, lasting for up to 8.5 minutes. Chen and others (1992) used a combination of DC electrocorticography and magnetoencephalography following MCAO (middle cerebral artery occlusion) in rats. These DC signals were measured at approximately twelve minute intervals throughout the ischemic period (for up to two hours). There was a high correlation between the electrical and magnetic signals.

Gardner-Medwin and others (1994) observed KCl-induced cortical SD in anaesthetized rats using gradient-echo magnetic resonance imaging (MRI). Both horizontal and coronal sections were obtained at 12 to 30 second intervals. The experimenters observed a zone of increased signal intensity moving away from the stimulation at ≈2.9 mm/min due to increased levels of venous oxygenation. The wave was up to two mm wide and lasted for approximately one minute at any given point.

Changes in the apparent diffusion coefficient $D_{app}$ have also been used to observe SD (Latour and others, 1994; Hasegawa and others, 1995; Rother and others l996a, 1996b; Els and others, 1997) in both potassium-evoked spreading depression

and spreading depression invoked in ischemic zones. These observations show swaths of decreased diffusion coefficient ≈2 mm to ≈4.5 mm wide, traveling at speeds of ≈2.7 to ≈3.3 mm/min, and lasting for approximately one minute at any particular point. More recently, diffusion weighted MRI observations have been made simultaneously to electrophysiological measurements in anaesthetized rats in both ischaemic and non-ischaemic spreading depression (Busch and others, 1995, 1996; De Crespigny and others, 1998).

There have been a number of reports of regional cerebral blood flow observations utilizing SPECT (single photon emission tomography) during migraine attacks (Diener and others, 1997). Lauritzen and Olesen (1984) observed a unilateral hypoperfusion consistent with spreading depression that lasted for up to six hours. These observations, made in eight patients who experienced classical migraine symptoms, were obtained following the inhalation of Xe-133 during the attack. Woods, Iacoboni and Mazziotta (1994) reported a bilateral hypoperfusion in a single patient who spontaneously developed a migraine headache approximately two hours into a six-hour series of PET observations that were being performed in an unrelated clinical experiment. Although migraines are usually unilateral (only occurring in one hemisphere) bilateral migraines are not unknown. It is also possible that an SD wave might occur bilaterally, but only contribute to a migraine in one hemisphere. As will be discussed below (section 2.4.2, “Migraine”) the link between spreading depression and migraine headache is still highly controversial.

Changes in the properties of scattered light during spreading depression made the chick retina one of the first preparations in which optical imaging was used to observe SD (De Oliveria Castro, Martins Ferreira and Gardino, 1997). Besides the chick retina, such measurements have also been made in amphibian, reptilian and fish retinas (Martins-Ferreira and De Oliveria Castro, 1966; Higashida, Sakakibara and Mitarai, 1977). Since the retina is avascular, these observations are not related to rCBF changes as are the other optical imaging techniques that have been applied to SD. It is believed that the changes are volumetric, and that they reflect changes in tissue thickness as the wave passes through the retina (De Oliveria Castro and Martins Ferreira, 1970). Changes in the light transmittance through rodent hippocampal slices during spreading depression have also been attributed to volume changes (Turner, Aitken and Somjen, 1995) or to the passage of calcium waves (Basarsky and others, 1998). SD has been observed with OIS (intrinsic optical signals) and surface fluorescence techniques in the exposed cortex of anaesthetized rodents (Evans and Smith, 1987; Yoon and others, 1996; Rex, Cannestra and Toga, 1997). Cortical observations most likely reflect regional cerebral blood flow changes. Similarly, laser Doppler flowmetry has been used *in vivo* to observe spreading depression induced in anaesthetized cats (Goadsby, 1992), rabbits (Florence and others, 1994), and rats (Fabricius, Akgoren and Lauritzen, 1995; Lauritzen and Fabricius, 1995; Fabricius and Lauritzen, 1996; Fabricius and others, 1997).

A number of other techniques have been utilized to observe SD. Changes in the electrical impedance of the rat cortex have been observed during spreading depression

using the technique of applied potential tomography (Holder and Gardner-Medwin, 1988; Holder, 1992). In this relatively non-invasive technique, impedance is measured via scalp electrodes operating at ≈50 kHz. Daffertshofer and Hennerici (1995) point out that rCBF changes have been observed during hypercapnia with transcranial Doppler sonography (ultrasound). Although this technique has a poor spatial resolution it has a high temporal resolution. They have suggested that it may be useful for the study of variety of pathologies attributed to spreading depression, including migraine with aura and ischemia. However, there have been no reports of its being used during SD. Cammack, Ghasemzadeh and Adams (1992) suggested that changes in ascorbic acid levels should be measurable using a carbon fiber electrode measurement technique that they have developed, but as yet no measurements of spreading depression have been published. Other techniques involve observing changes in NADH fluorescence (that have been correlated with changes in metabolic activity) as discussed above (see section 2.2.7, “Metabolic Activity) (Mayevsky and Chance, 1975). Mayevsky has developed a multi-parametric probe that combines a large number of miniaturized sensors on a single electrode. These sensors can simultaneously measure metabolic, ionic and electrical activity. The probe was designed to diagnose traumatic brain injury. Such devices have been used to observe SD in both rodents and humans (Rogatsky and others, 1996; Mayevsky and others, 1996). The multi-parametric observations have been discussed in more detail earlier (see section 2.2.7, “Metabolic Activity”).

## 2.4. Clinical Significance of Spreading Depression

Spreading depression has been observed, implicated, or theorized to occur in several clinically significant situations: ischemia, brain injury, migraine headache, seizure, epilepsy, and concussion (see Table 2.3). Furthermore, there is some indication that it may be involved in some forms of transient global amnesia (TGA), and the existence of a "spreading depression syndrome" has been suggested to explain the pathologies of certain non-traumatic head injuries in children and adolescents. The scientific community is yet to reach a consensus as to whether spreading depression actually plays a causative role in the pathology of any of these conditions. The following sections will review the clinical evidence and evaluate it in terms of the neuro-protective theory of spreading depression stated at the outset of this chapter.

Table 2.3. Clinically relevant observations regarding spreading depression. See the text for more details or an analysis of some of the seemingly contradictory observations.

| | |
|---|---|
| Injury | SD can be induced by mechanical stimuli. |
| | SD threshold is lower than concussion threshold. |
| Ischemia & Stroke | Spontaneous SD occurs in ischemic regions. |
| | SD before ischemia correlated with reduced cell damage. |
| | SD during ischemia correlated with increased cell damage. |
| | Hypoxia can induce SD. |
| Migraine | Wave of SD passing through visual cortex is theoretically consistent with aura. |
| | Vascular changes occur during both SD and Migraine. |
| | Similar cortical wave speed. |
| | Changes in prostaglandin and NO levels during SD may cause vascular changes. |
| Transient global amnesia | TGA memory loss is theoretically consistent with a wave of hippocampal SD. |
| Epilepsy | SD will not propagate into a seizure zone. |
| | Prodromal voltage spikes in SD resemble epileptic discharge. |
| | Prodromal hallucinations during epilepsy are theoretically consistent with a wave of SD passing through appropriate sensory cortex. |
| | Migraines are more prevalent in seizure patients than controls. |
| | SD has been observed following administration of sub-convulsive dosages of agents that also induce seizures. |

### 2.4.1. TRAUMA

That spreading depression can occur in response to neural injury is well established. Simple mechanical stimuli, such as poking the cortex or dropping a blunt instrument on its surface are sufficient to induce spreading depression (see section 2.1.4, "Mechanical Stimulation," for more details). It is not necessary to actually break the surface, and the energy stimulation threshold for spreading depression is significantly exceeded during concussion (Marshall, 1959; Zachar and Zacharová, 1961; Bures, Buresová and Krívánèk, 1974). Focal injury will frequently induce spreading depression, as will hypoxia (Irwin and others, 1975; Kubota and others, 1989; Jing, Aitken and Somjen, 1994). Spontaneous episodes of spreading depression occur more frequently following lesions (Kelley and Steward, 1996). Following ischemia spontaneous waves of spreading depression have been observed in both the core and the rim of the infarct zone. In either case the waves usually spread distally (Dietrich and others, 1994).

One obvious indicator of membrane perforation, a rapid increase in $[K^+]_{out}$ beyond a threshold of ≈10 mM to ≈20 mM, is usually sufficient to induce spreading depression. The ionic redistribution and waves of depolarization that occur in ischemic zones (ID, ischemic depolarization) or anoxic zones (AD, anoxic depolarization) have many similarities to those that occur during SD. In each of these instances, there is a slow initial rise of extracellular potassium lasting for perhaps a

few minutes until a threshold (typically ≈10 mM to ≈12 mM, sometimes as high as ≈20 mM) is reached. Once the threshold is reached, there is typically a rapid increase of $[K^+]_{out}$ to ≈20 mM to ≈60 mM. The jump tends to be steeper during SD than AD or ID, but this may be due to the stimulation protocol and may not indicate different underlying physiological mechanisms (Hansen and Olson, 1980; Hansen and Nedergaard, 1988; Nedergaard and Hansen, 1993)

Spreading depression alone is not thought to cause irreversible brain injury (Gido, Kristian and Siesjo, 1994). Nedergaard and Hansen (1988) repeatedly elicited spreading depression in rats with hyperosmolar concentrations of KCl for up to four hours. Histological examinations performed four days later revealed no significant injury. Haselgrove and others (1990) observed the NADH redox state during spreading depression in Mongolian gerbils and determined that the energy demand placed on the rodent's brain during spreading depression is sufficient to cause temporary hypoxia. Ischemia has also been observed to occur in response to SD in rodents by Dreier and others (1998).

The effect of spreading depression may vary depending upon whether it occurs prior to or during an injury. When spreading depression occurs before an injury experiments suggest that the tissue develops a tolerance against subsequent ischemic damage. When experimental pre-treatments of SD were applied one to three days before injury, less cellular necrosis occurred and the infarct was smaller (Kawahara,

Ruetzler and Klatzo, 1995; Kobayashi, Harris and Welsh, 1995; Matsushima, Hogan and Hakim, 1996; Taga and others, 1997; Yanamoto and others, 1998).

When spreading depression does occur following an injury (e.g., in a lesion an ischemic zone) it seems to make matters worse. The severity of injury, the extent of cellular necrosis, and the rate of recovery have been correlated with the presence (Gill and others, 1992; Beck and others, 1996; Takano and others, 1996), magnitude (Alexis and others, 1996) and number of spontaneous waves of SD that occur (Kubota and others, 1989). Busch and others (1996) induced spreading depression in the ischemic zone of anaesthetized rats at 15-minute intervals for two hours by microinjecting potassium acetate into the frontal cortex. Ischemic brain infarcts had been previously induced in these animals by middle cerebral arterial occlusion (MCAO). The cortex was observed both electrophysiologically (to observe the membrane depolarization) and with diffusion-weighted imaging (to measure lesion size). In these experiments the volume of the lesion increased in a step-wise fashion after each injection. In another set of animals, SD was prevented by the application of the NMDA-antagonist MK-801 (dizocilpine). In these animals, no increase in lesion size was observed. This data supports the hypothesis that peri-infarct depolarizations can accelerate the rate at which the lesion will grow. Other authors have also concluded that SD-induced damage in the ischemic penumbra can be reduced by blocking NMDA receptors (Gill and others, 1992; Obrenovitch and Richards, 1995). It is not clear if this occurs because the magnitude of the spreading depression is reduced or because glutamate

toxicity is prevented. The sooner the spreading depression occurs, or the longer it lasts, the more likely it is that the tissue will not recover from hypoxia (Crowe, Mayevsky and Mela, 1981; Balestrino and Somjen, 1986; Balestrino, Aitken and Somjen, 1989). Following the application of gap-junctional blockers that have been observed to prevent spreading depression (Largo and others, 1997) the rate at which infarcts grew (in volume) following middle cerebral arterial occlusion (MCAO) in rats was reduced (Rawanduzy and others, 1997). More recently, however, Koroleva and others (1998) have reported increased necrosis following photothrombotic MCAO in rats when spreading depression is blocked with MK-801.

The autoregulatory mechanisms controlling vasodilation may also change during spreading depression. Florence and others (1994) have related this to an increase in the cAMP concentration. Prostaglandins and nitric oxide (NO) also may mediate circulatory changes, as has been discussed earlier (see section 2.2.9, "Circulatory Changes"). Somjen has hypothesized that the signal leading to selective neuronal vulnerability is initiated by calcium entry. In this theory, the duration of depolarization is critical to cell survival, and the presence of a normal blood supply tends to resist protracted spreading depolarizations (Somjen and others, 1990).

### 2.4.2. MIGRAINE

Although there is considerable disagreement over whether the relationship between SD and migraine is causal or epiphenomenal there is compelling circumstantial evidence linking the two phenomena (Lauritzen, 1985, 1987a, 1987b, 1992, 1994; Sand, 1991; Lance, 1993; Diener and others, 1997). The earliest arguments were based on the similarity between the propagation of a wave of SD and the visual disturbances, or auras, that are often seen during or preceding a migraine. Lashley (1941) described his auras in great detail and estimated the location of and speed of the propagating disturbance in the visual cortex. Recently published computational models have demonstrated that a wave of membrane depolarization passing through the occipital cortex could produce hallucinations similar to visual migraine auras (Reggia and Montgomery, 1996).

A typical migraine starts with a unilateral hypoperfusion in the occipital lobe. The hypoperfusion subsequently propagates anteriorly at a rate of ≈2 mm/min to ≈3 mm/min. Propagation is more-or-less isotropic, independent of both the vasculature and neuronal architecture, although the wave sometimes stops at major sulci. After wave passage, blood flow usually remains low for four to six hours, or as long as the attack persists (Lauritzen, 1985). Similar rCBF changes have been observed after cortical spreading depression in animals. Reduced rCBF typically lasts only for one to two hours in these experiments, but this may reflect the difference between animal and

human physiology. On the other hand, there is no clear evidence that spreading depression is specifically aversive in these animals (beyond the obvious discomforts of confinement, chronically implanted electrodes, or the exposed dura). In one series of experiments Koroleva and Bures (1993) reported that rats do not avoid entering into a compartment that is associated with cortical SD. Rats also did not show any preference between drinking faucets when one was associated with hippocampal SD, even though the SD would cause an interruption in drinking activity. Both of these observations suggest that spreading depression was not aversive in these instances.

The spreading electrochemical wave parallels vascular changes that occur during migraines with aura. As was described in the preceding paragraph, a typical migraine aura begins with a reduction in blood flow that spreads to encompass the entire occipital cortex, and continues to propagate across much of the remaining cortex (Oleson, 1981; Lauritzen, 1983, 1984). The aura appears early during this hypoperfusion, as the wave passes through visual cortex, and usually lasts for some fifteen to thirty minutes. In the spreading depression theory of migraine with aura, a wave of SD actually induces this spreading hypoperfusion. The aura ends when the disturbance leaves the visual cortex, but the wave of hypoperfusion continues, spreading into the parietal and temporal lobes. Recent experiments with transcranial magnetic stimulation suggest that the occipital cortex may be more excitable in migraine-with-aura patients (Aurora and others, 1998). This may be why the attacks start there, and not elsewhere. As the SD wave continues to spread (in this theory)

other brain regions should remain unaffected until the propagating depolarization reaches them. Somatosensory symptoms (e.g. tingling in the extremities) may occur as the electrophysiological wave reaches the sensory cortex. Various other abnormal perceptions including olfactory and gustatory hallucinations and distortions of body image have also been associated with migraine attacks. In the SD theory of migraine, these symptoms are also induced by the spreading wave of membrane depolarization as it passes through the corresponding sensory cortical regions (Morrison, 1990). As the SD wave passes, circulatory changes remain, and last for a much longer duration than the membrane depolarization. These circulatory effects may be induced by refinements in the release of vasoactive substances such as NO and various eicosanoids. These agents are usually released during SD (see section 2.2.9, "Circulatory Changes" and 2.2.7, "Metabolic Activity"). This might explain the delay between the aura and a migraine, based on the theory that spreading depression induces protein production as a response to some unidentified neural injury. In this theory, it might take some time for protein production to become fully upregulated. Local metabolic stores might not become sufficiently depleted to induce substantial vasodilation until this occurs. The gap between visual aura and migraine typically lasts for less than an hour, but in some patients has been reported to persist for at least five hours (Blau, 1992). The disturbance usually stops at the central sulcus, but modifications in protein production continue for several hours to several days.

In a second spreading depression based theory of migraine with or without aura, a trigeminal wave of SD activates meningeal C-fibers thereby causing neurogenic inflammation and pain (Moskowitz, Nozaki and Kraig, 1993). There is insufficient data to either accept or reject either theory. However it seems likely that migraines are caused by a wide range of processes, and for this reason both theories may be valid but in different patient populations.

The pharmacological data for the effect of anti-migraine compounds on SD is mixed. DHE (dihydroergotamine), acetylsalicylic acid, lignocaine, metoprolol, clonazepam, lisuride, ergotamine, iprazochrome and valproate failed to modulate SD in some studies while propranolol, sumatriptan, methysergide, paracetamol, and aceytlsalicylic acid were observed to decrease the velocity and accelerate the recovery of optical and electrical signals in other studies (Kaube and Goadsby, 1994; Wiedemann, Fernandes de Lima and Hanke, 1996). Sumatripan completely blocked spreading depression (Maranho-Filho and others, 1997). Barbiturates increased the velocity and amplitude of the potential shift (Wiedemann, Fernandes de Lima and Hanke, 1996). Anesthetics have been variously reported to inhibit (halothane), reduce (isoflourane) or have no affect whatever (α-chloralose) on spreading depression (Saito 1995; Piper and Lambert, 1996).

Nitric oxide, a known vasodilator (see section 2.2.9), may be released by the activation of metabatropic glutamate receptors and may provide a causal connection between SD and migraine (Brian and others, 1996). NO also has anaesthetic effects.

Various experiments indicate that NO directly decreases the velocity and magnitude of SD waves in a concentration and time dependent manner (Ulmer, Fernandes de Lima and Hanke, 1995; Piper and Laurent, 1996). This data would support a theory in which there are multiple different mechanisms for various forms of migraine.

### 2.4.3. EPILEPSY

A relationship between migraines and epilepsy has been postulated since the 1800s; Gowers (1907) labeled migraines as "the border-land of epilepsy." The prevalence of migraines in patients with comorbid seizure disorders is twice is high as it is in patients without any family history of seizures (Ottman and Lipton, 1994). The similarity in prodromal sensory hallucinations (*e.g.*, uncal seizures and migraine with aura) and the propagating nature of the disturbance (*e.g.*, the Jacksonian march) are suggestive of a wave of membrane depolarization passing through the appropriate cortical area. Anecdotal reports of migraine patients with a history of seizure have also been published (Donnet and Bartolomei, 1997).

The rhythmic spiking activity that precedes the DC-voltage shift of spreading depression has led many researchers to use spreading depression as an animal model of epilepsy. These spikes typically occur as bursts of neuronal activity that last for a few seconds (Grafstein, 1956a). They start as saw-tooth shaped voltage transients at a frequency of ≈60 Hz to ≈70 Hz and subsequently develop into voltage spikes of the same frequency. The spikes are coordinated (in phase) through all neuronal layers (Herreras and others, 1994) and usually disappear during the DC-voltage shift. Additional bursts of epileptiform-like activity, which are characteristic of clonic seizures, occasionally reoccur during wave passage (Leão, 1972). This rhythmic activity is probably at least partly due to sodium currents, as it can be prevented by the sodium-channel blocker TTX (tetradotoxin). When a wave of SD crosses the

boundary from a region that has not been treated with TTX into a region that has been treated with TTX, all spiking and rhythmic activity disappears. With the exception of the disappearance of the spikes, the wave propagates normally through the treated region. The spikes reappear when the wave leaves the treated area and enters an untreated area. Blocking synaptic transmission does not prevent the spike bursts, so they are probably not related to glutamatergic activity (Herreras and others, 1994). Antidromic spikes in the locus coereleus (LC) of anaesthetized rats (spikes that originate in or near the soma and propagate "back" through the dendritic tree, instead of or in addition too down the axon) have been observed at ≈15 mS to ≈90 mS intervals as SD propagated through the regions whose neurons synapse onto LC neurons (Arakawa and others, 1997). This suggests that the source of spikes may not be local but instead they may occur as a result of interactions with other neurons that are not directly affected by the SD wave. However, the LC spikes reported in this case were somewhat lower in frequency (≈11 Hz to ≈60 Hz) then the spikes usually observed during SD (≈60 Hz to ≈70 Hz, as stated above).

One set of experiments used human cortical tissue that had been removed from an epilepsy patient to relieve chronic seizures. When this tissue was placed in a magnesium-free bath, both spontaneous epileptiform activity and spontaneous spreading depression occurred. Both of these phenomena disappeared when NMDA antagonists were added to the bath, but were unaffected by non-NMDA glutamate receptor blockers (Avoli and others, 1995). This suggests that NMDA-receptors could

play roles in both spreading depression and seizure. NMDA receptors are normally blocked by endogenous $Mg^{++}$.

Spontaneous waves of spreading depression have also been observed following the application of chemical agents that induce seizure, such as picrotoxin and penicillin (Hablitz and Heinemann, 1989; Sutor and Hablitz, 1989; McLachlan, 1992). Both thalamic and cortical spreading depression have been observed following peritoneal applications of sub-convulsive dosages of PTZ (pentylenetetrazol, another convulsant) (Koroleva, Vinogradova and Bures, 1993).

The above observations suggest that spreading depression and seizure may share common mechanisms. It is even possible that they are two different levels of a graded response to the same stimulation, with SD occurring in response to a weaker stimulation, and seizure in response to a stronger one. Other observations, however, suggest that seizures and spreading depression are mutually incompatible. This is because they have not been observed to occur at the same location of the same tissue at the same time. It seems that either one or the other will occur, but not both. This is not necessarily incompatible with the first interpretation, since it may be that the mechanisms of SD and seizure, while similar, are sufficiently different that once one begins, the other cannot.

In one theory either membrane depolarization or spreading depression is able to prevent the spread of a seizure. This conjecture is based on the following series of

observations. First, while neuronal depolarization has been observed in deep cortical layers during a seizure, it appears that the magnitude of this depolarization is inadequate to trigger SD (Bures, Von Schwarzenfeld and Borzek, 1975). Second, waves of spreading depression seem unable to propagate into the area where a seizure is occurring, but have been observed to reverberate around the focus of a seizure (Ueda and Bures, 1977; Koroleva and Bures, 1979, 1980, 1982, 1983). Third, Reddy and Bures (1980) observed that SD did not penetrate into a region of rodent cortex that had been electrically stimulated (10 Hz, 20 to 30 mV). Although potassium levels returned to normal in twenty to thirty seconds, SD could not be stimulated for up to another three minutes. They suggested that the electrical stimulation induced the activation of an ion pump. According to Reddy and Bures the increased pump activity prevents spreading depression by enhancing potassium reabsorption into neurons. While this type of AC-activity does not take the same form as the spiking observed during a seizure, the effects of AC-stimulation could (in theory) be related to the events that occur during a seizure. Finally, other experiments have suggested that spreading depression cannot be induced in a region in which either anodic or cathodic currents have been applied to the cortical surface for at least five minutes (Richter and others, 1994; Richter, Fechner and Haschke, 1996).

### 2.4.4. Transient Global Amnesia

During an episode of transient global amnesia (TGA) the affected individual is unable to form new memories for a period lasting as long as six hours. Patients are also usually unable to recall events that occurred just prior to the attack. TGA is (by definition) not caused by trauma, ischemia, neural injury, stroke or any known seizure disorder. In some cases attacks of TGA are precipitated by stress, but usually TGA occurs without any warning. Recovery is usually complete, with the exception of some retrograde amnesia for the period just prior to and during the attack. The prevalence of TGA is 5 cases per 100,000 individuals annually (in the U.S.).

The cause of TGA is not known. It has been hypothesized that a wave of spreading depression passing through the hippocampus causes a temporary functional ablation (Olesen and Jorgensen, 1986; Nichelli and Menabue 1988). The higher interstitial concentration of glutamate (resting levels) in the hippocampus, compared to other parts of the brain, may favor the incidence of spreading depression in the hippocampus, since blocking glutamate receptors usually will prevent spreading depression (see section 2.2.2, “Amino Acids and Neurotransmitters,” and section 2.2.4, “Glutamate Receptors”). Additional stress-induced glutamate release may cause waves of SD to be generated in susceptible individuals.

Observations of the temporal lobe during TGA using diffusion-weighted magnetic resonance imaging have shown a decrease in extracellular space and cellular

swelling. This swelling is compatible with the passage of waves of spreading depression through the region (Strupp and others, 1998; Zorzon and others, 1998). The prevalence of migraine headache is significantly higher in TGA patients compared to controls. The fact that the expression of TGA symptoms is no different in patients who present with migraines than in TGA patients who do not present with migraines is consistent with an argument that both pathologies are caused by a common factor that predisposes the brain to some type of dysregulation (Schmidtke and Ehmsen, 1998). It is possible that this dysregulation takes the form of spreading depression. The nature of the predisposing factors remains unknown.

Cortical dysfunction during a bout of spreading depression is well documented. Since a nearly complete recovery of neural function usually occurs, even following repeated episodes of experimentally induced spreading depression, it has frequently been cited in the literature as a method for selective functional ablation. This method is imprecise at best, because of the tendency for SD to propagate. It is more useful for temporarily "turning-off" a complete brain organ than a brain region. SD can not always be confined to a single organ. The most common experimental utilization of SD in this manner has been to temporarily ablate a large brain region, or even the entire cortex (Freedman and Pote, 1969; Shibata and Bures, 1974; Best, Orr and Pointer, 1975; Buresová and Bures, 1975, 1976, 1985; Islam and Buresová, 1975; De Luca, Cerciello and Monda, 1982; Klosterhafen and Klosterhafen, 1985; Rampin and Morain, 1987; Bianki, Murik and Filippova, 1989; Tassoni, Bucherelli and Bures,

1992). SD has also been used to "functionally ablate" the olfactory bulb (Amemori and Bures, 1988), the caudate (Saavedra de Camargo, Brust-Carmona and Roig, 1981), and the cerebellar vermis (Storozeva, and Pletnicov, 1994). Because it is comparatively non-invasive and fully recoverable (with respect to selective lesioning) spreading depression has even been suggested as a diagnostic tool that could be used during neurosurgery (Sramka and others, 1977). There are no reports in the literature of SD having been used in this manner.

In a number of experiments cortical interactions with sub-cortical nuclei have been reported in which sub-cortical activity was suppressed. For example, cortico-thalamic oscillations have been studied using SD as an investigative tool. Thalamic activity was suppressed when SD arrived at particular cortical areas, with different cortical areas corresponding to different thalamic nuclei (Able-Fessard, Condes-Lara and Sanderson, 1983; Condes-Lara and Omana-Zapata, 1988; Condes-Lara and others, 1989; Condes-Lara, Omana-Zapata and Talavera, 1991; Condes-Lara, Sanchez-Moreno and Omana-Zapata, 1996). In other experiments a change in the usual nigro-striatal interaction has been observed by inducing SD in the striatum (Able-Fessard, Sanderson and Mavoungou, 1990). Anomalous antidromic spikes originating in the locus coereleus (LC) have been observed during cortical SD along with a decrease in spontaneous LC oscillations (Arakawa and others, 1997; Fujii and others, 1997). These are all examples of the suppression of normal activity as a result of SD, even though the SD did not actually occur in the region where the reduction in activity was

observed. The suppression was presumably due to cortical interactions with sub-cortical nuclei.

There is, in fact, some evidence that hippocampal SD has induced amnesia (Avis and Carlton, 1968; Kapp and Schneider, 1971). Thus it is not inconceivable that spontaneous waves of spreading depression, induced by emotional stress or some form of mild subclinical neural trauma would lead to temporary hippocampal ablation and interfere with memory formation.

### 2.4.5. Spreading Depression Syndrome

One group of researchers has hypothesized spreading depression as the cause of a class of dysfunction following mild head injury (Oka and others, 1977). Their conjectures are based on a number of clinical observations. Unfortunately, spreading depression has not actually been observed in any of these situations, and no follow-ups to this theory have been published. The theory proceeds as follows. Traumatic brain injury is frequently accompanied by a loss of consciousness, amnesia (retrograde or anterograde), and seizure. In most of these cases, the location of neural injury (the lesion) can be visibly identified (*e.g.*, on a CT scan). In a small number of cases, however, particularly among children, seizures have occurred following a mild injury that was not accompanied by a loss of consciousness, and in which no identifiable lesion could be found. Such patients usually made a full recovery without subsequent residual neurological deficits. Oka and others (1977) surveyed 1476 patients with various types of head injury and found 37 such cases, in which minor head injury was followed by transient neurological disorder. Excluded from the study were patients with a family history of seizure disorders, febrile convulsions or migraines; who lost consciousness immediately or shortly after the injury; who showed any form of skull fracture or hematoma; or who required any form of surgical treatment. Neurological dysfunction did not occur initially, but only after a lucid interval subsequent to the injury. Seizures occurred in ≈75% of the patients, and were always preceded by non-convulsive symptoms, such as somnolence, nausea and vomiting, or headache. In a

few cases, a pale complexion, irritability, restlessness, stupor, hemiparesis, hemiplegia, motor aphasia or coma occurred. Two thirds of the convulsive cases were in patients under three years of age. The lucid period typically was less than an hour in duration, but in some cases up to six hours. Oka concluded that the non-convulsive symptoms are the basic disturbance, and that a developmental boundary occurs at around three years of age that makes it increasingly difficult for the non-convulsive symptoms to change into convulsive ones. All of the patients completely recovered and showed no subsequent neurological disorders. The authors suggest that repeated waves of spreading depression occur as a result of the injury. The cranial malleability of younger patients increases the likelihood of mechanical stimulation.

Based on the observations that have been surveyed in the preceding sections, the theory of a generalized spreading-depression syndrome is not unreasonable. It is unfortunate that no follow-up studies have been published. It may be that the reason for this is due at least in part to the substantial improvements in imaging technology that have occurred in the past two decades since the original paper was published. Because of the improved resolution now available, it may have been that very small lesions that could not be observed in the earlier studies are now being found.

## 2.5. MODELS OF SPREADING DEPRESSION

This section surveys the mathematical models of spreading depression that have been previously published. With the exception of one model that utilizes the theory of cellular automata, all published descriptive models of spreading depression are based in some way on the extracellular diffusion of potassium. In the simplest form, the model is comprised of a single diffusion equation with a cubic reaction term. This equation describes the extracellular potassium concentration, and is an example of the class of equations called "bistable equations." This model is discussed in section 2.5.1 ("Bistable Equation").

While the bistable equation provides a mechanism for excitability, it does not provide a mechanism for recovery. A simple method that can be used to describe recovery in a bistable equation-based model is to introduce a second variable to the system. This recovery variable evolves according to a second differential equation. This technique is similar to the Fitzhugh-Nagumo model of nerve excitation, and the Morris-Lecar model of muscle fiber (Fitzhugh, 1961; Nagumo, Arimoto and Yoshizawa, 1964; Morris and Lecar, 1981). A set of models that have been used to describe spreading depression in this manner is presented in section 2.5.2 ("Bistable Equation with Recovery"). This class of models has been successfully used to describe the interaction between SD and the surrounding tissue. Examples include the simulation of the aura phase of a migraine headache, or the interaction between

ischemia and a wave of spreading depression. The only causative mechanism that they provide for spreading depression is the extracellular diffusion of potassium. The reaction term is heuristic, in the sense that it provides an analytical description of the changes in the interstitial potassium concentration, but does not provide a physiological process (such as ion pumps and currents through membrane channels) that produces these changes. Finally, in the models described in section 2.5.3 ("System of Reaction-Diffusion Equations"), the reaction terms are replaced by terms that represent ion channels, pumps and neurotransmitter interactions, and a separate equation is used for each ionic species.

Table 2.4. Published mathematical models of spreading depression. RDE: reaction diffusion equation; DE: differential equation.

| Class of Model | Salient Features of Model | References |
|---|---|---|
| Bistable equation | Driven by extracellular diffusion of $K^+$ | a |
| Bistable equation with recovery | Driven by extracellular diffusion of $K^+$<br>Second state variable for recovery<br>Applied to migraine, ischemia | b, c, d |
| System of RDE | RDE for extracellular $K^+$, $Ca^{++}$, $Na^+$, $Cl^-$<br>Local DE for cytoplasmic $K^+$, $Ca^{++}$, $Na^+$, $Cl^-$<br>Includes membrane currents and pumps<br>Includes neurotransmitter | e, f, g, h |
| Cellular Automaton | Purely descriptive model | i |
| Magnetic Dipole | Describes magnetic field produced by SD.<br>Makes no attempt to describe SD | j |

a. Bures, Buresová and Krívánèk, 1974; b. Reggia and Montgomery, 1996; c. Revett and others, 1998; d. Ruppin and others, 1999; e. Tuckwell and Miura, 1978; f. Tuckwell, 1980; g. Tuckwell, 1981; h. Tuckwell and Hermansen, 1981; i. Reshodko and Bures, 1974; j. Tepley and Wijesinghe, 1996

All of these models share a common deficiency: they are based purely on extracellular diffusion, and do not allow for the cytoplasmic movement of ions. One significant observation cannot be described by any model that is based purely on extracellular diffusion: the inhibitory effect upon spreading depression of agents that block gap junctions (see section 2.2.6, “Gap Junctions”). That these agents do appear to prevent spreading depression suggests that some cytoplasmic movement does occur during spreading depression.

Two additional models are included in this part of the review because they pertain to SD. Both of these models are purely descriptive, and neither is based on biophysical mechanisms. The first model, presented in section 2.5.4 (“Cellular Automaton”) describes spreading depression in terms of cellular automata (Reshodko and Bures, 1975). While this model does not provide a physiological explanation for spreading depression, it provides a possible mathematical framework for describing any excitable phenomena. The second model, presented in section 2.5.5 (“Magnetic Dipole Model”) describes the magnetic field at a point exterior to the cortex caused by a passing SD wave (Tepley and Wijesinghe, 1996). This model assumes that a spreading depression wave exists and causes a local membrane depolarization, but it does not actually describe spreading depression. The magnetic dipole model should be useful for analyzing magnetoencephalographic measurements.

### 2.5.1 BISTABLE-EQUATION BASED MODEL

Either Hodgkin, Huxley or Grafstein first suggested that spreading depression might be described by a reaction-diffusion (RD) equation for the extracellular potassium concentration (Bures, Buresová and Krívánèk, 1974). In this model, the RD equation takes the form

$$\frac{\partial c}{\partial t} = D\frac{\partial^2 c}{\partial x^2} + f(c) \tag{1}$$

where $c$ is the extracellular potassium concentration and $f(c)$ has three zeros, at $c=K_0$, $K_1$ and $K_2$ where $K_2>K_1>K_0$. A typical $f(c)$ is illustrated qualitatively in Figure 2.2. $K_0$ is the normal resting potassium concentration and $K_2$ is the concentration of extracellular potassium during wave passage (the excitation state). $K_1$ is an intermediate concentration that is usually interpreted as the threshold for excitation, in the sense that any perturbation of the potassium concentration exceeding $K_1$ will induce a traveling wave. Typical physiological values of these parameters are given in Table 2.4. Because the authors attribute this model to Grafstein, it will be referred to as the "Grafstein model" in the following paragraphs.

A reaction-diffusion equation of this form is one example of the so-called bistable equation (see section 9.2 of Keener and Sneyd, 1998 for a survey). The bistable equation is of interest because it admits traveling wave solutions.

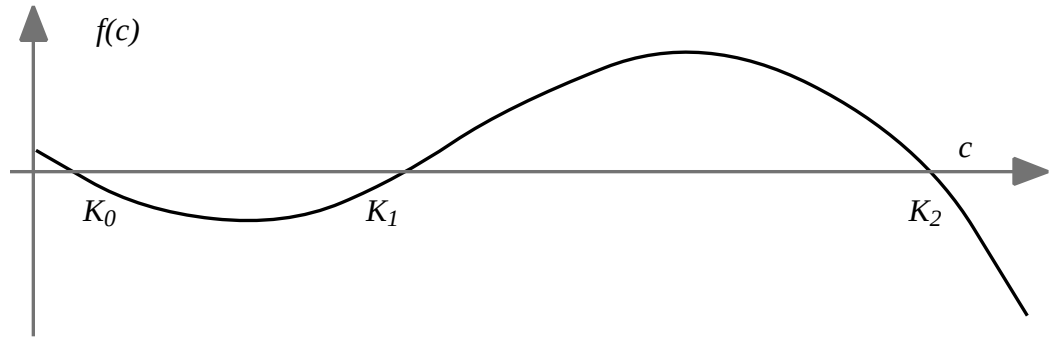


Figure 2.2. Reaction term for bistable-equation model of spreading depression. The function $f(c)$, where $c$ is the interstitial potassium concentration, has three zeroes, at $K_0$ (resting value), $K_1$ (threshold) and $K_2$ (wave magnitude). The slope of $f(c)$ must be negative at $K_0$ to make this steady state stable. A closer examination of this model reveals that the interpretation of $K_1$ as a "threshold" is not entirely correct, because it is possible for trajectories to move to the right even when $K < K_1$. This observation is clearer from an examination of the phase plot shown in Figure 2.3 in section 2.5.1.1.

Table 2.4. Typical parameter values for the bistable equation based model.

| Parameter | Description | Typical Value |
|---|---|---|
| $K_0$ | Resting $[K^+]_{out}$ | 3 – 4 mM |
| $K_1$ | Threshold for excitation | 12 – 20 mM |
| $K_2$ | Magnitude of $K^+$ wave | 25 – 60 mM |

Unfortunately, the equation 1 has only been solved analytically in two special cases: when *f* is either piecewise linear or a cubic polynomial. Furthermore, just because it admits traveling wave solutions does not mean that equation 1 is an appropriate model for SD. Many equations have wave solutions. And it is not necessary to restrict oneself to equations that admit wave solutions. Spreading depression has a number of wave-like properties that were presented in detail in the first part of this chapter. But the existence of wave-like properties does not prove that SD actually is a wave-phenomenon, and it may be that another model would describe these phenomena more correctly, even if the results were not true traveling waves in the strictest mathematical sense. Unlike the situations that occur in optics or quantum mechanics, there is no fundamental physical principal (actually, physiological principal would be a more accurate expression in this situation) that requires that SD be described as a wave.

In Grafstein's model of spreading depression the reaction term is taken explicitly as a cubic polynomial,

$$f(c) = \frac{1}{TK_2^2}(c - K_0)(K_1 - c)(c - K_2) \qquad (2)$$

where *T* is an as-yet-to-be determined time constant of the system. Because the subsequent solution is tractable, and because it produces a framework in which to interpret more complex solutions, it is worth looking at the solution in more detail.

The derivation is given in section 2.5.1.2, which serves as an appendix to this section. The solution is

$$c(x,t) = \frac{K_2}{2}\left[1 + \tanh\left(\frac{x + Vt}{VT_C} - C\right) + \frac{K_0}{K_2}\exp\left(-\frac{x + Vt}{VT_C} + C\right)\operatorname{sech}\left(\frac{x + Vt}{VT_C} - C\right)\right] \quad (3)$$

where $V$ is the wave speed (see equations 5 and 10 of section 2.5.1.2)

$$V = \left(\frac{K_2 + K_0 - 2K_1}{K_2}\right)\sqrt{\frac{D}{2T}} \quad (4)$$

$T_C$ is defined as

$$T_C = \frac{\sqrt{8DT}}{V(1 - K_0 / K_2)} \quad (5)$$

and $C$ is a constant determined by the initial conditions (see equation 14 of section 2.5.1.2 ). Bures, Buresová and Kríváněk (1974) interpret $T_C$ as the time when the depolarization is "practically complete" (typically ≤ 10 sec).

The following interpretation (which is not presented by the authors) can be made of this result. Solving for $V$ in equation 5

$$V = \frac{\sqrt{8DT}}{T_C(1 - K_0 / K_2)} \quad (6)$$

Equating the two expressions for the wave speed (equations 4 and 6) gives

$$\frac{K_2\sqrt{8DT}}{T_C(K_2-K_0)} = \left(\frac{K_2+K_0-2K_1}{K_2}\right)\sqrt{\frac{D}{2T}} \tag{7}$$

Solving equation 7 for T

$$T = \frac{T_C\left(K_2+K_0-2K_1\right)\left(K_2-K_0\right)}{4K_2^2} \tag{8}$$

Using $T_c$=4 sec,$K_0$=3 mM, $K_1$=10 mM and $K_2$=40 mM gives $T$≈ 532 msec. Since the diffusion constant of $K^+$ in free solution is $D_K$≈2000 μm$^2$/sec, and in a physiological medium $D \leq D_2$, the largest possible wave speed allowed by equation 4 (with these parameters) is $V$≈ 1.5 mm/min. This is substantially slower than the observed speed of spreading depression. Since $V$ is inversely proportional to $\sqrt{T}$ (by equation 4) and $T$ is proportional to $T_C$ (by equation 6), a smaller value for the critical time is needed to obtain a physiological wave speed.

An alternative calculation to that given in the preceding paragraph was actually presented by the authors (Bures, Buresová and Krívánèk, 1974). They assumed, based on observations of spreading depression, that the wave speed would be $V$≈3.0 mm/min (or greater), and used the above equations to estimate the minimum required diffusion constant. Eliminating $\sqrt{T}$ from equations 4 and 5 gives

$$\left(\frac{K_2+K_0-2K_1}{VK_2}\right)\sqrt{\frac{D}{2}} = \sqrt{T} = \frac{V(K_2-K_0)T_C}{K_2\sqrt{8D}} \tag{9}$$

Solving equation 9 for the diffusion constant

$$D = \frac{T_C V^2 (K_2 - K_0)}{2\left(K_2 + K_0 - 2K_1\right)} \tag{10}$$

With the same values for $K_0$, $K_1$, and $K_2$ used above, equation 10 gives $D \approx 8000$ $\mu m^2$/sec, which is some four times higher than the diffusion coefficient in free solution. It is unlikely that the diffusion coefficient would be this large. In fact, it is more likely that $D$ would be somewhat less than the value in free solution. Hence, Bures, Buresová and Krívánèk concluded that the propagation of spreading depression is not driven by extracellular diffusion alone, but by some sort of electrotonic mechanism.

### 2.5.1.1. Phase Plane Interpretation of Bistable Model

The dimensionless form of the bistable equation model of spreading depression can be obtained by substituting equation 2 of section 2.5.1 into equation 1 of the same section.

$$\frac{\partial \tilde{c}}{\partial \tau} = \frac{\partial^2 \tilde{c}}{\partial \xi^2} + (\tilde{c} - k_0)(k_1 - \tilde{c})(\tilde{c} - 1) \tag{1}$$

where $\tilde{c} = c / K_2, k_0 = K_0 / K_2,\ \ k_1 = K_1 / K_2,\ \xi = x / \sqrt{DT}$ and $\tau = t / T$. Traveling wave solutions to equation 1 take the form $\tilde{c}(\xi, \tau) = y(\zeta)$, for some function $y(\zeta)$ where $\zeta = \xi + v\tau$, and $v$ is a constant that is related to the wave speed, the form of which is yet to be determined (see equation 5 of section 2.5.1.2). This ansatz reduces equation 1 to the following ordinary differential equation

$$y'' - vy' + (y - k_0)(k_1 - y)(y - 1) = 0 \tag{2}$$

where the prime denotes differentiation with respect to $\zeta$ (see the following section for details). Equation 2 is equivalent to the following first order system,

$$y' = z \tag{3}$$

$$z' = vz + (k_0 - y)(k_1 - y)(y - 1) \tag{4}$$

The Jacobian matrix $J$ of this system is

$$J = \begin{bmatrix} 0 & 1 \\ (1-y)(k_0-y)+(1-y)(k_1-y)+(k_0-y)(k_1-y) & v \end{bmatrix} \tag{5}$$

The eigenvalues of $J$ are

$$\lambda = \frac{1}{2\sqrt{2}}\Big[1+k_0-2k_1 \pm\sqrt{1+k_0^2+4k_1^2+4k_1(1-4y)+2k_0(5+2k_1-8y)-16y+24y^2}\Big] \tag{6}$$

Critical points of the system occur at $(y, z) = (0, k_0)$, $(0, k_1)$, and $(0, 1)$. Evaluating equation 6 at $z=k_0$, $z=k_1$, and $z=1$ gives

$$\lambda = \begin{cases} \dfrac{1-k_0}{\sqrt{2}} \\ \dfrac{k_0-k_1}{\sqrt{2}} \end{cases} \quad \text{at } z = k_0, \tag{7}$$

$$\lambda = \frac{1+k_0-2k_1 \pm \sqrt{1+10k_0+k_0^2-12k_1-12k_0k_1+12k_1^2}}{2\sqrt{2}} \quad \text{at } z = k_1, \tag{8}$$

$$\lambda = \begin{cases} \dfrac{k_0-1}{\sqrt{2}} \\ \dfrac{1-k_1}{\sqrt{2}} \end{cases} \quad \text{at } z = 1, \tag{9}$$

Using the same values for these parameters as in the previous section, the eigenvalues at these points are approximately $\lambda = \{0.65, -.25\}$ at $z = k_0$, $\lambda = \{0.20 \pm 0.30i\}$ at $z = k_1$,

and $\lambda = \{1.06, -0.65\}$ at $z = 1$. Thus the critical points at $k_0$ and $k_2$ are saddles and the critical point at $k_1$ is an unstable spiral. The phase portrait for these values is illustrated in Figure 2.3. The traveling wave front corresponds to a heteroclinic trajectory from $(k_0, 0)$ to (1,0). The wave leaves the saddle node at $z = k_0$ along its unstable manifold in the upper half plane, and approaches $z$=1 along a stable manifold. Figure 2.3 reveals that it not necessary to have $y > k_1$ to obtain traveling waves from the bistable equation. Thus the usual physiological interpretation of this parameter can be misleading.

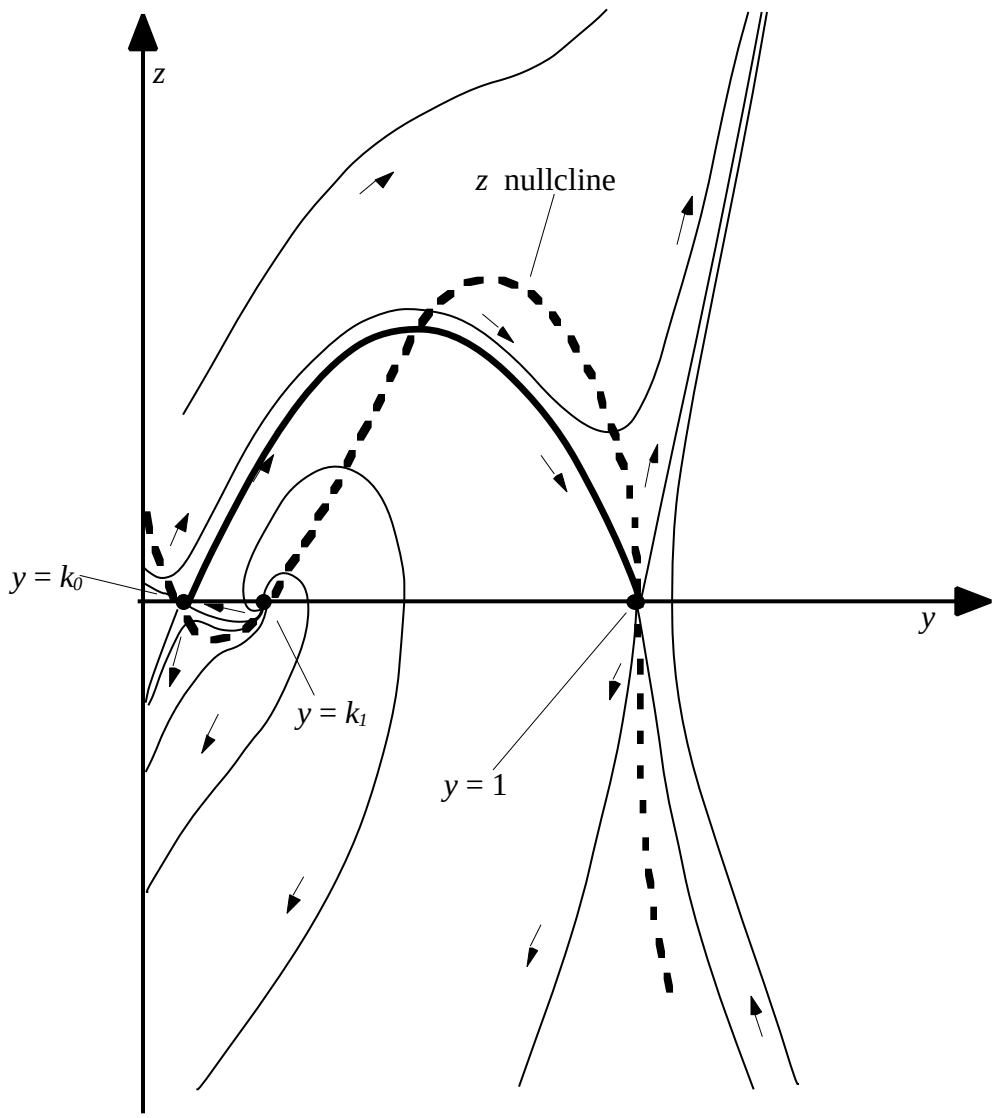


Figure 2.3. Phase portrait for equations 3 and 4 using $K_0$ = 3 mM, $K_1$ = 10 mM and $K_2$ = 40 mM. Traveling wave fronts correspond to the heteroclinic trajectory from ($k_0$, 0) to (1,0), which is shown in bold. The *z* nullcline is shown as a dashed line.

### 2.5.1.2. APPENDIX TO BISTABLE MODEL: DERIVATION OF WAVE SOLUTION

The solution to the bistable equation (equation 1 of section 2.5.1) given by Bures, Buresová and Krívánèk (1974) interprets *f*(*c*) (equation 2 of section 2.5.1) as the excess potassium concentration above the resting value. This is equivalent to assuming that $k_0 = 0$. A similar treatment is given in section 9.2.1 of Keener and Sneyd (1998). The solution that they obtain is equivalent to equation 3 of section 2.5.1 when $K_0 = 0$, i.e., the third, and most complicated, term in the brackets is missing. Since I am interested in the total potassium concentration and the form of the total potassium wave, the following derivation is slightly different from that presented in the references cited above.

From equation 1 of section 2.5.1.1,

$$\frac{\partial \tilde{c}}{\partial \tau} = \frac{\partial^2 \tilde{c}}{\partial \xi^2} + (\tilde{c} - k_0)(k_1 - \tilde{c})(\tilde{c} - 1) \qquad (1)$$

where $\tilde{c} = c / K_2, k_0 = K_0 / K_2$, $k_1 = K_1 / K_2$, $\xi = x / \sqrt{DT}$ and $\tau = t / T$. A wave-like solution traveling with a fixed speed $v$ should take the form

$$\tilde{c}(\xi, \tau) = y(\zeta) \qquad (2)$$

where $y$ is some function to be solved for that describes the shape of the wave, and

$$\zeta = \xi + v\tau = \frac{1}{\sqrt{DT}}\left(x + vt\sqrt{\frac{D}{T}}\right) \tag{3}$$

To obtain initial conditions, assume that the potassium concentration is raised to some value $K_{stim}$ at $x = 0$ and $t = 0$. Then

$$y(\zeta = 0) = \tilde{c}(\xi = 0, \tau = 0) = k_{stim} = \frac{K_{stim}}{K_2} \tag{4}$$

The fully-dimensioned wave speed $V$ is

$$V = \frac{dx}{dt} = \frac{\sqrt{DT}}{T}\frac{d\xi}{d\tau} = \sqrt{\frac{D}{T}}\frac{d\xi}{d\tau} = v\sqrt{\frac{D}{T}} \tag{5}$$

Substituting equations 2 and 3 into equation 1 gives

$$y'' - vy' + (y - k_0)(k_1 - y)(y - 1) = 0 \tag{6}$$

where the prime indicates differentiation with respect to $\zeta$. Equation 6 can be solved analytically as follows. First, let $z = y'$, and observe that

$$y'' = \frac{dz}{d\zeta} = \frac{dz}{dy}\frac{dy}{d\zeta} = y'\frac{dz}{dy} = z\frac{dz}{dy} \tag{7}$$

Substituting equation 7 into equation 6 gives

$$z\frac{dz}{dy} - vz + (y - k_0)(k_1 - y)(y - 1) = 0 \tag{8}$$

By direct substitution it may be verified that

$$z = \frac{(y - k_0)(1 - y)}{\sqrt{2}} \tag{9}$$

is a solution, so long as the (dimensionless) wave speed is

$$v = \frac{1 + k_0 - 2k_1}{\sqrt{2}} = \frac{K_2 + K_0 - 2K_1}{K_2\sqrt{2}} \tag{10}$$

Keener and Sneyd (1998) explain why one might postulate a solution like equation 9. The bistable equation admits traveling wave front solutions. A traveling wave front is a wave whose magnitude (the concentration in this situation) starts at one value initially (*e.g.*, $K = K_0$) and eventually reaches another value (*e.g.*, $K = K_2$). Or in terms of the wave variable $\zeta$, $\lim_{\zeta \to -\infty} y(\zeta) = k_0$ and $\lim_{\zeta \to \infty} y(\zeta) = 1$. It is a heteroclinic trajectory between two steady states. It would be nice if the analytic form of this trajectory – if it even exists – were to take a very simple form. The "simplest" function that has the necessary shape (in a qualitative sense) is a parabola. Equation 9 is such a candidate parabola. Since it works, it was a very lucky guess.

Equation 9 is an ordinary differential equation in y,

$$\frac{dy}{d\zeta} = \frac{(y - k_0)(1 - y)}{\sqrt{2}} \tag{11}$$

which can be solved by direct integration

$$\int \frac{d\zeta}{\sqrt{2}} = \int \frac{dy}{(y-k_0)(1-y)} = \frac{1}{1-k_0}\left[\int \frac{dy}{y-k_0} + \int \frac{dy}{1-y}\right] \tag{12}$$

where the last terms follows by expanding the integrand using the method of partial fractions. Hence

$$\frac{\left(1-k_0\right)}{\sqrt{2}}\zeta = \ln\frac{y-k_0}{1-y} + C \tag{13}$$

where $C$ is a constant of integration. From the initial condition (equation 4),

$$C = \ln\frac{1-k_{stim}}{k_{stim}-k_0} = \ln\frac{K_2 - K_{stim}}{K_{stim}-K_0} \tag{14}$$

Solving equation 13 for $y$ gives

$$y = \frac{e^{2\alpha}+k_0}{e^{2\alpha}+1} \tag{15}$$

where

$$\alpha = \frac{1}{2}\left[\frac{1-k_0}{\sqrt{2}}\zeta - C\right] = \frac{1}{2}\left[\frac{1-K_0/K_2}{\sqrt{2DT}}\left(x+Vt\right) - C\right] \tag{16}$$

Equation 15 can be stated more concisely in terms of hyperbolic functions. To do this, split it into two terms,

$$y = \frac{e^{2\alpha}}{e^{2\alpha}+1} + \frac{k_0}{e^{2\alpha}+1} \tag{17}$$

The first term in equation 17 is

$$\frac{e^{2\alpha}}{e^{2\alpha}+1} = \frac{e^{\alpha}}{e^{\alpha}} \; \frac{e^{\alpha}}{e^{\alpha}+e^{-\alpha}} = \frac{1}{2}\frac{e^{\alpha}+e^{\alpha}-e^{-\alpha}+e^{-\alpha}}{e^{\alpha}+e^{-\alpha}} = \frac{1}{2}\left[1+\tanh\alpha\right] \qquad (18)$$

The second term in equation 17 becomes

$$\frac{k_0}{e^{2\alpha}+1} = \frac{k_0 e^{-\alpha}}{e^{\alpha}+e^{-\alpha}} = \frac{k_0 e^{-\alpha}}{2\cosh\alpha} = \frac{k_0}{2}e^{-\alpha}\mathrm{sech}\alpha \qquad (19)$$

Substituting equations 18 and, 19 into equation 17 gives

$$y = \frac{1}{2}\left[1+\tanh\alpha + k_0 e^{-\alpha}\mathrm{sech}\alpha\right] \qquad (20)$$

Equation 20 is an expression for the shape of the traveling wave front. Equation 3 of section 2.5.1 is obtained by substituting equation 16 into equation 20.

## 2.5.2. BISTABLE EQUATION WITH RECOVERY

One difficulty with the method described in the previous section is that it does not provide a complete description of spreading depression. It is a traveling wave front, and not a traveling wave pulse, in that it approaches the rest state ($K = K_0$) as $t \to -\infty$ and the excited state ($K = K_2$) $t \to +\infty$ (for a discussion of the distinction between traveling wave fronts and traveling wave pulses, see chapter 9 of Keener and Sneyd, 1998). It does not provide a mechanism for recovery. An additional equation (or equations) that cause the form of $f(c)$ to vary with time could do this. For example, if the steady state at $K_2$ disappears after some time $\Delta t$, then the system would return to $K_0$.

Reggia and Montgomery (1994, 1996) provide a recovery mechanism inspired by the Fitzhugh-Nagumo (FN) model of action potentials (Fitzhugh, 1961; Nagumo, Arimoto and Yoshizawa, 1964). In the Fitzhugh-Nagumo model, an excitable system is described in terms of two variables instead of one. The first variable, say $K$, describes the phenomenon that becomes excited. Traditionally, this is voltage; in the present situation, it is potassium concentration. The second variable, $R$, controls the recovery of the system. Each variable is governed by a separate differential equation. A typical form that the FN model might take to describe the concentration $K$ is

$$\frac{dK}{dt} = f(K, R) \tag{1}$$

$$\frac{dR}{dt} = g(K, R) \tag{2}$$

where $f$ and $g$ are functions of both $K$ and $R$. In one commonly used form, $f$ is cubic in $K$ and linear (with negative slope) in $R$.

To get a traveling wave, Reggia and Montgomery add a diffusional term to equation 1

$$\frac{\partial K}{\partial t} = D\frac{\partial^2 K}{\partial x^2} + f(K, R) \tag{3}$$

Equation 3 is similar to Grafstein's mode (see equation 1 of section 2.5.1). In the earlier case (of section 2.5) $f$ was a cubic in $K$. Here it is fourth-order in $K$ and linear in $R$:

$$f(K, R) = A(K - K_0)(K - K_1)(K - K_2)(K + 0.1) - RK \tag{4}$$

where $K$ is the potassium concentration, $A$ (< 0) is a rate constant and $R$ is a potassium reuptake pump rate that acts as a recovery variable. Small perturbations in the potassium level are stable, and the system returns to $K \approx K_0$ when they occur. If the interstitial potassium concentration is raised above the threshold $K = K_1$, however, there is an "explosive" increase (Reggia and Montgomery's quotations) to a "ceiling" at $K_2$. The potassium reuptake rate $R$ is governed by a second equation

$$\frac{dR}{dt} = B\left[K - K_0 - CR\right] \tag{5}$$

where $0 < B < |A|$ and $C>0$. The rise in interstitial potassium causes the pumping rate to increase; this will eventually overtake the quartic release of potassium and lead to recovery.

Equations 3 through 5 form a Fitzhugh-Nagumo type model in the sense that it is a system of two differential equations with two state variables (*K* and *R*), one of which is an excitable variable (*K*) and the other is a negative-feedback recovery variable (*R*). Reggia and Montgomery demonstrated that wave-like solutions exist for equation 3. They then introduced a two dimensional lattice of neurons interconnected by a "Mexican-Hat" mutual activation function. When a wave was induced to pass through this neural net they found spatiotemporal patterns of neuronal activation that behaved in a manner similar to the visual hallucinations and scintillating scotomas experienced by migraine-with-aura patients.

The model was later modified to study the interactions between spreading depression and ischemia (Revett and others, 1998; Ruppin and others, 1999) by including the effects of tissue damage.

$$\begin{aligned} f(K) = {} & AI(K - K_0)(K - K_1)(K - K_2)(K + 0.1) \\ & + B(S - I)(K_2 - K) - CRK \end{aligned} \tag{6}$$

where $S$ is the cytosolic potassium concentration, $I$ is a measure of "cortical intactness" (which is related to the extent of injury), and $A$, $B$, and $C$ are constants. The first term describes extracellular excitability as before, in the sense that there is an “explosive” increase in the interstitial concentration from near $K \approx K_0$ to $K \approx K_2$ when when $K > K_1$. The second term in equation 6 describes pathological leakage due to membrane damage from the cytosol into the interstitial space, and the third term ($CRK$) is reuptake via membrane pumping (where $R$ is the pump rate). The reuptake rate changes according to

$$\frac{dR}{dt} = c_1 PIM(K - K_0) - c_2(K_2 - K + c_3)R \qquad (7)$$

where $c_1$, $c_2$, and $c_3$ are constants, $M$ describes the metabolic stores (*e.g.*, glucose, phosphates), and $P$ describes partial impairment of individual cortical elements. The variables $I$, $P$, $S$, and $M$ are described by their own set of differential equations. The form of these additional equations is not pertinent to the present study.

The salient point is that equations 6 and 7 are used to describe the effects of spreading depression on the surrounding tissue. The mechanisms that underlie spreading depression are described by this system only in the sense that the function $f$ describes the sensitivity of the interstitial potassium concentration with respect to any perturbations thereof. Since the first and third terms in equation 6 are presumably due to normal membrane channels and pumps, this formulation provides an heuristic description and not a mechanistic description, and its accuracy is based upon the

success of fitting the total membrane current with a polynomial. In this way it provides a useful tool to explore the way a wave of SD interacts with the brain. The waveform shape and time-dependent behavior of spreading depression is accurately described. However, Reggia's model does not provide any insight into the cause of excitability, the nature of the threshold or ceiling levels of potassium, mechanisms of propagation and recovery, or even why there are traveling waves at all. For this we must turn to a more complex model.

### 2.5.3. SYSTEM OF REACTION-DIFFUSION EQUATIONS

Tuckwell and Miura (1978) extended the reaction-diffusion approach by applying the reaction-diffusion equation four times, once for each of the extracellular concentrations of $Na^+$, $Cl^-$, $K^+$ and $Ca^{++}$.

$$\frac{\partial c_j^{out}}{\partial t} = D_j \frac{\partial^2 c_j^{out}}{\partial x^2} + F_j \qquad (1)$$

where $F_j$ is the membrane flux of species $c_j$ (positive out). They also modeled cytosolic concentrations but explicitly stated (as an assumption) that no charge movement occurred within the cytoplasm

$$\frac{\partial c_j^{in}}{\partial t} = -\frac{\alpha}{1-\alpha} F_j \qquad (2)$$

where $\alpha$ is the extracellular space fraction. Membrane fluxes of $Na^+$, $Cl^-$ and $K^+$ were assumed to be limited to post-synaptic regions, and were either neurotransmitter-induced or were due to metabolic pumps. This was expressed as

$$F_j = \sum_i k_{ij} T_i (V - V_j) + P_j \qquad (3)$$

where $k_{ij}$ describes the effect of transmitter $T_i$ on species $j$, $P_j$ describes membrane pumping for species $j$, $V$ is the membrane voltage (described with the Goldman-

Hodgkin-Katz equation) and $V_j$ is the Nernst potential for species $j$. Calcium release is purely voltage dependent, and the transmitter concentration is assumed to be proportional to the calcium flux. The calcium conductance is taken as a sigmoidal function of voltage

$$g \quad 1 + \tanh[p(V + V_1)] \tag{4}$$

where $p$ and $V_1$ are constants. A single ion pump was modeled for each species, described as a saturating function of the appropriate concentration

$$P_j \quad 1 - \exp(-r_j(c_j - C_j)) \tag{5}$$

where $r_j$ and $C_j$ are constants.

The authors found that this model was extremely computationally demanding. To reduce computer time, they developed a reduced model in which the $Na^+$ and $Cl^-$ concentrations were kept constant. With this simplified model they were able to describe spreading depression-like phenomena with bell-shaped wave forms that propagated at speeds ranging from ≈1 mm/min to ≈2.9 mm/min and which lasted for some ≈10 sec to ≈30 sec at any given point. The magnitude of the potassium wave was ≈15 to ≈20 mM and the change in voltage from the resting potential ≈20 mV (Tuckwell, 1980, 1981). In a later version of the full model (Tuckwell and Hermansen, 1981) transmitter release was described using a series of kinetic models. Waves generated in the full model had a speed of ≈0.6 mm/minute, and the qualitative

behavior of the ionic redistribution was described properly. The propagating waveform remained bell shaped, however.

It could be argued that the numerical inaccuracies of the model were due to the uncertainties in the large number of parameters (e.g., ionic conductivity, pump strength, half-activation concentrations, Hill coefficients, etc.), and that by a satisfactory parametric variation the physiological observations could be more accurately described. Tuckwell and his colleagues, however, were unable to do this. It could also be argued that very little was known about the behavior and variety of ionic currents when the model was developed, and that more modern biophysical models might be expected to improve the accuracy of the model. In this view, volumetric and metabolic changes are consequential but not causative and would be correctly described once all membrane-biophysical properties are taken into account. Since the model does correctly describe several qualitative features of spreading depression, this is not an unreasonable argument. However, one significant observation cannot be described by any model that is based purely on extracellular diffusion: the inhibitory effect upon spreading depression of agents that block gap junctions (see section 2.2.6, “Gap Junctions”).

## 2.5.4. CELLULAR AUTOMATON-BASED THEORY

Reshodko and Bures (1975) applied the technique of cellular automata to model a wave of spreading depression propagating in a circular pathway around an obstruction. In this description they modeled the cortex as a planar array of mutually interconnected cells. In the simplest arrangement, the array is rectangular, and each cell has four inputs (and outputs), but this geometry is not necessary. Each cell is in one of three states: quiescent, depressed, or refractory. Cells in the quiescent state are at rest (unstimulated). Cells in the depressed state are those through which a wave of SD is currently passing (currently depolarized). Cells in the refractory state are those through which the SD wave has already passed, and are not yet re-excitable to SD, *i.e.*, they are hyperpolarized. Cells remain in the depressed state for a duration $\tau_{SD}$, and in the refractory state for a duration $\tau_{ref}$.

The model is formulated as follows. Let $x$ denote a particular cell, and $x(t)$ the state of $x$ at time $t$. Then

$$x(t) = \begin{cases} Q, \text{ if } x \text{ is quiescent} \\ D, \text{ if } x \text{ is depressed} \\ R, \text{ if } x \text{ is refractory} \end{cases} \tag{1}$$

Similarly, let $\{y_1, y_2, \ldots, y_k\}$ be the $k$ cells that are connected to $x$, and let $y_i(t)$ denote the state $y_i$ at $t$. Time is discretized into a steps of length $\Delta t$. The state of a cell at

time $t + \Delta t$ depends only on (a) the state of the cell at time $t$, and (b) the states of the all the cells to which it is connected at time $t$. At time $t+\Delta t$, a state transition may occur, depending on the current state $x(t)$ and the states of the neighbors $y_i(t)$. If $x(t)$ = Q, and if one or more of the $y_i(t)$=D, then

$$x(t') = \begin{cases} D \ \ for\ t' = t + \Delta t, t + 2\Delta t, \ldots, t + \tau_{SD} \\ R \ \ for\ t' = \tau_{SD} + \Delta t, \tau_{SD} + 2\Delta t, \ldots, \tau_{SD} + \tau_{ref} \\ Q \ \ for\ t' = \tau_{SD} + \tau_{ref} + \Delta t \end{cases} \qquad (2)$$

This approach provides a technique for describing any disturbance that propagates as a function of cell-cell interactions; the only input parameters are the cell-cell connectivity and the duration of the depressed and refractory states. Beyond this it does not provide any mechanism for the physiological nature of spreading depression. Thus it provides a useful framework for understanding the geometry of wave propagation. But it is not clear how such a framework can be used to describe the dependence of wave shape and magnitude on physiological parameters such as membrane conductances and diffusion constants.

## 2.5.5. MAGNETIC DIPOLE MODEL

Tepley and Wijesinghe (1996) have theorized that the large amplitude magnetic waves observed during migraine headaches (Barkley and others, 1990) occur as a result of spreading depression. They model the cortex as a sheet of pyramidal cells. Each cell has an area of $10^{-4}$ $mm^2$ and is represented as a single magnetic dipole. The cortical sheet is then curved into a single sulcus of width *d* oriented along the *x* axis according to the function

$$z(x,y) = \frac{5y^2 d}{4(1+y^2)} \qquad (1)$$

as illustrated in Figure 2.4. Equation 1 is intended to describe the geometry qualitatively, as an indentation in the face of a planar conductor. It is not to be interpreted as a quantitatively accurate form of sulcus shape. The πspecific analytic shape is chosen for purely mathematical reasons – so that they could obtain an analytic solution.

Spreading depression is assumed (in this model) to be traveling as a plane wave that meets the sulcus at some angle β, where β=0 indicates propagation along the length of the sulcus. The authors are interested in modeling the magnetic field at a point exterior to the head in the vicinity of the sulcus. This assume that a SQUID (super-conducting quantum interference device) magnetometer is be oriented parallel to the z-axis. In this configuration, the magnetometor will measure only the z-

component of the magnetic field. The authors then proceed to derive an expression for the *z*-component of the magnetic field at any particular spatial location **r** caused by a traveling wave of spreading depression as passes by a single point **r′** in the tissue. Thus the result is a function of both **r** and **r′**. This derivation and the exact mathematical form of the result are not pertinent to the present discussion; for details the reader is referred to the above-cited reference. By integrating this expression numerically over a sulcus with the geometry described by equation 1 Tepley and Wijesinghe estimate the total magnetic field that should actually be detected by the SQUID coil. As a result, they concluded that it was possible to relate the shape, duration, polarity and amplitude of the spreading depression wave form, as measured by a particular model magnetometer, to the location of the detector with respect to the sulcus. They report that both the amplitude and duration of the simulated signal increase with both the active area and sulcus depth.

Tepley and Wijesinghe interpret their results in the following manner. As the active area (the area of tissue that is affected by the passing spreading depression wave) increases, more dipoles are involved; therefore the signal should be larger. Furthermore, as the active area increases, it takes longer for the SD wave to pass; therefore the signal should last longer. Next, when the depth of the sulcus increases, it takes longer for the wave to propagate down and then back out of the sulcus. Thus the overall duration of any magnetic disturbance should increase with sulcus depth. Additionally, the time period during which the wave is only on one side of the sulcus

increases with sulcus depth (for the same reason). When the wave is only on one side of the sulcus (before it has reached the bottom and turned back up) there is no cancellation of nearly adjacent dipoles, and the magnetic signal is predicted to be stronger. All of these results are compatible with observations.

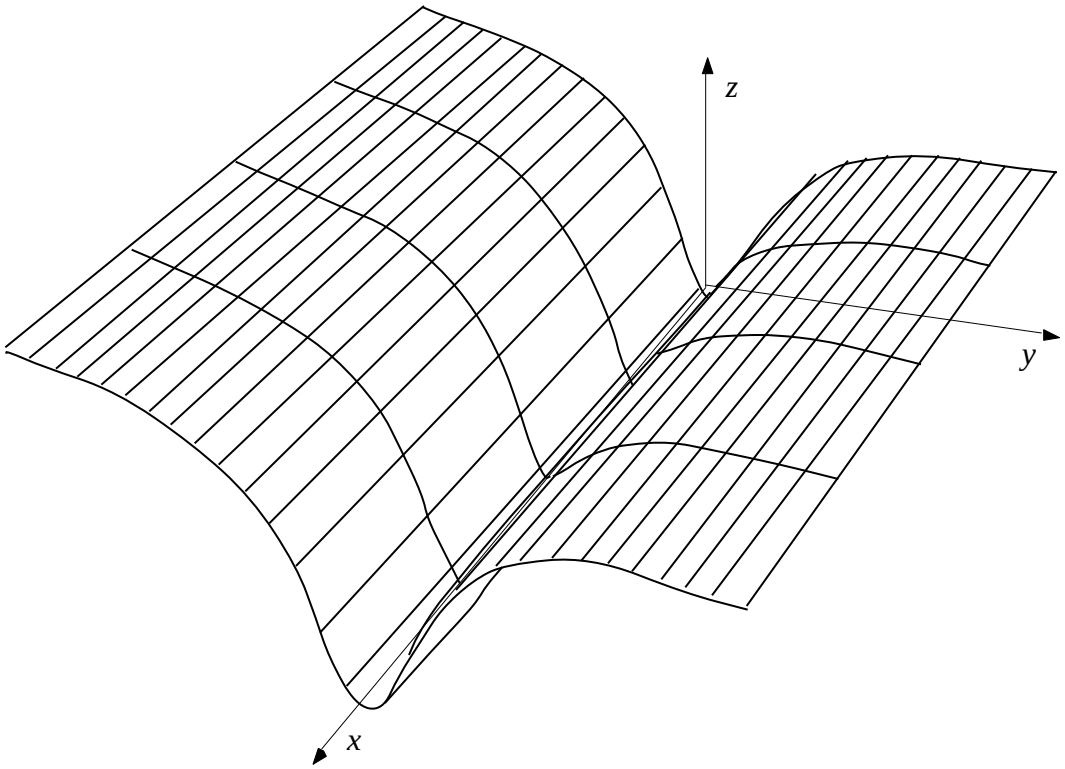


Figure 2.4. Sulcus geometry used by Tepley and Wijesinghe (1996). The sulcus is oriented along the *x*-axis with the *z*-axis pointing perpendicularly outward from the cortical surface.

# CHAPTER 3

# METHODS

This chapter presents the model that the dissertation proposes, its mathematical formulation, and the techniques utilized for its numerical (computational) implementation. An overview and motivation for what follows is presented in section 3.1 ("Overview of the Model"). The electrodiffusion equation, which is central to the model, is derived in section 3.2 ("Electrodiffusion Equation"). The reaction terms used in this formulation of the electrodiffusion equation are due to currents that pass through either neuronal or glial membranes, as described in section 3.3 ("Membrane Currents"). The models used for these currents are all standard biophysical models. The treatment of gap junctions is based on the diffusional movement between cells as presented in section 3.4 ("Gap Junctions"). The glial model is given in section 3.5 ("Glial Cells"). The effect of osmotic forces on cell volume, which has never before been studied in a mathematical treatment of spreading depression, is described in section 3.6 ("Osmotic Forces and Cell Volume"). The ways in which intracellular calcium stores are incorporated into the model, including buffering and release models, are described in section 3.7 ("Calcium Stores"). Numerical techniques are presented in section 3.8 ("Implementation").

## 3.1. MODEL OVERVIEW

The processes that are hypothesized to contribute to spreading depression are illustrated schematically in Figure 3.1. When a hyperosmotic concentration of extracellular $K^+$ is applied to neuronal tissue, the Nernst potential for potassium,

$$E_K = (RT/F)\ln(K_{out}/K_{in}) \tag{1}$$

immediately rises to a new value. Since the membrane is primarily permeable to potassium, the membrane potential *E* attempts to follow. Because the depolarization is spatially limited there are local voltage gradients along the length of all neuronal processes that pass through the area of perturbed ionic concentration

There are also likely to be voltage gradients within extracellular space, leading to ephaptic effects, but because extracellular space is widely connected and of relatively high conductivity (compared to the membranes and intracellular space) the usual assumption of a fixed extracellular ground potential is maintained. One might argue that the interstitial conductivity is approximately the same as the cytosolic when it is examined locally, but on the spatial scales of interest in spreading depression, such an argument is probably not valid. This is because there are numerous intracellular organelles, as well as gap junctions, that would serve to reduce the conductivity. Thus while both the intracellular and extracellular *fluids* might have nearly the same conductivity, the interstitial and cytosolic *spaces* probably do not.

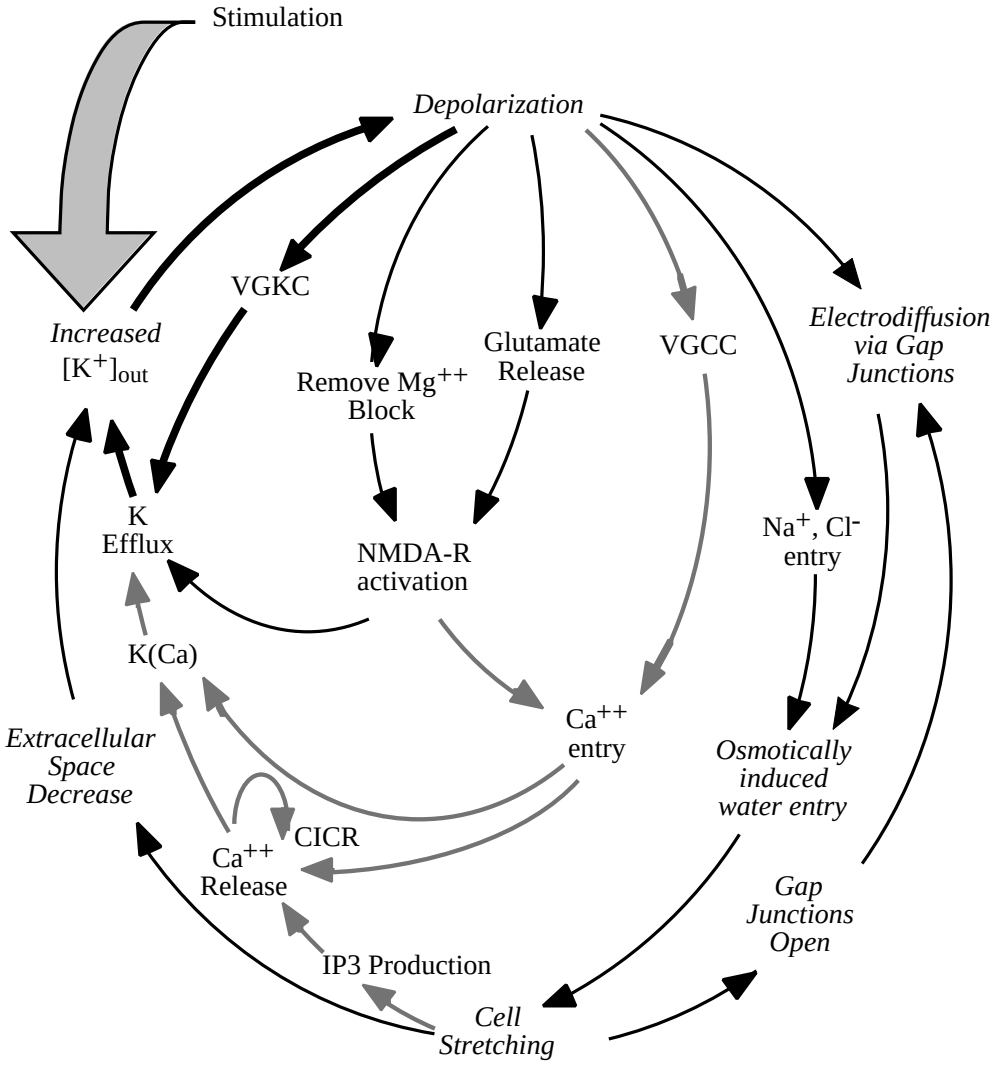


Figure 3.1. Schematic of processes involved in the model of spreading depression. The usual diffusional K+ wave model is indicated with bold arrows. The novel osmotic pathwal are shown around the edge of the circle, and the membrane current pathways are shown on its interior.

The model proceeds as follows. Local depolarization will open voltage-gated ion channels, leading to a potassium efflux out of the cells and into the area of high potassium concentration. This creates a cytoplasmic $K^+$ deficit (measured with respect to resting values, and also as measured with respect to the surrounding cytosolic regions) at the stimulation point. Extracellularly, $K^+$ diffuses away (*i.e.*, downhill) from the stimulation point of application. This causes the voltage gradient to spread. Cytoplasmic diffusion can also occur. Initially, of course, there are no cytoplasmic concentration gradients. But voltage gradients within the cytoplasm push $K^+$ away from the point of stimulation. This compounds the local sub-stimulation $K^+$ deficiency just described. Even after this cytosolic $K^+$ concentration gradient develops, $K^+$ will continue to be pushed away (uphill) from the stimulation point, due to electrodiffusive forces. To see why this "uphill" movement of $K^+$ continues, consider the Nernst-Plank equation, which gives the axial potassium flux in a dendrite oriented along the *x*-axis as

$$J = -D\left(\frac{\partial c}{\partial x} + \frac{zF}{RT}\, c\, \frac{\partial E}{\partial x}\right) \qquad (2)$$

where $D$ is the diffusion constant, $c$ the intracellular potassium concentration, $z = 1$ the ionic valence, $R$ the ideal gas constant, $T$ the temperature, and $E$ the voltage. The first term is Fick's Law, which states that in the absence of any other forces the natural stochastic movement of particles will be down the concentration gradient. The second term is Planck's equation, which tells us that in a viscous fluid positively charged

particles will be pushed at a constant speed down a voltage gradient, from an area of higher voltage to an area of lower voltage. Initially $c(x)$ is constant and there is no concentration gradient. Suppose the stimulus is applied as a bell-shaped increase in the interstitial potassium concentration centered at $x = 0$. Because there is no initial concentration gradient, the first term in equation 2 is zero (initially). However, the membrane at $x$=0 is depolarized with respect to all $x \neq 0$. Thus $\partial E / \partial x < 0$ for all $x > 0$ and $\partial E / \partial x > 0$ for all $x < 0$. Because of the minus sign in equation 2, there is a potassium flux inside the cell away from the point of stimulation. This leads to the initial local decrease in $K^+$ concentration, surrounded by areas of increased $K^+$ concentration. As this $K^+$ pulse develops, the first term in equation 2 becomes nonzero. The natural (intuitive) reaction would be for the concentration gradient to induce diffusional forces that push the potassium back in the direction from which it came, *i.e.*, towards the origin. However, as long as the magnitude of the second term (in equation 2) exceeds the magnitude of the first term (in equation 2), the net flux will continue to be away from the origin, even if that movement is uphill and against the concentration gradient. The two terms balance when

$$\frac{\partial c}{\partial x} = -c\frac{\partial \varphi}{\partial x} \qquad (3)$$

where $\varphi = zEF / RT$ is the dimensionless membrane potential. Dividing by the concentration and integrating *along the length of the membrane* for a distance $x$ starting at the point of stimulation,

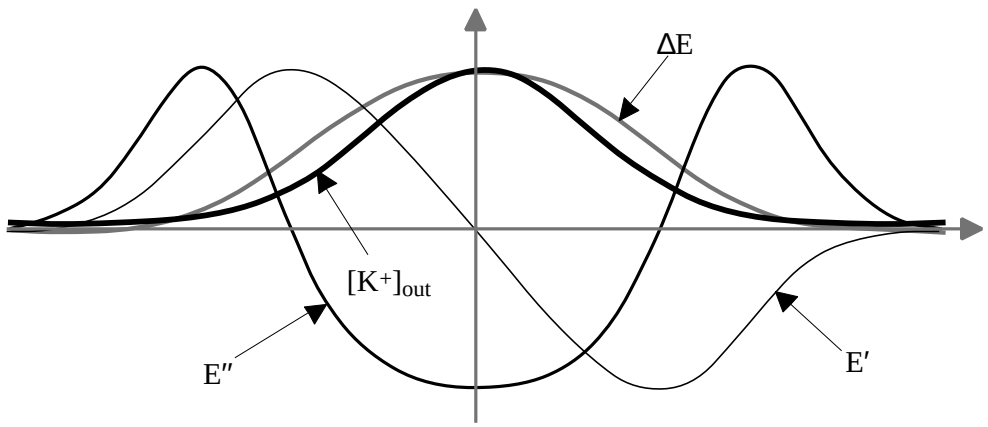


Figure 3.2. Electrodiffisive force as described by the electrodiffusion equation. The extracellular potassium stimulation, resulting membrane potential change ($\Delta E = E - E_{rest}$) and the first and second derivatives of $E$ are all normalized with respect to their maximum values.

$$\int_{x'=0}^{x'=x} \frac{1}{c}\frac{\partial c}{\partial x'}\,dx' = -\int_{x'=0}^{x'=x} \frac{\partial \varphi}{\partial x'}\,dx' \qquad (4)$$

gives

$$\ln\frac{c(x)}{c(0)} = \varphi(0) - \varphi(x) \equiv \Delta\varphi > 0 \qquad (5)$$

Thus ions will continue to move against the concentration gradient until $c(x) = c(0)e^{\Delta\varphi}$. Despite the similarity of equation 5 to the Nernst equation, we have not integrated across a membrane, but along the length of a (dendritic) process. However, the mathematics is the same. The formulation of this electrodiffusive force illustrated in Figure 3.2. During spreading depression at room temperature (where $RT/F \approx 25$ mV) depolarizations ranging from 25 to 75 mV (in round numbers) have been observed. Thus $\Delta\varphi \approx 1$ to $\approx 3$, giving hypothetical concentration ratios $c(x)/c(0)$ that approach ≈20. As long as there is a voltage gradient, the natural movement of potassium is (counter-intuitively) uphill, against the concentration gradient, until this hypothetical concentration ($c(x) = c(0)e^{\Delta\varphi}$) is reached.

The process of electrodiffusion, which has just been described, causes an additional term to be added to the reaction-diffusion equation. This will be shown more rigorously in the next section. At the same time that this cytoplasmic $K^+$ electrodiffusion is taking place, membrane depolarization causes an even more significant flow of $Na^+$ and $Cl^-$ into the cell. Both of these factors – electrodiffusion and ionic entry - contribute to osmotic imbalances. These imbalances are equalized

by the flow of water across the cellular membrane. This causes the cell to expand (or shrink) and forces the membrane to stretch. Stretch receptors may cause gap junctions between neurons to open, allowing cytoplasmic ionic movement to occur over even greater distances. It is also possible that the gap junctions are always open; as the preceding argument suggests, even if the gap junctions are always open, potassium will not flow back toward the stimulation point until the depolarization ends, or until the hypothetical concentration ratio is surpassed.

Cellular expansion, induced by osmosis, compresses interstitial space. This compression has been observed at levels reaching 50%, effectively doubling interstitial concentrations. This combination of two factors - cytoplasmic ionic movement and osmotically induced cellular expansion - is sufficient (mathematically) to induce wave propagation.

To formulate the model mathematically, the electrodiffusion equation is used to describe the cytoplasmic concentration of each ion. Interstitial concentrations are described by reaction-diffusion equations. The reaction terms are due to membrane currents and calcium buffers. Membrane currents are described by standard biophysical models, many of which use the Hodgkin-Huxley formalism as presented in section 3.3. The mathematical formulation has 29 state variables that are summarized in Table 3.1. Other variables used in the model are summarized in Table 3.2. These variables are described in more detail in the remainder of this chapter.

Table 3.1. State variables used in the model. HH is Hodgkin-Huxley variable. Equation is the equation and section number where the parameter is first defined. For example, equation 3.2.4 refers to equation 4 of section 3.2.

| Variable | Equation | Description |
|---|---|---|
| $[Ca^{++}]_{in}$ | 3.2.4 | Cytosolic $Ca^{++}$ concentration. |
| $[Ca^{++}]_{out}$ | 3.2.13 | Interstitial $Ca^{++}$ concentration. |
| $[Ca^{++}]_{ER}$ | 3.7.12 | $Ca^{++}$ concentration in buffer. |
| $[Cl^{-}]_{in}$ | 3.2.9 | Cytosolic $Cl^{-}$ concentration. |
| $[Cl^{-}]_{out}$ | 3.2.15 | Interstitial $Cl^{-}$ concentration. |
| [ITP] | 3.7.6 | Cytosolic ITP concentration |
| $[K^{+}]_{in}$ | 3.2.2 | Cytosolic $K^{+}$ concentration. |
| $[K^{+}]_{out}$ | 3.2.12 | Interstitial $K^{+}$ concentration. |
| $[Na^{+}]_{in}$ | 3.2.7 | Cytosolic $Na^{+}$ concentration. |
| $[Na^{+}]_{out}$ | 3.2.14 | Interstitial $Na^{+}$ concentration. |
| $f$ | 3.2.11 | Neuronal volume fraction |
| $h_{ITP}$ | 3.7.6 | ITP sensitive $Ca^{++}$ channel HH variable |
| $m_{stretch}$ | 3.7.9 | Inactivation of stretch-induced ITP production. |
| $m_A$, $h_A$ | 3.3.1.1 | A-channel HH variables. |
| $m_{BK}$ | 3.3.2.1 | Large conductance (BK) K(Ca) HH variable. |
| $m_{DR}$, $h_{DR}$ | 3.3.1.10 | Delayed rectifier HH variables. |
| $m_F$, $h_F$ | 3.3.4.1 | Fast $Na^{+}$ channel HH variables. |
| $m_{IK}$ | 3.3.1.5 | Intermediate conductance (IK) K(Ca) HH variable. |
| $m_M$ | 3.3.1.6 | M-channel HH variable. |

Table 3.1 (Continued)

| Variable | Equation | Description |
|---|---|---|
| $m_{HVA}$,$h_{HVA}$ | 3.3.5.12 | HVA $Ca^{++}$ channel HH variables. |
| $m_{LVA}$,$h_{LVA}$ | 3.3.5.1 | LVA $Ca^{++}$ channel HH variables. |
| $m_P$ | 3.3.4.12 | Persistent $Na^{+}$ channel HH variable. |
| $m_{ryanodine}$ | 3.7.12 | Ryanodine sensitive $Ca^{++}$ channel HH variable |
| $m_{SK}$ | 3.3.1.10 | Small conductance (SK) K(Ca) HH variable. |

Table 3.2. Symbols used in the model equations, excluding parameters and state variables. State variables are shown in Table 3.1 and parameters are summarized in Tables 4.1 through 4.3. The listing is not an exhaustive list of all symbols used in the text, but only comprises those variables that are pertinent to the model as implemented and described in the text. Equation is the equation number where the symbol is defined, or where it is first used if it does not have a specific defining equation. . For example, equation 3.2.1 refers to equation 1 of section 3.2. An asterisk (*) following an equation number indicates that the symbol is defined in the text following the referenced equation.

| Symbol | Equation | Description |
|---|---|---|
| $B(E,M)$ | 3.3.3.3 | Probability that NMDA channel is not blocked by Mg. |
| $c_{in}$ | 3.2.1 | Concentration in cytosol (mM/l). |
| $c_{out}$ | 3.2.11 | Interstitial concentration (mM/l). |
| $d$ | 3.2.1* | Diameter (μm). |
| $D_{c,in}$ | 3.2.1 | Diffusion constant in cytosol ($\mu m^2$/sec). |
| $D_{c,out}$ | 3.2.11 | Interstitial diffusion constant ($\mu m^2$/sec). |
| $E$ | 3.2.1 | Membrane potential (mV). |
| $E_c$ | 3.3.4 | Nernst potential for species $c$ ($c$ = $K^+$, $Na^+$, $Ca^{++}$) |
| $F$ | 3.2.1 | Faraday's constant (≈96 Coul/mM). |
| $g_A$ | 3.3.1.1 | Membrane conductance (pS/$\mu m^2$) due to KA channel. |
| $g_{BK}$ | 3.3.2.1 | Membrane conductance (pS/$\mu m^2$) due to BK channel. |
| $g_{c,NMDA}$ | 3.3.3.2 | Membrane conductance (pS/$\mu m^2$) for species $c$ ($c$ = $K^+$, $Na^+$, $Ca^{++}$) due to NMDA-receptor gated ion channels. |
| $g_{DR}$ | 3.3.1.10 | Membrane conductance (pS/$\mu m^2$) due to delayed rectifier. |
| $g_F$ | 3.3.4.1 | Membrane conductance (pS/$\mu m^2$) due to fast $Na^+$ channel. |
| $g_{HVA}$ | 3.3.5.12 | Membrane conductance (pS/$\mu m^2$) due to high voltage activated $Ca^{++}$ channel. |
| $g_{IK}$ | 3.3.1.5 | Membrane conductance (pS/$\mu m^2$) due to IK channel. |

Table 3.2 (Continued)

| Symbol | Equation | Description |
|---|---|---|
| $g_{LVA}$ | 3.3.5.1 | Membrane conductance (pS/μm$^2$) due to low voltage activated $Ca^{++}$ channel. |
| $g_M$ | 3.3.1.6 | Membrane conductance (pS/μm$^2$) due to M channel. |
| $g_P$ | 3.3.4.12 | Membrane conductance (pS/μm$^2$) due to persistent $Na^+$ channel. |
| $g_{SK}$ | 3.3.2.10 | Membrane conductance (pS/μm$^2$) due to SK channel. |
| $h_{DR,\infty}$ | 3.3.1.17 | Steady state value of $h_{DR}$. |
| $h_{F,\infty}$ | 3.3.4.9 | Steady state value of $h_F$. |
| $h_{HVA,\infty}$ | 3.3.5.19 | Steady state value of $h_{HVA}$. |
| $h_{ITP,\infty}$ | 3.7.7 | Steady state value of $h_{ITP}$. |
| $h_{LVA,\infty}$ | 3.3.5.8 | Steady state value of $h_{LVA}$. |
| $j_A$ | 3.3.1.1 | Membrane $K^+$ flux through A-channel (mM/cm$^2$-sec). |
| $j_{BK}$ | 3.3.2.1 | Membrane $K^+$ flux through large-conductance (BK) K(Ca) channel (mM/cm$^2$-sec). |
| $J_{c,glia}$ | 3.2.11 | Glial uptake rate (mM/l-sec) for species $c$ ($c$ = $K^+$, $Na^+$, $Cl^-$). |
| $J_{c,m}$ | 3.2.1 | Membrane flux for species $c$ (mM/cm$^2$-sec). |
| $j_{c,NMDA}$ | 3.3.3.1 | Membrane flux of species $c$ ($c$ = $K^+$, $Na^+$, $Ca^{++}$) through NMDA channel (mM/cm$^2$-sec). |
| $j_{Ca,ATPase}$ | 3.3.6.4 | Membrane $Ca^{++}$ flux through neuronal ATP-dependent $Ca^{++}$ pump (mM/cm$^2$-sec). |
| $j_{DR}$ | 3.3.1.10 | Membrane $K^+$ flux through delayed rectifier (mM/cm$^2$-sec). |
| $j_F$ | 3.3.4.1 | Membrane $Na^+$ flux through fast $Na^+$ channel (mM/cm$^2$-sec). |

Table 3.2 (Continued)

| Symbol | Equation | Description |
|---|---|---|
| $j_{HVA}$ | 3.3.5.12 | Membrane $Ca^+$ flux through HVA channels (mM/cm$^2$-sec). |
| $j_{IK}$ | 3.3.1.6 | Membrane $K^+$ flux through intermediate-conductance (IK) K(Ca) channel (mM/cm$^2$-sec). |
| $j_{ITP}$ | 3.3.7.6 | $Ca^{++}$ flux through ITP-sensitive channels in ER membrane (mM/sec). |
| $j_{ITP\text{-}removal}$ | 3.3.7.11 | Rate at which ITP is degraded in the cytoplasm (mM/l-sec). |
| $J_{K,glia}$ | 3.5.1 | Glial uptake rate (mM/cm$^2$-sec) for $K^+$. |
| $j_{Leak}$ | 3.3.7.1 | Leak flux (mM/cm$^2$-sec). |
| $j_{LVA}$ | 3.3.5.1 | Membrane $Ca^+$ flux through LVA channels (mM/cm$^2$-sec). |
| $j_M$ | 3.3.1.6 | Membrane $K^+$ flux through M-channel (mM/cm$^2$-sec). |
| $J_{Na,glia}$ | 3.5.1 | Glial uptake rate (mM/cm$^2$-sec) for $Na^+$. |
| $j_{Na/Ca}$ | 3.3.6.3 | Membrane $Ca^{++}$ flux through Na/Ca exchanger (mM/cm$^2$-sec). |
| $j_{Na/K}$ | 3.3.6.1 | Membrane $K^+$ flux through neuronal Na/K exchanger (mM/cm$^2$-sec). |
| $j_{Na/K/Cl}$ | 3.3.6.5 | Membrane $K^+$ flux through neuronal Na/K/Cl exchanger (mM/cm$^2$-sec). |
| $j_P$ | 3.3.4.12 | Membrane $Na^+$ flux through persistent $Na^+$ channel (mM/cm$^2$-sec). |
| $j_{Pump}$ | 3.7.5 | $Ca^{++}$ flux through pump in ER membrane (mM/sec). |
| $j_{ryanodine}$ | 3.7.12 | $Ca^{++}$ flux through ryanodine-sensitive ER channels (mM/sec). |
| $j_{SK}$ | 3.3.3.10 | Membrane $K^+$ flux through small-conductance (SK) K(Ca) channel (mM/cm$^2$-sec). |
| $m_{BK,\infty}$ | 3.3.2.4 | Steady state value of $m_{BK}$ |

Table 3.2 (Continued)

| Symbol | Equation | Description |
|---|---|---|
| $m_{DR,\infty}$ | 3.3.1.13 | Steady state value of $m_{DR}$. |
| $m_{F,\infty}$ | 3.3.4.5 | Steady state value of $m_F$. |
| $m_{HVA,\infty}$ | 3.3.5.15 | Steady state value of $m_{HVA}$. |
| $m_{IK,\infty}$ | 3.3.2.8 | Steady state value of $m_{IK}$. |
| $m_{LVA,\infty}$ | 3.3.5.4 | Steady state value of $m_{LVA}$. |
| $m_{SK,\infty}$ | 3.3.2.13 | Steady state value of $m_{SK}$. |
| $m_{M,\infty}$ | 3.3.1.9 | Steady state value of $m_M$. |
| $m_{P,\infty}$ | 3.3.4.15 | Steady state value of $m_P$. |
| $m_{stretch,\infty}$ | 3.7.10 | Steady state value of $m_{stretch}$. |
| $m_{ryanodine,\infty}$ | 3.7.13 | Steady state value of $m_{ryanodine}$. |
| $m(E)$ | 3.3.3.4 | Fraction of unblocked NMDA channels that are activated by neurotransmitter. |
| M | 3.3.3.3* | Interstitial magnesium concentration (mM/l). |
| $N_A$ | 3.6.1 | Total number impermeant anions in volume $V$. |
| $p_{HVA}$ | 3.3.5.1 | Ratio of membrane permeability to conductance of $Ca^{++}$ due to LVA channels ((cm/sec)/(μm$^2$/pS)). |
| $P_{LVA}$ | 3.3.5.1* | Membrane permeability (cm/sec) of $Ca^{++}$ due to LVA channels. |
| $p_{HVA}$ | 3.3.5.12 | Ratio of membrane permeability to conductance of $Ca^{++}$ due to HVA channels ((cm/sec)/(μm$^2$/pS)). |
| $P_{HVA}$ | 3.3.5.12* | Membrane permeability (cm/sec) of $Ca^{++}$ due to HVA channels. |
| $q_{max}$ | 3.3.8.1 | Maximum open probability due to stretch |

Table 3.2 (Continued)

| Symbol | Equation | Description |
|---|---|---|
| $Q_{open}$ | 3.3.8.1 | Open probability of ion channel due to membrane stretch. |
| $R$ | 3.2.1 | Ideal gas constant. |
| $r$ | 3.2.1 | Surface area to volume ratio. |
| $s_c$ | 3.2.1 | Source term for species c (mM/l-sec). |
| $[S]_{out}$ | 3.6.2 | Interstitial solute concentration (mM/l). |
| $T$ | 3.2.1 | Temperature (K). |
| $T_{max}$ | 3.3.3.4 | Maximum interstitial concentration of ligand for NMDA receptor (e.g., glutamate). |
| $x$ | 3.3.1 | Hodgkin-Huxley variable. |
| $x_\infty$ | 3.3.1 | Steady state value of Hodgkin-Huxley variable $x$. |
| $z$ | 3.2.1 | Valence. |
| $\alpha_{h,F}$ | 3.3.4.10 | Forward rate constant for $h_F$ ($sec^{-1}$). |
| $\alpha_{h,HVA}$ | 3.3.5.21 | Forward rate constant for $h_{HVA}$ ($sec^{-1}$). |
| $\alpha_{h,LVA}$ | 3.3.5.10 | Forward rate constant for $h_{LVA}$ ($sec^{-1}$). |
| $\alpha_{IK}$ | 3.3.2.8* | Forward rate constant for $m_{IK}$ ($sec^{-1}$). |
| $\alpha_{m,DR}$ | 3.3.1.14 | Forward rate constant for $m_{DR}$ ($sec^{-1}$). |
| $\alpha_{m,F}$ | 3.3.4.6 | Forward rate constant for $m_F$ ($sec^{-1}$). |
| $\alpha_{m,P}$ | 3.3.4.16 | Forward rate constant for $m_P$ ($sec^{-1}$). |
| $\alpha_{m,HVA}$ | 3.3.5.17 | Forward rate constant for $m_{HVA}$ ($sec^{-1}$). |
| $\alpha_{m,LVA}$ | 3.3.5.6 | Forward rate constant for $m_{LVA}$ ($sec^{-1}$). |
| $\alpha_x$ | 3.3.2 | Forward rate constant for Hodgkin-Huxley variable $x$ ($sec^{-1}$). |
| $\beta_{h,F}$ | 3.3.4.11 | Backward rate constant for $h_F$ ($sec^{-1}$). |
| $\beta_{h,HVA}$ | 3.3.5.22 | Backward rate constant for $h_{HVA}$ ($sec^{-1}$). |

Table 3.2 (Continued)

| Symbol | Equation | Description |
|---|---|---|
| $\beta_{h,LVA}$ | 3.3.5.11 | Backward rate constant for $h_{LVA}$ ($sec^{-1}$). |
| $\beta_{m,DR}$ | 3.3.1.15 | Backward rate constant for $m_{DR}$ ($sec^{-1}$) |
| $\beta_{m,IK}$ | 3.3.2.9 | Backward rate constant for $m_{IK}$ ($sec^{-1}$). |
| $\beta_{m,F}$ | 3.3.4.7 | Backward rate constant for $m_F$ ($sec^{-1}$). |
| $\beta_{m,P}$ | 3.3.4.17 | Backward rate constant for $m_P$ ($sec^{-1}$). |
| $\beta_{m,LVA}$ | 3.3.5.7 | Backward rate constant for $m_{LVA}$ ($sec^{-1}$). |
| $\beta_x$ | 3.3.4 | Backward rate constant for Hodgkin-Huxley variable $x$ ($sec^{-1}$). |
| $\Delta A$ | 3.7.9 | Fractional change in membrane area due to stretch. |
| $\Delta P$ | 3.3.8.1 | Change in pressure due to membrane stretch (mm Hg). |
| $\gamma$ | 4.4.1 | Maximum expansion into interstitial space. |
| $\tau_{h,\mathrm{A}}$ | 3.3.1.5* | Time constant for $h_A$ (sec). |
| $\tau_{h,\Delta\mathrm{P}}$ | 3.3.1.17* | Time constant for $h_{DR}$ (sec). |
| $\tau_{h,\,HVA}$ | 3.3.5.20 | Time constant for $h_{HVA}$ (sec). |
| $\tau_{h,\,LVA}$ | 3.3.5.9 | Time constant for $h_{LVA}$ (sec). |
| $\tau_{m,DR}$ | 3.3.1.16 | Time constant for $m_{DR}$ (sec). |
| $\tau_{m,\mathrm{A}}$ | 3.3.1.5* | Time constant for $m_A$ (sec). |
| $\tau_{m,\mathrm{BK}}$ | 3.3.2.3 | Time constant for $m_{BK}$ (sec). |
| $\tau_{m,\,HVA}$ | 3.3.5.16 | Time constant for $m_{HVA}$ (sec). |
| $\tau_{m,\,HVA}$ | 3.3.5.9 | Time constant for $m_{LVA}$ (sec). |
| $\tau_{m,\mathrm{IK}}$ | 3.3.2.7 | Time constant for $m_{IK}$ (sec). |

Table 3.2 (Continued)

| Symbol | Equation | Description |
|---|---|---|
| $\tau_{m,\mathrm{M}}$ | 3.3.1.8 | Time constant for $m_M$ (sec). |
| $\tau_{m,ryanodine}$ | 3.7.14 | Time constant for $m_{ryanodine}$ (sec). |
| $\tau_{m,\mathrm{SK}}$ | 3.3.2.12 | Time constant for $m_{SK}$ (sec). |
| $\tau_x$ | 3.3.4 | Time constant of Hodgkin-Huxley variable $x$. |

## 3.2. ELECTRODIFFUSION MODEL

A separate equation is used to describe the intracellular and extracellular concentrations of each species ($Ca^{++}$, $Cl^{-}$, $K^{+}$ and $Na^{+}$). The intracellular concentration $c_{in}$ of each ion is described by the electrodiffusion equation (Qian and Sejnowski, 1989)

$$\frac{\partial c_{in}}{\partial t} = \frac{\partial}{\partial x}\left(D_{c,in}\frac{\partial c_{in}}{\partial x}\right) + \frac{zF}{RT}\frac{\partial}{\partial x}\left(c_{in}D_{c,in}\frac{\partial E}{\partial x}\right) - rJ_{c,m} + s_c \qquad (1)$$

where $D_c$ is the cytoplasmic diffusion constant of $c$, $z$ is the valence, $E$ is the membrane voltage, $r$ is the average dendritic surface area to volume ratio ($r = 4/d$ for a cylindrical process of diameter $d$), $J_{c,m}$ is the membrane ion flux of $c$ (in mM/cm$^2$-sec), including ion pumps, and the source term $s_c$ describes the intracellular production of $c$ ($Ca^{++}$ only). The movement of ions through gap junctions is described by $D_{c,in}$ (Keener and Sneyd, 1998). The diffusion constant $D_{c,in}$ is left inside the derivatives in equation 1 because gap junction gating is usually voltage- and calcium-dependent, and hence position-dependent. The expression "cytoplasmic diffusion" is taken to refer to diffusion through an intracellular continuum of separate cells connected via gap junctions and does not necessarily mean that ions are spatially restricted to the interior of a single cell.

Figure 3.3 (Following Page) . Summary of the ionic fluxes included in the model. There are three voltage gated potassium channels (VGKC), the delayed rectifier (DR), the muscarinic (M) and the A-type channel. Three calcium-sensitive potassium channels (K(Ca)) are included, the large conductance (BK) that is Ca and voltage depdendent, the small conductance (SK) channel that is voltage insensitive, and an intermediate conductance channel (IK) that is both voltage and calcium dependent. Voltage gated calcium channels (VGCC) include high-voltage activated (HVA) and low-voltage activated (LVA) currents. Voltage gated sodium channels (VGNaC) include both fast and persistent channels. Cl flux is passive. The NMDA-receptor allows passage of Ca, Na, and K, which are all treated independently from one another. Neuronal pumps include an Na, K exchanger; a Na, Ca exchanger; an ATP-dependent Ca pump; and a Cl, bicarbonate pump. Glial pumps include the Na, K exchanger; the Cl,bicarbonate pump; and a Na, Cl, K pump. Leakage of Ca, Na, and K is described by a Goldman equation. The endoplasmic reticulum functions as a large buffer, with both IP3-sensitive and Ryanonide-sensitive channels, and a Ca pump. Both of the ion channels are also sensitve to cytoplasmic calcium concentrations. IP3 is generated by membrane stretch, and both the BK-channel and the DR-channel are stretch senstive. Water is allowed to pass into or out of the cell in response to osmotic forces.

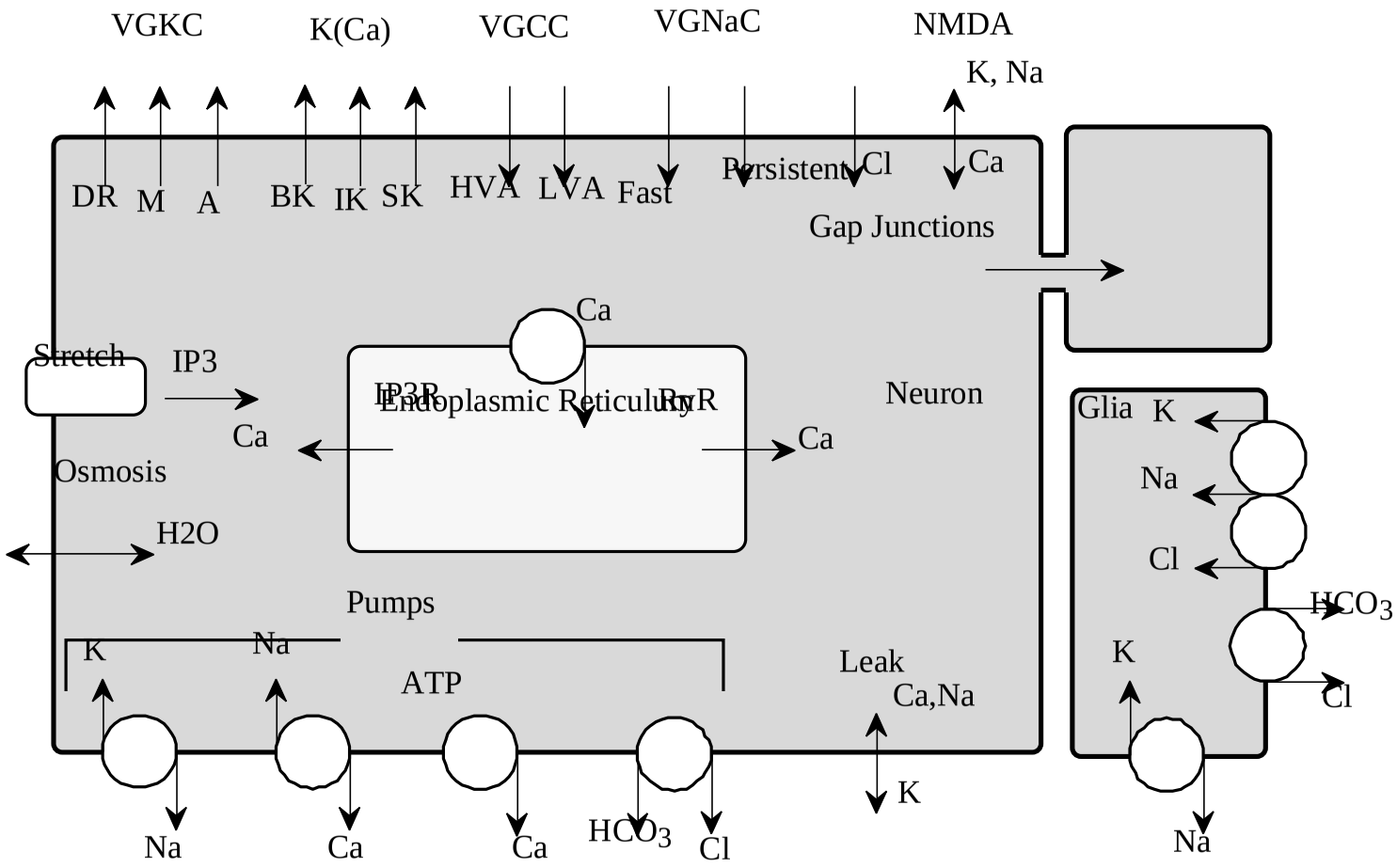
VGKC
K(Ca)
VGCC
VGNaC
NMDA
K, Na
DR
M
A
BK
IK
SK
HVA
LVA
Fast
Persistent
Cl
Ca
Gap Junctions
Ca
Stretch
IP3
IP3R
Endoplasmic Reticulum
RyR
Neuron
Ca
Ca
Osmosis
H2O
Pumps
K
Na
ATP
Leak
Ca,Na
K
Na
Ca
Ca
HCO3
Cl
Glia
K
Na
Cl
HCO3
K
Cl
Na

The electro-diffusion equation has not been previously used to describe spreading depression and is rarely used in neuronal simulations. The derivation given by Qian and Sejnowski (1989) assumes cylindrical symmetry but it is possible to derive equation 1 under less severe restrictions (as will be done in the following section).

The individual membrane currents are illustrated in Figure 3.3, and are described in more detail in section 3.3. For potassium, equation 1 becomes

$$\frac{\partial\left[\mathrm{K}^{+}\right]_{in}}{\partial t} = \frac{\partial}{\partial x}\left(D_{K,in}\frac{\partial\left[\mathrm{K}^{+}\right]_{in}}{\partial x}\right) + \frac{F}{RT}\frac{\partial}{\partial x}\left(\left[\mathrm{K}^{+}\right]_{in} D_{K,in}\frac{\partial E}{\partial x}\right) - rJ_{K,m} \qquad (2)$$

where the $K^+$ membrane flux is

$$J_{K,m} = j_A + j_M + j_{DR} + j_{BK} + j_{IK} + j_{SK} + j_{K,NMDA} + j_{K,leak} - j_{Na/K} \qquad (3)$$

Membrane currents are taken to be positive out. However, the expression for $j_{Na,K}$ given in section 3.6 is expressed as the magnitude of the $K^+$ flux, hence the minus sign in equation 3. For calcium equation 1 becomes

$$\frac{\partial\left[\mathrm{Ca}^{++}\right]_{in}}{\partial t} = \frac{\partial}{\partial x}\left(D_{Ca,in}\frac{\partial\left[\mathrm{Ca}^{++}\right]_{in}}{\partial x}\right) + \frac{2F}{RT}\frac{\partial}{\partial x}\left(\left[\mathrm{Ca}^{++}\right]_{in} D_{Ca,in}\frac{\partial E}{\partial x}\right) - rJ_{Ca,m} + s_{Ca} \qquad (4)$$

where the $Ca^{++}$ membrane flux is

$$J_{Ca,m} = j_{LVA} + j_{HVA} + j_{Ca,Leak} + j_{Ca,Na/Ca} + j_{Ca,ATP} + j_{Ca,NMDA} \qquad (5)$$

and the $Ca^{++}$ sources are described by

$$s_{Ca} = j_{IP3} + j_{Ryanodine} - j_{Pump} \qquad (6)$$

In equation 6 ions are removed from the cytosol and pumped into the ER by the ER-membrane pump term $j_{Pump}$. The terms in equation 6 are taken to be positive for pumping out of the ER (i.e., positive for pumping into the cytosol). For $Na^+$ equation 1 becomes

$$\frac{\partial[\mathrm{Na}^+]_{in}}{\partial t} = \frac{\partial}{\partial x}\left(D_{Na,in}\frac{\partial[\mathrm{Na}^+]_{in}}{\partial x}\right) + \frac{F}{RT}\frac{\partial}{\partial x}\left([\mathrm{Na}^+]_{in} D_{Na,in}\frac{\partial E}{\partial x}\right) - rJ_{Na,m} \qquad (7)$$

where the $Na^+$ membrane flux is

$$J_{Na,m} = j_F + j_P + \frac{3}{2} j_{Na,K} - j_{Na,Ca} + j_{Na,NMDA} + j_{Na,Leak} \qquad (8)$$

The sign of the $j_{Na,Ca}$ is negative because the expression for $j_{Na,Ca}$ in section 3.3.6 gives the inward current. The factor of 3/2 multiplies $j_{Na,K}$ because this ATP-driven pump removes 3 $Na^+$ ions for every 2 $K^+$ ions pumped into the cytosol. The expression for $j_{Na,K}$ in section 3.3.6 gives the $K^+$ flux. For $Cl^-$ equation 1 becomes

$$\frac{\partial[\mathrm{Cl}^-]_{in}}{\partial t} = \frac{\partial}{\partial x}\left(D_{Cl,in}\frac{\partial[\mathrm{Cl}^-]_{in}}{\partial x}\right) - \frac{F}{RT}\frac{\partial}{\partial x}\left([\mathrm{Cl}^-]_{in} D_{Cl,in}\frac{\partial E}{\partial x}\right) - rJ_{Cl,m} \qquad (9)$$

Since chlorine is the only cation included in the model, a passive membrane $Cl^-$ current is calculated to balance the total anion current.

$$J_{Cl,m} = J_{Cl,bicarb} + J_{K,m} + J_{Na,m} \qquad (10)$$

Because the total $Ca^{++}$ current is several orders of magnitude smaller, it is omitted from this calculation.

Extracellular ionic concentrations are described by a standard reaction-diffusion equation with glial uptake,

$$\frac{\partial c_{out}}{\partial t} = D_{c,out}\frac{\partial^2 c_{out}}{\partial x^2} + \frac{rf}{1-f}J_{c,m} - J_{c,glia} \tag{11}$$

where $D_{c.out}$ is the extracellular diffusion constant of $c$, $f$ is the neuronal volume fraction, and $J_{c,glia}$ describes glial uptake. For potassium, equation 11 becomes

$$\frac{\partial[\mathrm{K}^+]_{out}}{\partial t} = D_{K,out}\frac{\partial^2[\mathrm{K}^+]_{out}}{\partial x^2} + \frac{rf}{1-f}J_{K,m} - J_{K,glia} \tag{12}$$

For calcium equation 11 becomes

$$\frac{\partial[\mathrm{C}a^{++}]_{out}}{\partial t} = D_{Ca,out}\frac{\partial^2[\mathrm{C}a^{++}]_{out}}{\partial x^2} + \frac{rf}{1-f}J_{Ca,m} \tag{13}$$

For sodium equation 11 becomes

$$\frac{\partial[\mathrm{N}a^+]_{out}}{\partial t} = D_{Na,out}\frac{\partial^2[\mathrm{N}a^+]_{out}}{\partial x^2} + \frac{rf}{1-f}J_{Na,m} \tag{14}$$

For chlorine equation 11 becomes

$$\frac{\partial[\mathrm{Cl}^-]_{out}}{\partial t} = D_{Cl,out}\frac{\partial^2[\mathrm{Cl}^-]_{out}}{\partial x^2} + \frac{rf}{1-f}J_{Cl,m} \tag{15}$$

### 3.2.1. Derivation of Electrodiffusion Equation

The derivation starts with the continuity equation for particle conservation (McQuarrie, 1976, pp. 380-381),

$$\nabla \cdot \mathbf{J}(\mathbf{x},t) + \frac{\partial c(\mathbf{x},t)}{\partial t} = f(\mathbf{x},t) \qquad (1)$$

where $\mathbf{J} = \mathbf{n}J$, $\mathbf{n}$ is a unit vector in the direction of particle flux, $J$ is the particle flux in mM/cm$^2$-sec, $c$ is the particle concentration in mM/l, and $f(\mathbf{x},t)$ is the rate of production of particles at $\mathbf{x}$. Ionic fluxes are given by the Nernst-Planck equation (Keener and Sneyd, 1998, page 54)

$$\mathbf{J}(\mathbf{x},t) = -D(\mathbf{x},t)\left(\nabla c(\mathbf{x},t) + \frac{zF}{RT} c(\mathbf{x},t)\nabla E(\mathbf{x},t)\right) \qquad (2)$$

where $D(x, t)$ is the diffusion constant in μm$^2$/sec (which is allowed to take on different values at different locations), $E$ is the voltage in mV, $R$ is the ideal gas constant (≈8.3143 J/mM-˚K), $T$ is the temperature in Kelvins, $F$ is Faraday's Constant (≈96.48 coulombs/mM), and $z$ is the valence. Substituting equation 2 into equation 1 gives the electrodiffusion equation in its most general form

$$\frac{\partial c(\mathbf{x},t)}{\partial t} = \nabla \cdot \left(D(\mathbf{x},t)\nabla c(\mathbf{x},t)\right) + \frac{zF}{RT}\nabla \cdot \left(D(\mathbf{x},t)c(\mathbf{x},t)\nabla E(\mathbf{x},t)\right) + f(\mathbf{x},t) \qquad (3)$$

In one dimension equation 3 reduces to equation 1 of the section 3.2 ("Electrodiffusion Model") as will be shown in section 3.2.2 ("Electrodiffusion in One Dimension"). The diffusion constant $D$ will generally not be a constant because of the presence of gap

junctions. These may open in response to membrane stretch, and may close in the presence of large voltage gradients or increased $Ca^{++}$ or $H^{+}$ concentrations. Equation 3 differs from the usual reaction-diffusion equation

$$\frac{\partial c}{\partial t} = \quad \cdot (D \quad c) + f \qquad (4)$$

by the presence of the second term on the right hand side. Equation 3 has been applied to ionic fluxes in plasmas (Chen, 1974, page 138) and electron and hole fluxes in a semiconductor (Sze, 1969, page 66; Ashcroft and Mermin, 1976, page 601). It was first applied to membrane ion fluxes by Qian and Sejnowski (1989) who showed that when the changes in the ionic concentrations are small with respect to the total ionic concentrations for each ion, equation 3 is equivalent to the cable equation for dendritic membranes

### 3.2.2. ELECTRODIFFUSION IN ONE DIMENSION

Qian and Sejnowski (1989) derived a one-dimensional electro-diffusion equation by assuming cylindrical symmetry. This assumption is not necessary. Consider a length of dendrite, of length $\Delta x$, oriented along the $x$-axis, with total volume $\Theta$ and surface area $\Sigma$, as illustrated in Figure 3.4. The dendrite may or may not have spines. The surface area $\Sigma$ is composed of three parts: the ends, which are normal to the $x$ -axis, and the dendritic membrane. Designate the membrane surface area, including the surface area of any spines, by $A$, and the cross-sectional area at $x$ by the function $S(x)$. The cross-sectional area may pass through some spines. Then

$$\lim_{\Delta x \to 0} \frac{\Delta x S(x)}{\Theta} = 1 \tag{1}$$

regardless of the shape of the cross-section. By conservation of particles, the rate at which the concentration $c$ of any ionic species changes in $\Theta$ is related to the flux of particles across $\Sigma$ by the continuity equation

$$\cdot \mathbf{J} + \frac{\partial c}{\partial t} = f \tag{2}$$

where $f$ is the rate at which particles are produced within $\Theta$. Integrating equation 2 over the volume $\Theta$,

$$\iiint_{\Theta} \left( f - \frac{\partial c}{\partial t} \right) dV = \iiint_{\Theta} \cdot \mathbf{J} dV \tag{3}$$

Define $\langle f \rangle$, the average rate of ionic production in $\Theta$, as

$$\langle f \rangle = \frac{1}{\Theta} \iiint_{\Theta} f dV \tag{4}$$

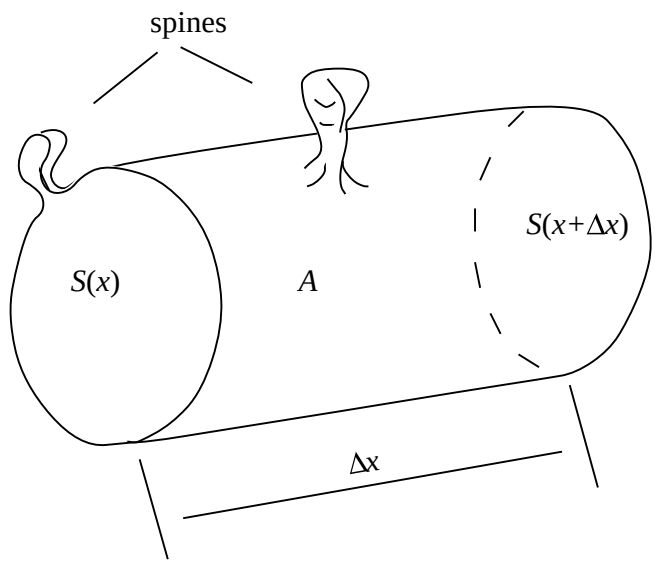


Figure 3.4. Volume element of dendrite used in derivation of the electro-diffusion equation. The dendrite may or may not have spines. The cross-sectional area normal to the $x$-axis is described by a function $S(x)$, and the membrane surface area is $A$. The total volume is $\Theta$ and the total surface area of the element is $\Sigma = S(x) + A + S(x+\Delta x)$

and $\langle c \rangle$, the average concentration in $\Theta$, as

$$\langle c \rangle = \frac{1}{\Theta} \iiint_{\Theta} c\,dV \tag{5}$$

Then the left side of equation 3 becomes

$$\iiint_{\Theta} \left( f - \frac{\partial c}{\partial t} \right) dV = \Theta \left[ \langle f \rangle - \frac{\partial}{\partial t} \langle c \rangle \right] \tag{6}$$

By the divergence theorem, the right hand side of equation 3

$$\begin{aligned} \iiint_{\Theta} \quad \cdot \mathbf{J}\,dV &= \iint_{\Sigma} \mathbf{J} \cdot d\mathbf{A} \\ &= \iint_{S(x)} \mathbf{J} \cdot d\mathbf{A} + \iint_{S(x+\Delta x)} \mathbf{J} \cdot d\mathbf{A} + \iint_{A} \mathbf{J} \cdot d\mathbf{A} \\ &= S\left[ \langle J_x(x+\Delta x) \rangle - \langle J_x(x) \rangle \right] + A \langle J_m(x) \rangle \end{aligned} \tag{7}$$

where $\langle J_x(x) \rangle$ is the average longitudinal ion flux at $x$ and $\langle J_m(x) \rangle$ the average ion flux across the membrane between $x$ and $x + \Delta x$. Dividing by the volume and taking the limit as $\Delta x \to 0$

$$\begin{aligned} &\lim_{\Delta x \to 0} \frac{1}{\Theta} \iiint_{\Theta} \quad \cdot \mathbf{J}\,dV \\ &= \lim_{\Delta x \to 0} \left\{ \frac{S\Delta x}{\Theta} \frac{\left[ \langle J_x(x+\Delta x) \rangle - \langle J_x(x) \rangle \right]}{\Delta x} + \frac{A \langle J_m(x) \rangle}{\Theta} \right\} \\ &= \frac{\partial \langle J_x(x) \rangle}{\partial x} + r(x) \langle J_m(x) \rangle \end{aligned} \tag{8}$$

The first term in the last line of equation 8 follows from equation 1 and the definition of a derivative. In the second term $r(x)$ is defined as the membrane-area-to-volume ratio at $x$,

$$r(x) = \lim_{\Delta x \to 0} \frac{A}{\Theta} = \frac{C(x)}{S(x)} \tag{9}$$

where $C$ is the circumference of $S$. For a cylindrical dendrite of diameter $d$, $r$(x)= 4/$d$. By equations 3 and 6,

$$\begin{aligned} \lim_{\Delta x \to 0} \frac{1}{\Theta} \iiint_{\Theta} \mathbf{J}\, dV &= \lim_{\Delta x \to 0} \frac{1}{\Theta} \iiint_{\Theta} \left( f - \frac{\partial c}{\partial t} \right) dV \\ &= \lim_{\Delta x \to 0} \frac{1}{\Theta} \left( \Theta \langle f \rangle - \Theta \frac{\partial \langle c \rangle}{\partial t} \right) \\ &= \langle f \rangle - \frac{\partial \langle c \rangle}{\partial t} \end{aligned} \tag{10}$$

By equating the last expression in equation 8 with the last expression in equation 10,

$$\frac{\partial \langle J_x(x) \rangle}{\partial x} + r(x) \langle J_m(x) \rangle = \langle f \rangle - \frac{\partial \langle c \rangle}{\partial t} \tag{11}$$

Rearranging terms and omitting the angle brackets,

$$\frac{\partial c}{\partial t} = -\frac{\partial J_x}{\partial x} - r J_m + f \tag{12}$$

Alternatively, one could assume that both the longitudinal current and the cytoplasmic concentration are constant across $S$, and that the membrane current is constant around $C$. In this case, the above derivation holds for the exact values of $J_m$, $J_z$ and $c$, without the need to resort to averaging. The longitudinal flux is given by Nernst-Planck equation, which in one dimension is

$$J_x = -D \frac{\partial c}{\partial x} - \frac{zFDc}{RT} \frac{\partial E}{\partial x} \tag{13}$$

where $z$ is the valence and $E$ is the voltage. The diffusion constants are assumed to be a function of position. Hence

$$\frac{\partial c}{\partial t} = \frac{\partial}{\partial x}\left(D\frac{\partial c}{\partial x}\right) + \frac{zF}{RT}\frac{\partial}{\partial x}\left(Dc\frac{\partial E}{\partial x}\right) - rJ_m + f \qquad (14)$$

which is the same equation derived by Qian and Sejnowski, with $4/d$ (in Qian and Sejnowski's version) replaced by $r$ (see equation 1 of section 3.2).

## 3.3. MEMBRANE CURRENTS

The membrane currents that are included in the model are illustrated in Figure 3.3. Standard biophysical models are used to describe the membrane currents; ion channels are described by the Hodgkin-Huxley formalism (Hodgkin and Huxley, 1952). In this formalism channel gating is described by activation or inactivation variables (*m*, *h*, *n*, and *x*) which relax exponentially to their steady state values $x_\infty$ with some time constant $\tau_x$,

$$\frac{dx}{dt} = \frac{x_\infty - x}{\tau_x} \tag{1}$$

Both $\tau_x$ and $x_\infty$ may be concentration and/or voltage dependent. In some cases, explicit formulas are given; in other cases they are given in terms of forward and backward rate constants $\alpha_x$ and $\beta_x$, where

$$\tau_x = \frac{1}{\alpha_x + \beta_x} \tag{2}$$

$$x_\infty = \frac{\alpha_x}{\alpha_x + \beta_x} \tag{3}$$

Then the membrane flux is

$$j = \frac{g m^p h^q}{F}\left(E - E_c\right) \tag{4}$$

where *g* is the membrane conductivity of the given channel in pS/μm$^2$, *p* and *q* are integers specified by the model, and $E_c = (RT / zF)\ln(c_{out} / c_{in})$ is the Nernst potential for *c*. The membrane voltage is calculated using the Goldman-Hodgkin-Katz equation (equation 2.7.21 of Johnston and Wu , 1995),

$$E = \frac{RT}{F} \ln \frac{P_K[\mathrm{K}^+]_{out} + P_{Na}[\mathrm{Na}^+]_{out} + P_{Cl}[\mathrm{Cl}^-]_{in}}{P_K[\mathrm{K}^+]_{in} + P_{Na}[\mathrm{Na}^+]_{in} + P_{Cl}[\mathrm{Cl}^-]_{out}} \tag{5}$$

The units in all equations are millimolar for concentration; seconds for time; and pico-Siemen/$\mu m^2$ for conductance unless otherwise specified. Specific biophysical models are used to describe ion channels for potassium, sodium and calcium. Chlorine, on the other hand, is the only membrane-permeant anion considered, and as such, a passive chlorine flux is calculated to balance the cation flux. Thus the chlorine flux presented here may actually represent the total membrane anion flux.

### 3.3.1. VOLTAGE GATED POTASSIUM CURRENTS

The model includes three voltage gated potassium channels as illustrated in Figure 3.3: the delayed rectifier (DR); the transient potassium current (A-channel or KA channel); and the non-inactivating muscarinic potassium current (M-channel). All three channels have been observed in gray matter.

The A-channel is a transient, rapidly activating and inactivating channel that is selective for potassium and is thought to contribute to spike repolarization. Transient A-channel currents have been observed in hippocampal pyramidal cell dendrites (Hoffman and others, 1997) with a conductance of $g_A \approx 20$ to $\approx 120$ pS/μm$^2$, while Traub estimates $g_A \approx 5$ pS/μm$^2$ (Traub and others, 1994). In cerebellar Purkinje cells $g_A \approx 2$ pS/μm$^2$ in dendrites and $g_A \approx 15$ pS/μm$^2$ in somata (De Schutter and Bower, 1994), while in soma of bullfrog sympathetic ganglion cells $g_A \approx 25$ pS/μm$^2$ (Yamada, Koch and Adams, 1998). The model of Yamada, Koch and Adams (1998) is used to describe this current.

$$j_A = \frac{g_A m_A h_A}{F}\left(E - E_K\right) \qquad (1)$$

where $E_K$ is the Nernst potential for potassium, $m_A$ is a Hodgkin-Huxley variable describing channel activation, and $h_A$ is a Hodgkin-Huxley inactivation variable,

$$\frac{dm_A}{dt} = \frac{m_{A,\infty} - m_A}{\tau_{m,A}} \qquad (2)$$

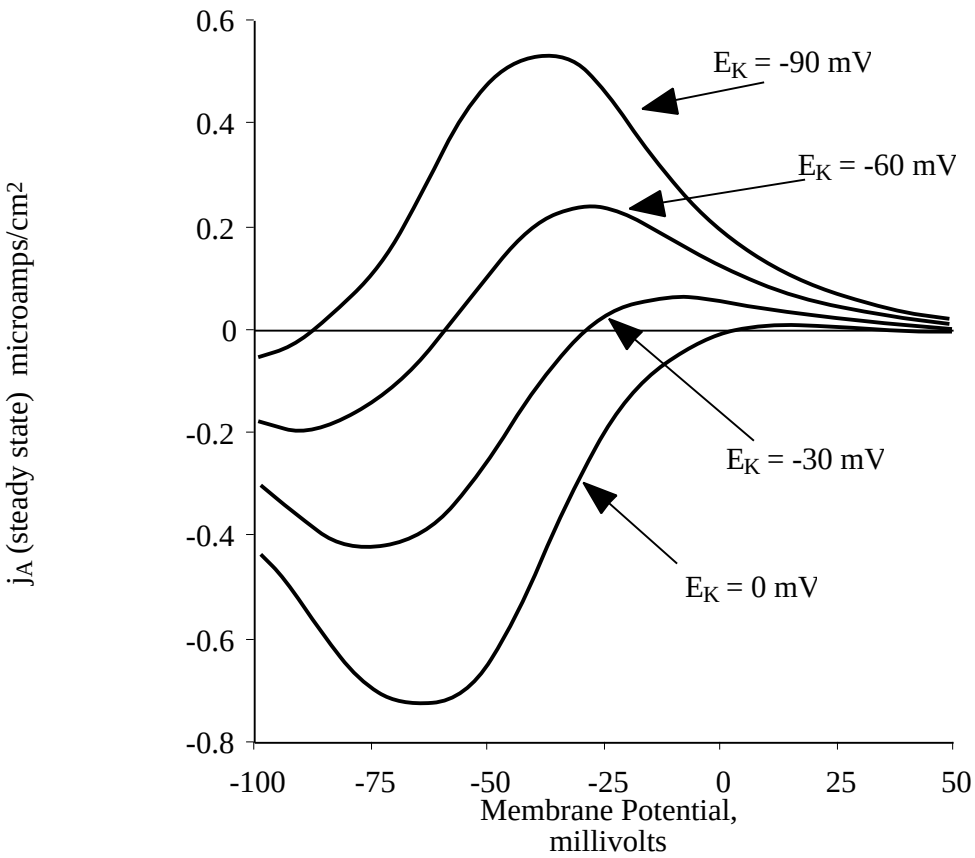


Figure 3.5. Steady state A-channel current for four different reversal potentials, for $g_A$=10 pS/μm$^2$. The current is given by equation 1 with $m_A = m_{A,\infty}$ and $h_A = h_{A,\infty}$ where $m_{A,\infty}$ is given by equation 4 and $h_{A,\infty}$ is given by equation 5.

$$\frac{dh_A}{dt} = \frac{h_{A,\infty} - h_A}{\tau_{h,A}} \tag{3}$$

The steady state values of the Hodgkin-Huxley variables are voltage dependent,

$$m_{A,\infty} = \frac{1}{1 + e^{-(E+42)/13}} \tag{4}$$

$$h_{A,\infty} = \frac{1}{1 + e^{(E+110)/18}} \tag{5}$$

\where $\tau_{m,A}$=1.38 msec and $\tau_{h,A}$=50 mS when $E$<-80 mV and $\tau_{h,A}$=150 mS when E ≥ -80 mV. The steady state A-channel current predicted by this model is illustrated in Figure 3.5.

The M-channel allows a non-inactivating potassium current that can be blocked by cholinergic muscarinic agonists (that actually act as antagonists at this particular channel). In pyramidal cell dendrites $g_M$ ≈20 pS/μm$^2$ (Mainen and Sejnowski, 1998), and in the bullfrog sympathetic ganglion cells $g_M$ ≈17 pS/μm$^2$ (Yamada, Koch and Adams, 1998). In the dendrites of cerebellar Purkinje cells $g_M$≈0.1 to 0.4 pS/μm$^2$, and in their somas $g_M$≈0.4 to 1.4 pS/μm$^2$ (De Schutter and Bower, 1994). The M-channel is described by the model of Yamada, Koch and Adams (1998).

$$j_M = \frac{g_M m_M}{F}\left(E - E_K\right) \tag{6}$$

where $m_M$ is a Hodgkin-Huxley activation variable, satisfying

$$\frac{dm_M}{dt} = \frac{m_{M,\infty} - m_M}{\tau_{m,M}} \tag{7}$$

The time constant and steady state activation are both voltage dependent,

$$\tau_{m,M} = \frac{1}{3.3\left[e^{(E+35)/40} + e^{-(E+25)/20}\right]} \tag{8}$$

$$m_{M,\infty} = \frac{1}{1+e^{-(E+35)/1}} \tag{9}$$

The steady state current predicted by this model is illustrated in Figure 3.6.

The delayed rectifier is expressed in various isoforms throughout the nervous system, and it is the principal contributor to post-spike repolarization after an action potential. It has slower kinetics than the A-channel and M-channel. The axonal DR-channel conductivity ranges from $g_{DR}$ ≈300 pS/μm$^2$ to ≈3000 pS/μm$^2$ (Hille, 1992). In hippocampal pyramidal cells, measurements indicate that $g_{DR}$ ≈ 15 to ≈ 23 pS/μm$^2$ in the dendrites and $g_{DR}$ ≈ 1350 pS/μm$^2$ in somata (Traub and others, 1994; Hoffman and others, 1997). In Purkinje cells the dendritic conductance has been estimated to be in the range from $g_{DR}$≈600 to $g_{DR}$≈900 pS/μm$^2$ and the somatic conductance to be in the range ≈6000 to 9000 pS/μm$^2$ (de Schutter and Bower, 1995). In bullfrog sympathetic ganglion cells $g_{DR}$ ≈ 230 pS/μm$^2$ (Yamada, Koch and Adams, 1998). The delayed rectifier is described by the model of Yamada, Koch and Adams (1998).

$$j_{DR} = \frac{g_{DR} m_{DR}^2 h_{DR}}{F}\left(E - E_K\right) \tag{10}$$

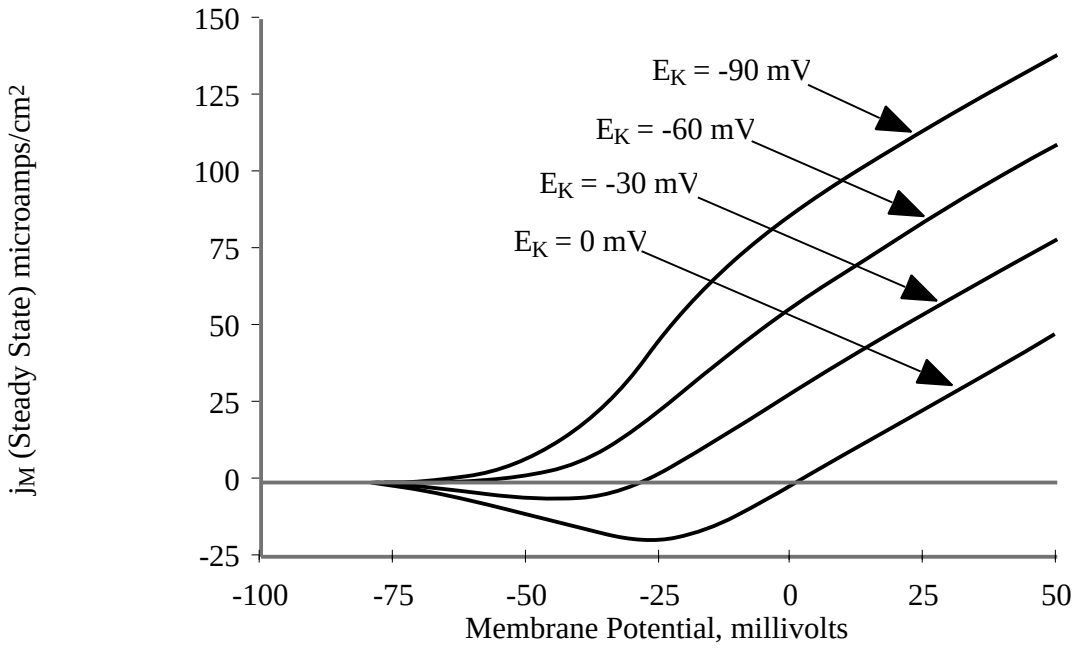


Figure 3.6. Steady state M-channel with $g_M$=10 pS/μm$^2$ for four different potassium reversal potentials. The steady state current is given by equation 6 with $m_M = m_{M,\infty}$, where $m_{M,\infty}$ is given by equation 9.

where $m_{DR}$ is a Hodgkin-Huxley activation variable, and $h_{DR}$ is an inactivation variable,that satisfy

$$\frac{dm_{DR}}{dt} = \frac{m_{DR,\infty} - m_{DR}}{\tau_{m,DR}} \tag{11}$$

$$\frac{dh_{DR}}{dt} = \frac{h_{DR,\infty} - h_{DR}}{\tau_{h,DR}} \tag{12}$$

The steady state activation is expressed in terms of the forward and reverse voltage-dependent rate constants $\alpha_{m,,DR}$ and $\beta_{m,DR}$, as

$$m_{DR,\infty} = \frac{\alpha_{m,DR}(E-20)}{\alpha_{m,DR}(E-20) + \beta_{m,DR}(E-20)} \tag{13}$$

where

$$\alpha_{m,DR}(E) = \frac{0.0047(E+12)}{1-e^{-(E+12)/12}} \tag{14}$$

$$\beta_{m,DR}(E) = e^{-(E+147)/30} \tag{15}$$

The activation time constant for $m_{DR}$ is given

$$\tau_{m,DR} = \frac{1}{\alpha_{m,DR}(E) + \beta_{m,DR}(E)} \tag{16}$$

The steady state value of the inactivation variable $h_{DR}$ is

$$h_{DR,\infty} = \frac{1}{1+e^{(E+25)/}} \tag{17}$$

where $\tau_{h,DR}$ = 6 sec for $E$ < -25 mV and 50 msec for E ≥ -25 mV (step function). The steady state current is illustrated in Figure 3.7 for several values of $E_K$.

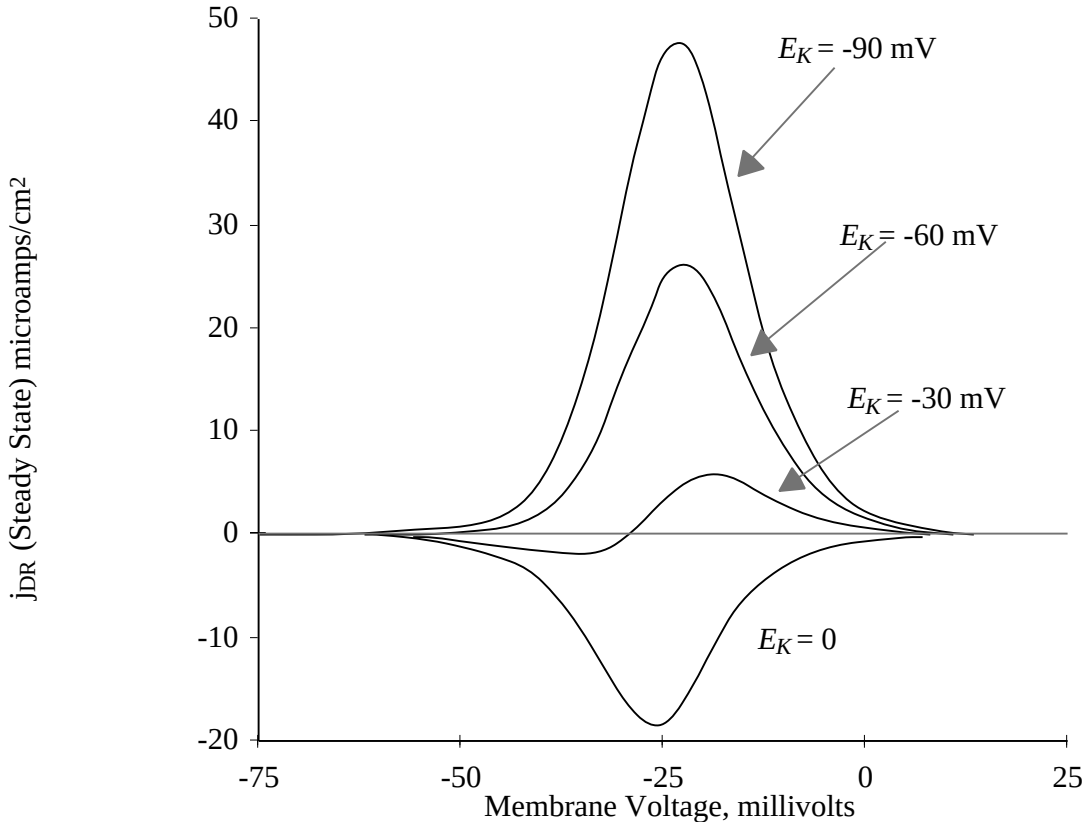


Figure 3.7. Steady state current for delayed rectifier model, with $g_{DR}$=250 pS/μm$^2$ for four different Nernst potentials for potassium. The steady state current is given by equation 10 with $m_{DR} = m_{DR,\infty}$ and $h_{DR} = h_{DR,\infty}$, where $m_{DR,\infty}$ and $h_{DR,\infty}$ are given by equations 13 and 17.

### 3.3.2. Calcium Dependent Potassium Currents

At least three classes of calcium-gated potassium channels (K(Ca)) have been identified in neurons (Blatz and Magleby, 1987; Sah, 1996; Vergara and others, 1998). These are classified based on their calcium and voltage sensitivity and pharmacological properties. The large conductance (BK) channel is both voltage- and calcium-dependent, is at least partially blocked by TEA (tetraethylammonium) and CTX (charybdotoxin), and has a single channel conductance of ≈200 pS to ≈250 pS. Small conductance (SK) channels have single channel conductances of ≈4 pS to ≈20 pS, are insensitive to both TEA and CTX, and have at least two subtypes: those that are sensitive to apamin and those that are insensitive to apamin. A third class of K(Ca) channels have intermediate single channel conductances (IK) ranging from ≈20 pS to ≈120 pS. IK channels are sensitive to both CTX and clotrimazole, and are both calcium-sensitive and voltage-sensitive. In many neurons two types of "slow after-hyperpolarization" (sAHP) currents have been identified: apamin-sensitive and apamin-insensitive. These are usually associated with SK or IK channels. In cerebellar Purkinje cells K(Ca) channels have been identified that activate at lower calcium concentrations than the BK channels and are sensitive to both TEA and CTX (Farley and Rudy, 1988; Reinhart, Chung, and Levitan, 1989; Groul and others, 1991); these may correspond to IK channels, or there may be two sub-populations of BK channels.

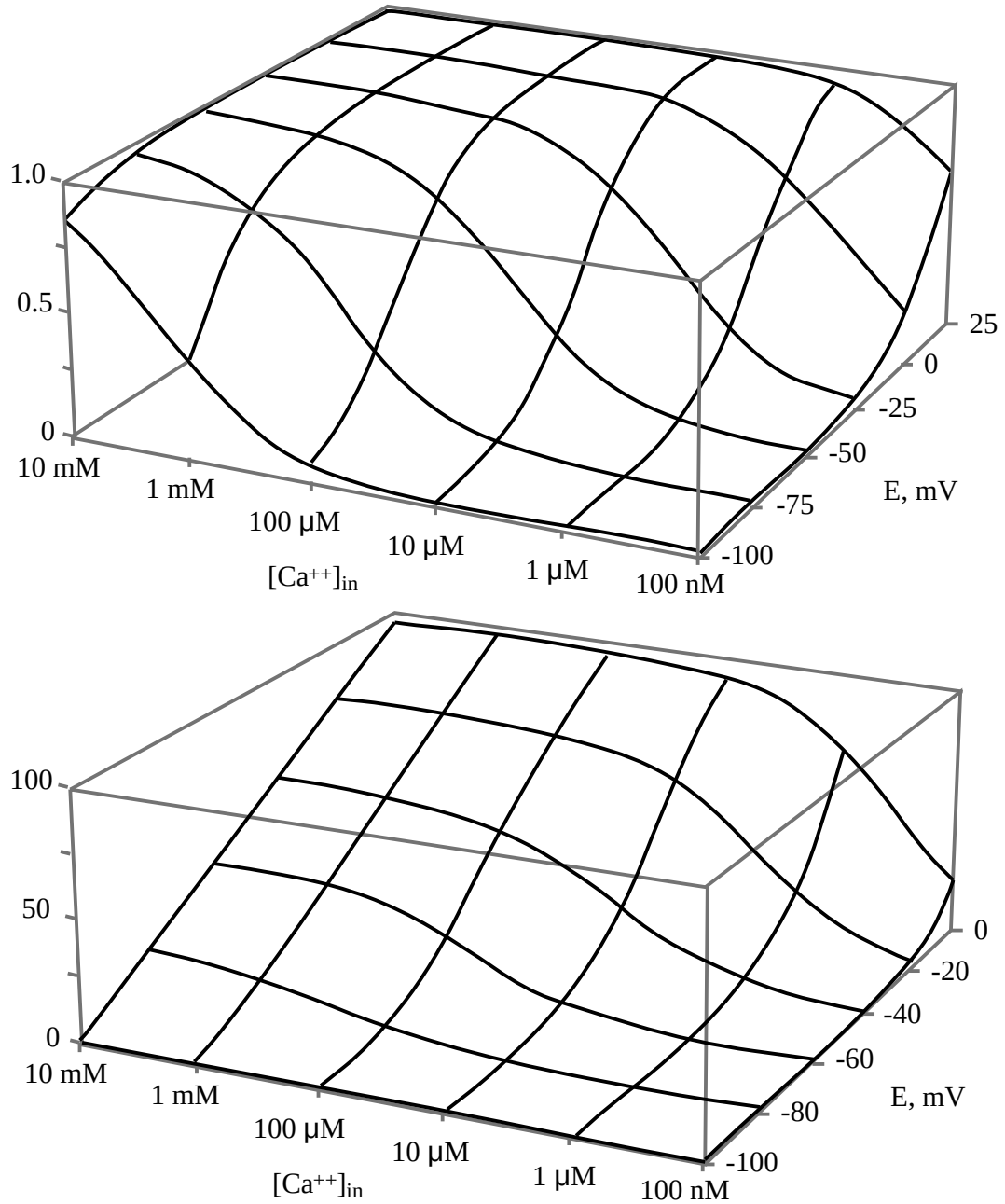


Figure 3.8. Steady state activation of BK channel. Top: activation variable $m_\infty$ (equation 4) assuming $E_K$=-100. Bottom: Steady state current in μA/cm$^2$ (equation 1 with $m = m_\infty$ and $g_{BK}$=10 pS/μm$^2$).

The contribution to membrane conductance by the BK channel has been estimated at $g_{BK}$ ≈800 pS/μm$^2$ in Purkinje cell dendrites (De Schutter and Bower, 1994), at $g_{BK}$ ≈40 to ≈120 pS/mμ$^2$ in hippocampal pyramidal cell dendrites, at $g_{BK}$ ≈200 pS/μm$^2$ in hippocampal pyramidal cell somata (Traub and others, 1994), and at $g_{BK}$ ≈240 pS/μm$^2$ in bullfrog sympathetic ganglion cells (Yamada, Koch and Adams, 1998). The model of Yamada, Koch and Adams (1998) is used for this conductance

. $$j_{BK} = \frac{g_{BK} m_{BK}}{F}\left(E - E_K\right), \tag{1}$$

where $m$ is a Hodgkin-Huxley activation variable that satisfies

$$\frac{dm_{BK}}{dt} = \frac{m_{BK,\infty} - m_{BK}}{\tau_{m,BK}} \tag{2}$$

where the time constant $\tau_{m,BK}$ and steady state activation $m_{BK,\infty}$ are given by

$$\tau_{m,BK} = \frac{0.001}{250\left[Ca^{++}\right]_{in} e^{E/24} + 0.1e^{-E/24}} \tag{3}$$

$$m_{BK,\infty} = \frac{250\left[Ca^{++}\right]_{in} e^{E/24}}{250\left[Ca^{++}\right]_{in} e^{E/24} + 0.1e^{-E/24}} \tag{4}$$

The steady state activation and steady state current for the BK channel model are illustrated in Figure 3.8.

The K2-channel model of De Schutter and Bower (1994), who estimate $g_{K2}$ ≈ 4 pS/μm$^2$ in Purkinje-cell dendrites, is used for the IK channel. In this model,

$$j_{IK} = \frac{g_{IK} m_{IK}}{F}\left(\frac{[Ca^{++}]_{in}}{[Ca^{++}]_{in} + 0.0002}\right)^2 (E - E_K) \tag{5}$$

where $[Ca^{++}]_{in}$ is measured in mM, and $m_{IK}$ is a Hodgkin–Huxley activation variable satisfying

$$\frac{dm_{IK}}{dt} = \frac{m_{IK,\infty} - m_{IK}}{\tau_{m,IK}} \tag{6}$$

The steady state activation and time constants are given in terms of the rate constants $\alpha_{IK}$ and $\beta=_{IK}$ as

$$\tau_{m,IK} = \frac{1}{\alpha_{IK} + \beta_{IK}} \tag{7}$$

and

$$m_{IK,\infty} = \frac{\alpha_{IK}}{\alpha_{IK} + \beta_{IK}} \tag{8}$$

In equations 7 and 8 $\alpha_{IK}$= 25 $sec^{-1}$ (fixed) and $\beta_{IK}$ is given by the voltage dependent function

$$\beta_m = 0.075e^{(E+5)/1(} \tag{9}$$

The IK channel steady state current is illustrated in Figure 3.9 for three different cytosolic calcium concentrations.

Topical applications of apamin have been observed to induce seizure activity (McCown and Breese, 1988). The mechanisms of seizure and spreading depression may be related (see section 2.4.3, “Epilepsy”). Waves of SD apparently will not propagate into a region that is undergoing a seizure (Ueda and Bures, 1977; Koroleva and Bures, 1980). However, the application of seizure-inducing agents sometimes leads to spontaneous SD waves (Hablitz and Heinemann, 1989), particularly at sub-

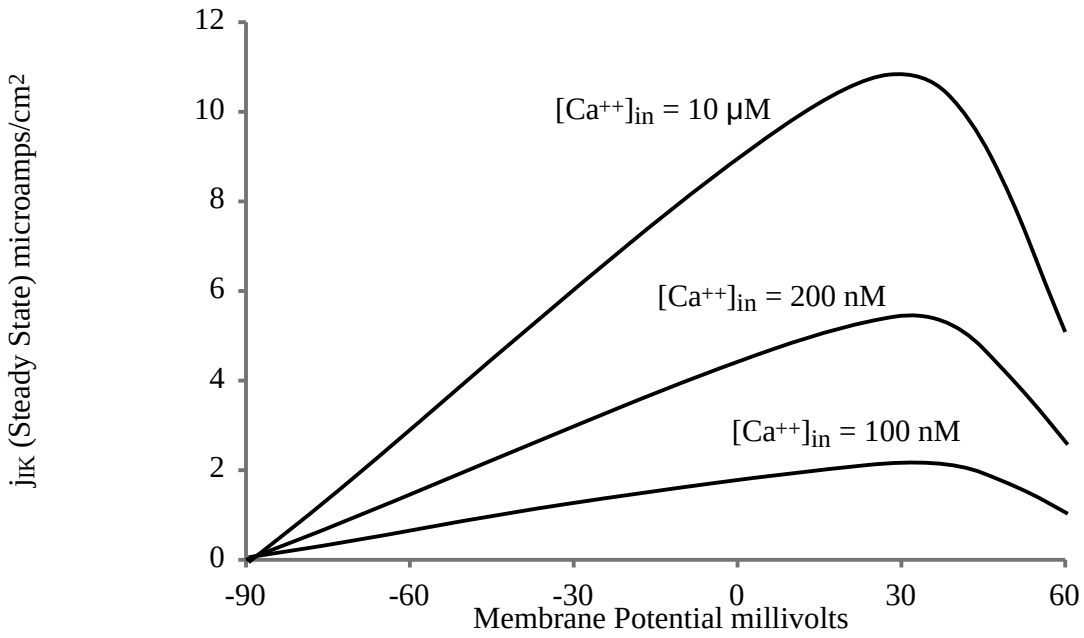


Figure 3.9. IK channel steady state current, assuming $g_{IK}$=1 pS/μm$^2$ and $E_K$=-90 mV. The steady state value of $j_{IK}$ (equation 5 with $m_{IK} = m_{IK,\infty}$, where $m_{IK,\infty}$ is given by equation 8) is shown for three different $[Ca^{++}]_{in.}$

convulsive dosages (Koroleva, Vinogradova and Bures, 1993). If agents that block SK-channels can induce a seizure, and if SD and seizures are mutually incompatible, then it may be that an increase in SK-channel conductivity (or the conductivity of some other K(Ca) channel) will induce spreading depression. Alternatively SD and seizure might be two levels of reaction to the same stimulus, with SD being the result of a weaker stimulus, and seizure the result of a stronger stimulus. In this hypothesis, a partial block of the SK channel should increase the susceptibility to spreading depression, while a complete block should increase the likelihood of seizure (see Figure 3.10).

Traub and others (1994) estimated the slow AHP current to have a conductivity of ≈8 pS/μm$^2$ in hippocampal pyramidal cell dendrites and soma; this current is associated with SK channels. In bullfrog sympathetic ganglion cells the contribution to membrane conductance due to the SK channel has been estimated to be $g_{SK} \approx 10$ pS/μm$^2$ (Yamada, Koch and Adams, 1998). The model of Yamada, Koch and Adams (1998) is used to describe the SK channel. The potassium flux in this model is

$$j_{SK} = \frac{g_{SK} m_{SK}^2}{F}\left(E - E_K\right) \tag{10}$$

where $m_{SK}$ is a Hodgkin-Huxley activation variable satisfying

$$\frac{dm_{SK}}{dt} = \frac{m_{SK,\infty} - m_{SK}}{\tau_{m,SK}} \tag{11}$$

**Hypothesis 1: SD and seizure are reactions to opposite stimuli.**

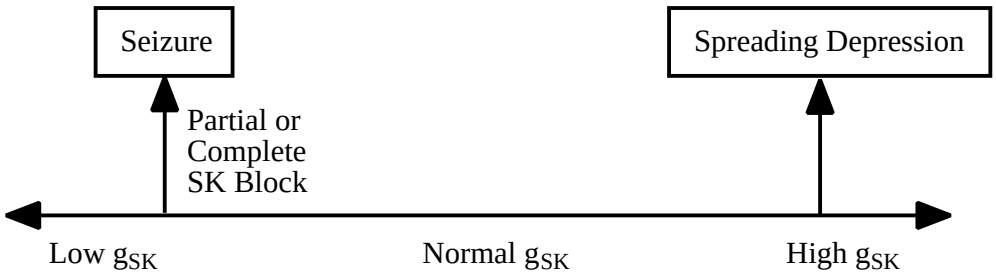


**Hypothesis 2: SD and seizure are reactions to the same stimuli.**

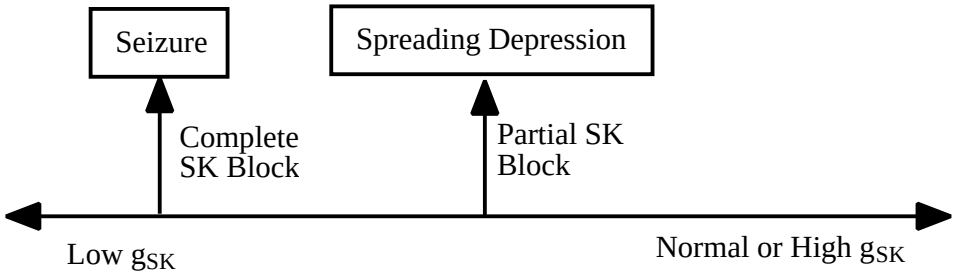


Figure 3.10. Two hypotheses for the relationship between spreading depression and seizure. In the first hypothesis, SD and seizure are mutually incompatible and are reactions to completely opposite stimuli. In the second hypothesis, SD and seizure are two different levels of reaction to the same class of stimuli, with SD being a reaction to a weaker stimulation (e.g., partial block of the SK channel) and seizure being a reaction to the strong stimulation (e.g. complete block of the SK channel).

The activation time constant and steady state activation are given by the voltage-independent but calcium dependent functions as

$$\tau_{m,SK} = \frac{1}{1.25 \times 10^{8}\left(\left[Ca^{++}\right]_{in}\right)^{2} + 2.5} \tag{12}$$

$$m_{SK,\infty} = \frac{1.25 \times 10^{8}\left(\left[Ca^{++}\right]_{in}\right)^{2}}{1.25 \times 10^{8}\left(\left[Ca^{++}\right]_{in}\right)^{2} + 2.5} \tag{13}$$

The SK channel current activation level, which is given by $m_{SK,\infty}^{2}$ (see equation 10), is illustrated in Figure 3.11.

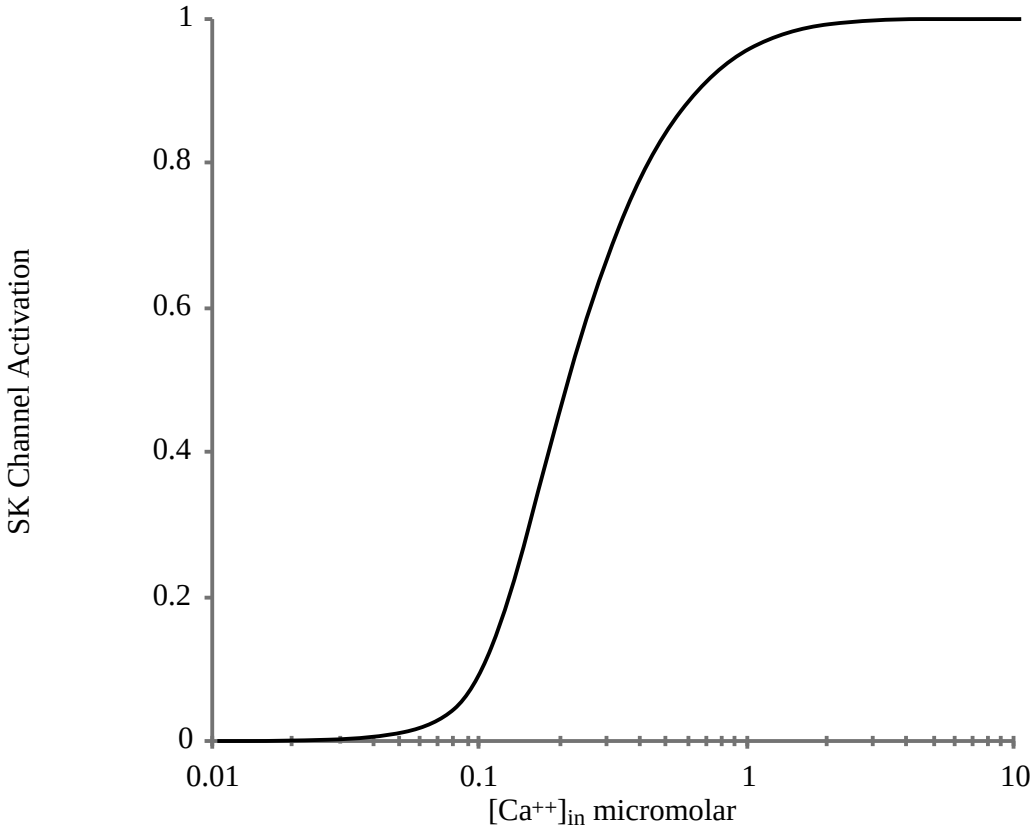


Figure 3.11. SK channel activation as a function of calcium concentration. The curve shows $m_{SK,\infty}^2$ where $m_{SK,\infty}$ is given by equation 13. The total activation is proportional to $m_{SK,\infty}^2$ as indicated by equation 10.

### 3.3.3. NMDA-RECEPTOR GATED CURRENTS

The human cerebral cortex contains approximately one synapse per square micron of dendritic tissue (Koch, 1998). Holmes (1995) has estimated that there are 200 to 2000 NMDA-mediated glutamate receptors in each hippocampal pyramidal cell synapse. Various measurements indicate that these receptors gate a channel that is permeable to $Ca^{++}$, $K^{+}$ and $Na^{++}$ with $P_K = P_{Na}$, $P_{Ca}/P_K \approx 3$ to 10.6, and that the currents can be accurately described by a constant field (Goldman) model (Mayer and Westbrook, 1987; Garaschuk and others, 1996; Schneggenburger, 1996). The typical calcium conductance at a single synapse has been estimated at ≈200 pS/μm$^2$ (Protopapas, Vanier and Bower, 1998). Using a constant field model, the ion flux for some species *c* through an NMDA channel is then

$$j_{c,NMDA} = g_{c,NMDA} E m(E) B(E,M) \frac{(c_{in}/c_{out}) e^{zEF/RT} - 1}{e^{zEF/RT} - 1} \qquad (1)$$

where $m(E)$ is the fraction of channels that have been activated by neurotransmitter, $B(E,M)$ is the fraction of channels from which the magnesium block has been removed, and the slope-conductance is defined at the reversal potential as

$$g_{c,NMDA} = \frac{PF^2 z^2}{RT} c_{out} \qquad (2)$$

The model of Destexhe, Mainen and Sejnowski (1998) is used to describe the voltage-dependent magnesium block function

$$B(E,M) = \frac{1}{1 + 0.028Me^{-0.062E}} \tag{3}$$

where $M$ is the interstitial magnesium concentration (assumed 1 mM for all simulations, Hansen, 1985). The channel activation function is given by the same authors as

$$m(E) = \left(1 + \frac{0.092}{T_{\max}}\left(1 + e^{-(E-2)/5}\right)\right)^{-1} \tag{4}$$

where $T_{max}$ is the maximum neurotransmitter concentration (assumed 1 mM for all simulations, Hansen, 1985). The total channel activation is illustrated in Figure 3.12.

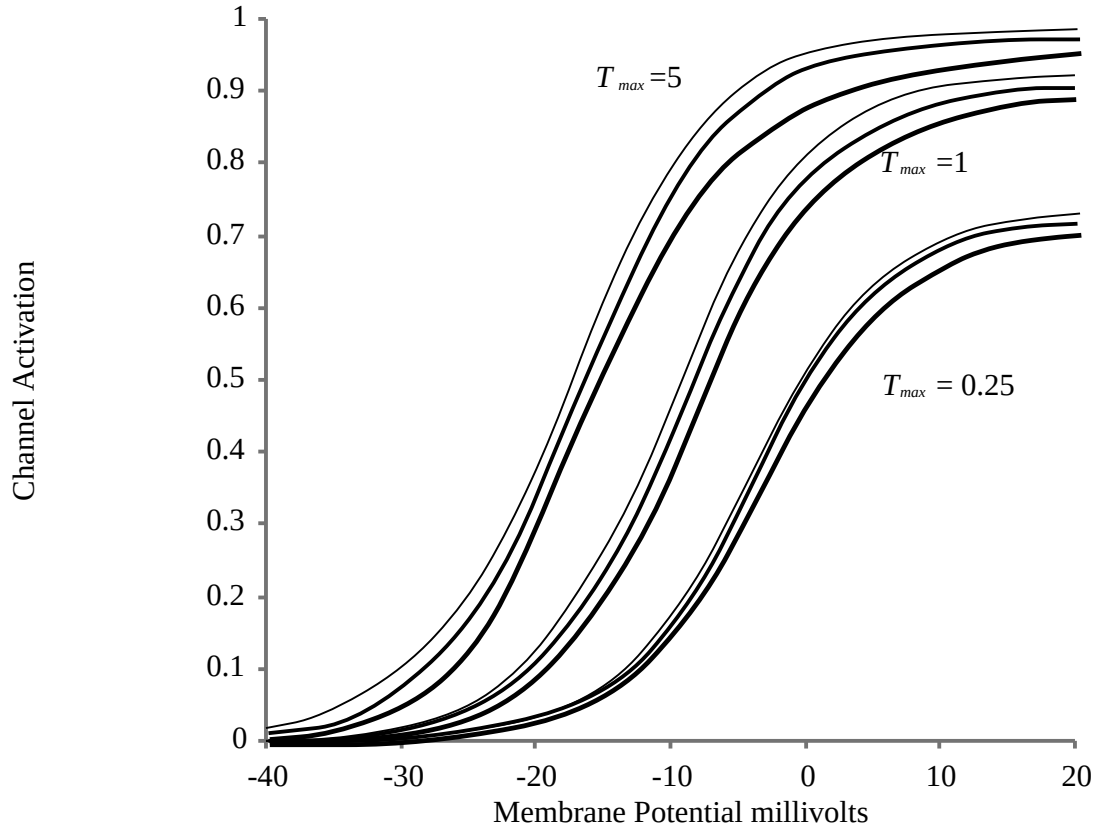


Figure 3.12. NMDA-receptor activated channel activation, i.e., the fraction of channels that are open at a given voltage, given by the product of equations 3 and 4. Activation is shown for three different values of $T_{max}$ (values indicated in mM on plot). For each value of $T_{max}$, a family of curves for three values of M is shown. For each family, left to right: $M$ = 0.1 mM, $M$=1.0 mM, and $M$=3 mM.

### 3.3.4. VOLTAGE GATED SODIUM CURRENTS

In axons, the fast sodium channel is responsible for the large voltage shift that occurs during an action potential. The sodium channel density at axonal nodes of Ranvier ranges from ≈2500 pS/μm$^2$ to ≈15000 pS/μm$^2$ (Hille, 1992). The gray-matter distribution of sodium channels varies, even within single neurons. Furthermore, this distribution is not consistent among different brain regions, even in the same type of neuron. Traub and others (1994) estimated a $Na^{++}$ conductance of ≈10 pS/μm$^2$ to ≈30 pS/μm$^2$ in the proximal dendrites of hippocampal pyramidal cells, zero in the distal dendrites, and ≈1000 pS/μm$^2$ in their somata. Stuart and Sakmann (1994), on the other hand, observed $g_{Na}$≈40 pS/μm$^2$, with no significant variation along the length of neocortical pyramidal cell dendrites. Magee and Johnston (1995a, 1995b) observed two to 10 sodium channels per patch in hippocampal dendrites with a single-channel conductivity of ≈16 pS. With a one micron diameter patch pipette, this would indicate $g_{Na}$≈ 40 pS/μm$^2$ to ≈200 pS/μm$^2$. Colbert and Johnson (1996) similarly estimate $g_{Na}$≈ 45 pS/μm$^2$ to ≈60 pS/μm$^2$ in the somata of neocortical pyramidal cells. The models of De Schutter and Bower (1995) are used to describe both of these conductances. De Schutter and Bower do not include any dendritic $Na^+$ currents in their model, perhaps because of a lack of such observations in Purkinje cells, but they estimate somatic conductances of ≈75,000 pS/μm$^2$ and ≈10 pS/μm$^2$, respectively, for the fast and persistent sodium channels. The fast sodium current is given by

$$j_F = \frac{g_F}{F} m_F h_F (E - E_{Na}) \tag{1}$$

where $m_F$ and $h_F$ are Hodgkin-Huxley activation and inactivation variables that satisfy the usual relaxation relations,

$$\frac{dm_F}{dt} = \frac{m_{F,\infty} - m_F}{\tau_{m,F}} \tag{2}$$

$$\frac{dh_F}{dt} = \frac{h_{F,\infty} - h_F}{\tau_{h,F}} \tag{3}$$

The steady state values and time constants are given in terms of the forward and backward rate constants $\alpha_{m,F}$ and $\beta_{m,F}$ (for $m_F$) and $\alpha_{h,F}$ and $\beta_{h,F}$ (for $h_F$). The time constant for activation is

$$\tau_{m,F} = \frac{1}{\alpha_{m,F} + \beta_{m,F}} \tag{4}$$

and the steady state activation variable is

$$m_{F,\infty} = \frac{\alpha_{m,F}}{\alpha_{m,F} + \beta_{m,F}} \tag{5}$$

The rate constants for activation are

$$\alpha_{m,F} = 35e^{(E+5)/1} \tag{6}$$

$$\beta_{m,F} = 7e^{-(E+65)/2} \tag{7}$$

The time constant for inactivation is

$$\tau_{h,F} = \frac{1}{\alpha_{h,F} + \beta_{h,F}} \tag{8}$$

and the steady state inactivation variable is

$$h_{F,\infty} = \frac{\alpha_{h,F}}{\alpha_{h,F} + \beta_{h,F}} \tag{9}$$

The rate constants for inactivation are

$$\alpha_{h,F} = \frac{0.225}{1 + e^{(E+80)/11}} \tag{10}$$

$$\beta_{h,F} = 7.5e^{(E-3)/11} \tag{11}$$

The steady state current for the fast sodium channel, as predicted by this model, is illustrated in Figure 3.13.

The $Na^+$ flux through the persistent sodium channel is given by

$$j_P = \frac{g_P}{F} m_P (E - E_{Na}) \tag{12}$$

where $m_P$ is a Hodgkin-Huxley activation variable. There is no inactivation variable for this channel. The activation variable decays exponentially to its steady state value, according to

$$\frac{dm_P}{dt} = \frac{m_{P,\infty} - m_P}{\tau_{m,P}} \tag{13}$$

The steady state value and time constant are both given in terms of the forward and backward rate constants $\alpha_{m,P}$ and $\beta_{m,P}$ as

$$\tau_{m,P} = \frac{1}{\alpha_{m,P} + \beta_{m,P}} \tag{14}$$

and

$$m_{P,\infty} = \frac{\alpha_{m,P}}{\alpha_{m,P} + \beta_{m,P}} \tag{15}$$

The rate constants for activation are

$$\alpha_{m,P} = \frac{200}{1 + e^{-(E-18)/16}} \tag{16}$$

$$\beta_{m,P} = \frac{25}{1 + e^{(E+58)/}} \tag{17}$$

The predicted steady state current due to the persistent sodium channel is illustrated in Figure 3.14.

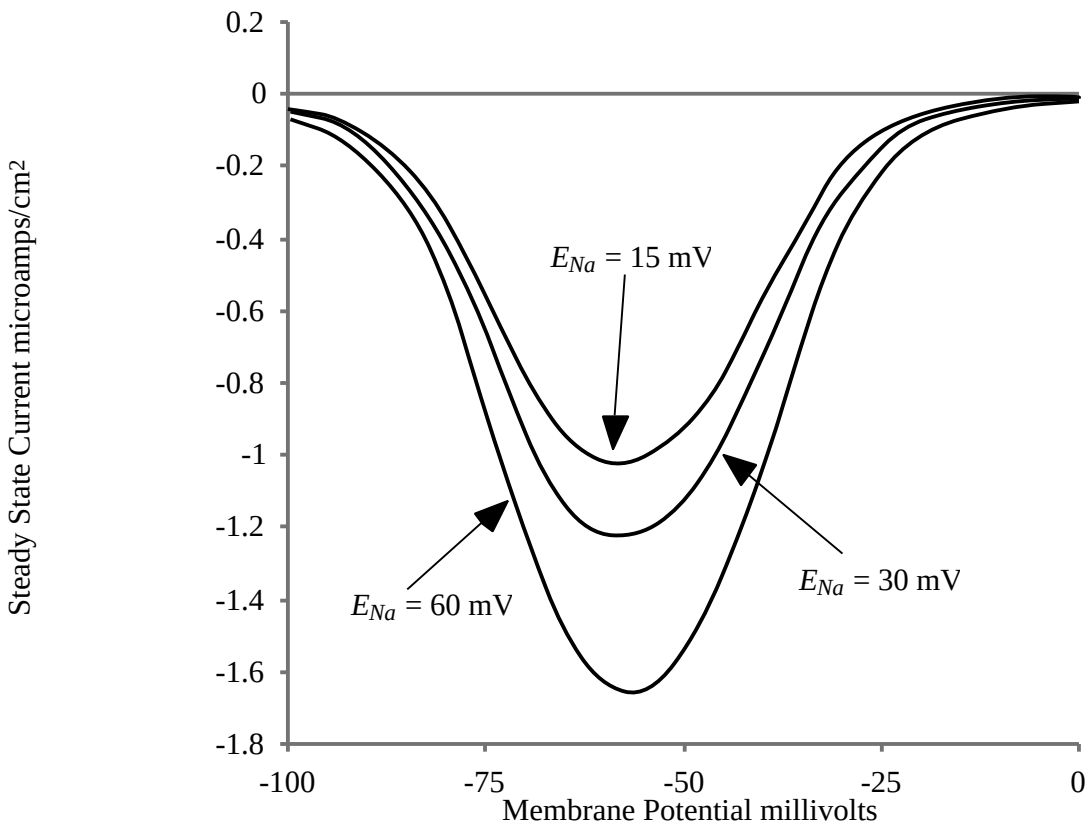


Figure 3.13. Steady state current of fast sodium channel for $g_F$ = 50 pS/μm$^2$ (equation 1 with $m_F = m_{F,\infty}$) for three different sodium Nernst Potentials.

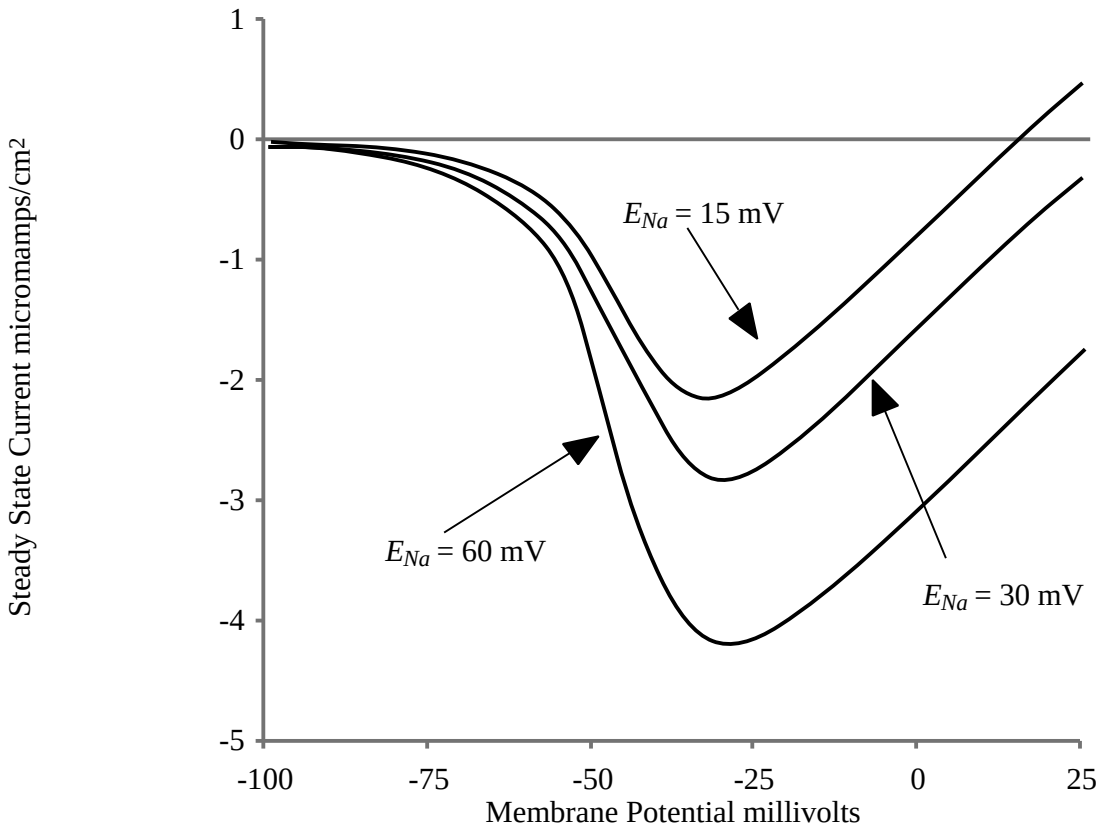


Figure 3.14. Steady state current of persistent sodium channel for $g_P$ = 0.5 pS/μm$^2$ (equation 12 with $m_P = m_{P,\infty}$) for three different sodium Nernst Potentials.

### 3.3.5. VOLTAGE GATED CALCIUM CURRENTS

Several subtypes of voltage gated calcium currents have been observed in the dendrites of hippocampal pyramidal cells, including both low-voltage activated (LVA) and high-voltage activated (HVA) currents. Traub and others (1994) estimated a total dendritic $Ca^{++}$ conductance of ≈10 pS/μm$^2$ to ≈30 pS/μm$^2$ and a somatic calcium conductance of ≈10 pS/μm$^2$ in hippocampal pyramidal cells. Magee and Johnston (1995a, 1995b) observed 2 to 7 calcium channels per patch; assuming a one-micron diameter patch pipette and a single channel conductivity of 10 pS, this gives $g_{Ca}$≈ 25 pS/μm$^2$ to 90 pS/μm$^2$. Various pharmacological studies have been consistent with the presence of T, N, L, P/Q, and R subtypes in these measurements (Christie and others, 1995; Gillessen and Alzheimer, 1997; Magee and Johnston, 1995a, 1995b; Kavalali and others, 1997). In the dendrites of Purkinje cells calcium channel densities have been estimated at $g_P$≈4.0 to ≈4.5 pS/μm$^2$ and $g_T$≈0.5 pS/μm$^2$ (De Schutter and Bower, 1994). The T-type and P-type channel models of De Schutter and Bower (1994) are used as being canonical of the LVA and HVA currents, respectively.

The membrane $Ca^{++}$ flux due to LVA channels is described in this model by

$$j_{LVA} = g_{LVA} p_{LVA} m_{LVA} h_{LVA} \frac{4FE}{RT} \frac{\left[\mathrm{Ca}^{++}\right]_{in} e^{2EF/RT} - \left[\mathrm{Ca}^{++}\right]_{out}}{e^{2EF/RT} - 1} \qquad (1)$$

where $p_{LVA} = P_{LVA}/g_{LVA}$ and $P_{LVA}$ is the permeability of this channel in cm/sec, $m_{LVA}$ is a Hodgkin-Huxley activation variable and $h_{LVA}$ is an inactivation variable. Their kinetics are described by

$$\frac{dm_{LVA}}{dt} = \frac{m_{LVA,\infty} - m_{LVA}}{\tau_{m.LVA}} \tag{2}$$

$$\frac{dh_{LVA}}{dt} = \frac{h_{LVA,\infty} - h_{LVA}}{\tau_{h,\,LVA}} \tag{3}$$

The steady state activation variable $m_{LVA,\infty}$ and time constant $\tau_{m,LVA}$ are

$$m_{LVA,\infty} = \frac{\alpha_{m,LVA}}{\alpha_{m,LVA} + \beta_{m,LVA}} \tag{4}$$

$$\tau_{m,LVA} = \frac{1}{\alpha_{m,LVA} + \beta_{m,LVA}} \tag{5}$$

where the forward and backward rate constants for activation are

$$\alpha_{m,LVA} = \frac{2.6}{1 + e^{-(E+21)/}} \tag{6}$$

$$\beta_{m,LVA} = \frac{0.18}{1 + e^{(E+40)/}} \tag{7}$$

The steady state inactivation variable $h_{LVA,\infty}$ and time constant $\tau_{h,LVA}$ are

$$h_{LVA,\infty} = \frac{\alpha_{h,LVA}}{\alpha_{h,LVA} + \beta_{h,LVA}} \tag{8}$$

$$\tau_{h,LVA} = \frac{1}{\alpha_{h,\,LVA} + \beta_{h,LVA}} \tag{9}$$

where the forward and backward rate constants for inactivation are

$$\alpha_{h,LVA} = \frac{0.0025}{1 + e^{(E+40)/}} \tag{10}$$

$$\beta_{h,LVA} = \frac{0.19}{1 + e^{-(E+50)/10}} \tag{11}$$

The membrane calcium flux due to HVA-channels is modeled as

$$j_{HVA} = g_{HVA} p_{HVA} m_{HVA} h_{HVA} \frac{4FE}{RT} \frac{\left[\mathrm{Ca}^{++}\right]_{in} e^{2EF/RT} - \left[\mathrm{Ca}^{++}\right]_{out}}{e^{2EF/RT} - 1} \tag{12}$$

where $p_{HVA} = P_{HVA}/g_{HVA}$ and $P_{HVA}$ is the permeability of this channel in cm/sec, $m_{HVA}$ is a Hodgkin-Huxley activation variable and $h_{HVA}$ is an inactivation variable. Their kinetics are described by

$$\frac{dm_{HVA}}{dt} = \frac{m_{HVA,\infty} - m_{HVA}}{\tau_{m.HVA}} \tag{13}$$

$$\frac{dh_{HVA}}{dt} = \frac{h_{HVA,\infty} - h_{HVA}}{\tau_{h,HVA}} \tag{14}$$

The steady state activation variable $m_{HVA,\infty}$ and time constant $\tau_{H,LVA}$ are

$$m_{HVA,\infty} = \frac{\alpha_{m,HVA}}{\alpha_{m,HVA} + \beta_{m,HVA}} \tag{15}$$

$$\tau_{m,HVA} = \frac{1}{\alpha_{m,HVA} + \beta_{m,HVA}} \tag{16}$$

where the forward and backward rate constants for activation are

$$\alpha_{m,HVA} = \frac{8.5}{1 + e^{-(E-8)/12.}} \tag{17}$$

$$\beta_{m,HVA} = \frac{35}{1 + e^{(E+74)/14.5}} \tag{18}$$

The steady state inactivation variable $h_{HVA,\infty}$ and time constants $\tau_{m,HVA}$ are

$$h_{HVA,\infty} = \frac{\alpha_{h,HVA}}{\alpha_{h,HVA} + \beta_{h,HVA}} \tag{19}$$

$$\tau_{h,HVA} = \frac{1}{\alpha_{h,HVA} + \beta_{h,HVA}} \tag{20}$$

where the forward and backward rate constants for inactivation are

$$\alpha_{h,HVA} = \frac{0.0015}{1 + e^{(E+29)/8}} \tag{21}$$

$$\beta_{h,HVA} = \frac{0.0055}{1 + e^{-(E+23)/8}} \tag{22}$$

The predicted steady state calcium currents are illustrated in Figure 3.15.

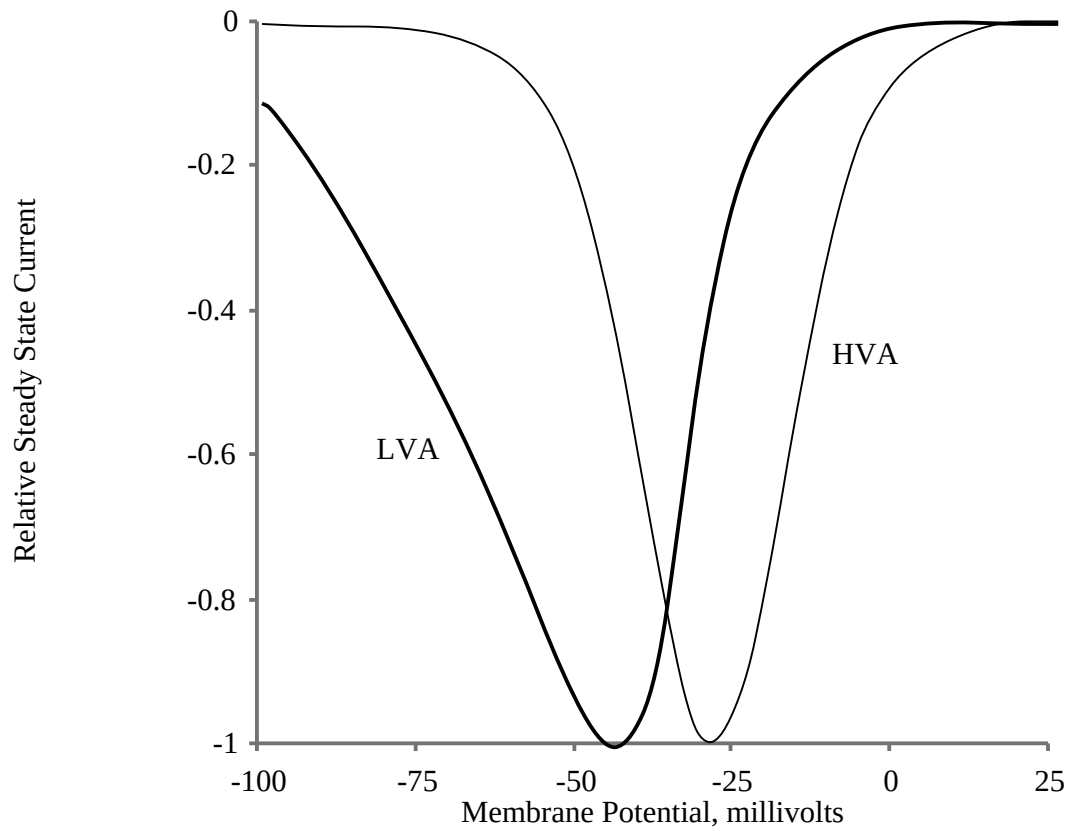


Figure 3.15. Comparison of steady state calcium currents. Currents are shown relative to the maximum current for each channel type (e.g., $j_{SS}(V)/\max_V |j_{SS}(V)|$). Currents are shown as negative values to emphasize the inward nature of the current. The steady state LVA-current is given by equation 1 with $m_{LVA} = m_{LVA,\infty}$ and $h_{LVA} = h_{LVA,\infty}$. The steady state HVA-channel current is calculated from equation 12 with $m_{HVA} = m_{HVA,\infty}$ and $h_{HVA} = h_{HVA,\infty}$.

## 3.3.6. ION PUMPS AND EXCHANGERS

Potassium and sodium concentrations are maintained by an electrogenic membrane sodium/potassium pump with a strength of 1 – 10 μA/cm$^2$ that pumps three sodium ions out of the cell for every two potassium ions pumped into the cell. The cardiac model given by Lemieux, Roberge and Joly (1992) is used to describe this current, which is weakly voltage dependent and is half-activated at $[K^+]_{out}$≈9 mM and $[Na^+]_{in}$≈14 mM. The magnitude of the $K^+$ flux is given by

$$J_{Na/K} = \frac{j_{max,\,Na/K}}{F}\left(\frac{[K^+]_{out}}{[K^+]_{out}+3.7}\right)^2\left(\frac{[Na^+]_{in}}{[Na^+]_{in}+0.6}\right)^3 \frac{0.052\sinh\tilde{V}}{0.026e^{\tilde{V}}+22.5e^{-\tilde{V}}} \qquad (1)$$

where

$$\tilde{V} = \frac{F}{RT}(E+176.5) \qquad (2)$$

The calcium gradient is maintained by a high-affinity low strength membrane-bound calcium ATP-ase and a lower affinity but higher strength Na/Ca exchanger. The sodium/calcium exchanger pumps three $Na^+$ ions out for every $Ca^{++}$ ion pumped in. The sodium/calcium exchanger is described by the cardiac model of Di Francesco and Noble (1985), with the magnitude of the $Na^+$ flux given by

$$J_{Na/Ca} = \frac{j_{\max,Na/Ca}}{Fc_0^3}\,\frac{[Na^+]_{in}^3[Ca^{++}]_{out}\,e^{0.02E} - [Na^+]_{out}^3[Ca^{++}]_{in}\,e^{-0.02E}}{1+0.0001\left([Na^+]_{out}^3[Ca^{++}]_{in}+[Na^+]_{in}^3[Ca^{++}]_{out}\right)} \qquad (3)$$

Di Polo and Beaugé (1983) estimate that the Na/Ca exchanger has a maximum pump rate of ≈2000 femtomoles/cm$^2$-sec in cardiac tissue (i.e. $j_{max,Na/Ca} \approx 0.2\ \mu A/cm^2$). The value of $c_0$ is calibrated so that equation 3 gives this saturation current (≈ 0.2 μA/cm$^2$) at physiological concentrations of sodium and calcium.

The calcium-ATPase is described by a Michaelis-Mentin curve with a Hill constant of 1 and a half-activation at 200 nM (Di Polo and Beaugé, 1979, De Schutter and Smolen, 1998), with the magnitude of the $Ca^{++}$ given by

$$J_{Ca,ATPase} = \frac{j_{max,ATPase}}{F} \frac{[Ca^{++}]_{in}}{[Ca^{++}]_{in} + 0.0002} \qquad (4)$$

Di Polo and Beaugé (1983) estimate that $j_{max,ATPase} \approx 0.02\ \mu A/cm^2$ (≈200 femtomoles/cm$^2$-sec). Sodium and potassium balance is also maintained by a glial $Na^+/K^+$ pump and an $Cl^-/Na^+/K^+$ cotransporter. The cotransporter drives all three atoms into the glia in the ratio of 2:1:1. The cotransporter model is dependent on extracellular potassium, sodium, and chlorine with Hill coefficients of 1, 1, and 2 and is half-activated at $[K^+]_{out}$ =2.7 mM, $[Na^+]_{out}$ =35 mM and $[Cl^-]_{out}$=40 mM (Tas, Massa and Koschel, 1986; Tas and others, 1987; Watz, 1995) with the magnitude of the $K^+$ flux given by

$$j_{Na/K/Cl} = \frac{j_{max,Na/K/Cl}}{F} \left( \frac{[K^+]_{out}}{[K^+]_{out} + 2.7} \right) \left( \frac{[Na^+]_{out}}{[Na^+]_{out} + 35} \right) \left( \frac{[Cl^-]^2_{out}}{[Cl^-]^2_{out} + 1600} \right) \qquad (5)$$

Chlorine balance is also maintained with a neuronal bicarbonate/chlorine exchanger that is reversible, half-activated at $[Cl^-]_{in}$=2 mM, and has a resting pump concentration of 4 mM, with the magnitude of the $Cl^-$ flux given by

$$j_{Cl-Bicarb} = \frac{j_{max,Cl-Bicarb}}{F} \frac{[\mathrm{Cl}^-]_{in} - 4}{[\mathrm{Cl}^-]_{in} + 2} \tag{6}$$

### 3.3.7. LEAK CURRENT

Leak conductances are calculated using the Goldman current equation (equation 2.68 of Keener and Sneyd, 1998),

$$j_{Leak} = \frac{Pz^2 F^2 E}{RT} \frac{c_{in} - c_{out} e^{-zFE/RT}}{1 - e^{-zFE/RT}} \tag{1}$$

The permeability for each species is calibrated to maintain equilibrium at the rest concentrations of that species. Leak currents are calculated for potassium, sodium, and calcium.

### 3.3.8 STRETCH RECEPTORS

Stretch activated ion currents have been observed in a large number of physiological systems. Various reports indicate that several voltage-sensitive potassium channels can be activated by membrane stretch. These include the delayed-rectifier (DR), muscarinic (M-channel), and BK-type K(Ca) channel. Stretch-activation of other ligand-gated and voltage-gated currents has also been reported. The probability of channel opening is sigmoidal, increasing with negative pressure (i.e., less pressure on the outside of the cell). Mienville, Barker and Lange (1996) quantitatively observed the stretch-activation of BK channels in rat neuroepithelial cells, and fit a Boltzmann distribution with a half-activation pressure at ≈66 mm Hg, slope of ≈10.2 mm Hg, and maximum open probability of ≈0.43. Stretch activation of the delayed rectifier has been observed in microvascular endothelial cells (Fan and Walsh, 1999) and guinea-pig ventricular myocytes (Sasaki, Mitsuiye and Noma, 1992). Cardiac potassium M-channels are stretch dependent and have shown activation that increases with increasing pressure for pressures as high as ≈80 mm Hg (Pleumsamran and Kim, 1995; Ji and others, 1998). In *xenopus* kidney proximal tubule cells, the open probability of a voltage-dependent stretch-activated $K^+$ channel increases from ≈0.01 to ≈0.75 as the pressure is varied from ≈12 to ≈25 mm Hg (Kawahara, 1990). In cultured rat mesencephalic and hypothalamic neurons, ion currents that are sensitive to both arachidonic acid and membrane stretch have been

observed. These currents are half-activated at a pressure of ≈18 mm Hg (Kim and others, 1995). Stretch-sensitive voltage-insensitive potassium currents in *nectarus* renal tubule begin to open with ≈8 to ≈15 mm Hg of pressure (Sackin, 1987; Kawahara, 1993). In pig articular chondrocytes, the activation of stretch-sensitive $K^+$ channel is half-maximual at ≈15 mm Hg (Martina, Mozrzmas and Vittur, 1997). A TEA-sensitive stretch-activated $K^+$ channel that is not voltage dependent has been observed in *drosophila* muscular tissue (Gorczyca and Wu, 1991). Fluid flow also affects the inward rectifier current in both rat and human skeletal muscle (Burton and Hunter, 1990); this effect may be due to pressure differences. Other stretch-activated channels have been reported in human fibroblasts (Stockbridge and French, 1988), guinea pig cochlear epithelial cells (Yeh and others, 1997), chick cardiac myocytes (Ruknudin, Sachs and Bustamante, 1993), rabbit corneal epithelial cells (activated at pressures of ≈20 to ≈80 mm Hg) (Watanabe, Tanizaka and Kaneko, 1997), in rat cerebellar astrocytes (half-activated at ≈45 mm Hg; Islas, Pasantes-Morales and Sanchez, 1993), in glial cells that ensheathe the abdominal stretch receptor neurons of crayfish (Erxleben, 1991) and in *xenopus* oocytes (Yang and Sachs, 1990). Based on these observations, it is likely that some stretch-activation of ion currents may occur in gray matter. Besides the NMDA-channel, the primary conductances that are significant in spreading depression (as predicted by the simulations that are presented in Chapter 4, "Results") appear to be the BK and delayed rectifier channels. To describe stretch-activation of these channels, their open-probability due to stretch $Q_{open}$ was modeled sigmoidally as

$$Q_{open} = \frac{q_{max}}{1 + e^{-(\Delta P - \Delta P_{1/2})/K}} \tag{1}$$

where $\Delta P$ is the applied pressure in mm Hg, $q_{max}$ is the maximum open probability due to stretch, $K$ is a slope constant, and $\Delta P_{1/2}$ is the half activation pressure. The pressure change is related to the volume by applying Boyle's law, which states that the product $PV$ is constant. Thus to first order (in absolute values), $\Delta P / P = \Delta V / V$, or

$$\Delta P = P_{rest} \left( \frac{f}{f_{rest}} - 1 \right) \tag{2}$$

where $P_{rest}$ is the resting pressure (taken as 760 mm Hg).

## 3.4. GAP JUNCTIONS

Although it is assumed that gap junctions are either always open or are open by stretch activated receptors, this is not specifically modeled. Instead, gap junctional permeability is described by a reducing the cytoplasmic diffusion constant, with a diffusion constant of zero indicating complete block. Keener and Sneyd (1998) show that in one-dimension the effective diffusion constant $D_{eff}$ through the intracellular continuum of cells is a function of the single-cell intracellular diffusion constant $D_{in}$ in a manner that depends on the geometrical distribution of gap junctions,

$$D_{eff} = \frac{D_{in}}{1 + 0.0016\,\frac{1-\Delta}{\Delta}} \qquad (1)$$

where $\Delta$ is a parameter satisfying $0 < \Delta < 1$ that describes the distribution of gap junctions. When the gap junctions are highly clumped in individual aggregates, $\Delta \to 1$, and when the gap junctions are uniformly distribution $\Delta \to 0$. Thus the actual diffusion constant for each species in the intracellular continuum should be somewhat smaller than the corresponding diffusion constant within a single cell, and the value of $D_{eff}$ depends on the gap junctional distribution. Since potassium, sodium and chlorine are not buffered as strongly as calcium, the ration $D_{in}/D_{free}$ is probably somewhat larger for these species than for calcium, where $D_{free}$ is the diffusion constant in free solution.

In some cell types, gap junctional conductivity decreases with applied voltage; furthermore, some gap junctions appear to be blocked by high levels of intracellular calcium. Vogel and Weingart (1998) reduce the total conductivity of gap junctions by the voltage dependent factor

$$\gamma_1(\vartheta) = \frac{2}{\exp\left(\frac{-\vartheta}{1+e^{\vartheta}}\right) + \exp\left(\frac{\vartheta}{1+e^{-\vartheta}}\right)} \tag{2}$$

where $\vartheta = \Delta V / V_H$, $\Delta$V is the voltage drop across a single gap junction, and the parameter $V_{\mathrm{H}} \approx$ 10 – 1000 mV. Since

$$\Delta V = \ell \frac{dV}{dx} \tag{3}$$

where the length $\ell$ of a typical gap junction is ≈15 nm (nanometer) and the voltage gradients are strongly bounded by, say 100 mV/μm, this would produce very little attenuation and hence is ignored in the present model.

Cardiac cells are widely coupled by gap junctions that are sensitive to divalent cations, especially calcium and magnesium, as well as pH (*i.e.*, $H^+$ concentration). Noma and Tsuboi (1987) estimate that the junctional conductivity between paired cardiac cells is reduced by a factor of

$$\gamma_2\left(\left[\mathrm{Ca}^{++}\right]\right) = 1 - \frac{1}{1 + \left[\left(\frac{K_{Ca}}{[\mathrm{Ca}^{++}]_{in}}\right)^{n}\left(1 + \left(\frac{K_H}{[\mathrm{H}^{+}]_{in}}\right)^{2n}\right)\right]} \qquad (4)$$

where $K_{\mathrm{Ca}}$= 316 nM, $K_{\mathrm{H}}$=112 nM, and $n$=3, when divalent cations are present. Although there is no evidence indicating whether this type of block is present in nerve cells, equation 4 was implemented and some simulations were run with various values of $K_{Ca}$. A fixed value of pH=7 was used for these studies.

## 3.5. GLIAL CELLS

The glial uptake models are designed to maintain extracellular homeostasis against small variations of the interstitial environment. The detailed glial kinetics are not considered. Potassium and sodium levels are maintained with a $Na^+/K^+$ pump and a $Na^+/K^+/Cl^-$ co-transporter. To maintain chlorine homeostasis a $Cl^-$/bicarbonate pump is also included in the model. The same pump models are used in glia and neurons. Because of the lack of good measurements of the relative pump concentrations in glial cells, the pump strengths are set to give each $K^+$ pump an equal role at steady state. The strength of all glial transporters and pumps is then controlled proportionally by a single maximum glial uptake rate. Unless otherwise specified, a total glial uptake rate of 2 mM/sec is used. For the equations given in this section a positive flux indicates material being removed from interstitial space and entering the glial cytoplasm (the opposite convention used for neuronal cytoplasm).

Potassium is pumped into the glia cytoplasm and out of interstitial space at the following rate

$$J_{K,glia} = j_{max,K,glia}\left(j_{Na/K/Cl,glia} + j_{Na/K,glia}\right) - j_{K,Leak,glia} \qquad (1)$$

where $j_{Na/K/Cl,glia}$ and $j_{Na/K,glia}$ take the same forms given in equations 1 and 5 of section 3.3.6, but normalized to give a maximum pump rate of 0.5 (dimensionless, putting all of the units in $j_{max,K,glia}$). This allows the total K pump rate to be controlled by the

parameter $j_{max,K,glia}$. The leak current takes the same form as equation 1 of section 3.3.7. The magnitude of the leak is calibrated so that equation 1 gives zero at rest.

Sodium is pumped out of interstitial space and into the glial cytoplasm at the following rate:

$$J_{Na,glia} = j_{max,K,glia}\left(j_{Na/K/Cl,glia} - \frac{3}{2} j_{Na/K,glia}\right) + j_{Na,Leak,glia} \quad (2)$$

where the pump currents are normalized for potassium as discussed in the preceding paragraph. Because the same pumps are referenced in equations 1 and 2 the coefficient of the first term in equation 2 is determined by the corresponding quantity in equation 1. The sign of the Na/K exchanger is negative because $Na^+$ is pumped into the interstitial space and, the sign of the leak current is positive because $Na^+$ leaks into glia rather than out of glia.

Chlorine is pumped out of interstitial space and into the glial cytoplasm at the following rate:

$$J_{Cl,glia} = j_{max,K,glia}\left(2j_{Na/K/Cl,glia} - j_{Cl/Bicarb,glia}\right) + j_{Cl,Leak,glia} \quad (3)$$

where the glial Na/K/Cl removes $Cl^-$ from the interstitial space at twice the rate that it removes $Na^+$ and $K^+$, and the $Cl^-$/bicarbonate exchanger extracts $Cl^-$ from glia. The bicarbonate pump is normalized to have a maximum dimensionless pump rate of 0.5, and the leak current is normalized to give a total Cl current of zero at rest.

## 3.6. Osmotic Forces and Cellular Volume

An imbalance in isotonicity will lead to osmotic forces and the passage of water into (or out of) a cell. The models used to describe these volume changes are described in this section. Given any particular ionic distribution, *e.g.*, the number of ions on either side of the neuronal membrane (non-neuronal cells are not included in this analysis), there is a particular neuronal volume fraction $f$ at which the cell is in osmotic balance with its environment. This volume fraction is referred to as the steady state volume fraction $f_\infty$ in the remainder of this dissertation. In the simplest model, whenever there is any ionic redistribution, the volume is instantaneously reset to the steady state volume, *e.g.*, $f = f_\infty$, without regard to the speed of water transport across the membrane. This steady state model is described in section 3.6.1 ("Steady State Model"). To account for the finite rate of water transport, a simple relaxation model is presented in section 3.6.2 ("Relaxation Model"). In this model, the volume relaxes exponentially to its steady state value with some time constant $\tau$. To justify the relaxation model the actual differential equation for water transport across the membrane as a function of the osmotic pressure difference is solved in section 3.6.3 ("Exact Model"). The "exact" model leads to an equation that is implicit in $f$ (the cytoplasmic volume fraction). It is not possible to analytically solve this equation to obtain an explicit expression for $f$; instead, it must be solved numerically. It turns out that this numerical solution is practically indistinguishable (numerically) from the

solution of the relaxation model. The reason for this, and a comparison of the exact and relaxation models, is presented in section 3.6.4 ("Comparison of Osmotic Models"). Finally, a fit of the exponential model to some real data is presented in section 3.6.5 ("Estimation of Osmotic Time Constant").

### 3.6.1. STEADY STATE MODEL

Consider a single volume element $V$ of CNS tissue. In an "ideal" model $V$ would include a concoction of neurons, glia, vasculature, extracellular matrix, interstitial space and various entities whose individual volumes are changing dynamically on various time scales, e.g.,

$$V = V_{Neuronal} + V_{Interstitial} + V_{Glial} + V_{Vascular} + V_{ECM} + \cdots \quad (1)$$

For the sake of simplifying the calculations, we assume that both the total volume $V$ is fixed due to anatomical constraints (e.g., the skull). Furthermore, let us assume that some of the component volumes are also fixed on the time scale during which spreading depression is initiated (seconds). Grouping those compartments that are individually fixed in volume into $V_{Fixed}$ and those that are individually variable into $V_{Variable}$ we obtain

$$V = V_{Fixed} + V_{Variable} \quad (2)$$

We will restrict $V_{Variable}$ to include only $V_{Neuronal}$ and $V_{Interstitial}$, which we then label in standard form as $V_{in}$ and $V_{out}$. It could be argued that both $V_{Glial}$ and $V_{Vascular}$ should also be included in $V_{Variable}$. Glial volume changes probably do occur during spreading depression, and could be described by the neuronal model that is presented below. However, one of the hypotheses that is being

tested (numerically) in this dissertation is whether it is possible to describe what is seen during spreading depression by neuronal volume changes. Since only a nominal glial model is included, it was decided to ignore glial volume changes in what follows. A complete glial model, including osmotic volume changes, is an important topic for further study. Vascular changes also have been observed during spreading depression; however, the time scale of these changes appears to be slower, occurring primarily after an SD wave has passed. Therefore these changes have also been excluded from the model. Then with these assumptions from equation (2) the quantity

$$V \equiv V_{Variable} = V - V_{Fixed} = V_{in} + V_{out} \tag{3}$$

is a constant. Defining $f$ as the neuronal volume fraction we have

$$V_{in} = fV \tag{4}$$

$$V_{out} = (1 - f)V \tag{5}$$

The total number of cytosolic impermeant anions $N_A$ in $V$ can be calculated if we assume initial electroneutrality,

$$N_A = V_{rest}\left([\mathrm{Na}^+]_{in,rest} + [\mathrm{K}^+]_{in,rest} - [\mathrm{Cl}^-]_{in,rest}\right) \tag{6}$$

The subscript "rest" indicates the values at rest, and $V_{rest}$ is $V_{in}$ at rest.

By isotonicity, the internal and external solute ionic concentrations must be balanced. Hence the total external solute concentration $[\mathrm{S}]_{out}$ is

$$[\mathrm{S}]_{out} = [\mathrm{Na}^+]_{in} + [\mathrm{K}^+]_{in} + [\mathrm{Cl}^-]_{in} + \frac{N_A}{fV} \tag{7}$$

both at rest as well as at all times later as isotonicity is maintained. To maintain this isotonicity, any change in the ionic concentration is balanced by a flow of water across the membrane such that $\Delta V / V = \Delta N_S / N_S$, where $N_S$ is the total number of interstitial solute ions in the volume element $V$. Hence (Jakobson, 1980)

$$\frac{df}{dt} = \begin{cases} \frac{1}{[S]_{out}} \sum \frac{d}{dt}\left([c]_{in} f\right), & f \le f_{max} \\ 0, & f > f_{max} \end{cases} \tag{8}$$

Neuronal cells resist swelling more than other cells (Aitken and others, 1998a). Thus cells are not allowed to expand beyond the limits imposed by the surrounding parenchyma, typically to no more than 95% of the total volume.

### 3.6.2. RELAXATION MODEL

In a relaxation model the volume fraction $f$ relaxes to its steady state value $f_\infty$ with some time constant $\tau$,

$$\frac{df}{dt} = \frac{f_\infty - f}{\tau} \tag{1}$$

Equation 1 can be solved by the method of integrating factors, by observing that

$$\frac{d}{dt}\left(fe^{t/\tau}\right) = \left(\frac{df}{dt} + \frac{f}{\tau}\right)e^{t/\tau} = \frac{f_\infty}{\tau}e^{t/\tau} \tag{2}$$

By the fundamental theorem of calculus, integration of equation 2 yields

$$\begin{aligned} f(t)e^{t/\tau} &= f(0) + \frac{f_\infty}{\tau}\int_0^t e^{T/\tau}\,dT \\ &= f_0 + f_\infty(e^{t/\tau} - 1) \end{aligned} \tag{3}$$

where $f(0) = f_0$. Multiplying by $e^{-t/\tau}$ gives

$$f(t) = (f_0 - f_\infty)e^{-t/\tau} + f_\infty \tag{4}$$

### 3.6.3. "EXACT" MODEL

The rate of water flow due to an osmotic pressure difference can be written as

$$\frac{d(fV)}{dt} = P_f S V_W \left(OSM_i - OSM_o\right) \qquad (1)$$

where $P_f$ is the osmotic water permeability of the membrane (typically $\approx 3 \times 10^{-5}$ m/sec), $S$ is the surface area of the membrane, $V_W$ is the partial molar volume of water (typically $\approx 1.8 \times 10^{-5}$ m$^3$/mol), $OSM = \phi[s]$ is the osmolality, $\phi \approx 0.93$ is the osmotic coefficient, $[s]$ is the solute concentration, $V$ is the total volume (cytoplasmic plus interstitial) and $f$ is the cytoplasmic volume fraction (Voets and others 1999). Since the cytoplasmic volume is $fV$ and the interstitial volume fraction is $(1-f)V$, the concentrations in equation 1 can be expressed in terms of the total numbers of solute ions $n_{in}$ and $n_{out}$ on either side of the membrane as $n_{in}/fV$ and $n_{out}/[(1-f)V]$,

$$\frac{d(fV)}{dt} = \phi P_f S V_W \left([s]_i - [s]_o\right) = \frac{\phi P_f S V_W}{V}\left(\frac{n_{in}}{f} - \frac{n_{out}}{(1-f)}\right) \qquad (2)$$

Since the total volume $V$ is a constant, equation 2 can be solved for $df/dt$ to give

$$\begin{aligned}\frac{df}{dt} &= \frac{\phi P_f S V_W}{V^2}\left(\frac{n_{in}}{f} - \frac{n_{out}}{(1-f)}\right) \\ &= \frac{\phi P_f S V_W}{V^2 f(1-f)}\left(n_{in} - f(n_{in} + n_{out})\right) \qquad (3) \\ &= \frac{\phi P_f S V_W (n_{in} + n_{out})}{V^2 f(1-f)}\left(f_\infty - f\right)\end{aligned}$$

where

$$f_\infty = \frac{n_{in}}{n_{in} + n_{out}} \tag{4}$$

The steady state volume fraction $f_\infty$ is the volume the cell is "trying" to reach assuming that there is no additional ionic transport into or out of the cell. The cell will be in osmotic balance with its environment when

$$f = f_\infty \tag{5}$$

The new variable $f_\infty$ is a function of the concentrations and could be thought of as an additional state variable of the model.

To solve equation 3 we must make some assumptions about neuronal geometry so as to relate the surface area ($S$) to the cytoplasmic volume ($fV$). Since the bulk of gray matter in the CNS is composed of dendrites we assume cylindrical geometry in what follows. Using spherical or other volumes will result in a different answer. If the model is to be applied to somata and glial cells, it will become necessary to take this fact into account. A compartmentalized scheme taking into account the geometry of each component separately may be one technique to utilize for this. For a cylindrical process of length $L$ and radius $r$ the membrane surface area is

$$S = 2\pi rL \tag{6}$$

and the cytoplasmic volume is

$$fV = \pi r^2 L \tag{7}$$

Solving equation 7 for $r$ gives

$$r = \sqrt{\frac{fV}{\pi L}} \tag{8}$$

Substituting equation 8 into equation 6 gives

$$S = 2\pi L\sqrt{\frac{fV}{\pi L}} = 2\sqrt{\pi LVf} \tag{9}$$

Substituting equation 9 into equation 3 gives

$$\frac{df}{dt} = \frac{\phi P_f 2\sqrt{\pi L}V_W(n_{in} + n_{out})}{V^{3/2}}\frac{1}{(1-f)\sqrt{f}}\left[f_\infty - f\right] \tag{10}$$

Define $k$ to be the leading constant in equation 10,

$$k = \frac{\phi P_f 2\sqrt{\pi L}V_W(n_{in} + n_{out})}{V^{3/2}} \tag{11}$$

With this definition, equation 10 becomes

$$\frac{df}{dt} = \frac{k}{(1-f)\sqrt{f}}\left[f_\infty - f\right] \tag{12}$$

Equation 12 is a separable differential equation. Hence

$$\int_0^t k\,dT = \int_{f_0}^{f}\frac{(1-F)\sqrt{F}}{f_\infty - F}dF \tag{13}$$

where $f(0) = f_0$. Integrating the left hand side of equation 13 gives

$$kt = \int_{f_0}^{f}\frac{(1-F)\sqrt{F}}{f_\infty - F}dF = I(f) - I(f_0) \tag{14}$$

where $I(f)$ is the indefinite integral

$$I(f) = \int\frac{(1-f)\sqrt{f}}{f_\infty - f}df \tag{15}$$

In our evaluation of equation 15 all arbitrary constants of integration will be ignored since the ultimate goal is to solve the definite integral given by equation 14. To evaluate I($f$) we begin by making the following substitution in equation 15

$$f = f_\infty \cos^2 x \tag{16}$$

Since equation 16 gives $dF = -2 f_\infty \cos x \sin x dx$ we have

$$\begin{aligned} I &= \int \frac{(1 - f_\infty \cos^2 x)\sqrt{f_\infty \cos^2 x}}{f_\infty - f_\infty \cos^2 x}(-2 f_\infty \cos x \sin x dx) \\ &= -2\sqrt{f_\infty} \int \frac{(1 - f_\infty \cos^2 x)\cos^2 x}{\sin x} dx \\ &= -2\sqrt{f_\infty} \left\{ \int \frac{\cos^2 x}{\sin x} dx - f_\infty \int \frac{\cos^4 x}{\sin x} dx \right\} \end{aligned} \tag{17}$$

Applying the identity $\sin^2 x + \cos^2 x = 1$ gives

$$\begin{aligned} I &= -2\sqrt{f_\infty} \left\{ \int \frac{1 - \sin^2 x}{\sin x} dx - f_\infty \int \frac{1 - 2\sin^2 x + \sin^4 x}{\sin x} dx \right\} \\ &= -2\sqrt{f_\infty} \left\{ \int \csc x dx - \int \sin x dx - f_\infty \left[ \int \csc x dx - 2\int \sin x dx + \int \sin^3 x dx \right] \right\} \\ &= -2\sqrt{f_\infty} \left\{ (1 - f_\infty) \int \csc x dx - (1 - 2 f_\infty) \int \sin x dx - f_\infty \int \sin^3 x dx \right\} \\ &= -2\sqrt{f_\infty} \left\{ (1 - f_\infty) \int \csc x dx + (1 - 2 f_\infty) \cos x - f_\infty \int \sin^3 x dx \right\} \end{aligned} \tag{18}$$

Observe that

$$\begin{aligned} \int \csc x dx &= \int \frac{1}{\sin x} dx = \int \frac{1}{\sin(2(x/2))} dx = \int \frac{1}{2\sin(x/2)\cos(x/2)} dx \\ &= \frac{1}{2} \int \frac{\cos(x/2)}{\sin(x/2)\cos^2(x/2)} dx = \frac{1}{2} \int \frac{\sec^2(x/2)}{\tan(x/2)} dx \\ &= \int \frac{1}{\tan(x/2)} d\tan(x/2) = \ln|\tan(x/2)| \end{aligned} \tag{19}$$

$$\int \sin^3 x dx = \int \sin x(1-\cos^2 x)dx = \int \sin x dx - \int \sin x \cos^2 x dx$$
$$= -\cos x + \frac{1}{3}\cos^3 x dx \tag{20}$$

Substituting equations 19 and 20 into the last line of equation 18 gives

$$I = -2\sqrt{f_\infty}\left\{(1-f_\infty)\ln\left|\tan\frac{x}{2}\right| + (1-2f_\infty)\cos x - f_\infty\left[-\cos x + \frac{1}{3}\cos^3 x\right]\right\}$$
$$= -2\sqrt{f_\infty}\left\{(1-f_\infty)\ln\left|\tan\frac{x}{2}\right| + (1-f_\infty)\cos x - \frac{f_\infty}{3}\cos^3 x\right\} \tag{21}$$
$$= -2\sqrt{f_\infty}(1-f_\infty)\ln\left|\tan\frac{x}{2}\right| - 2\sqrt{f_\infty}(1-f_\infty)\cos x + \frac{2}{3}f_\infty^{3/2}\cos^3 x$$

Next, let

$$\alpha = f / f_\infty = \cos^2 x \tag{22}$$

$$\alpha_0 = f_0 / f_\infty \tag{23}$$

Then during cellular expansion

$$f_0 \le F \le f_\infty \qquad \alpha_0 = \frac{f_0}{f_\infty} \le \frac{F}{f_\infty} = \alpha \le 1$$

$$\alpha_0 \le \alpha \le 1 \qquad 0 \le \sqrt{\alpha_0} \le \sqrt{\alpha} \le 1$$

$$0 \le 1-\sqrt{\alpha} \le 1 \le 1+\sqrt{\alpha} \tag{24}$$

$$0 \le \frac{1-\sqrt{\alpha}}{1+\sqrt{\alpha}} \le 1 \qquad \left|\frac{1-\sqrt{\alpha}}{1+\sqrt{\alpha}}\right| = \frac{1-\sqrt{\alpha}}{1+\sqrt{\alpha}}$$

The order of terms in the numerator is reversed (in the last step) during cellular contraction. The following argument applies specifically to expansion; the corresponding argument for contraction is completely analogous. From equations 22 and 24

$$\ln\left|\tan(x/2)\right| = \ln\left|\sqrt{\frac{1-\cos x}{1+\cos x}}\right| = \ln\left|\sqrt{\frac{1-\sqrt{\alpha}}{1+\sqrt{\alpha}}}\right| = \frac{1}{2}\ln\frac{1-\sqrt{\alpha}}{1+\sqrt{\alpha}} \tag{25}$$

Substitution of equation 25 into equation 21 gives

$$I = -\sqrt{f_\infty}(1-f_\infty)\ln\frac{1-\sqrt{\alpha}}{1+\sqrt{\alpha}} - 2\sqrt{f_\infty}(1-f_\infty)\sqrt{\alpha} + \frac{2}{3}f_\infty^{3/2}\alpha^{3/2} \tag{26}$$

and thus by equation 14

$$\begin{aligned} kt = &-\sqrt{f_\infty}(1-f_\infty)\ln\left[\frac{1-\sqrt{\alpha}}{1+\sqrt{\alpha}}\frac{1+\sqrt{\alpha_0}}{1-\sqrt{\alpha_0}}\right] \\ &-2\sqrt{f_\infty}(1-f_\infty)\left(\sqrt{\alpha}-\sqrt{\alpha_0}\right) + \frac{2}{3}f_\infty^{3/2}\left(\alpha^{3/2}-\alpha_0^{3/2}\right) \end{aligned} \tag{27}$$

With the following substitutions

$$\tau = \frac{\sqrt{f_\infty}(1-f_\infty)}{k} \tag{28}$$

$$\beta = \frac{1-\sqrt{\alpha_0}}{1+\sqrt{\alpha_0}} \tag{29}$$

$$\gamma = \frac{2f_\infty}{3(1-f_\infty)} \tag{30}$$

equation 27 becomes

$$\frac{t}{\tau} = \ln\left[\beta\frac{1+\sqrt{\alpha}}{1-\sqrt{\alpha}}\right] - 2\left(\sqrt{\alpha}-\sqrt{\alpha_0}\right) + \gamma\left(\alpha^{3/2}-\alpha_0^{3/2}\right) \tag{31}$$

It is not possible to analytically invert this formula to get an expression for $\alpha(t)$. We can obtain an approximate expression by observing that $\alpha$ is typically close to 1, and approaches 1 in the limit as $t \to \infty$. In the long term limit, the first term on the right hand side of equation 31 strongly dominates the other two terms. Note that this is only

the case for large $t$; for smaller times the third term may dominate because of the leading factor of $\gamma$. In the long-term time limit only, we can approximate $t \approx \tilde{t}$, where

$$\frac{\tilde{t}}{\tau} = \ln\left[\beta \frac{1+\sqrt{\alpha}}{1-\sqrt{\alpha}}\right] \tag{32}$$

Exponentiating both sides of equation 32 gives

$$e^{\tilde{t}/\tau} = \beta \frac{1+\sqrt{\alpha}}{1-\sqrt{\alpha}} \tag{33}$$

Solving for $\alpha$ gives

$$\alpha = \left(\frac{e^{\tilde{t}/\tau} - \beta}{e^{\tilde{t}/\tau} + \beta}\right)^2 \tag{34}$$

From equation 22 the approximate volume fraction is therefore

$$f(\tilde{t}) \approx f_\infty \left(\frac{e^{\tilde{t}/\tau} - \beta}{e^{\tilde{t}/\tau} + \beta}\right)^2 \tag{35}$$

Although the solution (equation 35) is only valid as $t \to \infty$, and may be rather inaccurate for smaller $t$, it interestingly retains two essential features, namely that

$$\lim_{t \to \infty} f(t) = f_\infty \tag{36}$$

and

$$\begin{aligned} f(0) &= f_\infty \left[\left(1 - \frac{1-\sqrt{\alpha_0}}{1+\sqrt{\alpha_0}}\right) \Big/ \left(1 + \frac{1-\sqrt{\alpha_0}}{1+\sqrt{\alpha_0}}\right)\right]^2 \\ &= f_\infty \left(\frac{1+\sqrt{\alpha_0} - 1 + \sqrt{\alpha_0}}{1+\sqrt{\alpha_0} + 1 - \sqrt{\alpha_0}}\right)^2 = f_\infty \alpha_0 = f_\infty \frac{f_0}{f_\infty} = f_0 \end{aligned} \tag{37}$$

The numerical solution of equation 31 can be found as follows. First let

$$\lambda = \ln\beta + 2\sqrt{\alpha_0} - \gamma\alpha_0^{3/2} \tag{38}$$

Then equation 31 can be rewritten as

$$\frac{t}{\tau} = \ln\left[\frac{1+\sqrt{\alpha}}{1-\sqrt{\alpha}}\right] - 2\sqrt{\alpha} + \gamma\alpha^{3/2} + \lambda \tag{39}$$

where $\gamma$ and $\lambda$ are constants determined by the initial conditions. Next, let

$$u = \sqrt{\alpha} = \sqrt{f / f_\infty} \tag{40}$$

which gives

$$\frac{t}{\tau} = \ln\left[\frac{1+u}{1-u}\right] - 2u + \gamma u^3 + \lambda \tag{41}$$

The problem is to numerically solve equation 41 for $u$ at a given $t$. This is equivalent to finding a root of the equation

$$g(u) = \ln\left[\frac{1+u}{1-u}\right] - 2u + \gamma u^3 + \lambda - \frac{t}{\tau} = 0 \tag{42}$$

The Newton-Raphson iteration formula for this type of problem is

$$u_{n+1} = u_n - \frac{g(u_n)}{g'(u_n)} \tag{43}$$

Once $t$ is given, it is a constant, so by differentiating equation 42

$$g'(u) = \frac{1}{1+u} + \frac{1}{1-u} - 2 + 3\gamma u^2 \tag{44}$$

Since $g$ is monotonic and has precisely one root (this is shown below following equation 54) the choice of starting value is not tremendously important (at worst case it will slow down computation). We thus use the large-time approximation (equation 35) as a first guess, and then iterate using equations 42 through 44. The (numerical) algorithm to solve for $f(t)$ at any given $t$ is then as follows. Given $f_0$, $f_\infty$ and $t$, compute

$$\alpha_0 = f_0 / f_\infty \qquad \text{(from 22)} \qquad (45)$$

$$\beta = \frac{1-\sqrt{\alpha_0}}{1+\sqrt{\alpha_0}} \qquad \text{(from 29)} \qquad (46)$$

$$\gamma = \frac{2 f_\infty}{3(1 - f_\infty)} \qquad \text{(from 30)} \qquad (47)$$

$$\lambda = \ln\beta + 2\sqrt{\alpha_0} - \gamma\alpha_0^{3/2} \qquad \text{(from 38)} \qquad (48)$$

$$u_1 = \frac{e^{t/\tau} - \beta}{e^{t/\tau} + \beta} \qquad \text{(from 34 and 40)} \qquad (49)$$

$$f_1 = f_\infty u_1^2 \qquad \text{(from 40)} \qquad (50)$$

Repeat until desired level of convergence:

$$g_n = \ln\left[\frac{1+u_n}{1-u_n}\right] - 2u_n + \gamma u_n^3 + \lambda - \frac{t}{\tau} \qquad \text{(from 42)} \qquad (51)$$

$$g_n' = \frac{1}{1+u_n} + \frac{1}{1-u_n} - 2 + 3\gamma u_n^2 \qquad \text{(from 44)} \qquad (52)$$

$$u_{n+1} = u_n - \frac{g_n}{g_n'} \qquad \text{(from 43)} \qquad (53)$$

$$f_{n+1} = f_\infty u_{n+1}^2 \qquad \text{(from 40)} \qquad (54)$$

At each integration time step the revised concentrations of all species are computed, the value of $f_\infty$ is revised, and $f$ is computed from eqs. 45 through 54. Then the concentrations are recalculated based on this new value of $f$. The entire process is repeated until all state variables (including $f$ and $f_\infty$) converge to a desired level of precision.

To demonstrate that $g(u)$ has precisely one root, observe first from equation 44 that $g(u)$ is strictly monotonically increasing on ( $0 < u < 1$), because

$$g'(u) = \frac{1}{1+u} + \frac{1}{1-u} - 2 + 3\gamma u^2 = \frac{2}{1-u^2} - 2 + 3\gamma u^2 = 2\frac{u^2}{1-u^2} + 3\gamma u^2 > 0 \qquad (55)$$

Hence there can be a most one root. To prove the existence of at least one root, let

$$h(u) = \ln\frac{1+u}{1-u} - 2u + \gamma u^3 + \lambda \tag{56}$$

We need to show that there is a root of the equation

$$h(u) = t/\tau \tag{57}$$

for all $t$. First, observe that for $t = 0$, $u = \sqrt{\alpha_0}$ is a solution of equation 57 (because $\alpha = \sqrt{\alpha_0}$ is a solution of equation 31 when $t = 0$). Next observe that

$$\lim_{u \to 1} \ln\frac{1+u}{1-u} = \infty \tag{56}$$

Hence $h(u)$ can be made arbitrarily large by choosing $u$ sufficiently close to 1. Since $h$ is differentiable (in fact it is monotonically increasing), it is continuous. Hence by continuity, the function can be made to take on nonnegative value. Hence equation 57 has a root.

Finally, for completeness we derive the exact version of equation 34. We may write equation 31 as

$$\frac{t}{\tau} = \ln\left[\beta\frac{1+\sqrt{\alpha}}{1-\sqrt{\alpha}}\right] - A(\alpha) + B(\alpha) \tag{57}$$

where $A(\alpha) = 2(\alpha^{1/2} - \alpha_0^{1/2})$ and $B(\alpha) = \gamma(\alpha^{3/2} - \alpha_0^{3/2})$. Equations 32 through 34 can be rewritten with $\tilde{t}/\tau$ replaced by $t/\tau + A - B$ to obtain

$$\alpha = \left[\frac{e^{t/\tau}e^{A-B} - \beta}{e^{t/\tau}e^{A-B} + \beta}\right]^2 \tag{58}$$

which is implicit in $\alpha$, since both $A$ and $B$ are functions of $\alpha$.

## 3.6.4. Comparison of Osmotic Models

To study the asymptotic behavior of the solution we first study the large-time ($t \to \infty$) approximation (equation 35 of the previous subsection),

$$f(t) \approx f_\infty \left( \frac{e^{t/\tau} - \beta}{e^{t/\tau} + \beta} \right)^2 = f_\infty \left( \frac{1 - \beta e^{-t/\tau}}{1 + \beta e^{-t/\tau}} \right)^2 \tag{1}$$

where the tilde has been dropped to simplify the notation. The inter-neuronal space typically shrinks by as much as half during SD. Since the neuronal volume fraction is typically $f \approx 0.8$ to $\approx 0.85$ at rest, $f$ should increase to a value between $f_\infty \approx 0.9$ (for $f_0 \approx 0.8$) and $f_\infty \approx 0.925$ (for $f_0 \approx 0.85$). Thus $f_0$ and $f_\infty$ are typically bounded by 0.8 and 0.925, with $f_0 / f_\infty < 1$ during expansion, $f_0 / f_\infty > 1$ during contraction, and equality only holding at steady state (*i.e.*, as $t \to \infty$). Consider the expansion problem (contraction is completely analogous). Then by equation 29 of the previous subsection,

$$|\beta| = \left| \frac{1 - \sqrt{\alpha_0}}{1 + \sqrt{\alpha_0}} \right| = \left| \frac{1 - \sqrt{f_0 / f_\infty}}{1 + \sqrt{f_0 / f_\infty}} \right| < \approx 0.043 \tag{2}$$

Thus it seems reasonable to expand equation 1 in terms of the small parameter $\beta$,

$$\begin{aligned} f &\approx f_\infty \left( (1 - \beta e^{-t/\tau})(1 - \beta e^{-t/\tau} + O(\beta^2) \right)^2 \\ &= f_\infty \left( 1 - 2\beta e^{-t/\tau} + O(\beta^2) \right)^2 \\ &\approx f_\infty (1 - 4\beta e^{-t/\tau}) \\ &= f_\infty + \frac{4\beta f_\infty}{f_\infty - f_0} (f_0 - f_\infty) e^{-t/\tau} \end{aligned} \tag{3}$$

Observe that by equation 29 of the previous subsection,

$$\frac{4\beta f_\infty}{f_\infty - f_0} = \frac{4 f_\infty}{f_\infty - f_0}\frac{\sqrt{f_\infty} - \sqrt{f_0}}{\sqrt{f_\infty} + \sqrt{f_0}} = \frac{4 f_\infty}{\left(\sqrt{f_\infty} + \sqrt{f_0}\right)^2} \tag{4}$$

where the last step follows because

$$f_\infty - f_0 = \left(\sqrt{f_\infty} + \sqrt{f_0}\right)\left(\sqrt{f_\infty} - \sqrt{f_0}\right) \tag{5}$$

Using the above mentioned limits for $f_0$ and $f_\infty$ gives

$$0.89 \approx \frac{0.8}{0.9} \le \frac{f_0}{f_\infty} \le \frac{0.85}{.925} \approx 0.92 \tag{6}$$

Thus

$$0.94 \le \sqrt{f_0 / f_\infty} \le 0.96 \tag{7}$$

and hence

$$3.76 \le \left(1 + \sqrt{f_0 / f_\infty}\right)^2 \le 3.85 \tag{8}$$

From equation 4

$$\frac{4\beta f_\infty}{f_\infty - f_0} = \frac{4 f_\infty}{f_\infty\left(1 + \sqrt{f_0 / f_\infty}\right)^2} = \frac{4}{\left(1 + \sqrt{f_0 / f_\infty}\right)^2} \tag{9}$$

so by equation 8

$$1.04 < \frac{4\beta f_\infty}{f_\infty - f_0} < 1.06 \tag{10}$$

Thus by equation 3

$$f \approx f_\infty + (f_0 - f_\infty)e^{-t/\tau} \tag{11}$$

is an under-estimate of equation 1 by some 4% to 6%. Equation 11 is identical to the solution of the simple relaxation model (see equation 4 of section 3.6.2). Thus the

approximate model (equation 35 of section 3.6.3) and the exponential-relaxation model (equation 4 of section 3.6.2) should give nearly the same results.

To analyze the error in using the exponential model as an estimate for the exact solution (equation 39 of section 3.6.3) we start with equation 58 of the previous section. In the derivation of equation 11 every step remains valid if we replace $t/\tau$ everywhere with $t/\tau + A - B$, giving

$$f \approx f_\infty + (f_0 - f_\infty)e^{-t/\tau}e^{B-A} \tag{12}$$

so long as $\beta e^{B-A}$ (rather than simply $\beta$) is a small parameter ($A$ and $B$ are functions of $\alpha$ defined following equation 57 of the previous section). To simplify calculations, the algebraic identity $x^3 - y^3 = (x-y)(x^2 + y^2 + xy)$ can be used to factor $B$ - $A$,

$$\begin{aligned} B - A &= \gamma(\alpha^{3/2} - \alpha_0^{3/2}) - 2(\alpha^{1/2} - \alpha_0^{1/2}) \\ &= (\alpha^{1/2} - \alpha_0^{1/2})\left[\gamma(\alpha + \alpha_0 + \sqrt{\alpha\alpha_0}) - 2\right] \\ &\le (1 - \alpha_0^{1/2})\left[\gamma(1 + \alpha_0 + \sqrt{\alpha_0}) - 2\right] \end{aligned} \tag{13}$$

where the last line follows because $\alpha_0 \le \alpha \le 1$ during expansion. For $\alpha_0$=0.8 and $f_\infty$=0.9 we obtain $\gamma$=6, $\beta \approx 0.056$ and $\beta e^{B-A} \le 0.08$; for $\alpha_0$=0.85 and $f_\infty$=0.925 we obtain $\gamma \approx 8.22$, $\beta \approx 0.041$ and $\beta e^{B-A} \le 0.21$. Since equation (12) neglects terms that are of order $\left(\beta e^{B-A}\right)^2$ we anticipate some 0.6% to 4% error (squaring the bounds on $\beta e^{B-A}$) in addition to the 4% to 6% underestimate discussed following equation 11. The net result is still an underestimate. A numerical comparison of the exact and exponential models is illustrated in Figure 3.16.

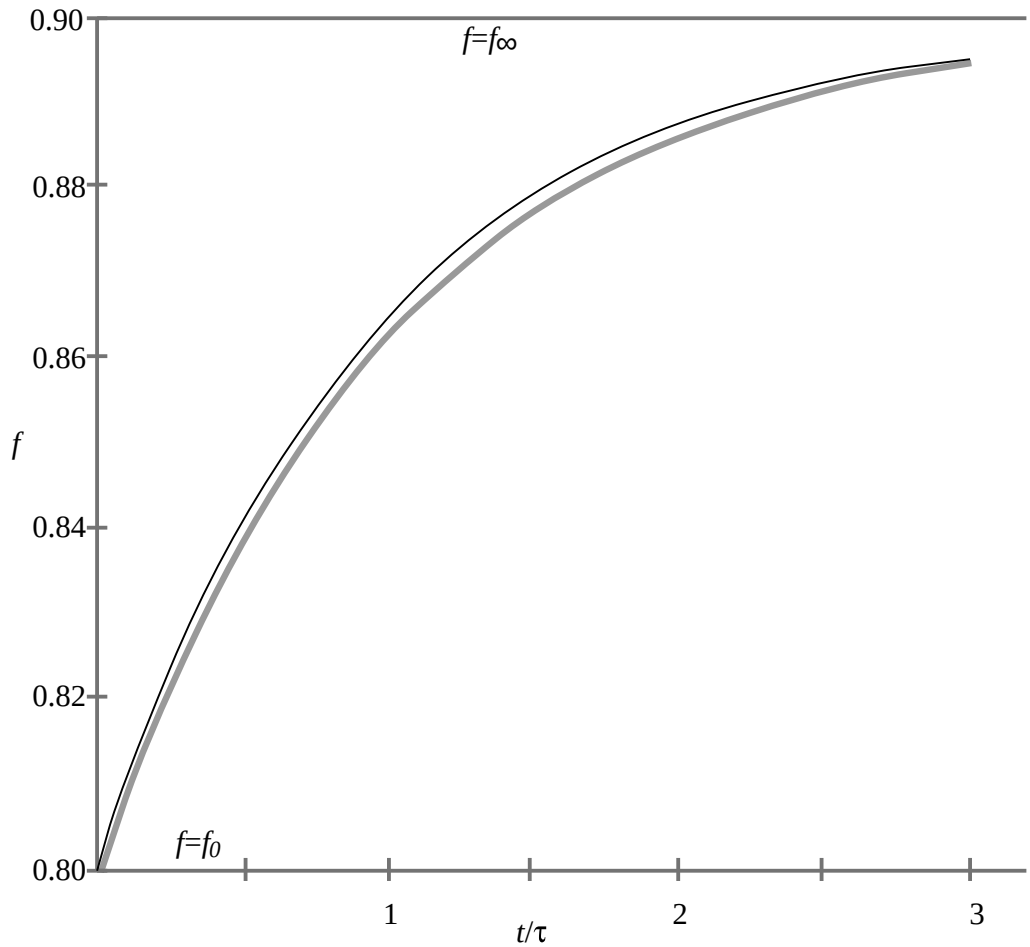


Figure 3.16. Comparison of solution to exact (thin black line) and exponential relaxation (heavy gray line) models for a situation with $f_0 = 0.8$ and $f_\infty = 0.9$. The asymptote for $f = f_\infty$ is shown as the straight line at $f = 0.9$. The abscissa corresponds to the line $f = f_0$, and is given in units of the time constant $\tau$. Observe that the exponential solution is an underestimate as predicted (see the text following equation 11).

### 3.6.5. ESTIMATION OF OSMOTIC TIME COEFFICIENT

From equations 11 and 28 of section 3.6.3 the time constant for volume changes should be given approximately by

$$\tau = \frac{\sqrt{f_\infty}(1-f_\infty)V^{3/2}}{2\phi P_f \sqrt{\pi L} V_W (n_{in}+n_{out})} \qquad (1)$$

Unfortunately many of the parameters in equation 1 are not well known or are difficult to estimate. In particular it requires that we know the absolute number of solute ions on both sides of the membrane, among other things. Instead, it should be easier to fit a value of $\tau$ to experimental data. This requires knowledge of the volume as a function of time after a change in osmolarity has occurred. Such an experiment has recently been reported for endothelial cells (Voets and others 1999). The investigators were interested in studying volume regulated anion channels. In a typical experiment (such as the one used to obtain the data shown in Figure 3.17) they reduced the interstitial osmolarity from 320 mOsm to 240 mOsm by changing the $Na^+$ concentration of the perfusate and observing cell thickness as a function of time. A fit of equation 4 of section 3.6.2 gives a time constant of $\tau \approx$ 20 seconds, as illustrated in Figure 3.17. However, the cells represented in Figure 3.17 were relatively flat, with a thickness of $\approx$2 μm and an area of $\approx$60 $\mu m^2$, and expansion was essentially restricted to a single dimension (the thickness of the "pancake"). It is not clear how to apply these data to neurons, which should expand in either two (with cylindrical geometry, as assumed in the previous section) or three (spherical geometry, e.g., somata) dimensions.

However, the general biophysical mechanisms driving cellular volume changes are probably similar and it should be reasonable to expect that the time constants would have the same order of magnitude. The observations in the non-neuronal cells give us an estimate of the range of time constants one might expect to see in all cells. The range of validity of the model can then be evaluated by stress testing the model over a wide range of time constants including those observed in the non-neuronal cells.

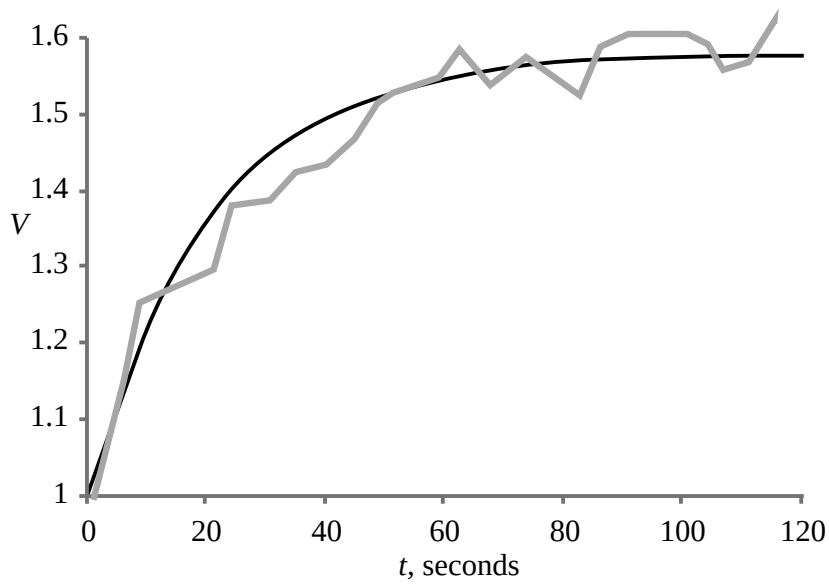


Figure 3.17. Estimation of time constant τ for osmotic expansion. The data (heavy, jagged gray curve) are taken from Voets and others (1999) Figure 2; the curve (thinner, smooth, black curve) is given by equation 4 of section 3.6.2 using $\tau = 16.56$ seconds, $V_0 = 1.0$ and $V_\infty = 1.585$.

## 3.7. INTRACELLULAR CALCIUM STORES

At typical physiological concentrations, at least 95% of the calcium that enters a cell is buffered (Berridge, 1993; Kostyuk and Verkhrasky, 1995). Free calcium is removed by two different processes that occur on different time scales. In the faster process, calcium is bound by an intracellular protein, such as calmodulin (Cam), calbindin, calreticulin or parvalbumin. It is this process that gives calcium its ability to rapidly trigger a cascade of signals even at very low concentrations. Calmodulin, for example, is present in gray matter at a concentration estimated to be between ≈30 μM and ≈50 μM (Neher, 1995; Gabso, Neher and Spira, 1997). A single molecule of calmodulin has four binding sites for calcium, giving it a total buffering capacity of ≈120 μM to 200 μm. Fully bound Ca-Cam complexes typically trigger activity via the so-called Cam-dependent protein kinases, phosphatases and adenylate cyclases. The calcium binding reaction

$$Ca + Cam \underset{b}{\overset{f}{\rightleftharpoons}} CaCam \qquad (1)$$

has rate constants of $b \approx 500$ sec$^{-1}$ and $f \approx 5\times10^4$ sec$^{-1}$mM$^{-1}$, giving a $K_d$ ( = $b/f$) of ≈ 0.01 mM. Applying the law of mass action, the corresponding differential equation is then

$$j_{buff} \equiv \frac{d[Ca]}{dt} = \frac{d[Cam]}{dt} = \frac{[Cam]_\infty - [Cam]}{\tau} \qquad (2)$$

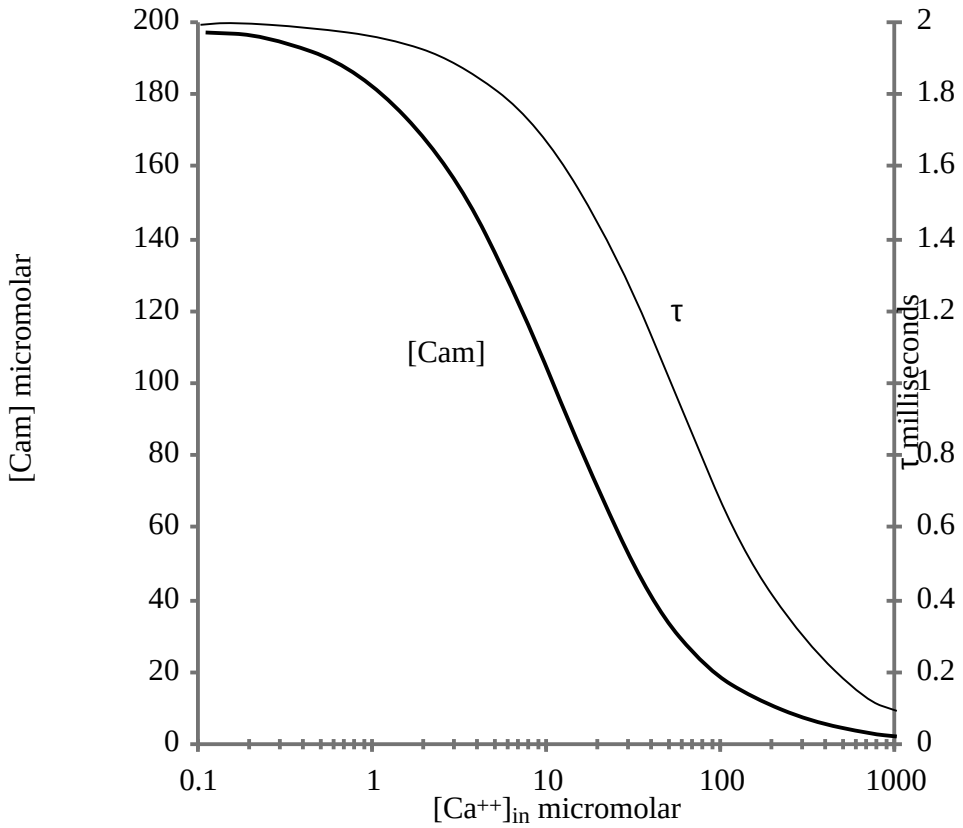


Figure 3.18. Steady state protein buffer concentration and time constant for relaxation toward steady state according to the law of mass action for equation 1, given the values of the rate constants listed in the text. The following parameters were used: $b = 500\ \text{sec}^{-1}$, $f = 5\times10^{4}\ \text{sec}^{-1}\text{mM}^{-1}$; $T = 200\ \mu\text{M}$.

where the steady-state concentration of free buffer is

$$[Cam]_{\infty} = \frac{T}{1 + [Ca]/K_d} \tag{3}$$

where T is the total buffer concentration (free plus bound buffer) and the time constant for relaxation to steady state is

$$\tau = \frac{1}{b + f[Ca]} \tag{4}$$

Equations 3 and 4 are illustrated in Figure 3.18 as a function of free calcium concentration. The high level of protein buffering capacity illustrated in Figure 3.18 probably only exists immediately beneath the membrane, typically in a layer ≈0.1 μm or thinner (Yamada, Koch and Adams, 1998). This implies that in typical dendrites (1 μm to 2 μm in radius) the total protein buffering capability averaged over a full dendritic cross-section is probably reduced by at least 80% to 90% from the quoted values. Because the resulting values are substantially lower than those due to intracellular organelles (which will be described in the following paragraphs) protein buffering is excluded from the model. However, this remains an important subject for further studies, particularly in the study of SD-associated calcium waves, and K(Ca) effects on SD propagation.

The second process by which free calcium is removed is via buffering to intracellular organelles, primarily the endoplasmic reticulum (ER) and mitochondria. While this process occurs on a much slower time scale – that of seconds rather than

milliseconds – these buffers are much larger. Neuronal measurements have indicated a capacity somewhere between 100 μM and 5 mM. (Kendall, Dormer and Campbell; 1992, Hofer and Machen, 1993; Llano, DiPolo and Marty, 1994; Fiero and Llano, 1996). In Purkinje cells, the binding rate has been estimated as $f \approx 1300$ $mM^{-1}sec^{-1}$ with $K_d \approx 0.02$ μM (De Schutter and Smolen, 1998; de Schutter, 1998).

Buffering occurs via a calcium – dependent ion pump in the ER membrane. This has been modeled as (Atri and others, 1993; Atri, 1996)

$$j_{Pump} = j_{Pump,Max} \frac{[Ca^{++}]_{in}}{0.0001 + [Ca^{++}]_{in}} \qquad (5)$$

Estimates for the pump rate $j_{ERPump,Max}$ range from ≈1 μM/sec in astrocytes, frog oocytes and airway epithelial cells (Atri and others, 1993; Roth and others, 1995; Sneyd and others, 1995) to at least 16 μM/sec in Purkinje cells (De Schutter, 1998; De Schutter and Smolen, 1998) and nearly 1 mM/sec in the bullfrog sympathetic ganglion (Friel, 1995, assuming a $T \approx 4$ mM) and cardiac cells (Keizer and Levine, 1996).

Calcium can also be released from these organelles; this occurs through at least two known types of channels. Both of these channels exhibit a biphasic response to calcium, in which calcium activates the channel at lower concentrations (sub-micromolar) and inactivates at higher concentrations. One of these channels also requires the presence of ITP (1,4,5-inositol trisphosphate). The other channel is sensitive to both ryanodine, which blocks the channel, and methyl xanthines (such as

caffeine and theophylline) that activate the channel by making it more sensitive to calcium) (Berridge, 1993; Coronado and others, 1994; Kostyuk and Verkhratsky, 1995; Goldbeter, 1996; De Schutter and Smolen, 1998). Agonist-induced calcium release can be stimulated by injecting cells with caffeine or ITP; in such experiments calcium transients or oscillations of ≈100 to ≈600 nM (nanomolar) $Ca^{++}$ have been observed. Calcium can be released from ITP-sensitive pools by activation of metabatropic glutamate receptors, muscarinic cholinergic receptors and metabatropic purinoreceptors on the cellular membrane, probably via G-proteins. It is not clear if both ITP and ryanodine receptors act on the same calcium stores in neurons, or whether two different pools of calcium are involved. In the models implemented in the present study, only a single calcium pool is utilized. This pool includes both ryanodine and ITP sensitive channels (Goldbeter, 1996).

ITP-sensitive calcium stores have been identified throughout the dendritic tree, particularly in Purkinje cells (De Schutter and Smolen, 1998). The calcium flux through the ITP sensitive channel is described with the model of Atri (1996) in which

$$j_{ITP} = j_{ITP,Max} h_{ITP} \left(0.567 + \frac{0.433[\mathrm{ITP}]}{0.004 + [\mathrm{ITP}]}\right)\left(0.111 + \frac{0.889[Ca^{++}]_{in}}{0.0007 + [Ca^{++}]_{in}}\right) \quad (6)$$

where $h_{ITP}$ is a Hodgkin-Huxley inactivation variable with a time constant of $\tau_h$=2 seconds and steady state activation of

$$h_{ITP,\infty} = \frac{1}{1 + \left([Ca^{++}]_{in} / 0.0007\right)^2} \quad (7)$$

Estimates of the maximum magnitude of the ITP-sensitive current range from ≈3 μM/sec in airway epithelial cells to ≈15 μM/sec in Purkinje cells (Sneyd and others, 1995; De Schutter and Smolen, 1998).

Stretch-activated IP3 production has been observed in airway epithelial cells; the rate of production is proportional to the increase in area, with the concentration tripling with an increase of ≈14% (Felix, Woodruff and Dirksen, 1996). This data has been fit with the simple model

$$\frac{d[\mathrm{ITP}]}{dt} = 0.04 m_{stretch} \Delta A \qquad (9)$$

where $m_{stretch}$ is a Hodgkin-Huxley activation variable with a time-constant of 3 seconds and step-function steady state value,

$$m_{stretch,\infty} = \begin{cases} 1, & [\mathrm{ITP}] \le [\mathrm{ITP}]_{threshold} \\ 0, & [\mathrm{ITP}] > [\mathrm{ITP}]_{threshold} \end{cases} . \qquad (10)$$

and ΔA is the relative change in membrane area. ITP is degraded at a rate give by (Keener and Sneyd, 1998)

$$j_{ITP-removal} = \frac{v_{ITP} k_{ITP} [\mathrm{ITP}]}{[\mathrm{ITP}] + k_{ITP}} \qquad (11)$$

The ITP concentration following inside a cell whose membrane has been stretch to 13% above its resting area is illustrated in Figure 3.19. A time constant of 1 sec was used for $m_{stretch}$ was used for this simulation. Other parameters used were $v_{ITP}$=1/sec and

$k_{ITP}$=1.25 μM. An activation threshold (in equation 10) of [ITP] = 1.8 μM is used (Felix, Woodruff and Dirksen, 1996).

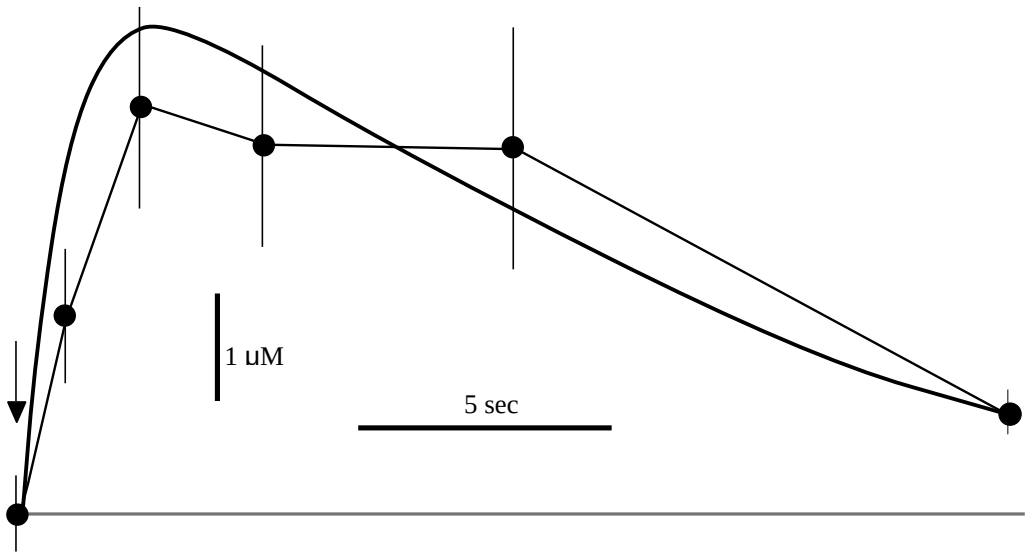


Figure 3.19. ITP production simulated using the model described by equations 9 and 10 following a membrane stretch by 13%. The curves give the total ITP concentration as a function of time following the beginning of the stimulation (arrow). The membrane is held stretched for the entire experiment. The data (including error bars) is taken from Felix, Woodruff and Dirksen (1996) for airway epithelial cells. The horizontal line indicates the baseline concentration (1.6 μM).

The ryanodine channel is described by the reduced quasi-steady-state model suggested by Keener and Sneyd (1998, page 183) which gives the $Ca^{++}$ flux as

$$j_{ryanodine} = m_{ryanodine} v_{ryanodine} \left( [Ca^{++}]_{ER} - [Ca^{++}]_{in} \right) \tag{12}$$

where $m_{ryanodine}$ is a Hodgkin-Huxley variable with steady-state value and time constant given by

$$m_{ryanodine,\infty} = \left[ 1 + \frac{0.05}{[Ca^{++}]_{in}} + \frac{[Ca^{++}]_{in}}{0.001} \right]^{-1} \tag{13}$$

$$\tau_{m,ryanodine} = \left[ 0.8 + \frac{800[Ca^{++}]_{in}}{1 + 0.5/[Ca^{++}]_{in}} \right]^{-1} \tag{14}$$

Estimates of the pump rate $v_{ryanodine}$ range from 15 $sec^{-1}$ to 40 $sec^{-1}$ in cardiac cells (Keizer and Levine, 1996; Keener and Sneyd, 1998) to 2.4 $sec^{-1}$ in the bull frog sympathetic neuron (Friel, 1995) and 0.02 $sec^{-1}$ in cerebellar Purkinje cells (De Schutter, 1998).

Figure 3.20 compares the various models for buffering and release by intracellular organelles.

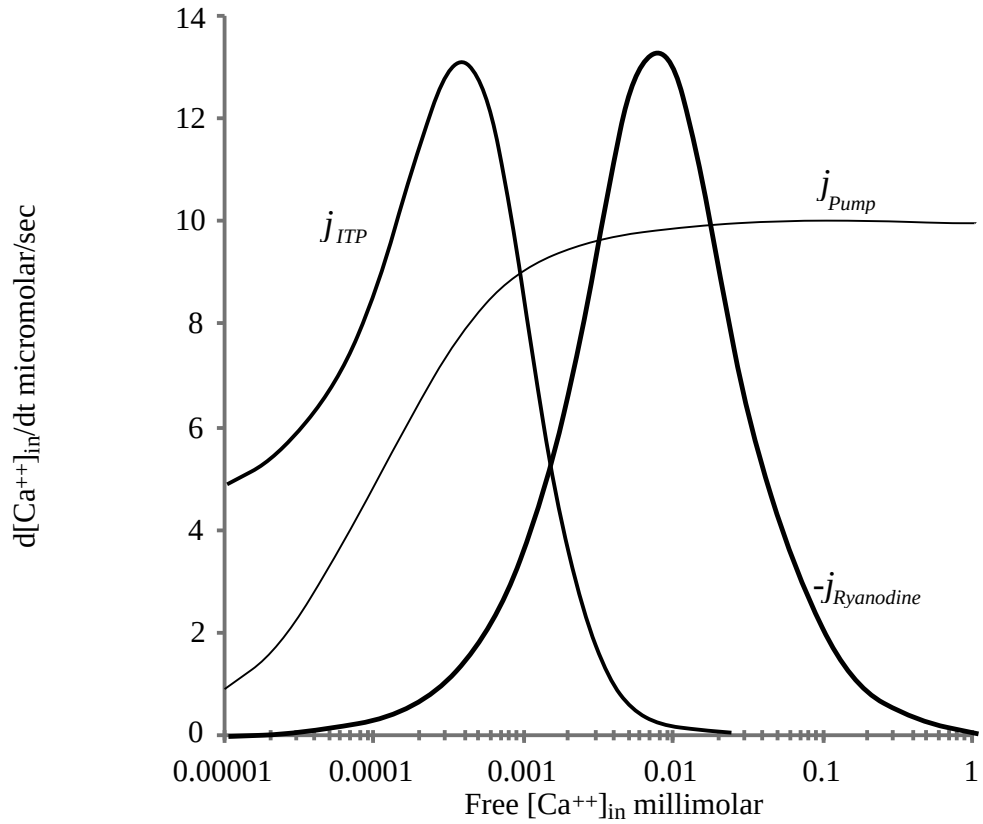


Figure 3.20. Comparison of models for calcium buffering by and release from intracellular organelles. $j_{Ryanodine}$ is calciulated from equation 12 with $v_{Ryanodine}$ =0.1 $sec^{-1}$ and $[Ca]_{ER}$=2 mM; $j_{ITP}$ is calculated from equation 6 with $j_{ITP,max}$=0.04 mM/sec in the limit of high [IP3] concentration (so that the first bracketed term in equation 6 is equal to one); $j_{Pump}$ is calculated from equation 5 with $j_{Pump,Max}$=0.01 mM/sec.

## 3.8. IMPLEMENTATION

To provide a simpler, and more general numerical implementation, equations 1 and 11 of section 3.2 were rewritten in the form

$$\frac{\partial c}{\partial t} = \frac{\partial}{\partial x}\left(D\frac{\partial c}{\partial x}\right) + g \tag{1}$$

where $c$ and $D$ represent $c_{in}$ and $D_{in}$ (equation 1) or $c_{out}$ and $D_{out}$ (equation 11). They are all are functions of $x$ and $t$. The forcing function is

$$g(x,t) = \frac{zF}{RT}\frac{\partial}{\partial x}\left(c_{in}D_{c,in}\frac{\partial E}{\partial x}\right) - rJ_{c,m} + s_c \tag{2}$$

for the cytosolic concentrations, and

$$g(x,t) = \frac{rf}{1-f}J_{c,m} - J_{c,glia} \tag{3}$$

for the interstitial concentrations. The electrodiffusion term (the first term on the right side of equation 2) was calculated at each time step using a cubic-spline interpolation for the voltage (Engeln-Müllges and Uhlig, 1996). The membrane ion flux $J_{c,m}$ for each species is just the simple sum of the ion fluxes for all currents for that species (see section 3.2). Equation 2 was solved numerically using the Crank-Nicholson method (Morton and Mayers, 1994).

The integration technique was implemented as follows. Space is discretized (see Figure 3.21) into individual points $x_j = \left(j - \frac{J}{2}\right)\Delta x$, with a total *J-1* intervals

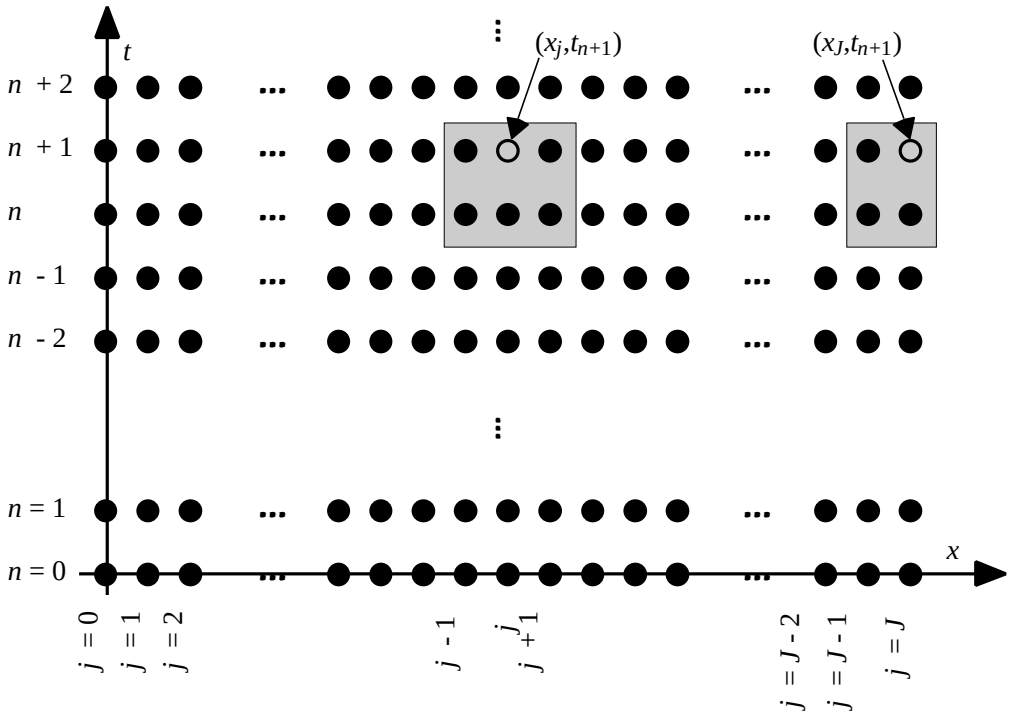


Figure 3.21. Spatial discretization used in numerical integration. The implicit relationship of state variables at six different grid points (four different grid points at a boundary point) is illustrated by the boxes. The implicit equations are then solved (numerically and interatively) for the indicated point (open circle) as described in the text of this section. The origin of the x-axis is chosen at $j$ = J/2 (not illustrated) and the origin of the time axis occurs at $n$ = 0.

of length $\Delta x$, where $J$ is an odd integer, so that $j = J/2$ corresponds to the origin ($x$=0). Time is discretized into individual points $t_n = n\Delta t$, where $n \geq 0$, with $t_0$ corresponding to the initial (start) time. The state variables at time $t_{n+1}$ and location $x_j$ are related to their values at the surrounding gridpoints $x_{j\pm1}$ at $t_{n+1}$, and their values at these three same spatial grid points at the previous time step $t_n$ according to the implicit formula (for $j = 2, \ldots, J\text{-}1$)

$$\begin{aligned}\frac{c_j^{n+1} - c_j^n}{\Delta t} = \frac{1}{2(\Delta x)^2}\Big[&D_{j+1/2}^{n+1}\left(c_{j+1}^{n+1} - c_j^{n+1}\right) - D_{j-1/2}^{n+1}\left(c_j^{n+1} - c_{j-1}^{n+1}\right) + \\ &D_{j+1/2}^{n}\left(c_{j+1}^{n} - c_j^{n}\right) - D_{j-1/2}^{n}\left(c_j^{n} - c_{j-1}^{n}\right)\Big] \\ &+ \frac{1}{2}\left[g_j^{n+1} + g_j^n\right]\end{aligned} \tag{4}$$

where $D_{j+1/2}^n$ is the diffusion constant evaluated at a spatial location halfway between grid points. At the spatial endpoints ($j$ = 1 and $j$ = $J$)

$$\begin{aligned}\frac{c_1^{n+1} - c_1^n}{\Delta t} = \frac{1}{2(\Delta x)^2}\Big[&D_{1+1/2}^{n+1}\left(c_2^{n+1} - c_1^{n+1}\right) - 2D_{1/2}^{n+1}c_1^{n+1} + \\ &D_{1+1/2}^{n}\left(c_2^{n} - c_1^{n}\right) - 2D_{1/2}^{n}c_1^{n}\Big] + \frac{1}{2}\left[g_1^{n+1} + g_1^n\right]\end{aligned} \tag{5}$$

$$\begin{aligned}\frac{c_J^{n+1} - c_J^n}{\Delta t} = \frac{1}{2(\Delta x)^2}\Big[&-2D_{j+1/2}^{n+1}c_j^{n+1} - D_{J-1/2}^{n+1}\left(c_J^{n+1} - c_{J-1}^{n+1}\right) + \\ &-2D_{j+1/2}^{n}c_J^{n} - D_{j-1/2}^{n}\left(c_J^{n} - c_{J-1}^{n}\right)\Big] + \frac{1}{2}\left[g_J^{n+1} + g_J^n\right]\end{aligned} \tag{6}$$

To account for voltage-dependent gap-junctional conductivity or calcium block, $D_{j+1/2}^n$ is calculated using a standard cubic-spline interpolation scheme. No

significant dependence was found in a small number of test runs that were performed. As the calcium threshold for gap-junction inactivation was increased (e.g., by slowly raising $K_{Ca}$ in equation 4 of section 3.4 from zero to several micromolar) no effect was seen until a sharp threshold was reached. Above threshold, no wave propagation occurred, and below threshold, no difference was seen between $K_{Ca} = 0$ and $K_{Ca} > 0$. The system behaved as if gap junctions were closed suddenly, and not in a graded fashion. Since there is no data that indicates the value of $K_{Ca}$ in neuronal tissue (if the gap junctions even are calcium-sensitive, and there is no data on this subject either), the phenomenon was not investigated further. Since the purpose of this study was to demonstrate the possibility of gap junction-mediated spreading depression, and not to elucidate the mechanisms of gap junction activity, a more complete study was deemed to be beyond the scope of the dissertation. A more complete study would include spatially-dependent and time-dependent diffusion, and would further examine the variables that may cause this dependence (such as calcium concentration or pH).

For implementation, equations (4) through (6) were first written more compactly in matrix form by defining $h = \dfrac{\Delta t}{2(\Delta x)^2}$ and $k = \Delta t / 2$ and observing that

$$\begin{aligned} c_1^{n+1} - c_1^n = {} & h\left[2D_{1+1/2}^{n+1} c_2^{n+1} - \left(D_{1+1/2}^{n+1} + D_{1/2}^{n+1}\right) c_1^{n+1}\right] \\ & + h\left[2D_{1+1/2}^{n} c_2^{n} - \left(D_{1+1/2}^{n} + D_{1/2}^{n}\right) c_1^{n}\right] + k\left[g_1^{n+1} + g_1^n\right] \end{aligned} \tag{7}$$

$$
\begin{aligned}
c_j^{n+1} - c_j^n = {} & h\left[D_{j+1/2}^{n+1} c_{j+1}^{n+1} - \left(D_{j+1/2}^{n+1} + D_{j-1/2}^{n+1}\right) c_j^{n+1} + D_{j-1/2}^{n+1} c_{j-1}^{n+1}\right] \\
& + h\left[D_{j+1/2}^{n} c_{j+1}^{n} - \left(D_{j+1/2}^{n} + D_{j-1/2}^{n}\right) c_j^{n} + D_{j-1/2}^{n} c_{j-1}^{n}\right] \\
& + k\left[g_j^{n+1} + g_j^n\right]
\end{aligned}
\tag{8}
$$

$$
\begin{aligned}
c_J^{n+1} - c_J^n = {} & h\left[-\left(D_{J+1/2}^{n+1} + D_{J-1/2}^{n+1}\right) c_J^{n+1} + 2D_{J-1/2}^{n+1} c_{J-1}^{n+1}\right] \\
& + h\left[-\left(D_{J+1/2}^{n} + D_{J-1/2}^{n}\right) c_J^{n} + 2D_{J-1/2}^{n} c_{J-1}^{n}\right] + k\left[g_J^{n+1} + g_J^n\right]
\end{aligned}
\tag{9}
$$

Then the following vectors are defined, where we continue to indicate the time step with a superscript index,

$$
\mathbf{c}^n = \begin{pmatrix} c_1^n \\ c_2^n \\ \vdots \\ c_j^n \end{pmatrix}, \quad \mathbf{G}^n = h\begin{pmatrix} g_1^n \\ g_2^n \\ \vdots \\ g_j^n \end{pmatrix}
\tag{10}
$$

as is the tridiagonal matrix $\mathbf{D}^n$

$$
\mathbf{D}^n = \begin{pmatrix} -D_{1.5}^n - D_{0.5}^n & 2D_{1.5}^n & 0 & & \\ D_{1.5}^n & -D_{2.5}^n - D_{1.5}^n & D_{2.5}^n & \vdots & \\ 0 & & \ddots & 0 & \\ \vdots & 0 & 2D_{J-1/2}^n & -D_{J-1/2}^n & -D_{J+1/2}^n \end{pmatrix}
\tag{11}
$$

In particular, when $D$ is a constant, then the matrix $\mathbf{D}$ is a constant:

$$
\mathbf{D}^n = \begin{pmatrix} -2D & 2D & 0 & \cdots & 0 \\ D & -2D & D & & \vdots \\ 0 & \ddots & \ddots & \ddots & 0 \\ \vdots & & D & -2D & D \\ 0 & \cdots & 0 & 2D & -2D \end{pmatrix}
\tag{12}
$$

With these definitions equation (5) becomes

$$
\mathbf{c}^{n+1} - \mathbf{c}^n = h\mathbf{D}^{n+1}\mathbf{c}^{n+1} + h\mathbf{D}^n\mathbf{c}^n + \mathbf{G}^n + \mathbf{G}^{n+1}
\tag{13}
$$

Equation (13) can be solved for the $n$+1'st state vector,

$$\mathbf{c}^{n+1} = \left(\mathbf{I} - h\mathbf{D}^{n+1}\right)^{-1}\left[\left(\mathbf{I} + h\mathbf{D}^{n}\right)\mathbf{c}^{n} + \mathbf{G}^{n} + \mathbf{G}^{n+1}\right] \tag{14}$$

It is convenient to define the matrices

$$\mathbf{A}(n) = \mathbf{I} - h\mathbf{D}^{n+1} \tag{15}$$

$$\mathbf{B}(n) = \mathbf{I} + h\mathbf{D}^{n} \tag{16}$$

The notation in equations (15) and (16) for the time step is not written as a superscript, but rather as a functional dependence on $n$, so as to avoid any confusion in equation (17) between time step and matrix inversion. With these definitions, equation (14) becomes

$$\mathbf{c}^{n+1} = \mathbf{A}(n)^{-1}\left[\mathbf{B}(n)\mathbf{c}^{n} + \mathbf{G}^{n} + \mathbf{G}^{n+1}\right] \tag{17}$$

where the "-1" superscript is indicates matrix inversion. When $D$ is a constant, the matrices **A** and **B** only have to be calculated once for all times. When $D$ is variable, the inversion of **A** can still be calculated efficiently in O($J$) steps because the matrix is tridiagonal. Inversion of a $J \times J$ matrix will in general require $O(J^3)$ steps (Engeln-Müllges and Uhlig, 1996).

Since equation 14 is implicit in $\mathbf{G}^{n+1}$, $\mathbf{c}^{n}$ was used to obtain a first estimate of $\mathbf{G}^{n+1}$ on the right side of the equation (**G** is a function of **c** through the membrane currents, etc.). Iteration for successive approximations to $\mathbf{G}^{n+1}$ was continued at each time step until the membrane voltage converged to within $10^{-7}$ mV.

The initial stimulation was modeled in most simulations by raising the interstitial concentration of potassium at $x$ = 0 to 50 mM/liter with a bell-shaped (Gaussian) distribution ($\sigma$ = 100 μm). Other initial concentrations were tested, but this variation had no significant effect on the results, as will be discussed in chapter 4 ("Results"). There was some concern that discontinuous initial conditions (e.g., step functions or spikes) might lead to instability in the integration algorithm, although there is no theoretical reason that this might be a problem with the Crank-Nicholson technique. It is possible to obtain some oscillations (resembling the Gibbs-phenomenon seen in Fourier Analysis) in such situations, but even this was not observed. However, because of these concerns, the Gaussian initial condition was chosen, which had none of the aforementioned potential difficulties. Furthermore, it was felt that a Gaussian stimulation would more correctly describe reasonable experimental conditions in which a "drop" of K+ enriched solution was "dropped" onto the tissue.

All models were implemented as FORTRAN-77 standard computer programs (using Pro-FORTRAN/F77, version 6.0, Absoft Corporation, Rochester Hills, MI) and were run on an Apple iMac (233 MHz, Apple Computer, Inc., Cupertino, CA). All floating point variables were implemented as double precision pseudo-real numbers (REAL*8) with ≈15 digits accuracy.

Because of the large amount of numbers calculated, only a subset of the predicted values were sampled for output. To produce the waveform-shape versus

position plots, typically one point every 50 microns (e.g., 20 points per millimiter) was sampled every 5 or 10 seconds. These results were copied into Microsoft *Excel* spreadsheets and plotted. Wave speed calculations were performed in *Excel* by measuring the time of the leading edge of the potassium wave at half-maximum magnitude. To produce the waveform shape versus time plots, values were output at a subset of locations (typically one to five *x*-values) at 100 mSec intervals.

## 3.9. PROGRAM VERIFICATION AND TESTING

The total program comprised approximately 8000 lines of FORTRAN code (including comments). All FORTRAN code was tested using standard program verification techniques. After each subroutine was implemented, a temporary driver program was written to execute that subroutine. In this way the transmission of information between the calling and the called subprogram could be verified.

Each physical model (*e.g.*, Hodgkin-Huxley variable, ion current, Goldman voltage calculation, *etc*.) was verified against the expected output. For example, a driver subroutine for a particular $m_\infty$ or $h_\infty$ variable would produce a table of that variable as a function of voltage, where the range of voltages encompassed (and significantly exceeded) the expected physiological range (*e.g.* ±250 mV). This table of values was plotted using a standard spreadsheet program (*e.g.*, Microsoft *Excel*). The plot was then compared with the published plot to verify correct behavior. At a higher level, the steady-state current-voltage relations were also plotted and compared with published models (for example, many of the models in this chapter are accompanied by such plots).

Additionally, each physical model was implemented in *Mathematica* as well as in FORTRAN. The advantage of a *Mathematica* implementation is the palette-based equation input and WYSIWYG display. Thus it was possible to visually compare the *Mathematica* equations with the model equations. Data tables and plots were also

generated with *Mathematica* that were subsequently compared with both published plots (where available) and the final FORTRAN implementation. All discrepancies were further examined until all coding errors were discovered and the discrepancies removed.

Calculation techniques were verified in a similar manner. For example, matrix multiplication routines (e.g., multiplication, addition, inversion) were passed several test matrices and manipulated. Analogous calculations were performed with *Mathematica*, which contains explicit matrix manipulation methods. Each element of a calculated matrix was compared with the same element of the *Mathematica* matrix. Finally, the FORTRAN program was utilized to verify such things as $\mathbf{AA}^{-1} = \mathbf{I}$. In a similar vein, the numerical interpolation algorithm was tested with various arrays of data representing either smooth data or high frequency data. The data arrays and interpolated values were plotted to verify reasonable interpolation values.

Integration subroutines were also tested with special driver programs. When all ion currents and electrodiffusion are inhibited only diffusion remains in the equations. The diffusion equation can be solved analytically with a spike-increase (*e.g.*, delta-function) initial condition. The solution is an expanding Gaussian; otherwise the solution is the convolution of a Gaussian-kernel with the initial condition. The concentration of each ion was independently raised at a single point to simulate a delta-function at $t = 0$. The program was then run forward for 60 seconds

and the resulting concentration profiles compared with the expected diffusive profiles in both their spatial and time dependence. No discrepancies were discovered.

The ability of the program to correctly integrate the ion currents with the diffusive drivers and predict wave propagation was verified as follows. First, a Hodgkin-Huxley voltage-driver was written to simulate a propagating action potential in a simulated axonal compartment with Sodium and Potassium channels. When the conductances were raised to physiologic axonal values, Hodgkin-Huxley type spikes were observed. These were plotted by sampling the data at 0.01 mSec intervals; for the spike tests, an integration step size of 0.001 msec was sufficient. No change in the results was observed with smaller time steps. Second, the calcium-models were tested with initial conditions comparable to those in published models (Atri and others, 1993; Keener and Sneyd, 1998). All wave-propagation and calcium-oscillation characteristics predicted by the program (*e.g.*, wave speed, wave magnitude, parametric dependence) were verified to agree with the published models. For the calcium models step sizes of 0.1 to 5 msec were found to be sufficient; further decreasing the step size produced no observable change in the output. Step sizes larger than 10 msec produced inconsistent results. Finally, when all ion currents and models were enabled but there was no simulation, the model system remained quiescent as would be expected (i.e., nothing should happen). This was verified with five-minute (simulated time) runs with step sizes of 0.1 to 5 mSec; voltages and concentrations remained unchanged to within one part in $10^5$ during this period.

When the complete model was integrated the system was tested with a wide range of spatial and time discretization step sizes. No advantage was found in reducing the step size beneath 50 μm, i.e., there was no change in the results when smaller steps were used. Inconsistent results occurred when the step size was increased above 100 μm. Similarly, when the time step was decreased, no change in the results was observed when the step size was decreased beneath 0.1 msec. Inconsistent results were obtained with step sizes exceed ≈10 msec, probably because at this point the time constants of some of the ion gates are exceeded. As a result, simulations were run with step sizes of 50 μm and 0.1 msec. Because voltage spiking was not an integral part of this study the lower step sizes needed to recover the voltage transients were not necessary. Furthermore, since the voltage calculation was performed using a Goldman calculation rather than the Hodgkin-Huxley current-integration driver, all high-speed transients that would have led to spiking were eliminated from the results.

# CHAPTER 4

# RESULTS

This chapter presents the results of numerical simulations that were used to evalulate the model. Table 4.1 gives the resting concentrations and diffusion constants which were assumed. Table 4.2 shows other parameters that were used in the simulations. In most of the simulations, a parametric subset was extensively varied to test the robustness of the model. In general, this involved a variation of some ionic conductance. Other parameters (besides ionic conductances) were set to the values shown in Tables 4.1 and 4.2, except as specified in the following sections. Typical ranges of ionic conductances are summarized in Table 4.3.

Table 4.1. Resting concentrations and diffusion constants used in simulations (except where specified otherwise in the text).

| | Resting Concentration | | Diffusion Coefficient | |
|---|---|---|---|---|
| | Intracellular | Extracellular | Intracellular | Extracellular |
| $Ca^{++}$ | 100 nM | 2 mM | 200 $\mu m^2$/sec | 790 $\mu m^2$/sec |
| $Cl^-$ | 4 mM | 124 mM | 508 $\mu m^2$/sec | 124 $\mu m^2$/sec |
| $K^+$ | 130 mM | 3 mM | 490 $\mu m^2$/sec | 1960 $\mu m^2$/sec |
| $Na^+$ | 10 mM | 140 mM | 332 $\mu m^2$/sec | 1330 $\mu m^2$/sec |

Table 4.2. Parameter values used in the simulations. Equation is the equation number in which the parameter is first used.

| Parameter | Description of Parameter | Equation | Value |
|---|---|---|---|
| $c_{stim}$ | $[K^+]$ stimulation | 4.1.1 | 40 mM |
| $d$ | Diameter | 3.2.1† | 2 mμ |
| $F$ | Faraday constant | 3.1.1 | 96 coul/mM |
| $f$ ($f_{min}$, $f_{max}$) | intercellular volume fraction | 3.2.11 | 0.85 (.7, .92) |
| [IP3] | IP3 resting concentration | 3.2.6 | 1.8 μM |
| $j_{max,ATPase}$ | ATPase maximum current | 3.3.6.4 | 0.02 μA/cm$^2$ |
| $j_{max,Glial}$ | maximum glial uptake rate | 3.5.1 | 2 mM/sec |
| $j_{max,Na/Ca}$ | Na/Ca pump maximum current | 3.3.6.1 | 0.2 μA/cm$^2$ |
| $j_{max,Na/K}$ | Na/K exchanger maximum current | 3.3.6.1 | 5 μA/cm$^2$ |
| $M$ | Interstitial $Mg^{++}$ concentration | 3.3.3.3 | 1 mM |
| $P_{Cl}/P_K$ | Cl resting permeability | 3.3.5 | 0.1 |
| $P_{Na}/P_K$ | Na resting permeability | 3.3.5 | 0.01 |
| $R$ | Gas Constant | 3.1.1 | 8.310 J/deg-mole |
| σ | Half-width of $[K^+]$ stimulation | 4.1.1 | 150 μm |
| $T$ | Temperature | 3.1.1 | 308 K |
| $T_{max}$ | Maximum neurotransmitter concentration | 3.3.3.4 | 1 mM |

†defined in text just following this equation

Table 4.3. Range of ionic conductances used in the simulations. Equation gives the equation number where the conductance is first used.

| Parameter | Description | Equation | Values |
|---|---|---|---|
| | Potassium Channels | | |
| $g_A$ | A-type $K^+$ channel | 3.3.1.1 | 0 to 50 pS/μm$^2$ |
| $g_{BK}$ | BK-type K(Ca) channel | 3.3.2.1 | 0 to 1000 pS/μm$^2$ |
| $g_{DR}$ | Delayed rectifier channel | 3.3.1.10 | 0 to 2000 pS/μm$^2$ |
| $g_{IK}$ | IK-type K(Ca) channel | 3.3.2.5 | 0 to 4 pS/μm$^2$ |
| $g_M$ | M-type (muscarinic) $K^+$ channel | 3.3.1.6 | 0 to 50 pS/μm$^2$ |
| $g_{SK}$ | SK-type K(Ca) channel | 3.3.2.10 | 0 to 1 pS/μm$^2$ |
| | Calcium Channels | | |
| $g_{HVA}$ | HVA type $Ca^{++}$ channel | 3.3.5.12 | 0 to 20 pS/μm$^2$ |
| $g_{LVA}$ | LVA type $Ca^{++}$ channel | 3.3.5.1 | 0 to 2 pS/μm$^2$ |
| | Sodium Channels | | |
| $g_F$ | Fast $Na^+$ channel | 3.3.4.1 | 0 to 100 pS/μm$^2$ |
| $g_P$ | Persistent $Na^+$channel | 3.3.4.12 | 0 to 1 pS/μm$^2$ |
| | NMDA Channels | | |
| $P_{Ca}/P_K$ | $Ca^{++}$ permeability (with respect to $K^+$) | 3.3.3.2 | 3 to 10.6 |
| $P_{Na}/P_K$ | $Na^+$ permeability (with respect to $K^+$) | 3.3.3.2 | 1 |
| $g_{K,NMDA}$ | Potassium conductance of NMDA channel | 3.3.3.1 | 0 to 2000 pS/μm$^2$ |

## 4.1. WAVE INITIATION

Spreading depression is induced (in the simulations presented in this dissertation) by a topical application of potassium. As an initial condition the following bell-shaped function was used:

$$c(x,0) = c_{rest} + (c_{stim} - c_{rest})e^{-x^2/2\sigma^2} \qquad (1)$$

where $c_{rest}$ is the resting concentration (e.g., $[K^+]_{out}$=3 mM), $c_{stim}$ is the magnitude of the stimulation, and $\sigma$ is a measure of the width of the stimulation. The results that will be presented in this chapter predict that spreading depression may be induced by this protocol whenever $c_{stim}$ exceeds some threshold that depends on the membrane conductances.

The initiation of a typical wave with $c_{stim}$ = 50 mM is illustrated in Figure 4.1. Conductance values used for this particular simulation are summarized in Table 4.4. The resting concentrations and diffusion constants are summarized in Table 4.1, and other parameters used are listed in Table 4.2. The initial increased $[K^+]_{out}$ (the $t$ = 0 curve in Figure 4.1) causes a depolarization (not illustrated). Intracellularly, $K^+$ is pushed away from the area of maximum stimulation, leaving a $K^+$ deficit in its wake. The cytosolic $K^+$ pulse propagates away from the origin; this is illustrated at $t$ = 2 sec

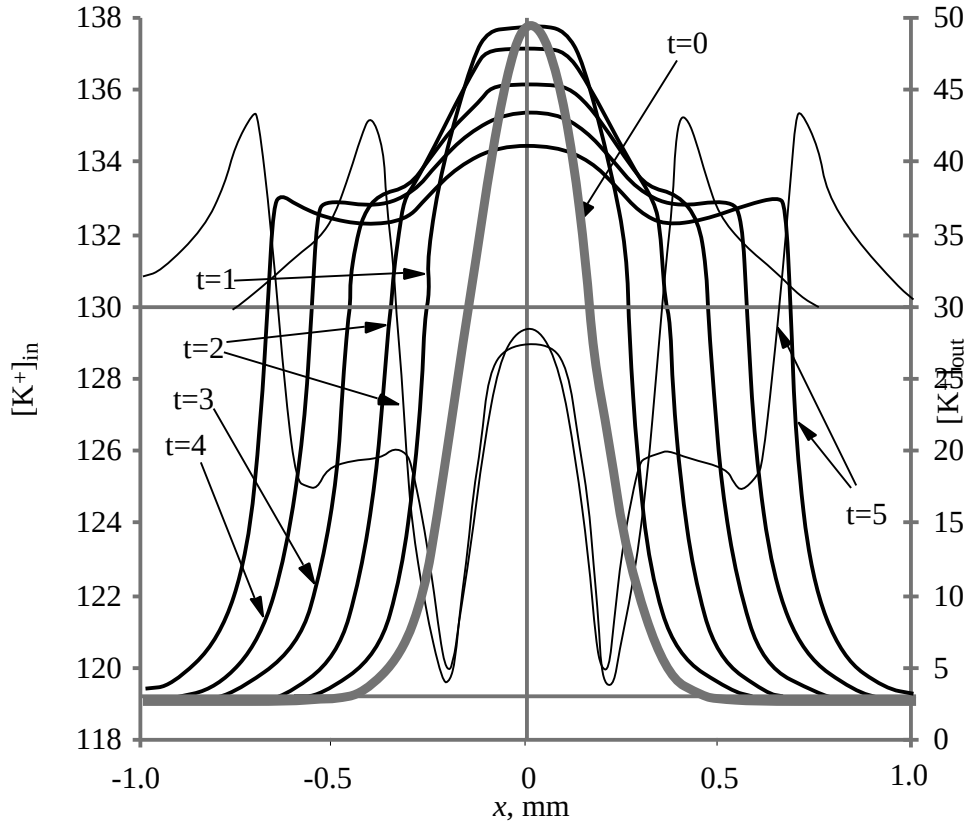


Figure 4.1. Initiation of spreading depression. The extracellular (heavy lines, right ordinate) and intracellular (thin lines, left ordinate) are shown at various times (shown in seconds) after stimulation. The concentrations are millimolar. The parameters used are given in Table 4.4; all other conductances are set to zero. K(Ca) currents are inhibited in this simulation. The initial stimulation was 50 mM of potassium applied with a bell shaped distribution ($[K^+]_{out}$ = 47 mM above rest, $\sigma$ = 150 μm).

and $t$ = 5 sec in Figure 4.1. The intracellular pulse leads to cellular expansion and the contraction of interstitial space. At the same time the interstitial $K^+$ is diffusing away from the origin. This leads to an interstitial $K^+$ pulse moving away from the origin at a fixed speed. This is illustrated in Figure 4.1 at one second intervals for the first five seconds following the stimulation.

Table 4.4. Membrane conductances used to initiate the $K^+$ wave illustrated in Figure 4.1.

| Parameter | Value |
|---|---|
| $g_{DR}$ | 1000 pS/μm$^2$ |
| $g_A$ | 10 pS/μm$^2$ |
| $g_M$ | 10 pS/μm$^2$ |
| $g_{K,NMDA}$ | 100 pS/μm$^2$ |
| $g_{NA,F}$ | 50 pS/μm$^2$ |
| $g_{NA,P}$ | 0.5 pS/μm$^2$ |

The shape of the waveform and its speed are independent of $c_{stim}$, so long as the concentration of potassium is above threshold. Figure 4.2 shows a wave which is induced with $c_{stim}$ = 0.5 molar; the wave propagates with the same speed (v ≈ 6.2 mm/min) and magnitude ($[K^+]_{out}$≈ 37 mM, $\Delta E$ ≈ 58 mV, voltage data not shown) as the wave shown in Figure 4.1. The wave appears to propagate further because it is initiated further away from the center of the stimulation, as demonstrated by Figure 4.2. The effect of stimulations that are both above and below threshold is illustrated in

Figures 4.3 and 4.4. The extracellular potassium concentration at the point of stimulation is shown in Figure 4.3 for three seconds following the stimulation. The concentration at a point one-half mm away from the stimulation point (3.33 $\sigma$) is shown in Figure 4.4. When the stimulation is sub-threshold the concentration decays to zero, in a manner similar to diffusion. For stimulations very close to the threshold, the concentration tends to linger near the threshold first for a while; this is true regardless of whether the stimulation is below or above threshold. The linger duration is longer the closer the stimulation is to the threshold. This behavior is suggestive of a saddle or unstable steady state at around 20.2 to 20.3 millimolar. As the super-threshold stimulation increases, the linger duration decreases until it disappears at around 50 mM. Following the linger, there is a rapid rise in concentration to at least 37 mM, which is the magnitude of the waves which are generated (with this parameter set). The concentration at the origin continues to increase at the origin for another ≈10 to ≈20 mM. For higher levels of stimulation (above ≈ 70 mM) there was no discernable concentration increase. The stimulation was varied over more than two orders of magnitude, with no observable difference in wave magnitude (≈37 mM) or wave speed (≈ 6.2 mm/sec).

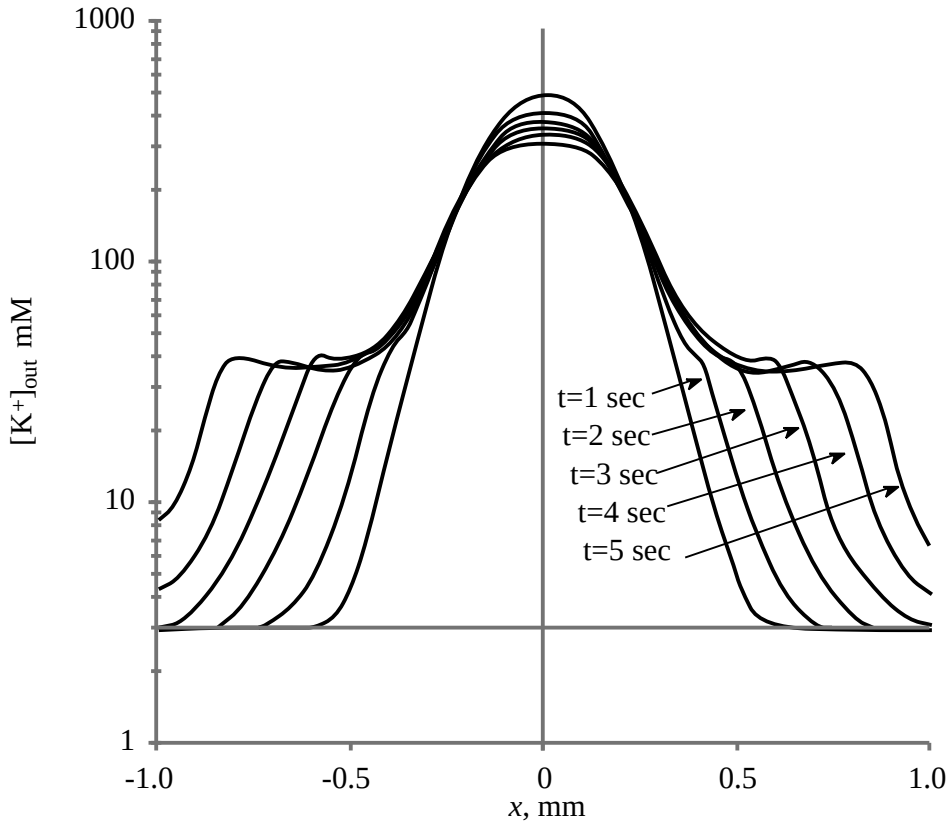


Figure 4.2. Initiation of spreading depression with $[K^+]_{out}$=0.5 M as the initial stimulation. All other parameters are the same as in Figure 4.1.

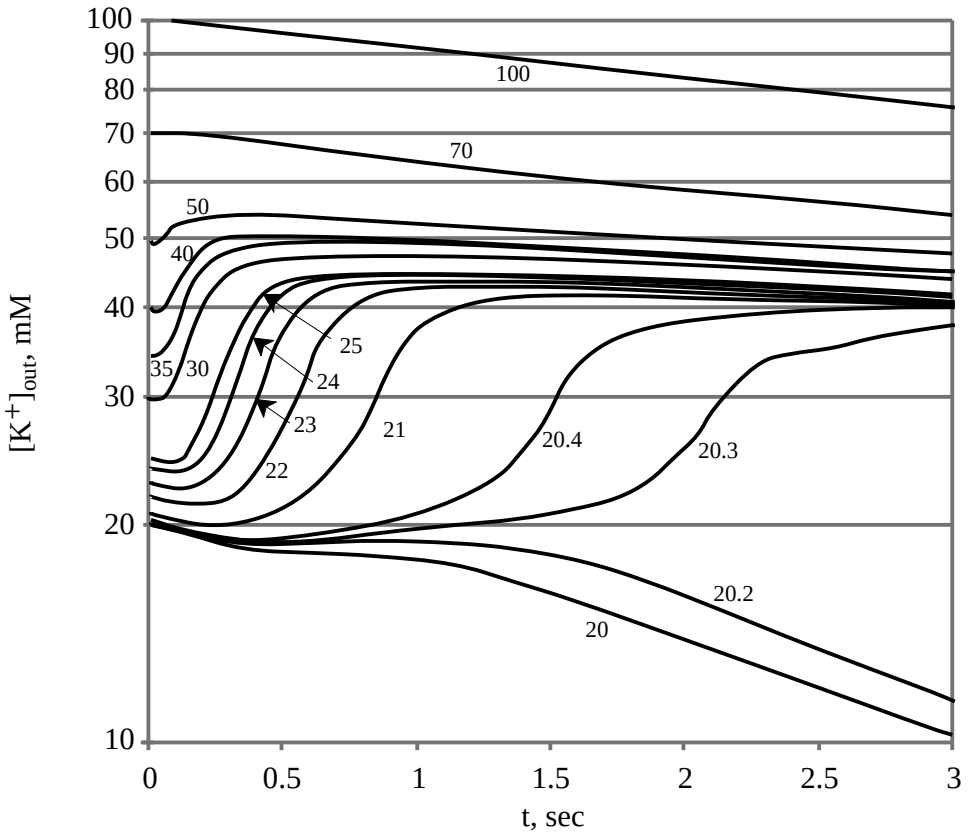


Figure 4.3. Extracellular potassium concentration at the point of stimulation. The curves are labeled with $c_{stim}$ in millimoles; all stimulations use $\sigma = 150$ μm, as before. These stimulations suggest that there is probably an unstable steady state between 20.2 and 20.3 mM for the parameter set of Tables 4.1 through 4.4. The closer a supra-threshold stimulation is to threshold, the longer it takes to induce the system to move away from threshold.

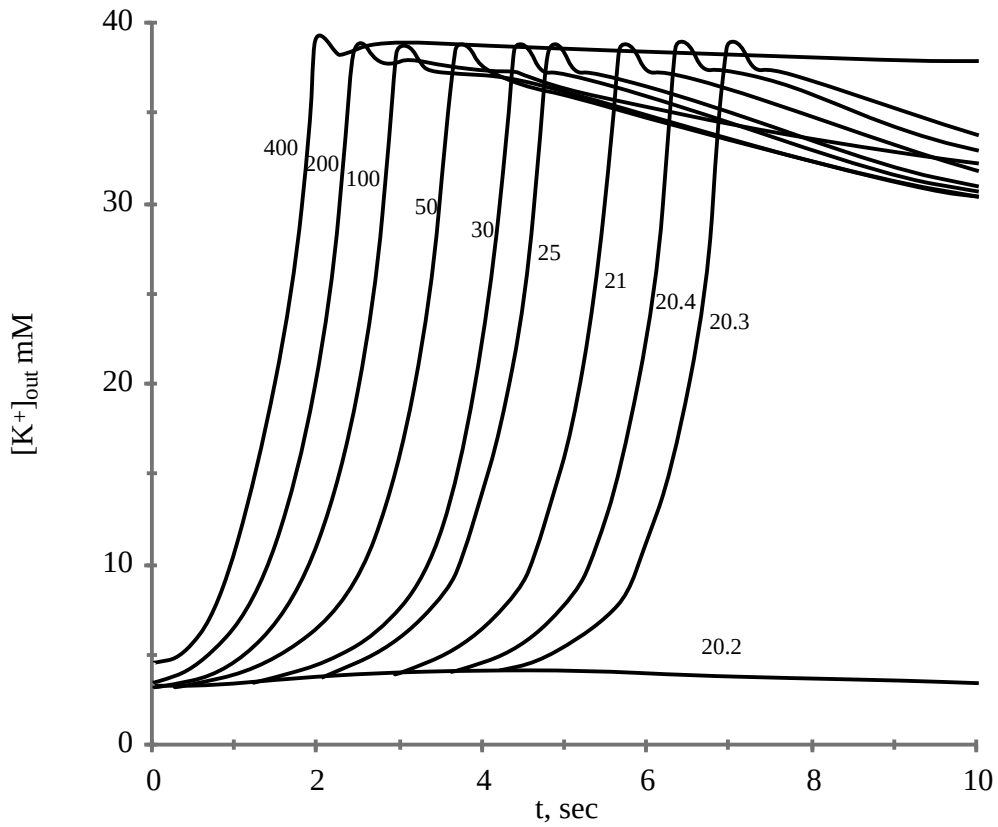


Figure 4.4. Extracellular potassium concentration at a point one-half millimeter from the stimulation. The curves are labeled with $c_{stim}$ in millimoles; all stimulations use $\sigma$ = 150 μm, as before. All stimlations induced waves which propagated at the same speed. Higher magnitude stimulations induce spreading depression more quickly, as illustrated in Figure 4.3. Thus the maximum stimulation at $x$ = 0.5 mm is also reached more quickly. The highest magnitude simulations recovered more slowly; the reason for this is not clear.

## 4.2. WAVEFORM SHAPE

By independently varying the conductance of each membrane current it was found that the potassium efflux is predicted to occur as a result of a combination of the following mechanisms: NMDA receptor gated potassium currents, voltage-gated potassium currents, and calcium-activated potassium currents. The shape of a typical waveform is illustrated in Figure 4.5, which shows the change in membrane voltage at two times as a function of position. There is a prolonged hyperpolarization following recovery from the depolarizing waveform. The start of this hyperpolarized period can be seen in the trailing edge of the *t*=30 sec waveform in Figure 4.5. The parameters which were used in this simulation are shown in Table 4.5. As suggested by the values in Table 4.5, this wave is propagated as a result of both NMDA-mediated and voltage-gated potassium currents.

Changes in interstitial ionic concentrations which occur along with the DC potential change are illustrated in Figure 4.6 at a point approximately one-half mm away from the stimulation point. The predictions shown in Figure 4.6 are from the same simulation used for Figure 4.5. The maximum predicted $[K^+]_{out}$ increases to ≈25 to ≈50 mM, depending on the actual combination of ionic conductances; the maximum is ≈28 mM for the single example shown in Figure 4.6. $Na^+$ and $Cl^-$ concentrations fall to ≈10 mM and ≈20 mM, respectively. There is a small increase (2 to 3 mM) in $[Na^+]_{out}$ and $[Cl^-]_{out}$ before the decreases in these species, probably due to cell

swelling that affects the interstitial volume. The peak cytosolic potassium concentration change, which seems to drive the process, precedes shifts in the other two species by approximately two seconds.

The top plot in Figure 4.6 shows the cytosolic pulse of $K^+$ that precedes the interstitial ionic changes. A wave of increased cytosolic potassium (≈5%) is seen to precede the oncoming wave; wave passage is accompanied by concentration drop of ≈10% over one to two seconds. The initial pulse occurs because of the electro-diffusive forces that drive cytosolic potassium away from the point of stimulation. Osmotic forces resulting from the subsequent charge imbalance cause water entry and cellular swelling. Thus the cytosolic concentration decrease is due in part to cellular expansion and not only because of ionic movement. Cellular swelling compresses extracellular space and leads to the rapid increase in interstitial potassium concentration. The predicted decrease in interstitial space is as large as ≈50% (data not shown).

Table 4.5 Parameters used for the simulations illustrated in Figures 4.5 and 4.6. Conductances not listed are zero.

| Parameter | Value |
|---|---|
| $g_{DR}$ | 300 pS/μm$^2$ |
| $g_F$ | 10 pS/μm$^2$ |
| $g_P$ | 0.1 pS/μm$^2$ |
| $g_{K,NMDA}$ | 1100 pS/μm$^2$ |
| $f_{REST}$ | 0.85 |

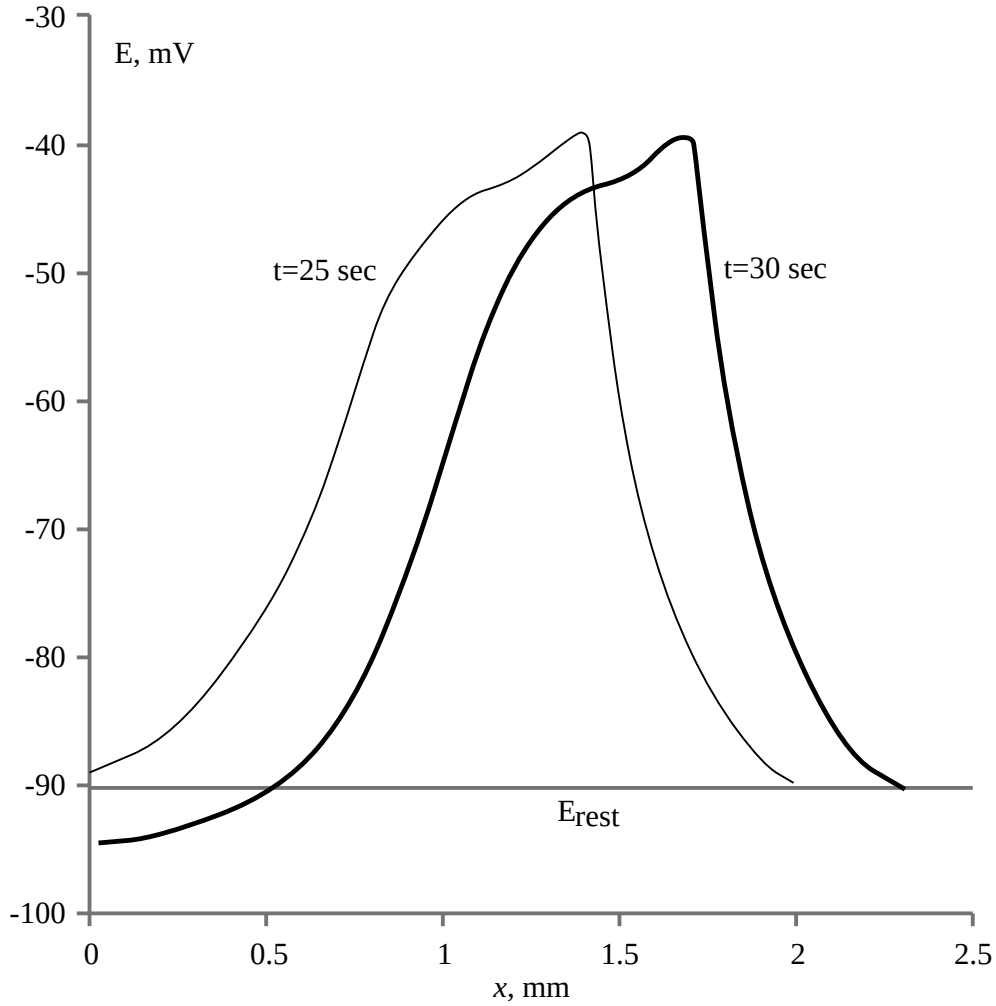


Figure 4.5. Predicted waveform at two times following the initial stimulation, showing a wave propagating to the right at ≈3.6 mm/min. The DC potential is shown as a function of the distance from the initial stimulation point at two different times following the stimulation. The wave was initiated at x = 0. Relevant parameter values are shown in Table 4.5

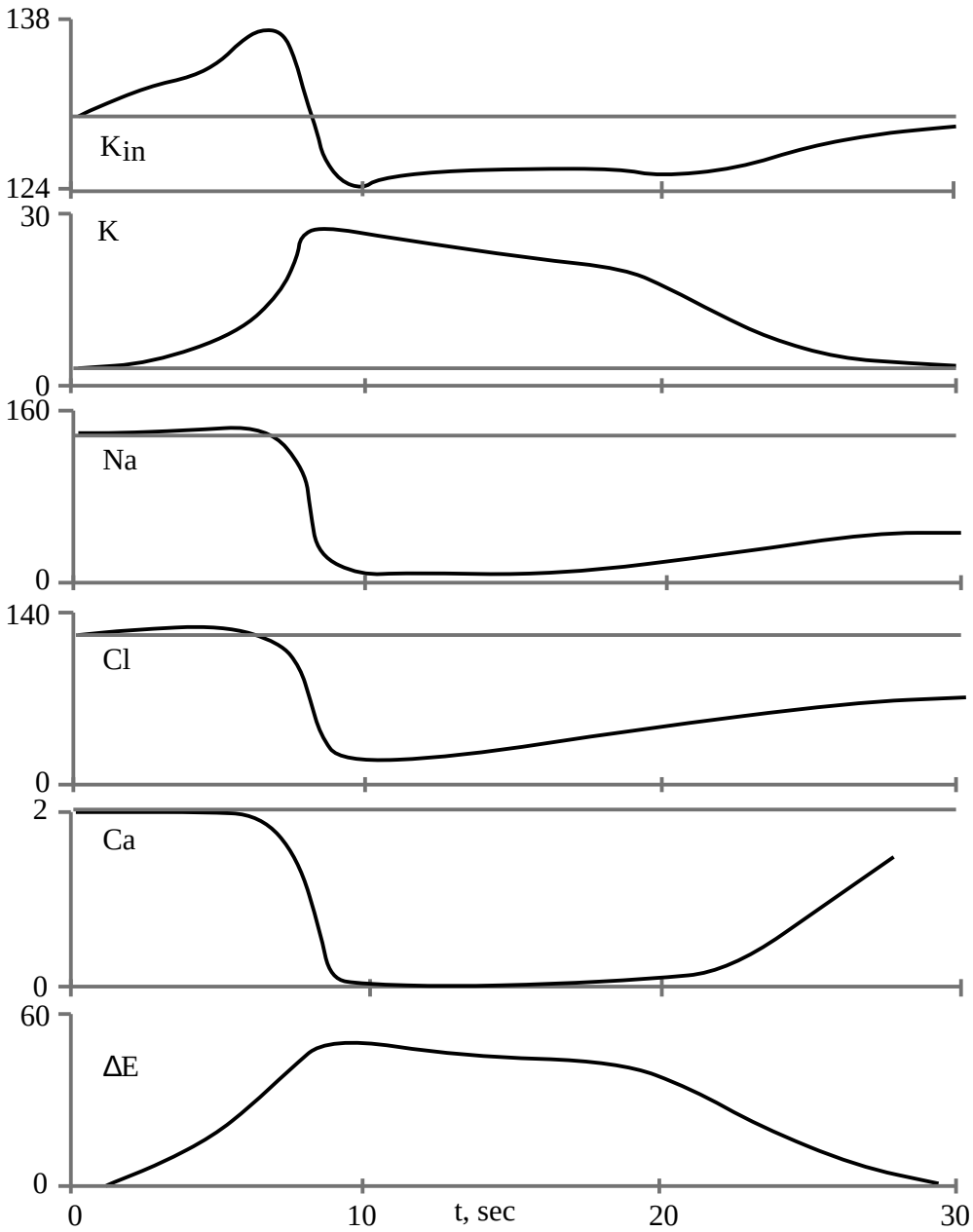


Figure 4.6. Changes in ionic concentrations observed at a point 0.5 mm from the simulation in the same simulation illustrated in Figure 4.5. The top plot gives the cytosolic potassium; all other concentrations are interstitial. All concentrations are millimolar, and membrane voltage is in millivolts.

## 4.3. GAP JUNCTIONS

In this model, wave propagation is strongly dependent on the opening of gap junctions between abutting cells. Gap junctions are simulated by a non-zero cytosolic diffusion constant. Cytosolic diffusion in the continuum model represents movement through gap junctions between adjacent cells. The mechanisms that cause the gap junctions to open were intentionally excluded from the scope of the simulation, but are probably due in part to osmotic pressure gradients and membrane stretch. It is also sufficient (to obtain the numerical results presented) that the gap junctions are always open.

While there is some evidence that high cytosolic calcium concentrations as well as large cytosolic voltage gradients between cells may cause gap junctions to close in cardiac cells, it is not clear whether such processes occur in neurons. Furthermore, the reported voltage gradients required to close gap junctions are much larger (≈50 to ≈400 mV between cells, Vogel and Weingart, 1998) than those which occur during spreading depression. In cardiac cells, there is some indication that pH may affect gap junction gating (Noma and Tsuboi, 1987), but there is no indication that any other ions are involved.

The effect of gap junction block is illustrated in Figure 4.7. The blocking of gap junctions is simulated by reducing all of the cytosolic diffusion constants by a constant factor between zero (complete block) and one (completely open). With the exception of calcium, measurements of the cytosolic diffusion constant have not been

published. For calcium the cytosolic diffusion constant $D_{Ca,in}$ has been estimated to be as large as 25% of diffusion constant $D_{Ca,free}$ in free solution (Albritton, Meyer and Stryer, 1992).

Table 4.6. Parameter values used to study gap junction block (Figures 4.7 and 4.8). Conductivity is given in pS/μm$^2$. Values of $g_{K,NMDA}$, $g_{BK}$, and $g_{DR}$ for specific curves in Figure 4.7 are illustrated on the figure. Unspecified conductivities are zero.

| Parameter | Value |
|---|---|
| $g_A$ | 10 |
| $g_{BK}$ | 200 |
| $g_{DR}$ | 800 |
| $g_F$ | 60 |
| $g_{HVA}$ | 4 |
| $g_{K,NMDA}$ | 110 |
| $g_{LVA}$ | 0.4 |
| $g_M$ | 10 |
| $g_P$ | 0.6 |

Table 4.7. Membrane conductances used to study dependence on cytosolic diffusion of potassium (Figures 4.9 and 4.10). Values are given in pS/μm$^2$.

| Parameter | Value |
|---|---|
| $g_{BK}$ | 250 |
| $g_{DR}$ | 250 |
| $g_F$ | 40 |
| $g_{HVA}$ | 4.0 |
| $g_{IK}$ | 1 |
| $g_{K,NMDA}$ | 250 |
| $g_{LVA}$ | 0.4 |
| $g_P$ | 0.4 |
| $g_{SK}$ | 1 |

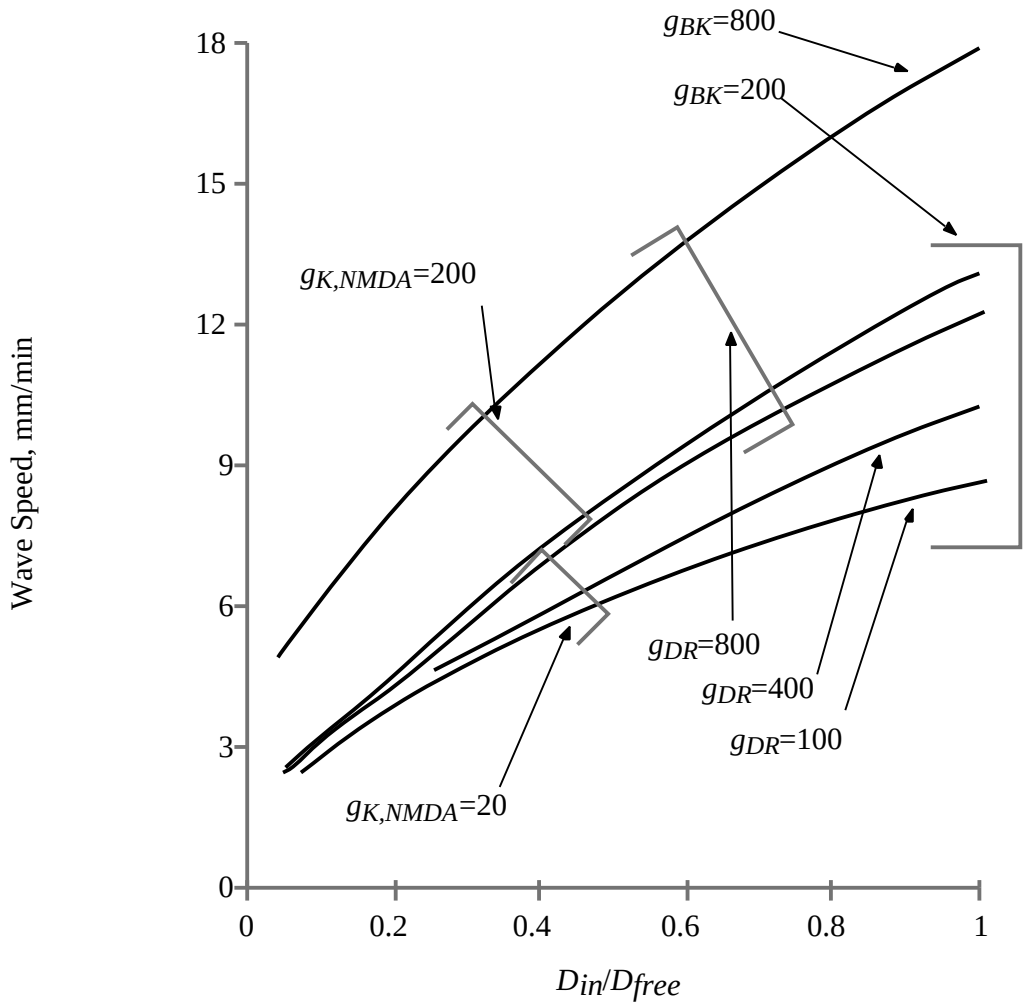


Figure 4.7. Cytoplasmic movement through gap junctions. Movement through the cytosolic syncytium of gap-junctionally connected cells is simulated by a nonzero cytosolic diffusion constant, shown on the abscissa a fraction of the corresponding interstitial diffusion constant. The interstitial diffusion constants are those in free solution. See Table 4.6 for parameter values. Curves are annotated with potassium conductances in pS/μm$^2$.

As shown by Keener and Sneyd (1998, pp. 236-246) gap-junction mediated intercellular permeation can be strongly dependent on the geometrical distribution of gap junctions. In the one-dimensional limit, the effective diffusion $D_{eff}$ through the cytosolic continuum is reduced in their model from the diffusion constant D in the cytosolic medium

$$\frac{D}{D_{eff}} \approx 1 + 0.0016\frac{1-\Delta}{\Delta} \tag{1}$$

where $\Delta$ is a geometrical measure of the gap junction distribution, with $\Delta \to 0$ for highly clumped aggregates of gap junctions and $\Delta \to 1$ for highly uniform distributions. Thus the actual diffusion constant for each species in the cytosolic continuum should be somewhat smaller than the corresponding diffusion constant within a single cell, and the value of $D_{in}$ depends on gap junctional distribution. Since potassium, sodium, and chlorine are not buffered as strongly as calcium, the ratio $D_{in}/D_{free}$ for these three species is probably somewhat larger than $D_{Ca,in}/D_{Ca,free}$. The range of wave speeds illustrated in Figure 4.7 compares favorably with values between 2 and 12 mm/min commonly quoted in the literature.

In order to determine which ions must diffuse via gap junctions for waves to propagate, the cytosolic diffusion constant of each ion (potassium, sodium, chlorine and calcium) was varied while holding the diffusion constants of other three ions fixed at 25% of that in free space ($D_{K,in}$=490 μm$^2$/sec, $D_{Na,in}$=332 μm$^2$/sec, $D_{Cl,in}$=508 μm$^2$/sec, $D_{Ca,in}$=200 μm$^2$/sec). The results are illustrated in Figure 4.8, which suggests

that the wave is carried almost entirely by potassium. Reducing the diffusion constant of calcium to zero resulted in a reduction of the wave speed of less that 1 %. Reducing the cytosolic diffusion constant of chlorine to zero resulted in a reduction in the wave speed by ≈4 %. Reducing the cytosolic diffusion constant of sodium to zero resulted in a reduction in the wave speed by ≈10 %. Finally, reducing the cytosolic diffusion constant of potassium to zero resulted in a wave speed reduction by ≈76 %.

In contrast to the wave speed, the wave magnitude depended only weakly on the diffusion constant, except at very low values. As the diffusion constant approached zero the magnitude of the wave dropped off precipitously towards zero. A comparison of the wave speed and magnitude as a function of the diffusion constant $D_{K,in}$ for potassium is illustrated in Figure 4.9. The parameters used for this simulation are given in Table 4.7. The effect of $D_{K,in}$ on the shape of the voltage waveform is illustrated in Figure 4.10. Reducing the diffusion constant decreases the slope of wave onset and extends the duration of the depolarization, as illustrated in that figure.

It has been argued that the interstitial diffusion constant should be reduced by a factor of $1/\lambda^2$ from values in free solution, where $\lambda$ represents the tortuosity of extracellular space. Values for $\lambda$ in the CNS typically range from 1.4 to 2.5 (Nicholson and Syková, 1998; Rusakov and Kullman, 1998). Extracellular tortuosity was not included in the model because extracellular diffusion does not play a significant role in the results. Reducing the interstitial diffusion constants of all species to zero reduced the wave speed by less than 1 % in this model (data not shown).

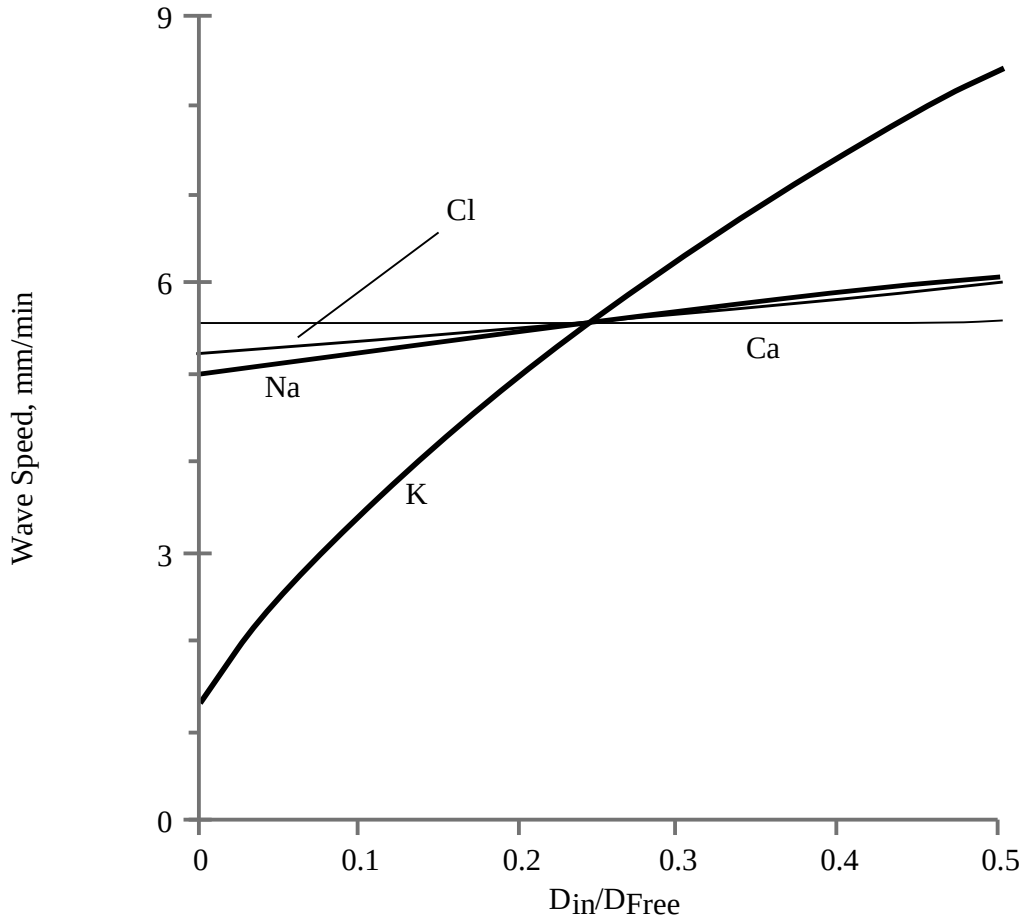


Figure 4.8. Comparison of cytosolic diffusion for different ionic species. Each curve shows the wave speed as a function of cytosolic diffusion constant for a single species, with all other diffusion constants held fixed at 25% of the value in free solution. The abscissa gives the diffusion constant as a fraction of its corresponding value in free solution. The prediction that the wave speed is strongly dependent on $D_{K,in}$ and relatively insensitive to $D_{Ca,in}$, $D_{Cl,in}$, and $D_{Na,\mathrm{in}}$, suggests that the diffusion of potassium through gap junctions is most crucial to the model. Parameter values are listed in Table 4.6.

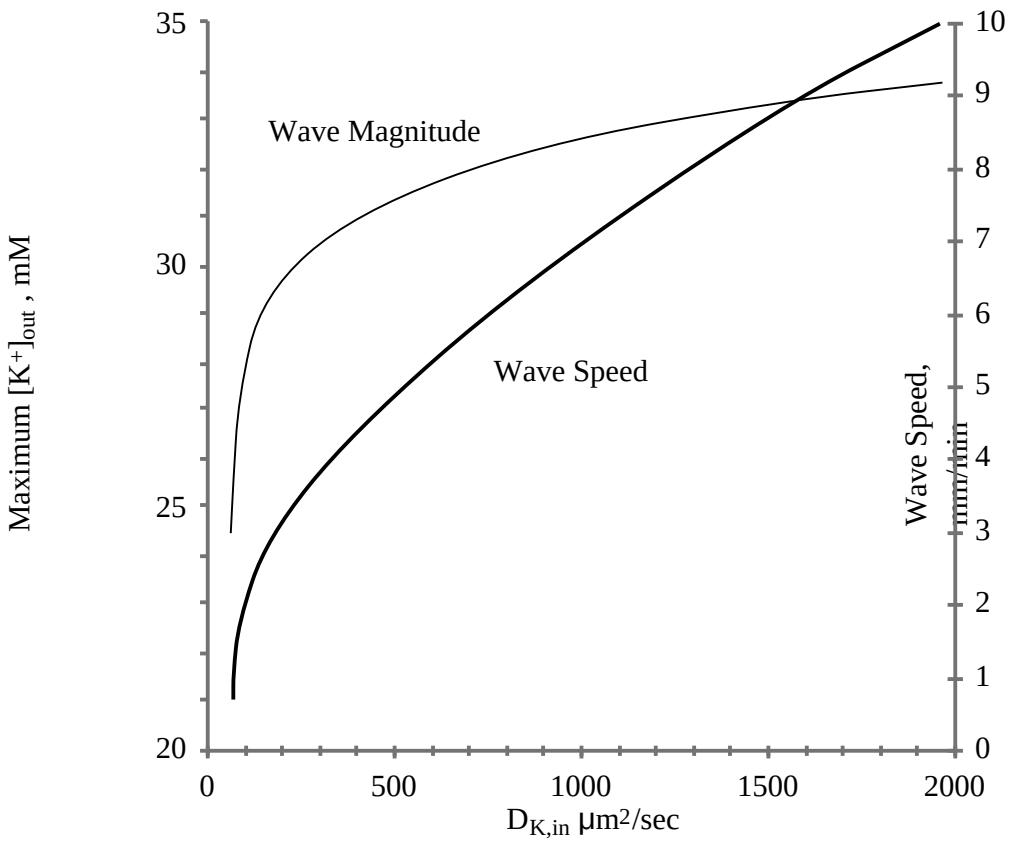


Figure 4.9. Predicted wave speed and wave magnitude as a function of the cytoplasmic diffusion constant for potassium. Parameter values are given in Table 4.7. Other diffusion constants are as given in Table 4.1. Typical DC-voltage waveforms for this same data set are illustrated in Figure 4.10

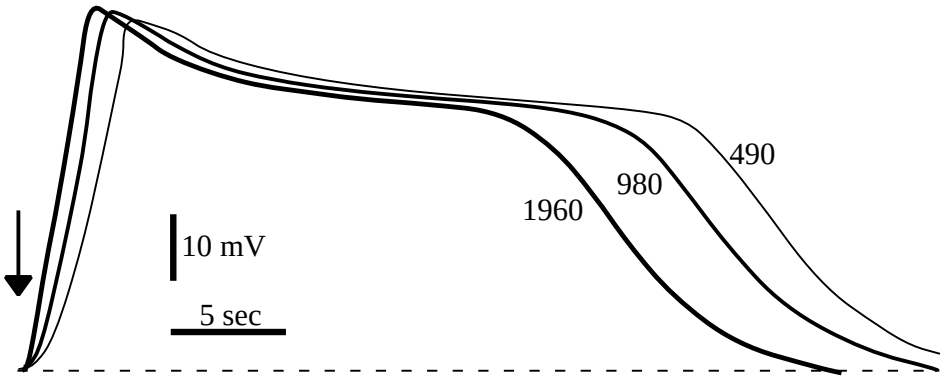


Figure 4.10. Effect of cytoplasmic diffusion constant on shape of waveform. The DC-voltage shift observed at a fixed point 0.5 mm from the stimulation is plotted as a function of time, for three different values of $D_{K,in}$. The arrow indicates the stimulation time and the resting potential is indicated by the dashed line. The three waveforms are annotated with the value of $D_{K,in}$ in $\mu m^2$/sec. Other diffusion constants are as shown in Table 4.1. Conductances used are given in Table 4.7.

## 4.4. Osmotic Volume Changes

Interstitial space comprises some ten to twenty percent of the neuropil (Nicholson and Syková, 1998). Measurements of the interstitial volume during the passage of a wave of spreading depression indicate a reduction in the volume of interstitial space that is between ≈30% and ≈50% (Van Harrevald and Khattab, 1967; Hansen and Olesen, 1980; Jing, Aitken and Somjen, 1994). This is presumably because the large net flow of permeable ions (primarily sodium and chlorine) into a cell introduces an osmotic pressure gradient. This pressure gradient results in the flow of water into the cell causing cellular expansion. In an arbitrarily stretchable cell, the water flow would be just exactly enough to counterbalance any concentration changes. However, neurons are not infinitely stretchable. If they occupy 80% of all available space, their expansion is geometrically limited to at most 25%, which would completely fill up all the available space. Even this amount of expansion is unlikely. Thus the allowed cellular expansion was limited by capping the reduction in interstitial space. A cap of 100% means that cells are allowed to expand to fill all available space, while a cap of 0% would correspond to a completely rigid membrane (equivalent to completely ignoring expansion). Analytically, the cap $\gamma$ is equivalent to a maximum cytosolic volume concentration, where

$$\gamma = \frac{f_{max} - f_{rest}}{1 - f_{rest}} \tag{1}$$

By varying the cap, the dependence of the model on osmotic forces was evaluated. This is illustrated in Figure 4.11. In this model, waves will not propagate unless the cells are allowed to expand. There is a sharp threshold in the allowed expansion at around 15% to 20%. When the cap is raised beyond ≈40%, there is no further increase in wave speed. Thus cells need to expand to occupy some 15% to 40% of the interstitial volume to allow wave passage. If spreading depression has a neuro-protective function, this might give an evolutionary advantage for organisms without a tightly packed neuropil.

The predicted volume change observed at a fixed point during wave passage is illustrated in Figure 4.12 (parameters listed in Table 4.9). The DC-voltage shift is superimposed on this plot for reference. Wave onset is shown on a more detailed scale in Figure 4.13. The first indication of the wave passage is a slow increase in cytoplasmic $K^+$, accompanied by a volume increase. The volume continues to grow as $[K^+]_{in}$ continues to increase over approximately the next three seconds. This is accompanied by rises in interstitial $K^+$, $Cl^-$, and $Na^+$, as interstitial space is compressed. The magnitude of the cytoplasmic potassium wave reaches maximum at t≈8 sec, and as $[K^+]_{in}$ decreases, water leaves the cell causing the volume to decrease for a short period of time. After approximately one third of a second, however, the depolarization induced $Na^+$ and $Cl^-$ entry exceeds potassium loss due to both depolarization and passage of the cytoplasmic wave. At this point the volume starts to increase again, continuing for another half-second until the wave peak is reached.

Slightly after recovery begins at around $t$=11 sec, a second wave of calcium-induced calcium release (CICR) from the endoplasmic reticulum occurs. The additional cytoplasmic calcium extends the activation of K(Ca) channels, and temporarily reverses recovery, leading to the "dimple" seen on Figure 4.12 between $t$=11 and $t$=12 seconds. This "dimple" could be made to disappear by turning off the CICR models in the simulation. No other observable change in the DC-voltage shift was seen as a result of this "dimple." Unfortunately, the correct parameters for CICR in dendrites are not known. Since all other predictions reported in this dissertation are qualitatively unchanged when CICR is excluded from the simulation, a further investigation of this phenomenon was deemed beyond the scope of the study. However, a detailed study of the role of calcium stores in spreading depression, and particularly in the generation of calcium waves in conjunction with spreading depression, is an important subject for further study.

To determine the impact of ignoring the finite rate of water entry in the simulations, the osmotic model was modified as described in section 3.6 to include an osmotic relaxation time constant $\tau$. Wave magnitude and wave speed both decreased with increasing $\tau$, as illustrated in Figure 4.14, but remain in the observed physiological range. The general properties of wave propagation are otherwise unchanged by the inclusion of this time constant.

Table 4.8. Parameters used in study of volume reduction cap (Figure 4.11). Conductance values are in pS/μm$^2$; conductances not shown are zero.

| Parameter | Value |
|---|---|
| $g_{DR}$ | 300 |
| $g_F$ | 40 |
| $g_{HVA}$ | 40 |
| $g_{K,NMDA}$ | 110 |
| $g_{LVA}$ | 0.4 |
| $g_P$ | 0.4 |

Table 4.9. Parameters used in simulation of volume changes (Figure 4.12 and 4.13). Conductivity is in pS/μm$^2$; conductances not listed are zero

| Parameter | Value |
|---|---|
| $g_A$ | 25 |
| $g_{BK}$ | 250 |
| $g_{DR}$ | 250 |
| $g_F$ | 40 |
| $g_{HVA}$ | 5 |
| $g_{IK}$ | 2 |
| $g_{K,NMDA}$ | 250 |
| $g_{LVA}$ | 0.5 |
| $g_M$ | 10 |
| $g_P$ | 0.4 |

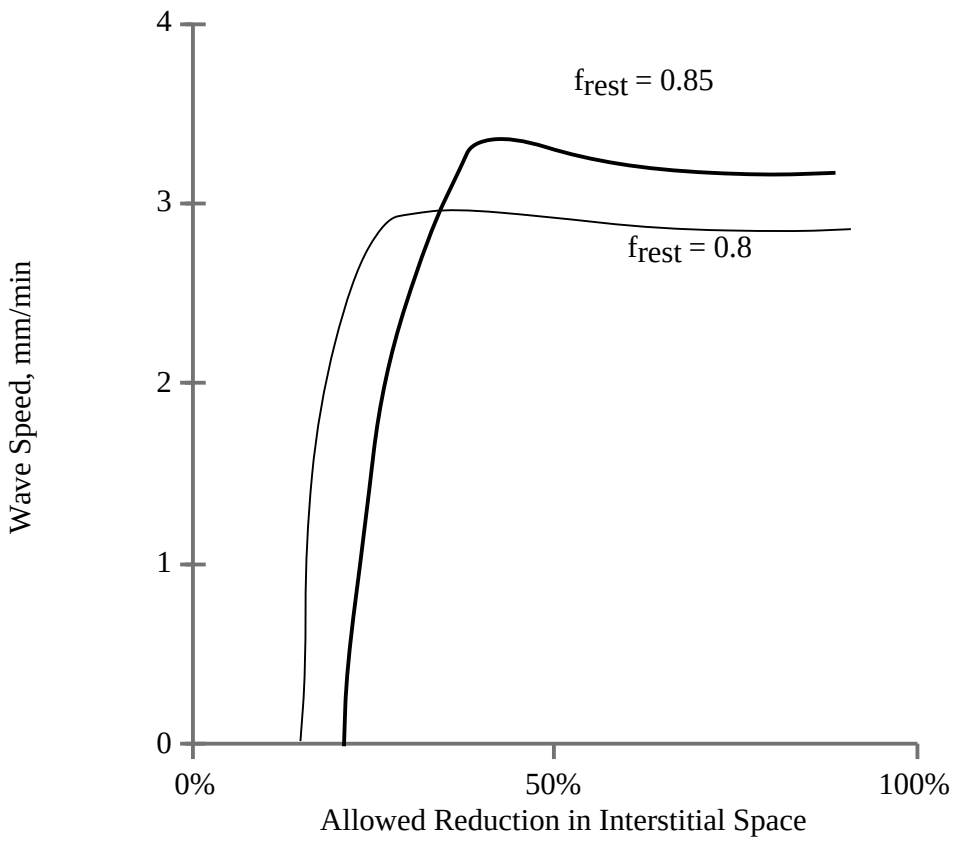


Figure 4.11. Dependence of predicted wave speed on the maximum allowed reduction in interstitial space due to osmotic forces. The two curves correspond to two different values of $f_{rest}$ as indicated. Parameter values used are given in Table 4.8.

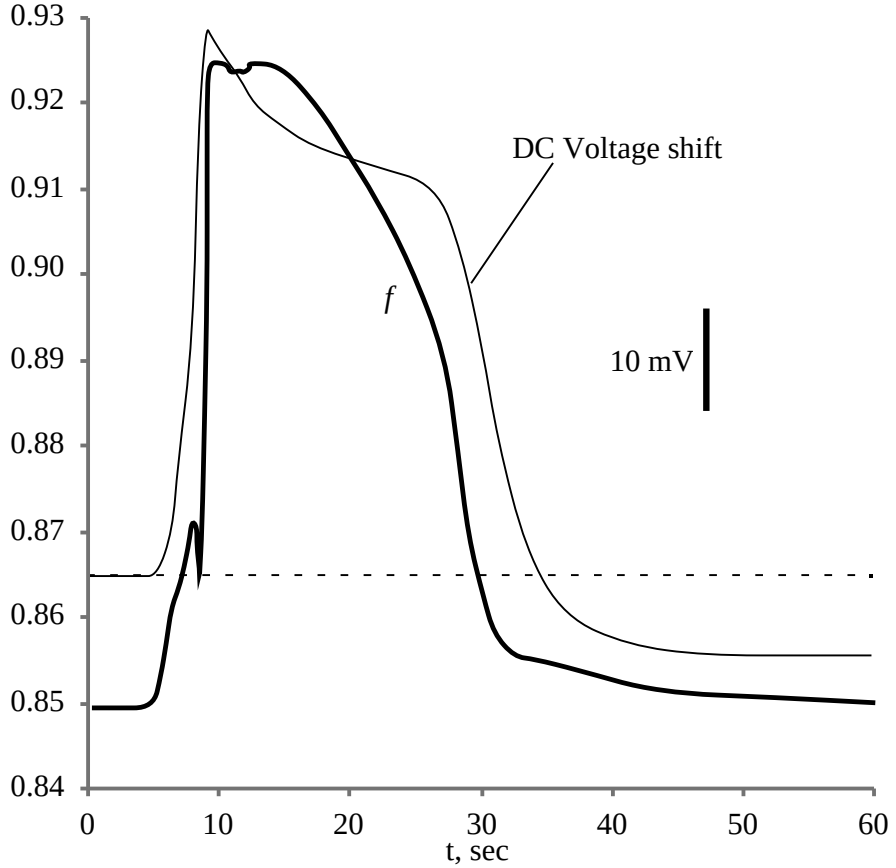


Figure 4.12. Volume fraction *f* as a function of time observed at a fixed point 1.0 mm from stimulation. The DC voltage shift is superimposed for reference; the scale bar refers to the voltage plot only. The resting potential is indicated by the dashed line. The stimulation occurs at $t = 0$. The "dimple" that occurs from 11-12 seconds is due to a second wave of calcium-induced calcium release (not shown in Figure 4.13). The parameters used are shown in Table 4.9.

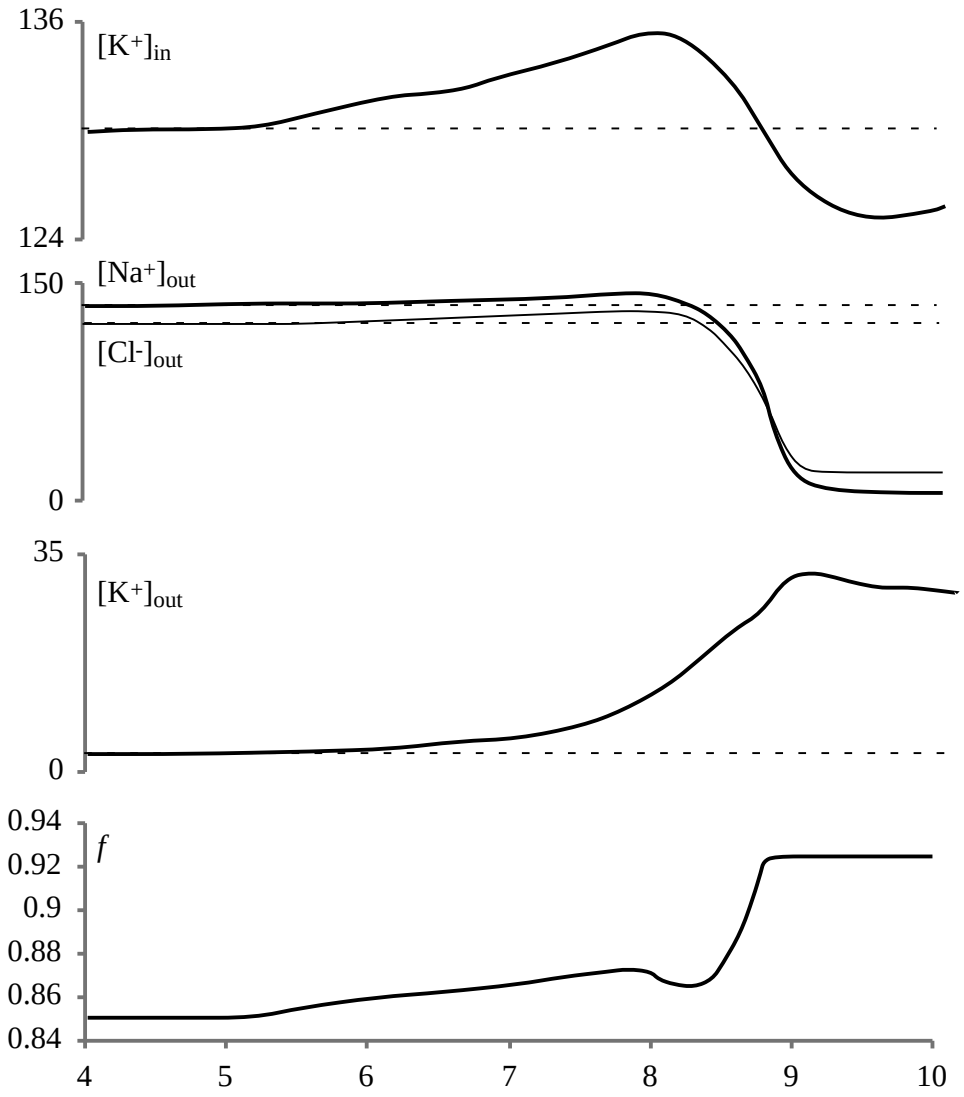


Figure 4.13. Volume change at onset of spreading depression wave passage. The predicted volume fraction f and several of the ionic concentrations are shown as a function of time (in seconds) following stimulation, as observed at a point 1.0 mm from the stimulation. The resting values are indicated by dashed lines. Parameters are as given in Table 4.9.

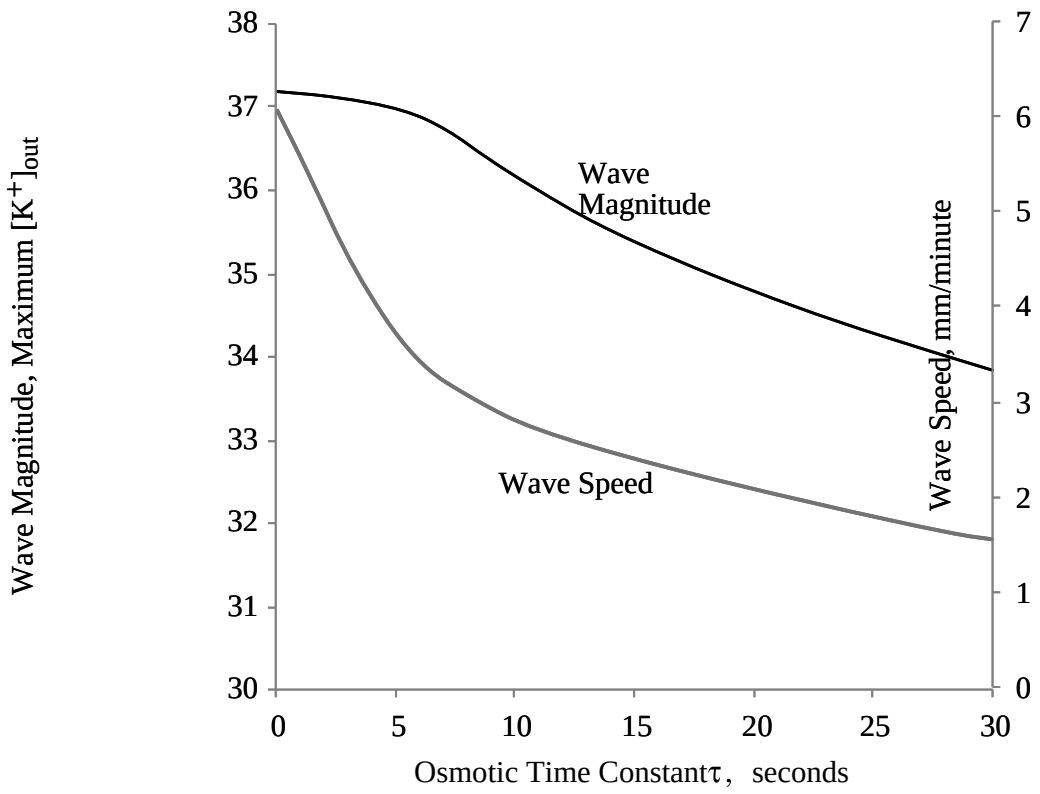


Figure 4.14. Effect of finite rate of water entry on wave propagation. Nonzero conductances used: $g_{DR}$ = 500 pS/μm$^2$, $g_{BK}$ = 500 pS/μm$^2$, $g_{HVA}$=5 pS/μm$^2$, $g_{LVA}$ = 0.5 pS/μm$^2$, $g_F$ = 50 pS/μm$^2$, $g_P$ = 0.5 pS/μm$^2$.

## 4.5. NMDA-RECEPTOR GATED ION CURRENTS

The simulations predict that spreading depression is mediated via several types of membrane conductances. In particular, since the large rises in interstitial potassium occur (in this model) because of neuronal potassium release, the membrane must have a sufficient permeability to potassium for this to occur. In fact, it is predicted that waves can be induced to propagate via any of three different potassium conductances, alone or in combination: n-methyl-d-aspartic acid receptor (NMDA-R) activated non-selective cation channels; voltage-gated potassium channels; and calcium-activated potassium channels. The NMDA receptor, putatively activated by glutamate, is widely present in post-synaptic locations throughout the central nervous system. Various studies have also indicated the presence of both voltage gated and calcium activated potassium channels in the dendrites and somata of cortical and hippocampal pyramidal cells and cerebellar Purkinje cells.

To study this dependence, each conductance was varied throughout its physiological range, with the other conductances held fixed. In all simulations in which a traveling wave could be induced, the magnitude of the interstitial potassium increase was in the range of ≈25 to ≈50 mM, and the depolarization lasted from 30 seconds to two minutes, depending on the combination of channels present in the neuronal membrane. Using both wave speed and wave magnitude as measures of excitability (with a wave speed of zero indicating that the conductance was sub-threshold) a family of curves of magnitude- or velocity-vs-conductance was plotted.

These simulations are summarized in Figures 4.15 (wave magnitude) and 4.16 (wave speed). Each curve in these figures corresponds to a different value of $g_{DR}$, and represents a large number of simulations. To obtain a particular curve, all parameters except for $g_{NMDA}$ were held fixed, and $g_{NMDA}$ was varied over its physiological range. In this context, $g_{NMDA}$ refers specifically to $g_{K,NMDA}$; however, all of the NMDA conductances were varied proportionally, i.e., the ratio $g_{Na,NMDA}/g_{K,NMDA}$ and $g_{Ca,NMDA}/g_{Na,NMDA}$ were held fixed during this particular set of simulations. In the remainder of this section, $g_{NMDA}$ will be used to indicate $g_{K,NMDA}$ to emphasize this fact. The calcium activated potassium channel conductivities were set to zero in this set of simulations to specifically elucidate the dependence on the post-synaptic (e.g. NMDA) conductance. Figure 4.15 illustrates that the wave magnitude is dependent on the number of NMDA channels that are present in the system, and is intensified by the strength of voltage-gated potassium channels (i.e., by $g_{DR}$). The corresponding wave speeds are shown in Figure 4.16. At lower delayed rectifier conductances ($g_{DR} < 321$ pS/μm$^2$) there is a sharp threshold NMDA conductance, illustrated by the vertical lines in the four curves on the right of Figure 4.15. Below the threshold, there is no propagating wave; above the threshold, the wave propagates at a speed that continuously depends on membrane conductivity. The threshold appears to be sharp, with waves appearing at threshold that propagate at speeds of ≈ 2.7 mm/minute (for the parameter set used in this figure). When $g_{DR} > 321$ pS/μm$^2$ a propagating wave

could always be induced (again, with the parameter set used for this particular simulation). The NMDA conductance threshold for wave propagation is illustrated in the inset of Figure 4.16. Propagating waves could not be induced (in this set of simulations) when the NMDA and delayed-rectifier conductances were in the shaded regions, whereas waves could always be induced in the unshaded region. Furthermore, the wave speed for the data shown in Figures 4.15 and 4.16 always exceeded 2.7 mm/minute. It is not known if a different minimum wave speed will occur with different parameter sets; this remains an important question for further study. In all cases wave speed increased with both $g_{DR}$ and $g_{NMDA}$; wave-magnitude increased with $g_{DR}$ but decreased with increasing $g_{NMDA}$. Although the wave speed increases with $g_{NMDA}$, the wave magnitude decreases. The only exception was at very high values of $g_{NMDA}$ (which are probably beyond the physiological range of any system). At the higher delayed-rectifier conductances in Figure 4.15 ($g_{DR}$=500 pS/μm$^2$) the $K^+$ levels ranged from ≈32 to ≈42 mM. In all cases in which a propagating wave could be induced during this set of simulations, the wave magnitude was greater than 20 mM.

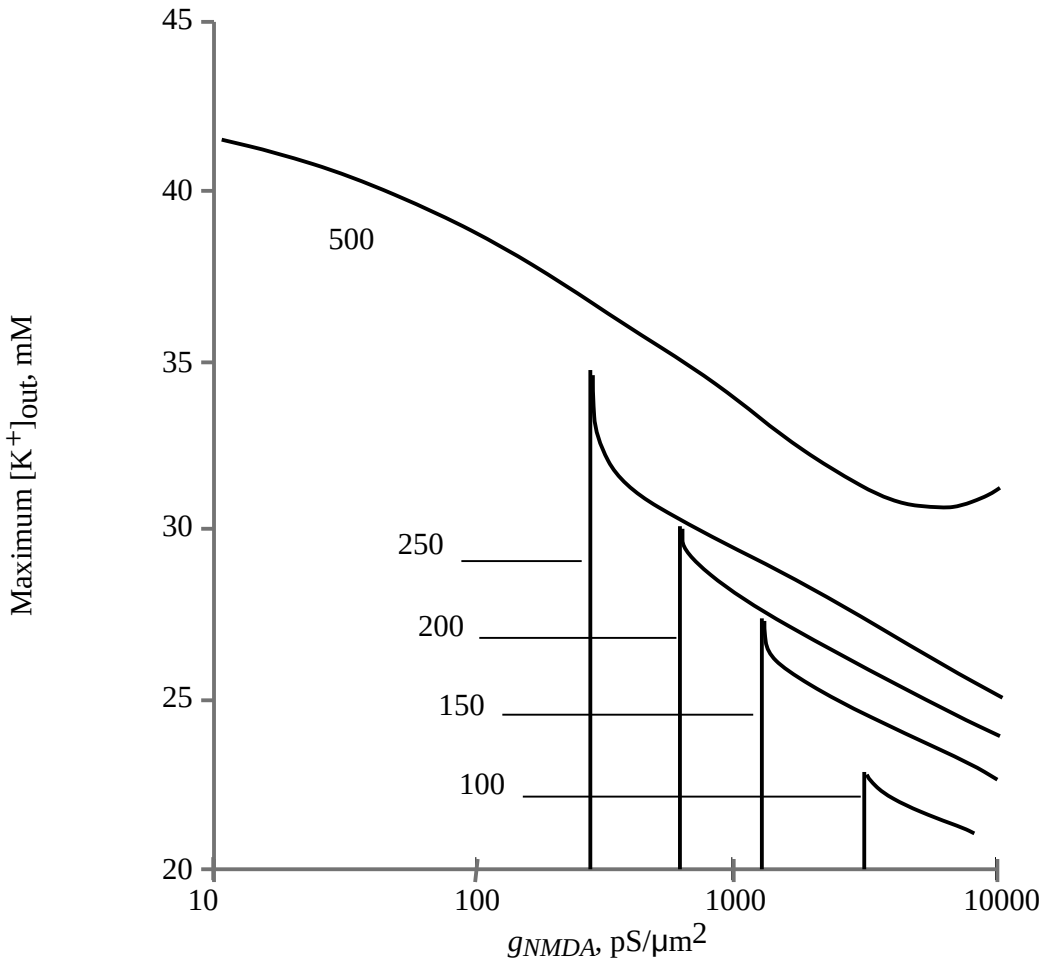


Figure 4.15. Magnitude of spreading depression wave as a function of NMDA-mediated potassium currents, for various values of $g_{DR}$ (shown in pS/μm$^2$ on the figure). The corresponding wave speeds are shown in Figure 4.16. The K(Ca) conductance is set to zero to specifically elucidate the NMDA-receptor mediated dependence, as are $g_M$ and $g_A$. The membrane sodium conductances used were $g_F$=10 pS/μm$^2$ and $g_P$=0.1 pS/μm$^2$.

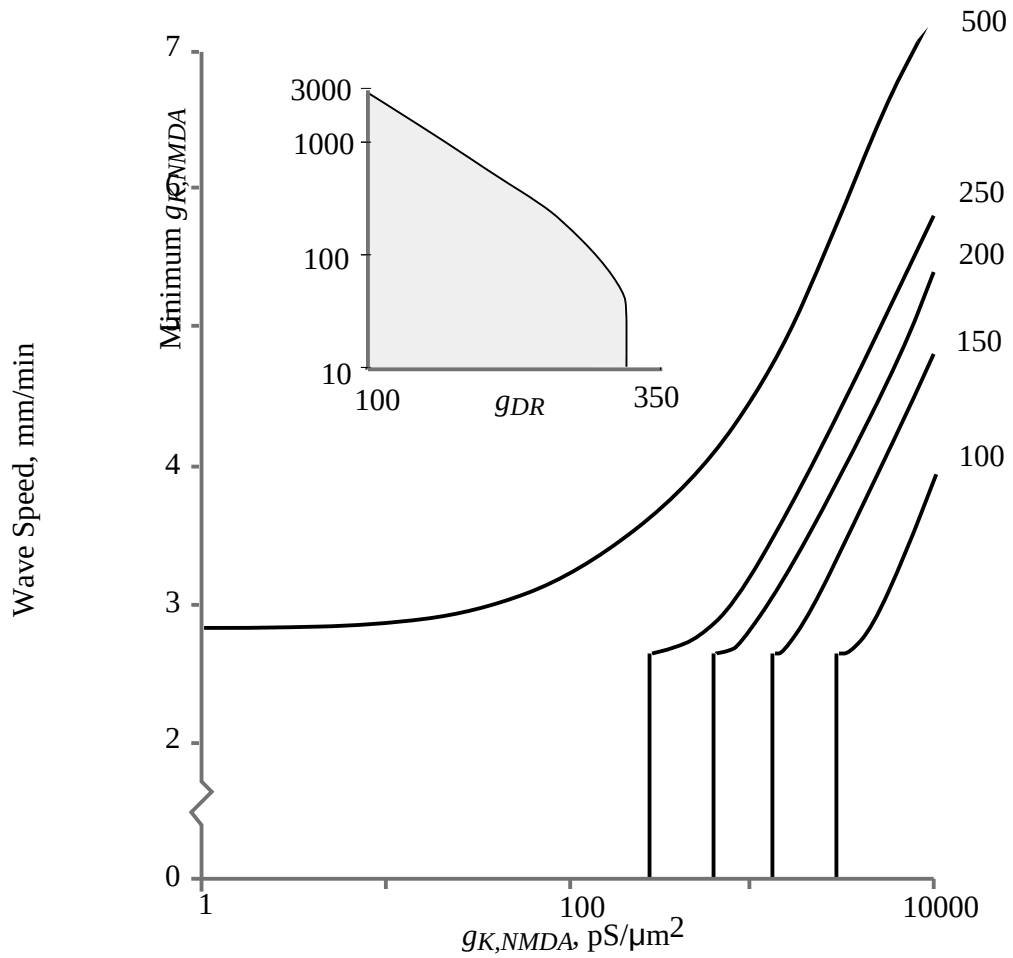


Figure 4.16. Predicted dependence of wave speed on NMDA-receptor mediated membrane currents. The inset shows the $g_{K,NMDA}$ threshold for wave propagation as a function of $g_{DR}$ (with $g_{BK}$=0). Waves will not propagate in the model in the shaded region.

## 4.6. CALCIUM ACTIVATED POTASSIUM CURRENTS

In a similar set of simulations, the novel possibility of spreading depression that is dependent on calcium-activated potassium channels (K(Ca) channels) was explored by varying the $g_{BK}$ while holding all other parameters fixed. The results are illustrated in Figures 4.17 and 4.18, which show that wave propagation can be affected by the presence of calcium-dependent potassium channels. The magnitude of the wave increased from $[K^+]_{out} \approx 25$ to $[K^+]_{out} \approx 47$ mM over the range of values shown, with a larger wave-amplitude at higher $g_{BK}$, as illustrated in Figure 4.17. Figure 4.18 shows the corresponding wave speed. The same conductivity-threshold phenomenon that was predicted for NMDA-mediated spreading depression was also predicted when the BK channel conductance was varied. The threshold region for this set of simulations is shown in the inset of Figure 4.18. While the threshold was still extremely steep, some curvature was observed in the wave-speed vs. $g_{BK}$ plot (Figure 4.18). The minimum supra-threshold wave speed that was predicted with this parameter set was ≈ 2.4 mm/min.

The calcium required to induce these waves could be supplied in either of two ways (data not shown): entry via voltage-gated calcium channels and release from intracellular stores. Stretch-activated IP3 release has been observed in non-neuronal tissue (Felix, Woodruff and Dirksen, 1996), and IP3-dependent calcium stores are known to be present throughout the dendritic tree (Kostyuk and Verkhratsky, 1995; De Schutter and Smolen, 1998). However, it is not known if the receptor and pump

sensitivities and strengths in neuronal tissue are sufficient to induce the required levels of calcium so this method is largely speculative. When IP3-activated and calcium-induced calcium release were excluded from the model, this type of SD-wave could be prevented by blocking voltage gated calcium channels.

The effect of $g_{BK}$ on the waveform shape is shown in Figure 4.19. Reducing $g_{BK}$ produced a graded response on waveform shape as well as velocity and magnitude. Block of the BK channel reduced the wave onset slope and increased the time to onset. Recovery was also delayed, but by a smaller amount than wave onset. A similar effect was obtained by blocking the HVA-type calcium channel or by reducing interstitial calcium, as will be discussed section 4.9 ("Calcium and Calcium Currents"). Conductance values used in these simulations are listed in Table 4.11.

The SK-channel seemed to have an inhibitory effect on spreading depression in the model. Figure 4.20 illustrates the DC-voltage shift, as observed at a point 0.5 mm from the stimulation, for three different values of $g_{SK}$. At the higher values of $g_{SK}$, the slope of onset of spreading depression was smaller, and the duration of the DC-voltage shift was much shorter. Furthermore, at higher values of $g_{SK}$, after an initial recovery that brought the membrane potential to within 10 mV of the resting value but still depolarized, the voltage took a much longer period of time to reach the resting value. The reason for this extended plateau is not known.

Table 4.10. Parameters used in K(Ca) dependence study (Figures 4.17 and 4.18). Membrane conductances are in pS/μm$^2$.

| Parameter | Value |
|---|---|
| $g_A$ | 50 |
| $g_F$ | 10 |
| $g_{HVA}$ | 4 |
| $g_{IK}$ | 4 |
| $g_{K,\ NMDA}$ | 100 |
| $g_{LVA}$ | 0.4 |
| $g_M$ | 10 |
| $g_P$ | 0.1 |
| $g_{SK}$ | 0 |
| $P_{Ca,NMDA}/P_{K,NMDA}$ | 3 |
| $P_{Na,NMDA}/P_{K,NMDA}$ | 1 |

Table 4.11. Conductance values (pS/μm$^2$) in simulation of waveform shape dependence on $g_{BK}$. Conductances not shown are zero.

| Parameter | Value |
|---|---|
| $g_{DR}$ | 250 |
| $g_{K,NMDA}$ | 250 |
| $g_{HVA}$ | 4 |
| $g_{LVA}$ | 0.4 |
| $g_F$ | 10 |
| $g_P$ | 0.1 |

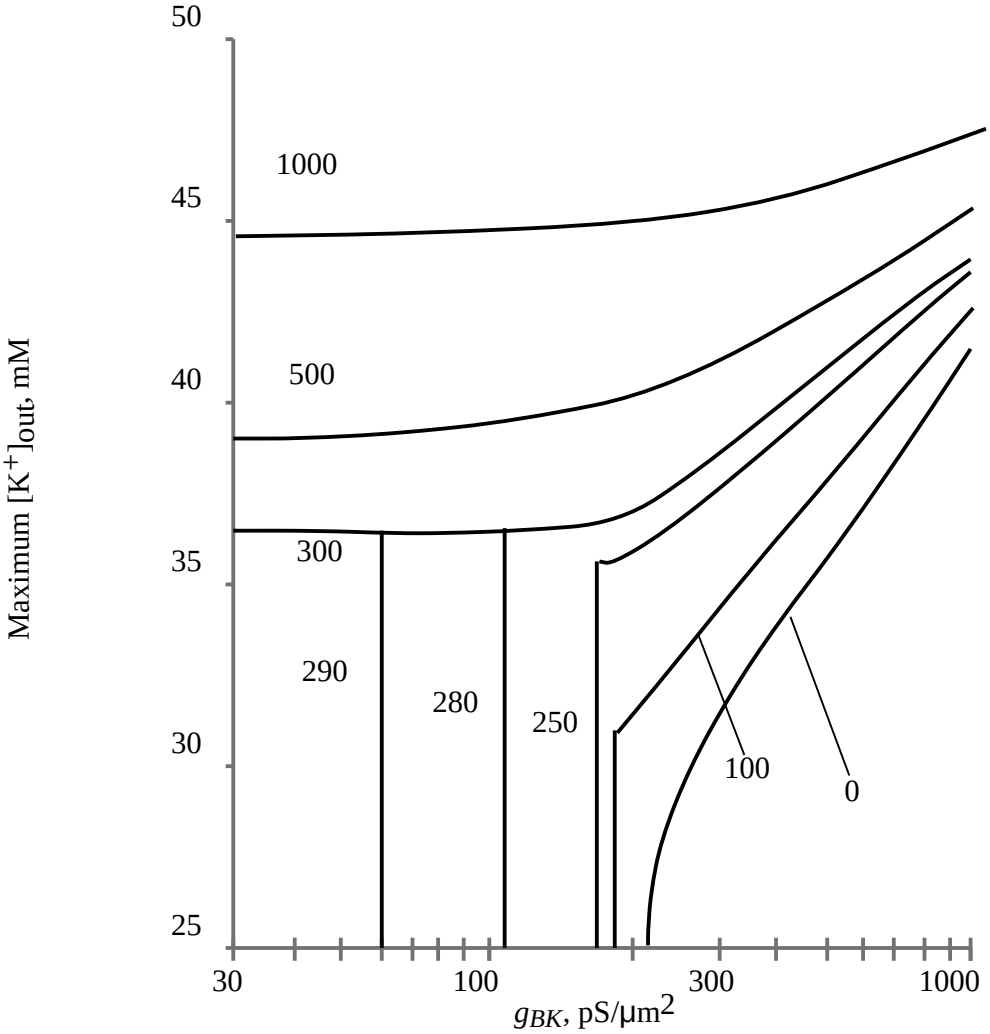


Figure 4.17. Wave magnitude as a function of $g_{BK}$ for various values of $g_{DR}$ (shown in pS/μm$^2$). The parameters used are listed in Table 4.10. The corresponding wave speeds are illustrated in Figure 4.18.

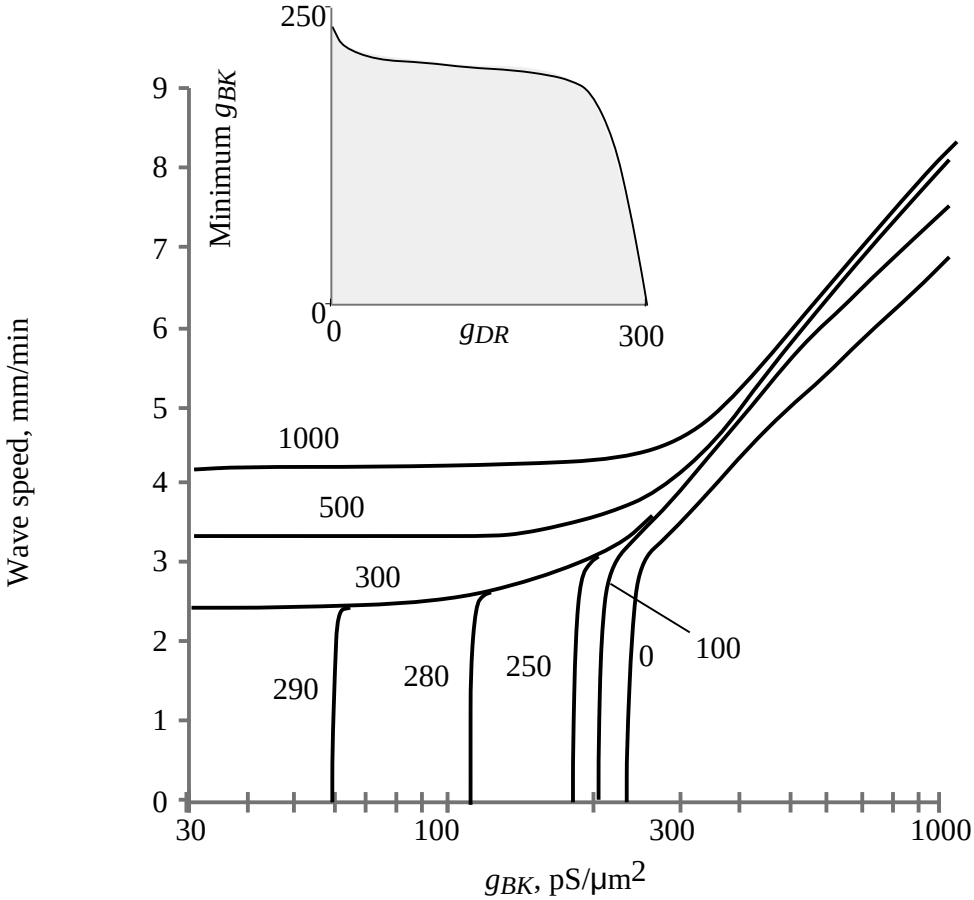


Figure 4.18. Wave speed as a function of $g_{BK}$ for the same set of simulations illustrated in Figure 4.17. The inset gives the BK-conductance threshold for wave propagation in this set of simulations.

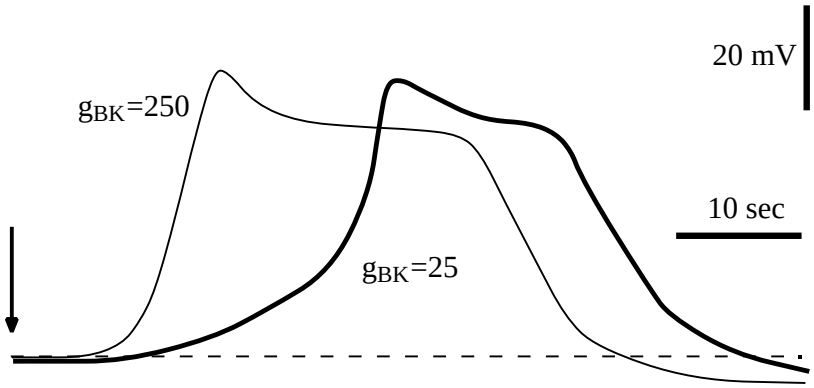


Figure 4.19. Effect of $g_{BK}$ on the shape of the DC-voltage waveform. The curves are annotated with the value of $g_{BK}$ in pS/μm$^2$. The dashed lines indicate the resting potential. Measurements are take at a point one mm from the point of stimulation. The arrows show the stimulation time. Membrane conductances used in the simulation are listed in Table 4.11

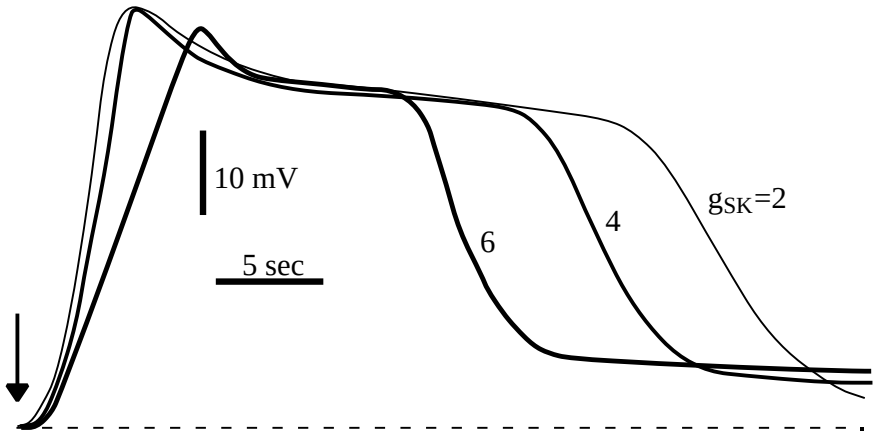


Figure 4.20. Effect of $g_{SK}$ on the shape of the DC-voltage waveform. The curves are annotated with the value of $g_{SK}$ in pS/μm$^2$. The dashed lines indicate the resting potential. Measurements are take at a point 0.5 mm from the point of stimulation. The arrows show the stimulation time. This simulation used $g_{BK}$ = 250 pS/μm$^2$; other membrane conductances used are listed in Table 4.11

## 4.7. VOLTAGE-GATED POTASSIUM CURRENTS

It might be inferred from Figures 4.15 through 4.18 that the predicted wave magnitude and predicted wave speed are both smoothly increasing functions of $g_{DR}$. This is in fact the case, as illustrated in Figure 4.21. To obtain the results shown, $g_{DR}$ was varied over its physiological range while holding all other parameters fixed at the values shown in Table 4.12. The effect of $g_{DR}$ on the waveform shape is shown in Figure 4.22. Reducing $g_{DR}$ produced a graded response on the predicted waveform shape as well as velocity and magnitude. Block of the delayed rectifier reduced the onset slope and increased the onset time. This effect was not as pronounced as with the BK channel. However, the predicted duration of the DC voltage was significantly reduced and the predicted slope of the recovery increased.

In contrast to the delayed rectifier, the model predicts that the A-type potassium channel would have an inhibitory, rather than a facilitatory influence on spreading depression. As this conductance is increased, both the slope of wave onset and the time of recovery decrease, as illustrated in Figure 4.23. This phenomenon is so pronounced that the model predicted a cutoff value of $g_A$, rather than a threshold value for $g_A$. For the simulation illustrated in Figure 4.23, this cutoff occurred between $g_A \approx 65$ pS/μm$^2$ and $g_A \approx 70$ pS/μm$^2$. This would suggest that tissue with lower average values of $g_A$ should be more susceptible to spreading depression, as they would not have the "natural protection" against SD that is conferred by the A-channel. This

prediction is consonant with the observations of spontaneous spreading depression that have occurred following application of agents such as 4-AP which selectively block the A-channel (Psarropoulou and Avoli, 1993, Avoli and others, 1996). The simulation did not predict any measurable dependence of either wave magnitude (maximum value of $[K^+]_{out}$ ) or wave speed on $g_A$.

To determine if the model predicted any dependence on the muscarinic (M-type) voltage-dependent K+ current, simulations were run at different values of $g_M$ (ranging from 0 to 100 pS/μm$^2$) with all other parameters held fixed. In contrast to the other voltage gated currents, no dependence on this conductance was found.

Table 4.12. Conductance values (pS/μm$^2$) in study of wave magnitude and wave speed dependence on $g_{DR}$ and $g_A$. Conductances not shown are zero.

| Parameter | Value |
|---|---|
| $g_{BK}$ | 250 |
| $g_{K,NMDA}$ | 250 |
| $g_{HVA}$ | 4 |
| $g_{LVA}$ | 0.4 |
| $g_F$ | 40 |
| $g_P$ | 0.4 |

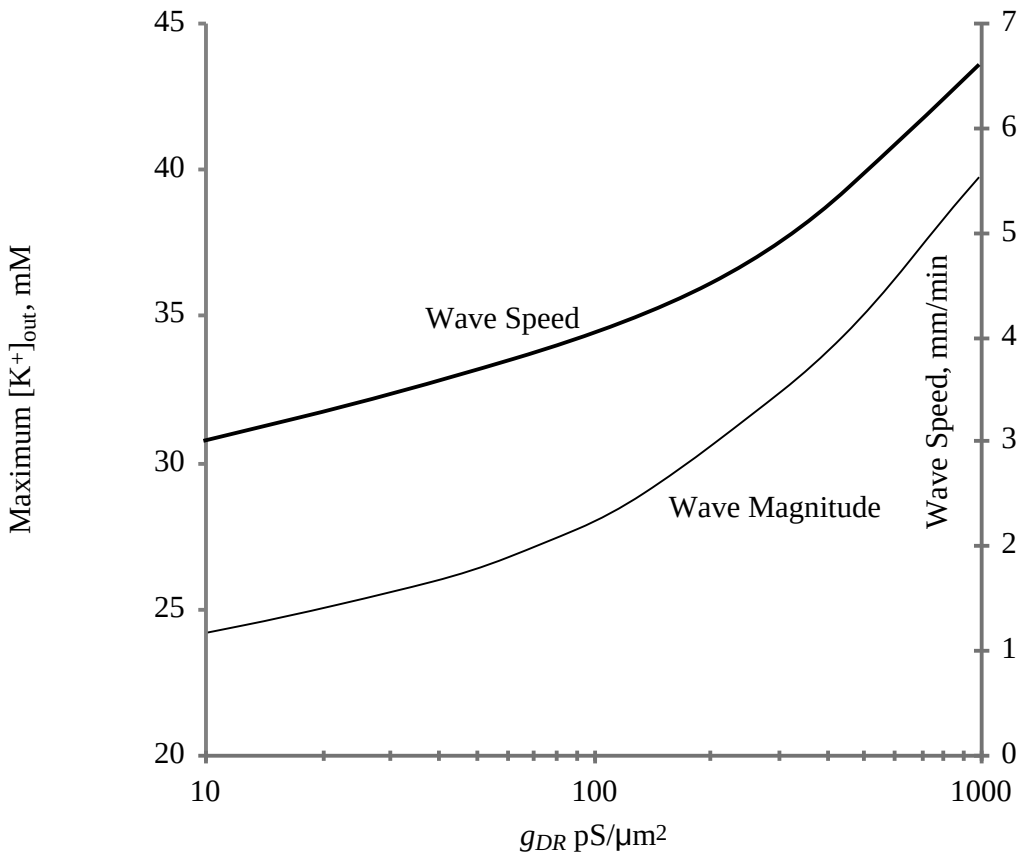


Figure 4.21. Dependence of wave speed and wave magnitude on delayed rectifier conductance. See Table 4.12 for parameter values.

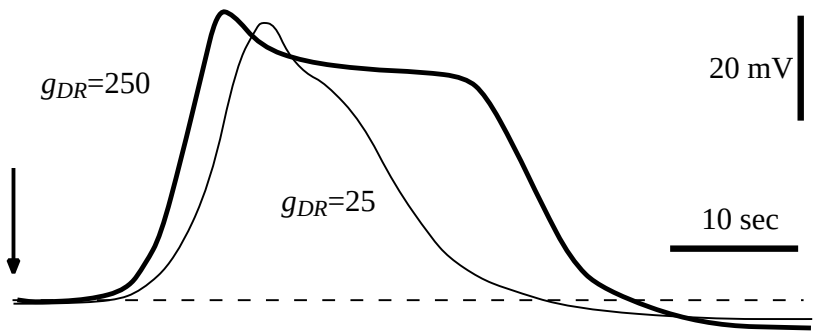


Figure 4.22. Effect of $g_{DR}$ on the shape of the DC-voltage waveform. The curves are annotated with the value of $g_{DR}$ in pS/μm$^2$. The dashed lines indicate the resting potential. Measurements are taken at a point one mm from the point of stimulation. The arrows show the stimulation time. Membrane conductance values used in this stimulation are listed in Table 4.12.

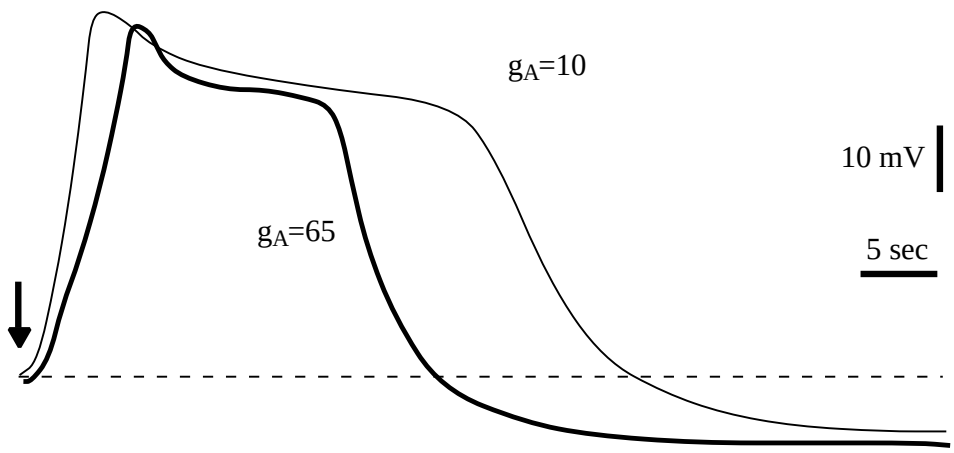


Figure 4.23. Effect of $g_A$ on the shape of the DC-voltage waveform. The curves are annotated with the value of $g_A$ in pS/μm$^2$. The dashed lines indicate the resting potential. Measurements are taken at a point one mm from the point of stimulation. The arrows show the stimulation time. For this simulation, $g_{DR}$ =25 pS/μm$^2$; other membrane conductance values used are listed in Table 4.12.

## 4.8. SODIUM CURRENTS

It has been observed that in some preparations SD can be induced by blocking inactivation of the sodium channel (Ashton and others, 1997), while a complete block of both calcium and sodium channels has been observed to prevent SD-like hypoxic depolarizations (Müller and Somjen, 1998). Both of these observations would suggest that sodium currents facilitate spreading depression. Changing the sodium conductivity also affected the simulated wave, as illustrated in Figure 4.24. This figure shows the DC-voltage change observed at a fixed point 0.5 mm from the stimulation as a function of time, for two different membrane sodium conductances. The dependence was smooth and continuous, without any threshold phenomenon occurring. At higher sodium conductivity, the potassium rise and DC-voltage shift were faster, and the duration of the depolarization lasted longer, while the wave amplitude decreased slightly. As shown in Figure 4.25 the predicted wave speed increased and the predicted wave magnitude decreased with sodium conductance.

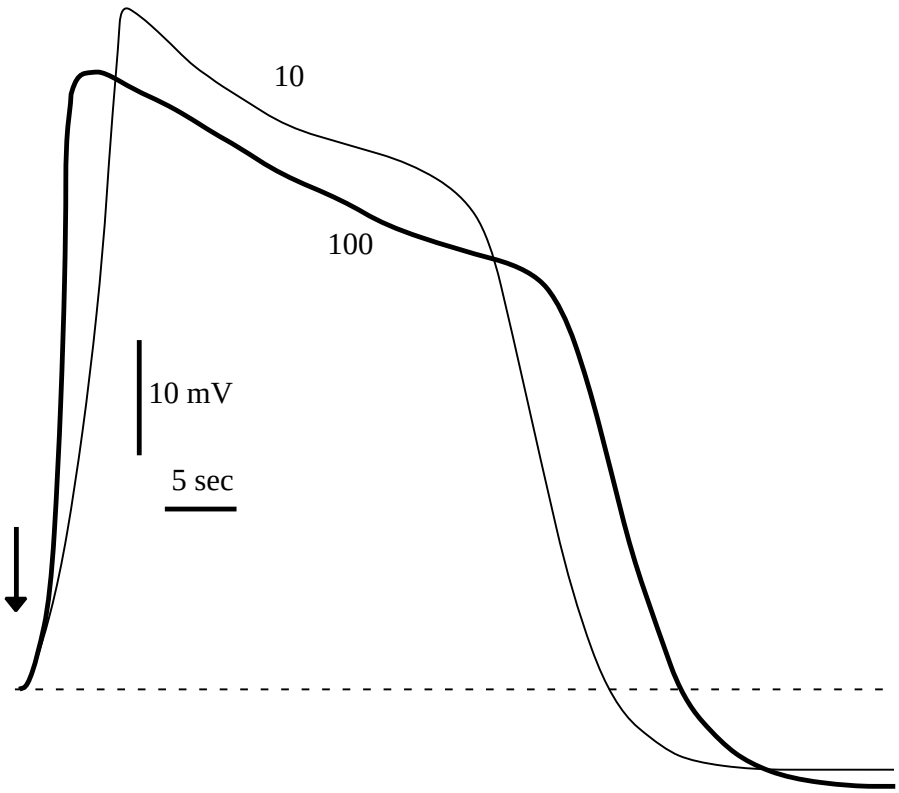


Figure 4.24. Effect of membrane conductance for sodium on waveform shape. The DC voltage shift is shown at a point 0.5 mm from the stimulation as a function of time (scale bars as shown), for two different values of $g_F$ (indicated in pS/μm$^2$ on the figure) with the ratio $g_P/g_F$=0.01 held fixed. The arrow indicates the stimulation time. The resting potential is shown as a dashed line. Values of other parameters: $g_M$=10 pS/μ$^2$m, $g_A$=10 pS/μm$^2$, $g_{K,NMDA}$=100 pS/μ$^2$, $g_{DR}$=1000 pS/μm$^2$. All other membrane conductances are set to zero.

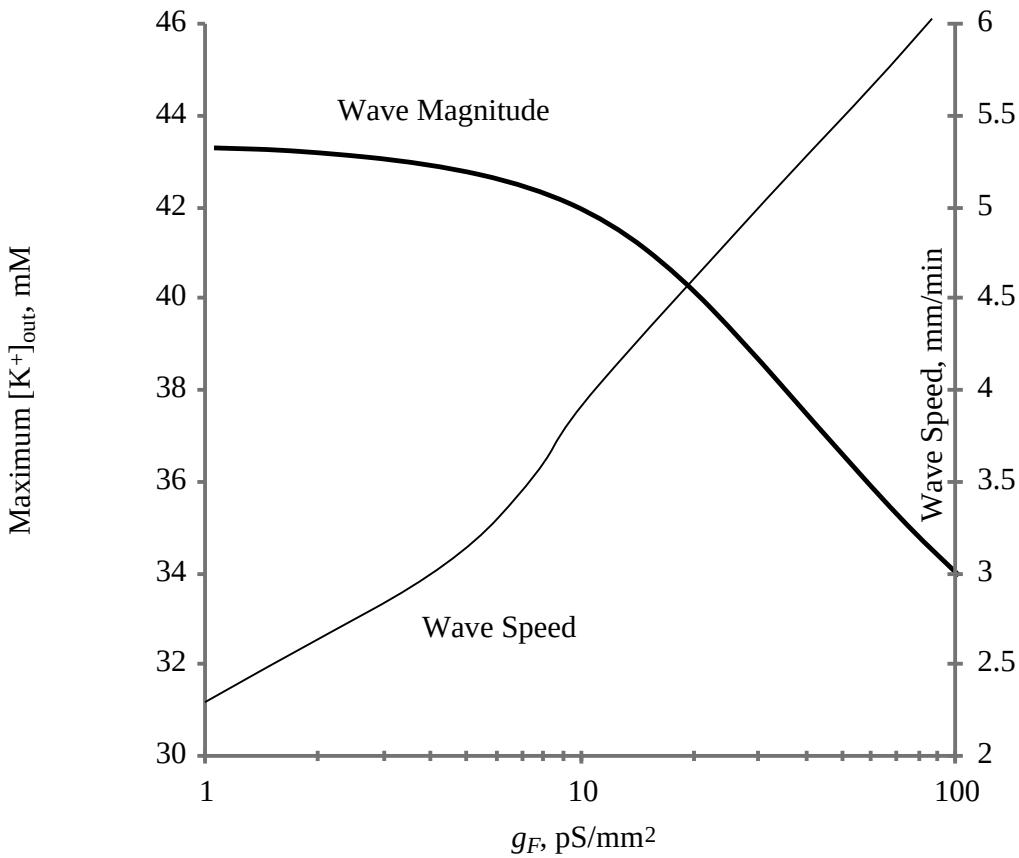


Figure 4.25. Wave speed and magnitude as a function of $g_F$. The ratio $g_P/g_F = 0.01$ is held fixed. Values of other parameters: $g_M$=10 pS/μm$^2$, $g_A$=10 pS/μm$^2$, $g_{K,NMDA}$=100 pS/μm$^2$, $g_{DR}$=1000 pS/μm$^2$. All other membrane conductances are set to zero.

## 4.9. CALCIUM AND CALCIUM CURRENTS

Each calcium conductance was varied independently while holding all other parameters fixed at the values given in Table 4.13. Both the predicted wave magnitude and wave speed increased approximately linearly with HVA-channel conductivity as illustrated in Figure 4.26. Wave magnitude was only weakly dependent on $g_{HVA}$, increasing by less than 3% as $g_{HVA}$ was increased from 0 to 20 pS/μm$^2$. The predicted wave speed was much more strongly dependent on $g_{HVA}$ increasing by over 50% from ≈4.3 mm/min to ≈6.6 mm/min (for the same parameter set). The HVA conductivity also affected the waveform shape. At higher calcium conductance, the slope of the onset of the wave, as observed at a fixed point, was steeper, and the wave recovered slightly sooner (Figure 4.27, top set of curves). A similar effect is predicted to occur when the interstitial calcium concentration is reduced to 10% of its original value (bottom set of curves in Figure 4.27). These predictions are consistent with the results of Basarsky and others (1998) who noticed a reduction in the wave onset slope when calcium was removed from the bath. Varying the LVA-channel conductivity over the same range (0 to 20 pS/μm$^2$) had no measurable effect on the predicted wave magnitude, the predicted wave speed or the predicted waveform shape.

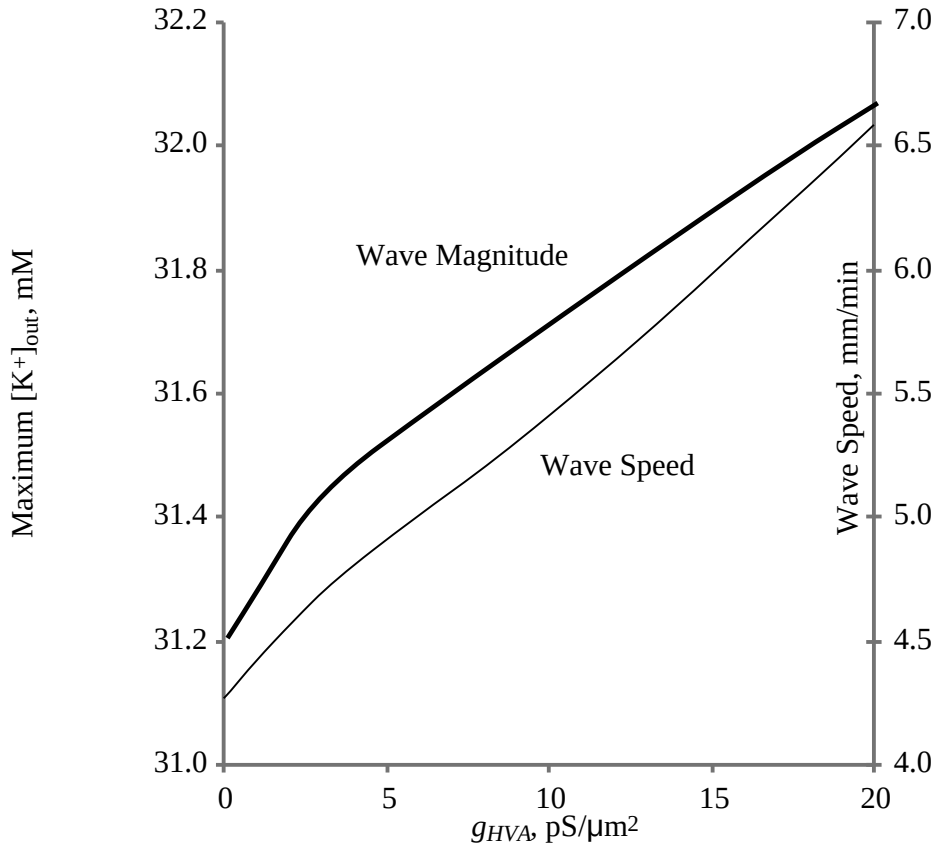


Figure 4.26. Predicted wave magnitude and wave speed as a function of HVA calcium current, with $g_{LVA}$=0.4 pS/μm$^2$ (fixed). Parameters as given in Table 4.13.

Table 4.13. Membrane conductances used in calcium study (pS/μm$^2$).

| Parameter | Value |
|---|---|
| $g_A$ | 25 |
| $g_{BK}$ | 250 |
| $g_{DR}$ | 250 |
| $g_F$ | 40.0 |
| $g_{IK}$ | 2.0 |
| $g_M$ | 10.0 |
| $g_{K,NMDA}$ | 250 |
| $g_P$ | 0.4 |
| $g_{SK}$ | 2.0 |

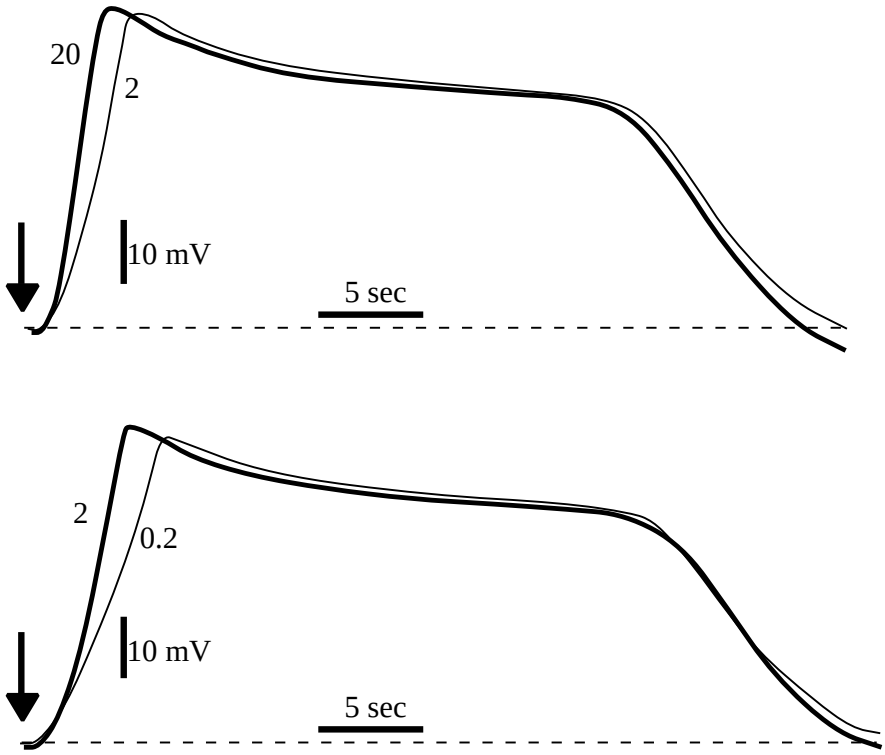


Figure 4.27. Predicted effect of interstitial calcium and HVA calcium current on the shape of the DC-voltage waveform as observed at a point 0.5 mm from the stimulation. The dashed line gives the resting potential. Top: Predicted effect of membrane calcium current through HVA channels for two different values of $g_{HVA}$. The curves are annotated with the values of $g_{HVA}$ in pS/μm$^2$. $[Ca^{++}]_{out}$ = 2.0 mM at rest. Bottom: Predicted effect of interstitial calcium concentation on the shape of the waveform, for two different values of $[Ca^{++}]_{out}$, shown in mM. In thte bottom plot, $g_{LVA}$=0.4 pS/μm$^2$. For both sets of curves $g_{HVA}$=4.0 pS/μm$^2$. Other parameters as given in Table 4.13.

## 4.10. CALCIUM WAVES

In all cases when spreading depression was induced, a cytosolic calcium wave was observed. The shape of a typical waveform at two times following the initial stimulation is illustrated in Figure 4.28. The peak of the calcium wave coincided approximately with the peak of the DC voltage shift (Figure 4.29) but has a much steeper onset and faster recovery, with magnitude ranging from 100 to 150 μM.

Preventing calcium release from intracellular stores by setting $j_{ITP,max}$=0 and $v_{ryanodine}$ =0 (in equations 6 and 12 of section 3.7) had no significant effect on the calcium waveform. The calcium wave could be abolished without preventing the SD wave by setting the conductivity of the voltage-gated calcium channels to zero. This indicates that the calcium wave predicted by this model is caused predominantly by calcium entry through membrane channels. If the bulk of the calcium which disappears from the intercellular space enters neurons (and not glial cells), the magnitude of the cytosolic calcium transient would approach

$$(1-\varepsilon)\times\frac{1-f}{f}\times[\mathrm{Ca}^{++}]_{out,rest}\approx 335\ \mu\mathrm{M} \qquad (1)$$

where $\varepsilon \approx 0.05$ is the fraction of calcium which remains, $f \approx 0.85$, and $[Ca^{++}]_{out,rest}\approx 2$ mM. This calculation assumes that the calcium is uniformly distributed throughout the cell. Buffering by intracellular organelles such as the endoplasmic reticulum and mitochondria, and by proteins such as calmodulin, should reduce the magnitude of this calcium transient. However, if the calcium is restricted to a smaller, sub-membrane area, such as dendritic spines, the transients in these areas could get much higher.

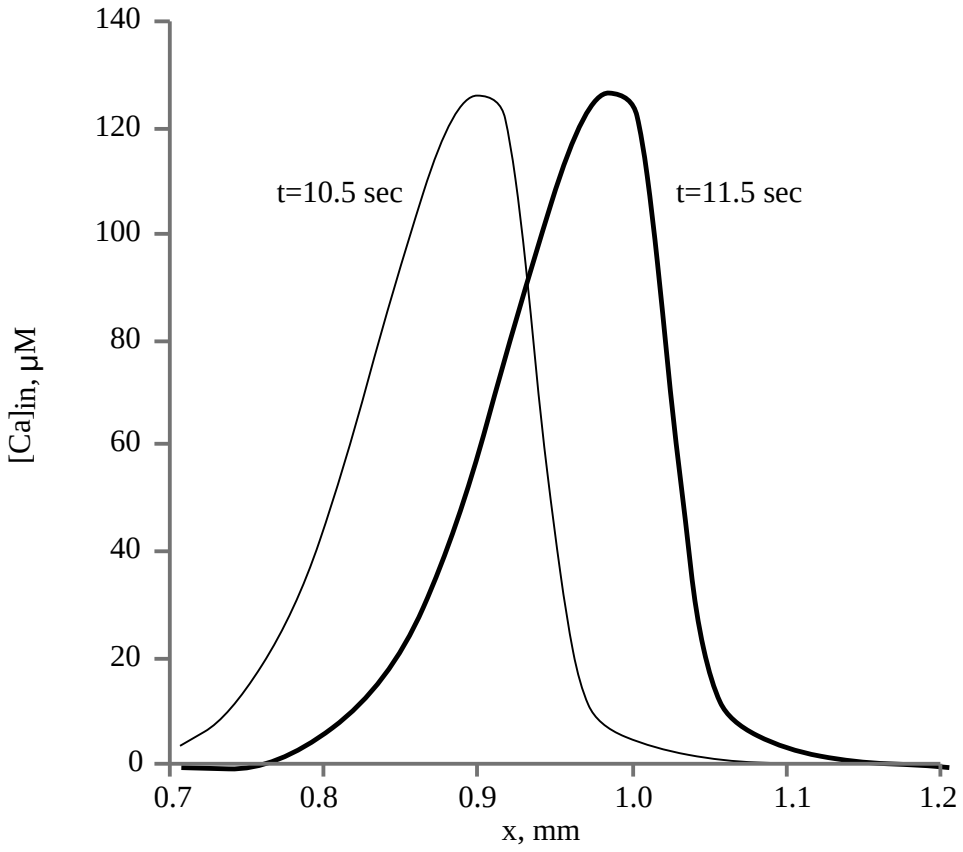


Figure 4.28. Cytosolic calcium wave traveling at same speed as SD wave. The waveform is shown at two times, t = 10.5 and *t* = 11.5 seconds after SD is induced by a stimulation at *x* = 0. The abscissa gives the distance from the stimulation in microns, and the ordinate gives the cytoplasmic calcium concentration in μM. In this simulation, the wave is traveling to the right at a speed of 4.7 mm/min. Parameters: $g_{DR}$=500 pS/μm$^2$, $g_A = g_M$ = 10 pS/μm$^2$, $g_{BK} = g_{SK} = g_{IK}$ = 0, $g_F$ = 50 pS/μm$^2$, $g_P$ = 0.5 pS/μm$^2$, $g_{HVA}$ = 4 pS/μm$^2$, $g_{LVA}$ = 0.4 pS/μm$^2$, $g_{K,NMDA}$ = 100 pS/μm$^2$, $j_{Pump,Max}$ = 0.01 mM/sec, $j_{IP3,Max}$ = 0.04 mM/sec, $j_{ryanodine,Max}$ = 0.1/sec.

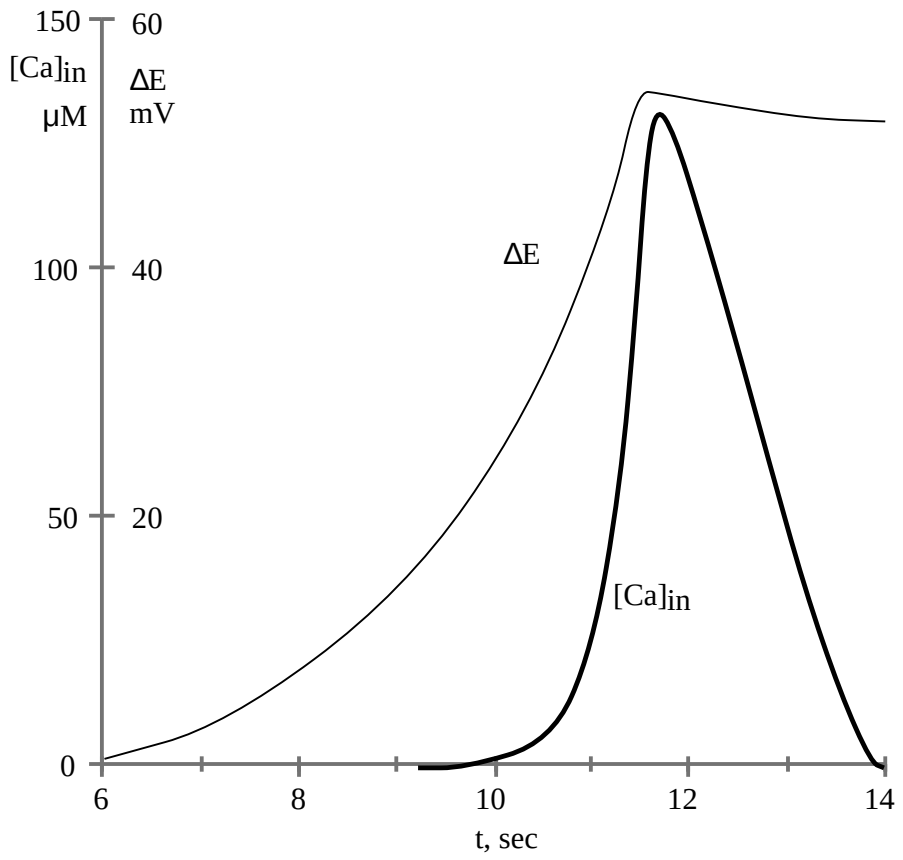


Figure 4.29. The calcium wave coincides with the peak of the DC voltage shift, both of which are illustrated at a point one millimeter from the point of stimulation, for the same simulation shown in Figure 4.27. The abscissa gives the time in seconds following the stimulation; the ordinates give the micromolar calcium concentration and the DC voltage shift from baseline in mV.

## 4.11. STRETCH-GATED ION CURRENTS

To determine if the activation of stretch-gated ion channels was necessary for wave propagation in the model, the proportion $q_{max}$ of BK and delayed rectifier channels which can be opened by stretch was varied from 0 to 1 (see equation 1 of section 3.3.8). The value of $q_{max,BK}$ had very little discernible effect on either the wave speed or wave magnitude except to set a threshold for wave propagation as illustrated in Figures 4.30 and 4.31. For $q_{max,BK}$ =0, the threshold occurred at $q_{max,DR} \approx 0.2$; for $q_{max,BK}$ =0.43 (the value suggested by Mienville, Barker and Lange, 1996), the threshold occurred at $q_{max,DR} \approx 0.16$; and for $q_{max,BK}$ =1, the threshold occurred at $q_{max,DR} \approx 0.03$. Between the threshold and $q_{max,DR} \approx 0.25$ minimal variation in the wave speed or magnitude was predicted by the simulations. For $q_{max,DR} > 0.25$, both the wave speed and wave magnitude showed a linear dependence on $q_{max,DR}$ which was independent of $q_{max,BK}$. The wave magnitude increased from $[K^+]_{out} \approx 27.5$ mM at ≈0.2 to 35 mM at $q_{max,DR}$ =1. Over the same range of $q_{max,DR}$, the wave speed increased linearly from ≈3.0 to 3.6 mM/min.

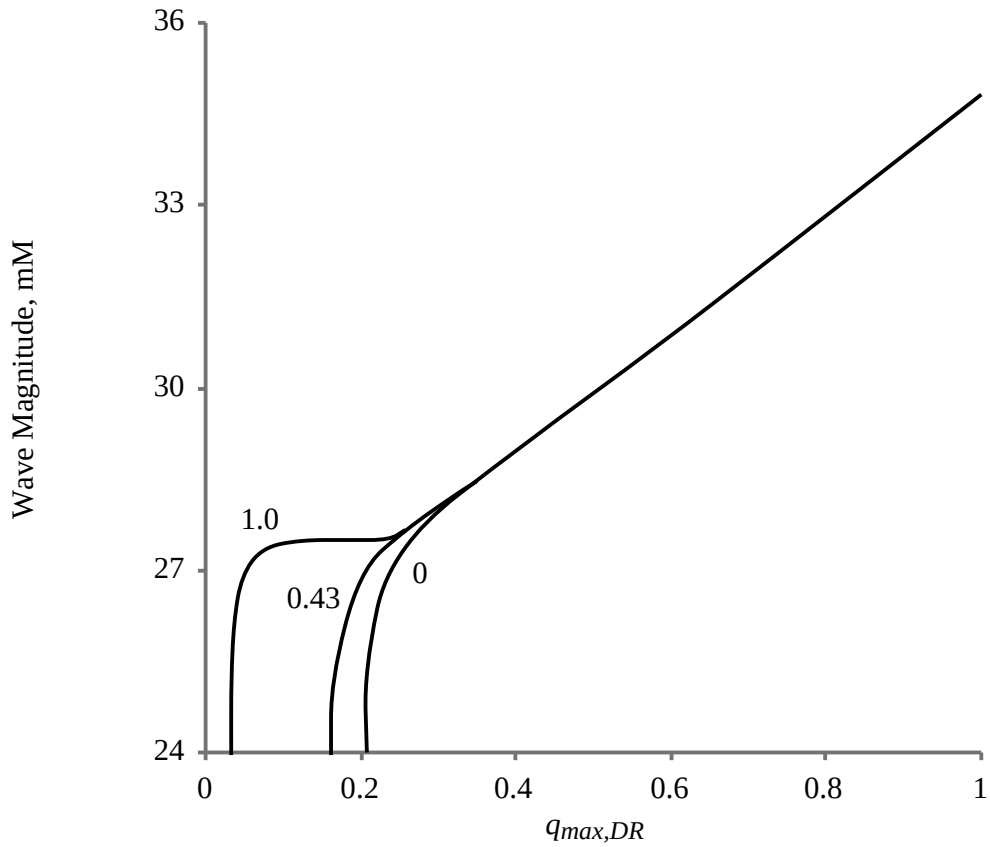


Figure 4.30. Significance of membrane stretch on model predictions. The wave magnitude is plotted as a function of $q_{max,DR}$ for three different values of $q_{max,BK}$, which are noted on the figure. The corresponding wave speeds are shown in Figure 4.31. Conductance values: $g_{DR}$=250 pS/μm$^2$, $g_{BK}$=250 pS/μm$^2$, $g_{K,NMDA}$=250 pS/μm$^2$, $g_{HVA}$=4.0 pS/μm$^2$, $g_{LVA}$=0.4 pS/μm$^2$, $g_F$=10 pS/μm$^2$, $g_P$=0.1 pS/μm$^2$, $g_M$=0, $g_A$=0.

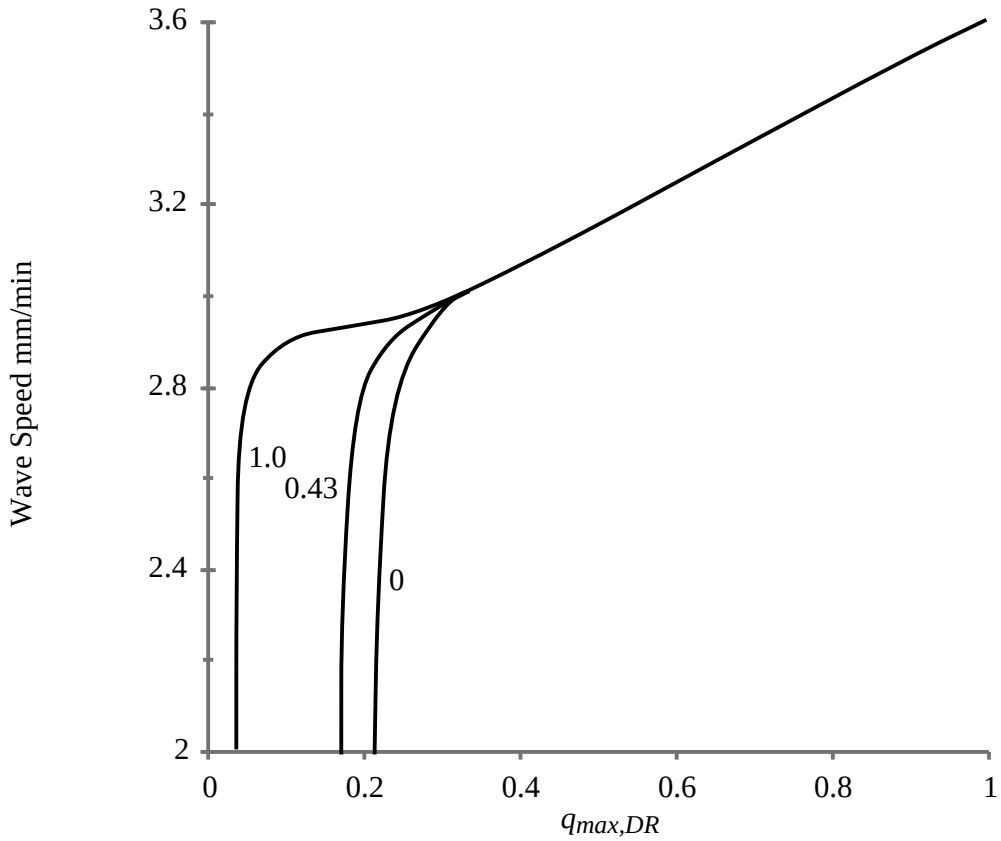


Figure 4.31. Wave speed as a function of $q_{max,DR}$ for three different values of $q_{max,BK}$, which are noted on the figure, for the same set of simulations illustrated in Figure 4.30.

## 4.12. NEURONAL GEOMETRY

To evaluate the dependence of the model on geometric parameters simulations were run over a range of dendritic diameters (0.75 μm to 8.0 μm) with all other parameters held fixed. The membrane conductances used are given in Table 4.14. The predicted wave magnitude, measured as the maximum total interstitial potassium concentration, decreased approximately linearly with diameter. The dependence was relatively weak, decreasing by approximately 15% from ≈ 32.7 mM to ≈27.5 mM over this range of diameters, as illustrated in Figure 4.32. The predicted wave speed was much more sensitive to variations in the diameter, decreasing by over 80% from ≈8.5 mm/min to ≈1.5 mm/min over this same parameter range. Wave speed is also shown in Figure 4.32. In addition, the onset of the DC voltage shift was slower (decreased slope) at larger diameters, and the predicted duration of the voltage shift was substantially longer. This is illustrated in Figure 4.33, which shows the DC voltage shift observed at a fixed point 0.5 mm from the stimulation point for two different diameters.

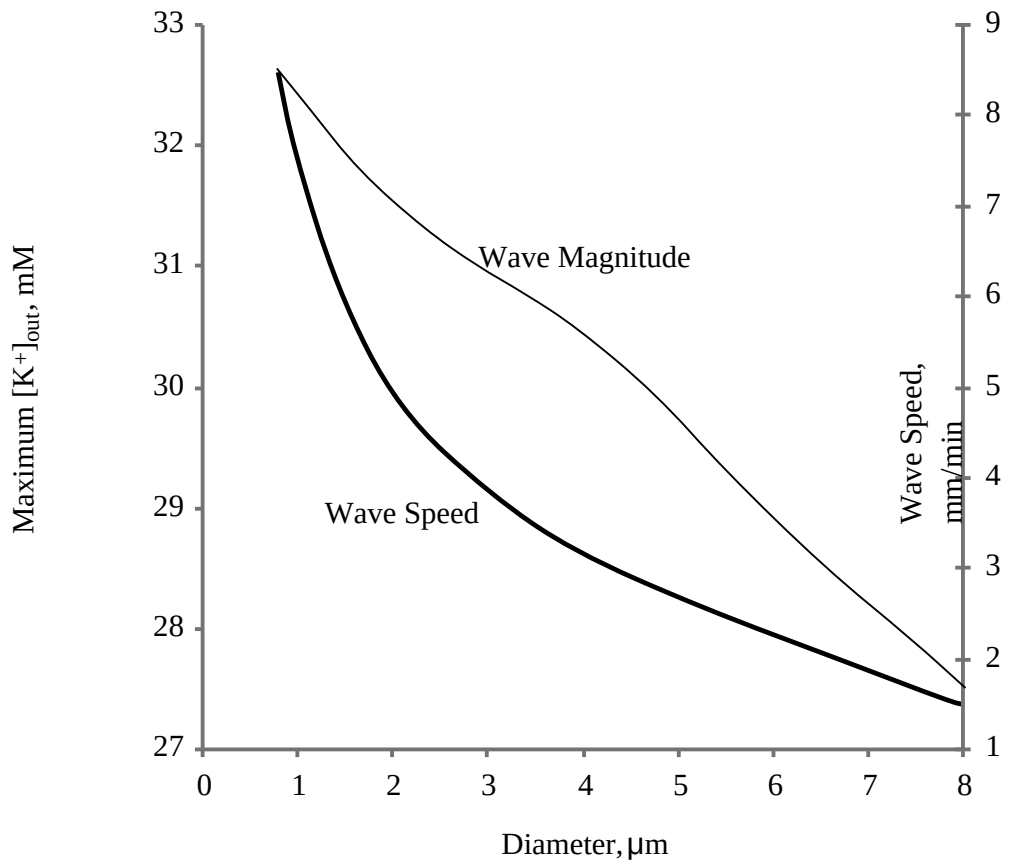


Figure 4.32. Dependence of predicted wave speed and wave magnitude on dendritic diameter. The parameters used are shown in Table 4.14.

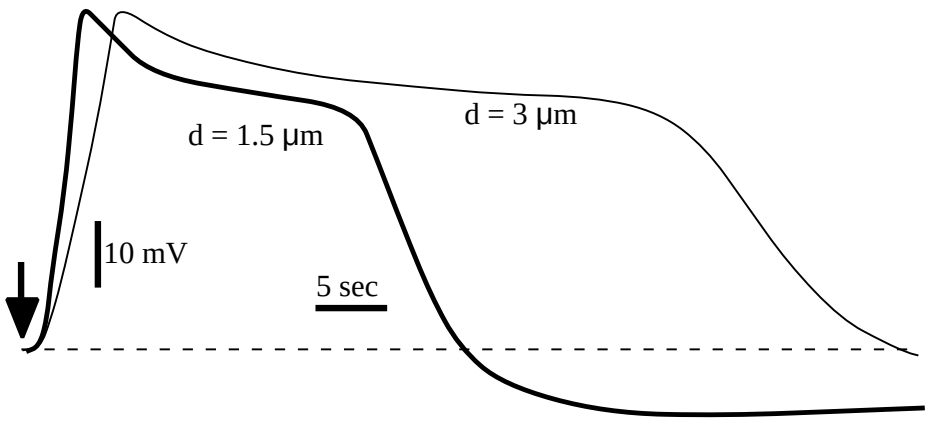


Figure 4.33. Effect of diameter on the shape of the predicted waveform. The DC-voltage shift as a function of time, as it would be observed at a fixed point 0.5 mm from the stimulation point, is illustrated for two different values of the dendritic diameter *d*. The resting potential is indicated by the dashed line, and the stimulation occurs at the time indicated by the arrow. The parameters used are listed in Table 4.14.

Table 4.14. Membrane conductances used to study dependence of model predictions on diameter.

| Parameter | Value, pS/μm$^2$ |
|---|---|
| $g_A$ | 25.0 |
| $g_{BK}$ | 250 |
| $g_{DR}$ | 250 |
| $g_F$ | 40.0 |
| $g_{HVA}$ | 5.0 |
| $g_{IK}$ | 2.0 |
| $g_{K,NMDA}$ | 250 |
| $g_{LVA}$ | 0.5 |
| $g_M$ | 10.0 |
| $g_P$ | 0.4 |
| $g_{SK}$ | 0 |

## 4.13. GLIAL PUMPING

To evaluate the dependence of the simulation on the glial pumping model, simulations were run over a range of glial pump strengths spanning the likely physiological parameter range (potassium pump strength from 0 to 10 mm/liter-sec). Other parameters used in this set of simulations are as shown in Table 4.15. As shown in Figure 4.34 both the predicted wave speed and predicted wave magnitude decreased smoothly as a function of total pumping strength. The decrease in predicted wave speed was more pronounced than the decrease in wave magnitude, decreasing by over 30% (from ≈5.03 mm/min to ≈3.25 mm/min) over the range of values tested. The predicted wave magnitude decreased by only ≈9% (from ≈31.8 mM to ≈29.2 mM). The predicted slope of wave onset also increased as glial pump strength was decreased (*e.g.*, in simulation of block), as illustrated in Figure 4.35. An increased slope is suggestive of a more rapid rise in activity, or a system that is more excitable to spreading depression; similarly, a decreased slope is suggestive of a less excitable system. The simulations predict that neural tissue is the most susceptible to spreading depression in the complete absence of glial cells. Even though the glial model is very simple, it predicts that glial cells, as modeled, act to inhibit, and not to facilitate spreading depression. This prediction is consonant with experimental findings, as discussed in section 2.2.8 ("Neuroglia") (Largo, Cuevas and Herreras, 1996, Largo and others, 1996, 1997).

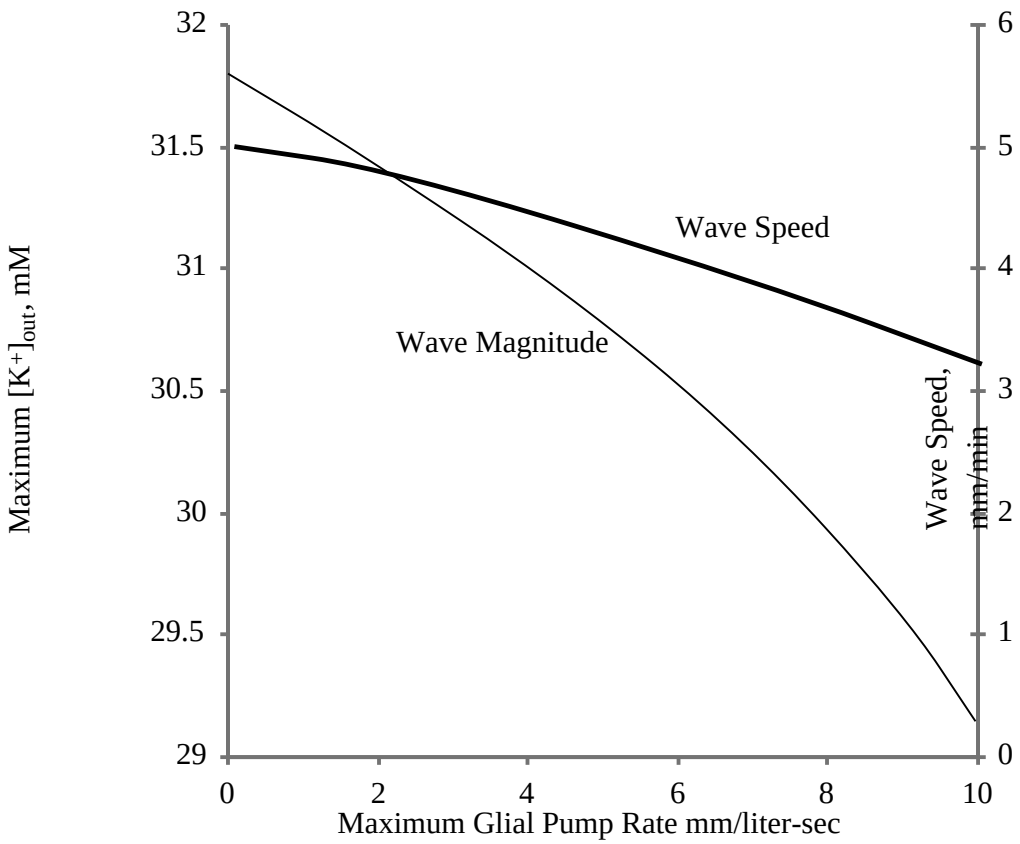


Figure 4.34. Effect of glial pump strength on model predictions. The wave magnitude (maximum interstitial $K^+$ concentration) are wave speed are plotted as a function of total glial pumping rate. The parameters used for this series of simulations are given in Table 4.15.

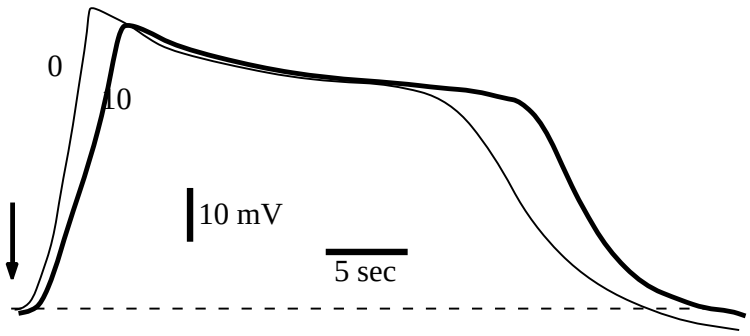


Figure 4.35. Effect of glial pump rate on shape of predicted waveform. The DC-voltage shift as observed at a fixed point 0.5 mm from the stimulation is shown for two different values of simulated total pump rate as a function of time. The stimulation time is indicated by the arrow. The resting potential is indicated by the dashed line. These predictions are representative of the simulations used in Figure 4.34. The membrane conductances used are listed in Table 4.15.

Table 4.15. Membrane conductances used to study glial model.

| Parameter | Value, pS/μm$^2$ |
|---|---|
| $g_A$ | 0 |
| $g_{BK}$ | 250 |
| $g_{DR}$ | 250 |
| $g_F$ | 40.0 |
| $g_{HVA}$ | 4.0 |
| $g_{IK}$ | 1.0 |
| $g_{K,NMDA}$ | 250 |
| $g_{LVA}$ | 0.4 |
| $g_M$ | 0 |
| $g_P$ | 0.4 |
| $g_{SK}$ | 1.0 |

# CHAPTER 5

# DISCUSSION

This chapter summarizes the dissertation, presents a critique of the methods used, and discusses the results predicted by the numerical simulations. The goals of the study were to model the predicted influence of (a) osmotic forces and (b) neuronal gap junctions in spreading depression (discussed in section 5.1, “Goals”). To study these objectives, a conceptual model of spreading depression was developed, formulated mathematically, and implemented as a computer program. Three crucial assumptions (discussed in more detail in section 5.2, “Crucial Assumptions”) were incorporated into this model: (a) that osmotic forces induce neuronal water entry; (b) that cytosolic voltage gradients exist and are described by the electrodiffusion equation; and (c) that neuronal gap junctions allow the direct movement of ions between cells.

The model that was developed in this dissertation has a number of novel features that have never before been applied to the study of spreading depression. These include the first use of standard, biophysical models of membrane currents to describe SD; the first application of the Hodgkin-Huxley formalism in the study of SD; the first study of gap junctions in a mathematical model of SD; the first

mathematical formulation of osmotic volume changes during SD; and the first application of the electrodiffusion equation to SD.

After the model was implemented as a computer program it was extensively studied (stress tested) by varying all parameters across their known physiological ranges. This parametric analysis produced a number of interesting predictions. One of these predictions is that the volume changes that have been observed during spreading depression are similar to what would be expected to occur as a result of osmotic forces. The simulations further predict that waves of SD cannot propagate unless some cellular expansion is possible. The model also predicts that ionic movement through a syncytium of neurons connected by gap junctions is sufficient to drive SD wave propagation, even in the complete absence of extracellular diffusion. Finally, a cytoplasmic calcium wave is predicted to propagate along with the wave of spreading depression. These predictions are discussed in section 5.3 in terms of a proposed neuroprotective theory of spreading depression. To reduce the computational demands of the numerical implementation, a number of simplifications were made. These simplifications, along with a critique of the model and suggestions for future study are summarized in section 5.4.

## 5.1. GOALS

The goals of this dissertation were (1) to model a putative mechanism (electrodiffusion) for the gap-junction mediated propagation of spreading depression, and (2) to evaluate the contribution of osmotic forces to SD wave propagation. The first goal was inspired by several experiments that have shown that spreading depression can be inhibited by selectively blocking gap junctions, while glial poisons do not prevent SD (Martins-Ferreira and Ribeiro, 1995; Nedergaard, Cooper and Goldman, 1995; Largo and others, 1997; Aitken and others, 1998b). The aim was to model a way in which SD might propagate via neuronal gap junctions; gating mechanisms were deemed beyond the scope of this study.

The second goal was based on the observations of substantial neuronal volume changes during SD (Kraig and Nicholson, 1978). It is not known if these volume changes are necessary for wave propagation. Osmotic forces and the consequent volumetric changes have not been included in any previous mathematical model of spreading depression. In the model presented in this dissertation, osmotic forces were hypothesized to induce water entry (and efflux) and volumetric change, and these volumetric changes were predicted to be crucial to wave propagation.

## 5.2. CRUCIAL ASSUMPTIONS

To obtain the results presented in this dissertation three crucial assumptions were made. The first assumption is based on the observations that cells expand during spreading depression (Jing, Aitken and Somjen, 1994). This expansion causes interstitial space to contract, thereby increasing the extracellular $K^+$ concentration. One possible mechanism for such expansion is osmosis. The existence of such osmotic forces constitutes the first crucial assumption. Increasing the ionic content of a cell leads to the generation of osmotic pressure gradients. To relieve these gradients water will enter the cell, causing it to expand. If the cells are not allowed to expand (in the present model) the depolarization-induced potassium efflux is insufficient to induce a propagating wave.

The second crucial assumption is that voltage gradients within the cytosolic fluid cannot be ignored. Interstitial voltage gradients are generally not taken into account in neuronal simulations because no advantage is conferred by acquiescing to the additional computational resources demanded. This is because the membrane voltage calculated electrodiffusively when all ionic concentration changes are small is almost indistinguishable from that predicted with a traditional compartmental approach (Qian and Sejnowski, 1989). However, there are significant concentration changes during spreading depression. Hence the usual model of a dendrite as a succession of ohmic compartments – as in the derivation of the cable equation – is not applicable. Electrodiffusion generates a cytosolic $K^+$ pulse, while depolarization

causes substantial $Na^+$ and $Cl^-$ fluxes into cells. The resulting osmotic forces lead to water entry and sufficient cellular expansion to induce a regenerative wave of spreading depression.

The third crucial assumption is that gap junctions open "as needed." It has been speculated that a wave of spreading depression causes normally closed gap junctions between neurons to open by some yet to be determined mechanism (Somjen and others, 1992). This view was taken here. There is some evidence indicating the widespread presence of gap-junctional proteins in the CNS, particularly during early development (Sloper and Powel, 1978; Bayer and Pickel, 1990; Bozhilova-Pastirova and Ovtscharoff, 1995; Simbürger and others, 1997). These may be necessary for the organization of neural circuits (Peinado, Yuste and Katz, 1993; Kandler and Katz, 1995; Rörig, Klausa and Sutor, 1995). It is not actually known whether these gap junctions are normally open or closed. How gap junctions activate during wave passage was specifically excluded from the scope of the present study, and remains a factor that should be examined more closely. This does not detract from the present results, since they suggest that an SD-like wave can be propagated via cytosolic transport if there is some mechanism that will open the gap junctions, and if the cell is allowed to expand and contract in response to osmotic forces. One possible mechanism for gap-junctional activation is membrane stretch.

## 5.3. MODEL PREDICTIONS

This section summarizes the model predictions and discusses them in terms of published results. The principal result is that standard electrophysiological modeling techniques are compatible with the phenomena observed during spreading depression. In particular, the properties of spreading depression depend upon the particular combination of membrane channels present in the tissue, and that while some membrane channels appear to facilitate SD, others may impede (or protect against) spreading depression. Furthermore, the simulations suggest that spreading depression will not occur unless there is sufficient space for the cells to expand in response to osmotic pressure gradients, and that wave propagation is dependent on the presence of neuronal gap junctions.

### 5.3.1. ELECTROPHYSIOGICAL PREDICTIONS

The simulations show that standard electrophysiological models may be used to describe spreading depression – or at least a variety of spreading depression-like phenomena. In particular these phenomena may be supported by a variety of electrophysiological mechanisms. The predicted wave magnitude, propagation velocity, and waveform shape depend on the mixture and quantity of membrane channels present in the tissue, as summarized in Table 5.1. Depending on the other channels that are present, the simulations predict a threshold conductance for NMDA-receptor gated ion currents (discussed in section 4.5, "NMDA-Receptor Gated Ion Currents"), the delayed rectifying (DR) potassium current (section 4.7, "Voltage

Gated Potassium Currents"), and the large conductance (BK-type) calcium-activated potassium (K(Ca)) channel (section 4.6, "Calcium Activated Potassium Currents"). Above threshold, the predicted wave magnitude is an increasing function of the DR and BK conductance, and a decreasing function of the NMDA conductance. The predicted wave speed is a continuously increasing function of all three conductances (above threshold). For some combinations of these conductances no threshold is predicted, i.e., waves can not always be induced. The model also predicts that both wave magnitude and wave speed should be an approximately linearly increasing functions of the HVA-calcium current, while no dependence on the LVA-calcium current is predicted (section 4.9, "Calcium and Calcium Currents"). Removing interstitial calcium is also predicted to decrease the likelihood that spreading depression will occur. The presence of voltage-gated $Ca^{++}$ channel antagonists or the removal of interstitial calcium will only inhibit spreading depression if the appropriate combination of ion channels is present. Consequently the partial or complete block of SD by NMDA-R antagonists (Hernandez-Caceres and others, 1987; Lauritzen and others, 1988; Marrannes and others, 1988; Lauritzen and Hansen, 1992; McLachlan, 1992; Nellgard and Wieloch, 1992), Magnesium ($Mg^{++}$) ions (van Harreveld, 1984; Lauritzen and others, 1988) and tetraethylammonium (TEA) ions (Scheller, Tegtmeir and Schlue, 1998) can be explained.

The simulations predict that both A-type voltage-gated potassium channel and the small conductance (SK-type) K(Ca) currents will have an inhibitory, rather than a facilitatory, role in spreading depression (refer to section 4.6, "Calcium Activated

Potassium Currents" and section 4.7, "Voltage Gated Potassium Currents"). One possible interpretation is that these two conductances act to stabilize the membrane against neuronal excitability (of the SD-type), while other conductances (particularly the NMDA, BK and DR channels) are destabilizing. The prediction that the A-type channel protects “against” spreading depression is consonant with the observations of spontaneous spreading that have been reported following application of 4-AP (a selective A-type channel blocker) (Psarropoulou and Avoli, 1993; Avoli and others, 1996). Furthermore, the prediction that the SK-channel is also protective against SD is consistent with the observation that seizures have been observed following application of apamin (a selective SK-channel antagonist) (McCown and Breese, 1990). These observations are also consistent with the theory that SD and seizure are two aspects of the same physiological response, with spreading depression the response to a weaker stimulation and seizure the response to a stronger stimulation.

Table 5.1. Summary of model predictions. Each column summarizes the effect of increasing the specified parameter. A "+" indicates an increasing dependence (i.e., magnitude increases with cytosolic diffusion constant), a "-" indicates a decreasing dependence, and "NC" indicates no change. "Mag" is wave magnitude, "Speed" is wave speed, "Slope" is magnitude of the onset slope, "Dur" is the duration of the DC-voltage shift.

| Parameter | Mag | Speed | Slope | Dur | Remark |
|---|---|---|---|---|---|
| Cytosolic diffusion constant | + | + | + | - | |
| NMDA conductance | - | + | NC | NC | threshold |
| BK conductance | + | + | + | + | threshold |
| SK conductance | NC | NC | - | - | cutoff |
| IK conductance | NC | NC | NC | NC | |
| DR conductance | + | + | + | + | threshold |
| A-channel conductance | NC | NC | - | - | cutoff |
| Na-channel conductance | - | + | + | + | |
| HVA-channel conductance | + | + | + | + | |
| LVA-channel conductance | NC | NC | NC | + | |
| Interstitial $Ca^{++}$ concentration | + | + | + | + | |
| Diameter | - | - | - | + | |
| Glial pumping rate | - | - | - | NC | |

### 5.3.2. Wave Propagation Requires Cellular Expansion

The simulations presented suggest that spreading depression will not propagate unless there is sufficient space for cellular expansion (see section 4.4, "Osmotic Volume Changes"). It has been reported that SD is more difficult to induce in species with more convoluted cortex (see, for example, McLachlan and Girvin, 1994). It is intriguing to speculate that the reason for this may be, in fact, that the neuropil is more tightly packed in these species. This may provide species with less tightly packed cortex, such as reptiles and fish, some protection against seizure.

### 5.3.3. Wave Propagation Requires Gap Junctions

Poisoning gap junctions (e.g., by reducing the cytosolic diffusion coefficient to zero) was predicted to have a strongly inhibitory effect on spreading depression (discussed in section 4.3, "Gap Junctions"). This is consistent with the theory that spreading depression requires the propagation of ionic currents through gap junctions, and the observation that agents which poison gap junctions prevent spreading depression (Martins-Ferreira and Ribeiro, 1995; Nedergaard, cooper and Goldman, 1995; Largo and others, 1996). Care must be taken in interpreting this result, however, since the agents used in these experiments can affect other processes (see section 2.2.6).

### 5.3.4. Calcium Waves Accompany Spreading Depression

Cytosolic calcium waves always accompany the SD wave in this model, with the calcium wave front propagating along with the DC voltage shift (see section 4.10, "Calcium Waves"). The propagating depolarization opens calcium channels, allowing calcium to enter the cell. It is also possible that a portion of the calcium would enter astrocytes or other glial cells. This could cause two independent calcium waves to occur: one in astrocytic space, and one in neuronal space. When multiple, complex calcium buffering and release mechanisms are taken into account, it might be possible to predict the propagation of multiple $Ca^{++}$ waves traveling at different speeds. For example, several laboratories have reported observing calcium waves with SD. Calcium waves have been observed in association with spreading depression in the chicken retina; the data indicate that glial mechanisms are involved (Fernandes de Lima, Goldermann and Hanke, 1994). Two distinct calcium waves were observed in hippocampal organ cultures (Kunkler and Kraig, 1998), with a fast wave traveling at ≈6 mm/min and a slow wave at ≈4 mm/min. The second wave traveled at the same speed as the SD wave but preceded it by 6 – 16 sec. The authors believe that it is likely that at least one of these waves is astrocytic. $Ca^{++}$ waves have also been observed in hippocampal slices during SD that are at least partially astrocytic (Basarsky and others, 1998). In this preparation both the SD and the $Ca^{++}$ wave propagate at ≈0.9 to 1.2 mm/min. These calcium waves were completely abolished by replacing the calcium in the bath with magnesium. Since calcium waves did not occur when calcium was not present in the bath, this supports the notion that

the $Ca^{++}$ waves are due to calcium passage across the membrane into neurons and/or astrocytes, rather than being due to release from internal stores. However, magnesium may have additional side-effects, such as NMDA block, and this phenomenon is likely to be examined in greater detail in the near future. Basarsky and others (1998) also predict a slowing in the rise (slope decrease) of the DC voltage shift when $Ca^{++}$ was removed from the bath. The results presented in section 4.9 are consistent with this slope change. The decrease in rise time may indicate the effect upon K(Ca) channel participation when calcium entry is prevented

In the present simulations, the expected sharp initial increase in $[Ca^{++}]_{in}$ occurs when the DC voltage wave passes, rather than several seconds earlier, as reported by Basarsky (1998). This is followed by a return to resting calcium concentrations within a few seconds as calcium is pumped into the ER. A more complete model may need to take into account multiple calcium buffers and release mechanisms, including both neuronal and glial syncyctia. This remains an important subject for further modeling.

### 5.3.5. Is Spreading Depression Neuroprotective?

The results of these simulations are consistent with a neuro-protective hypothesis of spreading depression. In this theory, spreading depression results from a combination of mechanisms that occur in response to the loss of cellular homeostasis. Typical stimuli that may induce SD (mechanical, electrical, chemical, hypoxic) will also lead to neural injury if presented in sufficient magnitude. The

large increases in interstitial $K^+$ or cytoplasmic $Na^+$ or $Cl^-$ observed during SD could be indicative of cellular damage. A cascade of cytoplasmic signals, starting with neuronal calcium entry, and eventually leading to the production of the proteins that are required for cellular repair and/or re-growth, could be the response to this injury. This production of regenerative proteins in response to neural trauma could be the evolutionary advantage that is provided by spreading depression. The propagating potassium wave characteristic of SD would, in this theory, be the mechanism by which the neuro-protective signal is propagated to the surrounding tissue. The consequent membrane depolarization could also be interpreted as a way of preventing further cell damage. Depolarization makes the membrane highly permeable to the usual inorganic ions of biological significance: $K^+$, $Na^+$, $Cl^-$, $Ca^{++}$. As these species approach their equilibrium concentrations, the driving forces for additional ionic fluxes disappear. Cells die if the membrane voltage is clamped. This occurs because extremely large currents are required to maintain the voltage clamp as the membrane resistance approaches zero. Cells recover when the voltage is allowed to float. Thus by equilibrating the voltage across the membrane (depolarizing to zero) the cells manage to protect themselves against potential damage or necrosis.

## 5.4. MODEL CRITIQUE

A number of simplifications were made to reduce the complexity of the model It could be argued that the predictions of this model are non-physiological because of the nature of these approximations. Without some sort of reduction, however, the model would not have been computable (with present technology). The biggest simplification is geometrical; all anatomical considerations, including specific neuronal connectivity, have been "averaged out" by the use of a continuum model. Furthermore, non-neuronal compartments (such as glial, axonal, and vascular) have been specifically excluded from the model. Axonal components are probably involved in high-voltage spiking and calcium waves that accompany spreading depression. Glial cells may be involved in calcium waves that accompany spreading depression, while vascular volume changes could affect tissue recovery. Calcium waves are predicted by the model, but only a single wave, and not the pair of waves that purportedly travel at different speeds that have been observed. Finally, gap junctions have been described by a non-gated diffusional approximation. The implications of this simplification are not entirely clear, but if neuronal gap-junctions can be activated (or inactivated) by changes in cytosolic ionic concentrations and voltage gradients, some modifications may need to be made. A critique of these simplifications is provided in the following subsections.

### 5.4.1. Geometrical Challenges

Perhaps the most daunting challenge is geometrical. Both the true three-dimensional nature of nervous tissue and the nature of neuronal connectivity have been ignored. A first step would be to extend the single-dimensional continuum model two a two-dimensional planar system representative of the cortical surface. Subsequent modifications and a third dimension could be added to account for gyral curvature.

A more complex issue is neuronal connectivity. In the continuum model a simple cylindrical geometry with a fixed radius has been assumed. In reality, dendrites form into three-dimensional tree-like structures with varying radius. The trees of adjacent neurons are highly intermixed. Compartmental models (e.g. GENESIS, NEURON) have been extremely successful at modeling single neurons as well as neuronal networks. These programs are implemented in terms of connected-ohmic compartments, and are designed to describe currents and voltages when the concentrations remain close to their usual physiological values. By extending such a model to include electrodiffusion, it might be possible to account for the extremely large ionic variations seen during spreading depression. In addition, ionic flows through gap junctions and osmotic volume changes have not been studied to any great extent in these models. It should still be possible to develop a NEURON-like simulation environment that is applicable to SD. The main problem (at present technological levels) would still be computability. These systems typically operate

on time scales of milliseconds, and spreading depression operates on time scales of seconds to minutes. Furthermore, the ionic changes that occur during SD affect all of the neurons in the given volume element being modeled. It would be necessary to account for as many of the different types of cells in the volume being modeled as possible, even if they are not networked together.

Another deficiency is that membrane channels are not uniformly distributed in the dendritic tree as has been assumed here. Much of this data is still not known. As this information becomes available and is taken into account it will probably add at least another order of magnitude to the complexity of the simulation.

There is also the question of geometric compartmentalization within cells. There may be multiple calcium buffers within many neurons that operate on different time scales and act in different locations. For example, protein buffers such as calmodulin are probably much denser in the sub-membrane regions and in dendritic spines. During spreading depression these buffers may saturate much more quickly than the intracellular organelles which are larger and more evenly distributed. It seems unlikely that this would affect the qualitative nature of the neuronal calcium waves, since it has been demonstrated (mathematically) that only one cytoplasmic pool of calcium is necessary for calcium waves to propagate (see Goldbeter, 1996 for a review). However, if there are multiple neuronal networks occupying the same volume elements, and each network has different calcium buffer distributions, it seems likely that calcium waves could propagate at different speeds in each network.

The same conclusion would follow if an astrocytic syncytium were added to the model.

### 5.4.2. Glial Contribution to Spreading Depression

Spreading depression can still be induced in preparations after glial poisons (e.g., fluorocitrate and fluoroacetate) are applied (Largo and others 1996, 1997). This result has been interpreted in the formulation of this model to imply that glial cells do not directly contribute to SD. However, as has been discussed above (see section 2.2.8, "Neuroglia") neither the cellular specificity nor the totality of the blocking effect of these agents is clear. If our interpretation of these observations is incorrect, then it may be that glia do, in fact, play an active role in spreading depression. However, with the exception of the parameter values used, there is nothing specifically "neuronal" about the cytosolic equations that have been used in this model. Thus with an appropriate parametric readjustment, it might be possible to reinterpret the simulations presented in Chapter 4 as indicating that it is an astrocytic, and not a neuronal, syncytium (or some combination of the two) of gap junctionally connected cells that effectively mediates spreading depression.

Very little is known about the active properties of astrocytes, although a wealth of information is being rapidly accumulated. A wide variety of ion channels have been identified in glial membranes. Whether these channels play an active role in astrocytic function remains to be determined. The role of vascular space and the astrocytic-vascular interaction may also be of interest. Gap junctions are known to be

present in astrocytes, and are assumed to play a significant role in the siphoning of excess potassium away from interstitial space. The mechanisms involved in this process are also not well understood. There is certainly some indication that calcium waves observed during spreading depression occur in glial cells; it may be that these waves propagate relatively independently of the properties of the nearby neuronal cells (see below in section 5.4.4 for more discussion of calcium waves).

Unfortunately, the particular distribution and quantity of ion channels present in glial membranes has not yet been very well characterized. Furthermore, although many of the same ion channels present in neurons have also been identified in astrocytic membranes, it is not known if they are "active" or operate in the same sense as in neuronal membranes. If these channels are active, it seems that many of the predictions obtained by the present model would still be valid in an astrocytic compartment.

### 5.4.3. Where are the Spikes?

The high-speed (AC) voltage spikes that precede an approaching SD wave have been completely ignored in this model. Various observations have suggested that these spikes can be blocked by the application of sodium channel blockers without otherwise affecting SD. The typical $Na^+$ channel density used in this model was ≈5 channels/$\mu m^2$, corresponding to measurements in gray matter. Since $Na^+$ channel densities are substantially higher in white matter, approaching 2000

channels/ $\mu m^2$ at nodes of Ranvier (Hille 1992) it was assumed in constructing this model that the spikes were axonal in origin. It seems likely that such spikes would occur if an axonal compartment were added to the model.

### 5.4.4. Gap Junction Gating Model

The need for neuronal gap-junctions to open "as needed" is probably the weakest assumption of this model. While there appears to be a widespread presence of gap junctions in the CNS, the neuronal geometry of these gap junctions has not yet been determined. It is not even known if these gap junctions are present in all neurons, or if they are at least present in sufficient quantity in some neuronal population to justify the model assumptions. More detailed measurements of the inter-neuronal ionic diffusion constants could help elucidate this issue. A mechanism for gap-junctional gating is also lacking. Possible mechanisms could be membrane stretch and calcium and/or acid/base changes that occur.

### 5.4.5. Calcium Wave Properties

Various theories have suggested that either (a) calcium waves and spreading depression are caused by a common mechanism or that (b) calcium waves may be one of the inducing factors of spreading depression. Certainly calcium waves have been observed in conjunction with spreading depression, and many of the same stimuli have been utilized to evoke both phenomena.

Recent experiments have suggested that (a) calcium waves can be dissociated from spreading depression by removing calcium from the perfusate and that (b) at least two calcium waves occur during spreading depression. The published results indicate that one of these calcium waves precedes the DC-voltage shift, perhaps by as much as 10-15 seconds, while the other calcium wave coincides with the DC-voltage shift. The first wave may also propagate at a faster speed. Furthermore, there is some indication that at least one of these waves is astrocytic in origin (Basarsky and others, 1998; Kunkler and Kraig, 1998).

Because of the experiments in which the calcium waves could be dissociated from spreading depression it was decided to focus on mechanisms of SD propagation that were calcium wave-independent. However, it is also possible that different forms of spreading depression could be caused by different mechanisms. Some of these could be calcium wave-dependent, and others could be calcium-wave independent.

The model as formulated in this dissertation does predict a calcium wave that coincides with the DC-voltage shift, but does not predict any leading calcium wave. The coincident calcium wave predicted by the present model occurs directly as a result of neuronal calcium entry as the voltage-gated channels open. The predicted wave magnitude is probably not correct because intracellular compartments have not been modeled. The buffering properties have instead been averaged over the dendritic cross section. The calcium buffering properties of sub-membrane layers and

dendritic spines are quite different from the properties of the deeper compartments because of the localization of protein buffers closer to the membrane. Furthermore, the geometric properties of spines and the localization of specific ion channels to either spines or the dendritic shaft probably have an effect.

It seems reasonable to conjecture that if a second, independent, astrocytic compartment were added to this model, that calcium waves would also propagate within the astrocytic compartment. Since this new compartment would have different calcium buffering properties the wave speed would very likely be different. It is not clear whether separate waves could propagate simultaneously within the same compartment (e.g., two astrocytic or two dendritic waves versus one of each) and what the interaction between these waves and the properties of the individual components would be.

In one calcium-wave dependent theory, the propagating calcium wave might activate K(Ca) channels (e.g., BK channels). The results presented in chapter 4 show that BK channels are (theoretically) capable of allowing sufficient potassium efflux to induce a propagating wave. In the simulations presented here this was primarily a voltage-dependent prediction. Depending on the calcium set-point of the K(Ca) channels it should also be possible to do this with a calcium wave. As potassium builds up in the interstitial space, the membrane would become depolarized. Even after the calcium wave has passed, the BK channels would continue to remain open (although to a lesser extent) because these channels are gated by a combination of

both depolarization and cytosolic calcium concentration. It may be that this combination would be sufficient to induce a regenerative wave. Since calcium-dependent mechanisms were not a major focus of this study, this type of mechanism was not investigated. Nevertheless, this is an important and interesting question for further study.

# GLOSSARY

| | |
|---|---|
| 4-AP | 4-aminopyridine, blocks potassium A-channel |
| 5-HT | serotonin |
| 5HT1D | a serotonin transporter protein |
| AA | arachidonic acid, 5,8,11,14-eicosatetraenoic acid |
| AC | alternating current |
| acetylcholine | a neurotransmitter, usually depolarizing |
| acetylcholinesterase | an enzyme which breaks down Ach |
| Ach | acetylcholine |
| A-channel | a type of voltage gated potassium channel |
| ACSF | artificial cerebro-spinal fluid |
| AD | anoxic depolarization |
| adenylate cyclase | an enzyme that facilitates the conversion of ATP to cAMP |
| ADP | adenosine diphosphate |
| agonist | a substance that binds to a receptor and evokes a response from that receptor |
| AHP | after-hyperpolarization current |
| alpha-bungarotoxin | a snake neurotoxin that is an antagonist of some nicotinic Ach receptors |
| alpha-cloralose | an anaesthetic |
| amnesia | memory loss |
| AMP | adenosine monophosphate |

| | |
|---|---|
| AMPA | α-amino-3-hydroxy-5-methyl-4-isoxalone propionic acid, a glutamate receptor agonist |
| anion | a negatively charged ion |
| anode | a positively charged electrode, it attracts anions |
| anoxia | a reduction in or the absence of oxygen in a tissue |
| antagonist | a substance that nullifies the effect of another substance, or one that blocks a receptor by binding to it and preventing the normal reaction of the receptor |
| anterograde amnesia | memory loss that occurs after an injury |
| antidromic spike | a voltage spike which starts in or near the soma of a neuron and propagates into the dendritic tree |
| antioxidant | a substance that inhibits oxidation |
| apamin | a natural toxin from honeybee venom |
| APH | amino-7-phosphonoheptanoate, an NMDA-receptor blocker |
| aphasia | the loss (or partial loss) of expressive ability in speech or writing or in language comprehension |
| apomorphine | a non-selective D1/D2-receptor agonist |
| APV | DL-2-aminophosphonovaleric acid, an NMDA-receptor blocker |
| asparagine | an amino acid |
| aspartate | an amino acid |
| astrocyte | a glial cell involved in maintaining interstitial homeostasis |
| ATP | adenosine triphosphate |
| atropine | an Ach receptor blocker |

| | |
|---|---|
| aura | visual hallucinations that sometimes precede migraine headaches |
| avascular | without blood vessels |
| BDNF | brain derived neurotrophic factor, a neurotrophin |
| benzocaine | an anaesthetic |
| bistable equation | a reaction-diffusion equation with two stable steady states; in this dissertation, it is usually an RDE with a cubic reaction-term |
| BK | large-conductance (e.g., big) K(Ca) channel |
| caffeine | 1,3,7-trimethyl xanthine, a stimulant tat (a) inhibits the phosphodiesterase that facilitates the hydrolysis of cAMP to AMP and (b) acts as an agonist to some $Ca^{++}$ channels in the ER membrane |
| calbindin | a protein that binds $Ca^{++}$ |
| calmodulin | a protein that binds $Ca^{++}$ |
| calreticulin | a protein that binds $Ca^{++}$ |
| cam | calmodulin |
| cAMP | cyclic adenosine monophosphate |
| carbachol | carbamylcholine, an Ach agonist |
| catecholamines | chemicals derived from tyrosine, including dopamine, epinephrine and norepinephrine |
| cathode | a negatively charge electrode, it attracts cations |
| cation | a positively charged ion |
| CBF | cerebral blood flow |
| CBV | cerebral blood volume |

| | |
|---|---|
| cGMP | cyclic GMP |
| CGP-40116 | D-(E)-2-amino-4-methyl-5-phosphone-3-pentenoic acid, an NMDA-receptor blocker |
| CGRP | calcitonin gene related peptide |
| CGS-19755 | cis-4-phosphonomethyl-2-piperidine carboxylate, an NMDA-receptor blocker |
| $CH_3COOH$ | acetic acid |
| channel | see ion channel |
| charybdotoxin | CTX |
| chloralose | an anaesthetic |
| cholinergic receptor | an Ach receptor |
| clonazepam | an antimigraine agent |
| concussion | a jarring shock to the brain that may induce the loss of consciousness or coma, amnesia, vertigo, nausea, bleeding, contusion, blurred vision, and/or headache |
| conotoxins | a set of calcium channel blockers |
| COX | cyclo-oxygenase |
| CPP | 3-((+-)-2-carboxypiperazin-4-yl)-propyl-l-phosphonic acid, a serotonergic agonist |
| Crank-Nicholson method | a numerical technique for solving a differential equation |
| CRE | cAMP response element, a regulatory region in genes that is activated by cAMP |
| CREB | CRE binding protein, a protein that interacts with CREs when it is phosphorylated and thereby is involved in control of gene transcription |

| | |
|---|---|
| CSF | cerebrospinal fluid |
| CTX | charybdotoxin, a natural toxin in scorpion venom |
| cubic spline | a numerical technique for fitting a smooth curve to a set of data points |
| curare | a poison (d-tubocurarine) that is extracted from plants of the *menispermaceae* family, it acts primarily by blocking nicotinic acetylcholine receptors |
| cyclandelate | a calcium channel antagonist |
| cytoplasm | the fluid within a cell |
| D1 | A class of dopamine receptors; activation stimulates adenylyl cyclase activity |
| D2 | a class of dopamine receptors; Activation inhibits stimulates adenylyl cyclase activity |
| DA | dopamine |
| DAME | d-Ala2-Met-enkephalinamide, an opiod |
| DC | direct current |
| depolarization | voltage increase (*e.g.*, less negative) |
| d-fen | d-fenfluramine, a serotonin reuptake inhibitor |
| DHE | an antimigraine agent, dihydroergotamine |
| dialysis | the passage of molecules down their concentration gradient and through a semi-permeable membrane |
| dipyridamole | DPR, an adenosine transport inhibitor |
| dizocilpine | MK-801, (+)-5-methyl,10,11-dihydro-5H-dibenzo[a,d]cyclohepten-5-10-imine maleate, an NMDA-receptor blocker |
| DNQX | dinitroquinoxaline-2,3-dione, an AMPA-receptor antagonist |

| | |
|---|---|
| Dopamine | a neurotransmitter |
| Doppler sonography | ultrasound imaging |
| DPCPX | An adenosine A1-receptor agonist, 8-cyclopentyl-1,3-dipropylzanthine |
| DPR | dipyridamole, an adenosine transport inhibitor |
| DR | delayed rectifier |
| d-tubocurarine | curare, an Ach receptor blocker, extracted from plants of the *menispermaceae* family |
| dura | a fibrous skin-like layer that surrounds the brain |
| EEG | electroencephalogram |
| EGR | a growth factor |
| electrodiffusion | diffusive motion in an electric field |
| electrodiffusion equation | The equation $\frac{\partial c}{\partial t} = \quad \cdot [D \quad c] + \frac{zF}{RT} \quad \cdot [Dc \quad E] + f$ or its one-dimensional analogue $\frac{\partial c}{\partial t} = \frac{\partial}{\partial x}\left(D\frac{\partial c}{\partial x}\right) + \frac{zF}{RT}\frac{\partial}{\partial x}\left(Dc\frac{\partial E}{\partial x}\right) - \frac{A}{V}J_{c,m} + s_c$ |
| electrodiffusion term | the term $\frac{zF}{RT}\frac{\partial}{\partial x}\left(cD\frac{\partial E}{\partial x}\right)$ in the electrodiffusion equation |
| endothelin | a vasoconstrictor |
| enkephalin | an endogenous opiod |
| epilepsy | a general term which refers to all seizure disorders; There is no such single disease as “epilepsy” |
| epinephrine | a neurotransmitter |
| ER | endoplasmic reticulum |
| ergotamine | an antimigraine agent |

| | |
|---|---|
| ethanol | an alcohol which inhibits adenosine transport and GABA-mediated chloride channels |
| Fitzhugh-Nagumo model | a system of two differential equations, where one equation describes an excitation variable and the other equation describes a recovery variable; it was originally developed to described nerve excitation |
| fluoroacetate | a metabolic poison that inhibits the Krebs cycle and is used to poison glial cells |
| fluorocitrate | a metabolic poison that inhibits the Krebs cycle and is used to poison glial cells |
| FN | Fitzhugh-Nagumo |
| FOS | a class of IEGs |
| GABA | gamma-amino-butyric acid, a common inhibitory neurotransmitter |
| gap junction | a pore-shaped protein that connects two cells allowing fluid to move directly from one cell to another |
| GDP | guanosine diphosphate |
| GFAP | glial fibrillary acid protein. |
| GHK equation | Goldman-Hodgkin-Katz equation |
| glia | the supporting cells of the nervous system, including astrocytes, oligodendrocytes, and microglia |
| gliosis | the growth of glial cells in response to an injury |
| glutamate | an amino acid neurotransmitter which is usually depolarizing |
| glycine | an amino acid |
| GMP | guanosine monophosphate |
| G-protein | a protein that specifically binds GTP (in its active state) and GDP (in its inactive state) |

| | |
|---|---|
| gray matter | neural tissue that consists primarily of cell bodies and dendrites |
| GTP | guanosine triphosphate |
| halothane | an anaesthetic |
| hemiparesis | the partial paralysis of one side of the body |
| hemiplegia | a paralysis of one side of the body |
| heptanol | an alcohol which poisons gap junctions |
| Hodgkin-Huxley formalism | a model which describes currents through ion channels; the current is proportional to $m^p h^q$, for some integers $p$ and $q$, where $m$ is an activation variable and $h$ is an inactivation variable, each of which decay exponentially to a steady state voltage-dependent value |
| HSP | heat shock protein |
| hypercapnia | the presence of high levels of $C0_2$ in the blood |
| hyperemia | increased blood flow |
| hyperpolarization | voltage decrease (i.e., more negative) |
| hypertonic | an above-normal concentration of an ion |
| hypotonic | a below-normal concentration of an ion |
| hypoxia | lower than normal oxygen level |
| ICP | intracranial pressure |
| ID | ischemic depolarization |
| IEG | immediate early genes and the proteins which they encode |
| IK | intermediate-conductance K(Ca) channel |
| *in vitro* | in an experimental situation which is not in a living animal |

| | |
|---|---|
| *in vivo* | in a living animal |
| indomethacin | a COX inhibitor |
| infarct | a localized area of ischemic damage |
| interstitial | the fluid-filled space between cells |
| ion channel | a pore shaped protein, usually in a cellular membrane, that allows selective passage to certain ions; sometimes ion channels are gated, i.e., the pore will open or close only under certain conditions |
| ion-selective microelectrode | a microelectrode whose tip is filled with a resin which is only permeable to a particular ionic species |
| iprazochrome | an antimigraine agent |
| ischemia | a reduction in blood flow due to arterial constriction or obstruction |
| ischemic penumbra | the region immediately adjacent to the ischemic zone |
| isoflurane | an anaesthetic |
| ITP | 1,4,5-inositol trisphosphate |
| JUN | a class of growth factors |
| K(Ca) | calcium-dependent potassium channel |
| kainic acid | a natural toxin from the red algae *digenea simplex*, an agonist of a subclass of glutamate receptors |
| KCl | potassium chloride, a potassium salt |
| ketamine | an NMDA-receptor blocker |
| L-701,324 | 7-chloro-4-hydroxy-3-(3-phenoxy)phenyl-2-(1H)-quinolone, a chemical which blocks the glycine binding site of the NMDA-receptor |
| LC | locus coereleus |

| | |
|---|---|
| lesion | an area of tissue injury |
| leu-enkephalin | an endogenous opiod |
| lidocaine | an anaesthetic |
| lignocaine | an antimigraine agent |
| LIPOX | lipoxygenase |
| lisuride | an antimigraine agent |
| L-NA | an NOS inhibitor, NG-nitro-L-arginine, also called L-NNA |
| L-NAME | an NOS inhibitor, NA-nitro-L-arginine methyl ester |
| L-NNA | an NOS inhibitor, NG-nitro-L-arginine |
| locus cereals | a brain organ in which high levels of NE are present |
| LTD | long term depression, a mechanism involved in learning at the cellular level |
| LTP | long term potentiation, the hypothetical mechanism involved in learning at the cellular level. |
| MCA | middle cerebral artery |
| MCAO | middle cerebral artery occlusion |
| M-channel | a voltage gated potassium channel which is sensitive to muscarinic agents |
| mecamylamine | an antagonist of nicotinic Ach receptors |
| metabatropic receptor | a receptor that acts indirectly via some intermediate messenger or cascade of messengers to produce its response |
| met-enkephalin | an endogenous opiod |
| methysergide | an antimigraine agent |
| metoprolol | an antimigraine agent |

| | |
|---|---|
| MHC | major histocompatibility class |
| microglia | a phagocytotic migratory glial cell |
| migraine | a headache that is usually severe and restricted to one side of the head, and is sometimes accompanied by nausea, vomiting or hallucinations |
| migraine with aura | migraines that are preceded by visual hallucinations |
| MK-801 | dizocilpine, (+)-5-methyl,10,11-dihydro-5H-dibenzo[a,d]cyclohepten-5-10-imine maleate, an NMDA-receptor blocker |
| Morris-Lecar model | a variant of the FN equation which describes muscle fibers in the barnacle |
| MRI | magnetic resonance imaging |
| mRNA | messenger RNA |
| muscarine | a chemical ($C_8H_{19}NO_3$) that occurs naturally in the fungus *amanita muscaria* and acts as an agonist on a subclass of acetylcholine receptors |
| NAD | nicotinamide adenine dinucleotide in its oxidized form |
| NADH | nicotinamide adenine dinucleotide in its reduced form |
| naloxine | a non-selective opiod receptor antagonist |
| NBK | nitrobenzylthioinosine, an adenosine transport inhibitor |
| NBQX | an AMPA receptor blocker, 2,3-dihydroxy-6-nitro-7-sulfamoylbenzo(F) quinoxaline |
| NE | norepinephrine |
| Nernst equation | the equation for the equilibrium membrane potential due to a single species, $E_1 - E_2 = (RT / zF)\ln([\mathrm{S}]_2 / [\mathrm{S}]_1)$ |
| neuroglia | glia |

| | |
|---|---|
| neurotrophins | a family of proteins which are involved in growth and development |
| NGF | neural growth factor, a neurotrophin |
| $NH_42SO_4$ | a salt of ammonium ($NH_4$) and sulfuric acid ($H_2SO_4$) |
| $NH_4Cl$ | ammonium chloride, a salt of ammonium ($NH_4$) |
| nicotine | an agonist of a class of Ach receptors |
| nigrostriatal system | the substantia nigra and the striatum, deep brain organs which are highly dopaminergic |
| nitroprusside | an NO donor |
| NMDA | n-methyl-d-aspartic-acid, an agonist of one class of glutamate receptors |
| NO | nitric oxide |
| norepinephrine | a neurotransmitter |
| NOS | nitric oxide synthase, an enzyme involved in the production of NO |
| NT | neurotrophin |
| nucleus accumbens | a septal nucleus of the brain adjacent to the ventromedial striatum |
| NURR | a growth factor |
| octanol | an alcohol that poisons gap junctions |
| OIS | optical intrinsic signal imaging |
| oligemia | a deficiency in blood volume |
| ouabain | a metabolic poison that inhibits the $Na^+/K^+$ exchanger |
| p75 | a membrane protein which bind some neurotrophins |

| | |
|---|---|
| paracetamol | an antimigraine agent |
| parallel fiber | the axons of cerebellar granule cells, they synapse on the dendrites of cerebellar Purkinje cells |
| parenchyma | the essential tissue of an organ |
| parvalbumin | a calcium binding protein |
| PCP | phencyclidine, and NMDA-receptor blocker, also a hallucinogenic agent known as angel dust |
| penicillin | a negatively charged antibiotic that blocks the $GABA_A$ channel by interacting with highly charged amino acid residues in the pore, and that acts as a convulsant at high dosages |
| perfusion | allowing a liquid to flow over something |
| PET | positron emission tomography |
| pH | a measure of the acidity of a tissue, calculated as $-\log[H^+]$ |
| phenylephrine | an adrenergic agonist |
| phosphatase | an enzyme that catalyzes the hydrolysis of phosphoric acid |
| photothrombosis | the formation of blood clots by a laser |
| pia | a thin, skin-like, protective membrane surrounding the brain |
| picrotoxin | a convulsive agent, blocks GABA-A receptors |
| PKC | protein kinase C |
| PLA | phospholipase A |
| population spike | voltage spikes which precede arrival of DC-voltage shift during passage of the SD wave |
| prodromal | preceding |
| proline | an amino acid |

| | |
|---|---|
| propanalol | an antimigraine agent |
| prostigmine | an acetylcholenesterase |
| PTU | propylthiouracyl, a drug which reduces thyroid secretions |
| PTZ | a convulsive agent, pentylenetetrazol |
| purine | a class of nitrogeneous bases with two rings; both adenine and guanine are purines |
| purinoreceptor | a receptor for that has a purine agonist |
| Purkinje cell | a candelabra-shaped cerebellar neuron whose primary inputs are climbing fibers from the inferior olive and the parallel fibers from the cerebellar granule cells |
| pyramidal cell | a type of neuron, which is widely expressed in the central nervous system, that has a pyramid-shaped body and separate apical and basal dendritic trees |
| quinpirole | a D2-receptor agonist |
| quisqualic acid | a natural toxin from the plant seed *quisquqalis indica*, an agonist of a subclass of glutamate receptors |
| RbCl | rubidium chloride, a rubidium salt |
| rCBF | regional cerebral blood flow |
| RDE | reaction-diffusion equation |
| reaction-diffusion equation | the equation $\frac{\partial c}{\partial t} = D\frac{\partial^2 c}{\partial x^2} + f(c)$ |
| reactive gliosis | the growth of glial cells in response to an injury |
| retrograde amnesia | the inability to recall memories of events that occurred prior to an injury |
| ryanodine | a plant alkaloid that binds (as an agonist) to a calcium channel in the ER membrane |

| | |
|---|---|
| sAHP | slow after-hyperpolarization current |
| SD | spreading depression |
| Serotonin | 5-hydroxytryptamine, a neurotransmitter which is also a vasodilatory agent |
| sigmoid | a class of curves described by a function such as the one illustrated that asymptotically approaches one value (e.g., zero) as $x \rightarrow -\infty$ and approaches a second value (e.g., one) as $x \rightarrow +\infty$ with a smooth transition in between 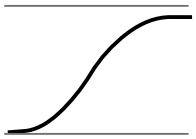 $y = \frac{1}{1+e^{-x}}$ |
| SK | small-conductance K(Ca) channel |
| SKF 38393 | a D1-receptor agonist |
| spatial buffering | the mechanism by which glial cells remove excess ions from the interstitial environment to a spatially distant location |
| SPC | slow potential change |
| SPECT | single photon emission computerized tomography |
| SQUID | superconducting quantum interference device, a sensitive magnetic field sensor |
| Sumatriptan | a 5HT1D agonist which is also a anti-migraine compound |
| synapse | the junction between neurons via which an impulse is transmitted |
| TEA | tetraethylammonium, blocks delayed rectifier and BK potassium channels |
| tetanus | an AC stimulation |
| tetrodotoxin | TTX |
| TGA | transient global amnesia |

| | |
|---|---|
| theophylline | 1,3-dimethyl xanthine, a non-selective adenosine receptor antagonist that also inhibits the hydrolysis of cAMP to AMP |
| thioembutal | an anaesthetic |
| transcranial Doppler sonography | ultrasound imaging of the brain taken across the skull |
| trauma | any injury (for the purposes of this dissertation) |
| TRK | receptor tyrosine kinases, the receptors for the neurotrophins. |
| TTX | tetrodotoxin, a $Na^+$ channel blocker poison that occurs naturally in order *tetraodontiformes* (which includes the puffer fish) |
| tyrosine | an amino acid |
| urethane | an anaesthetic |
| valproate | an antimigraine agent |
| vasoactive | an agent that effects blood vessels, by either constrictive or dilating them |
| veratridine | a poison that occurs naturally in the lily family (*veratrum*) and which slows inactivation of the sodium channel |
| white matter | neural tissue consisting primarily of myelinated axons |
| WYSIWYG | what you see is what you get |
| xanthine | a purinergic base |

# REFERENCES


Aitken PG, Jing J, Young J, Somjen GG (1991) Ion channel involvement in hypoxia-induced spreading depression in hippocampal slices. Brain Res. 541:7-11.

Aitken PG, Borgdorff AJ, Juta AJA, Kiehart DP, Somjen GG, Wadman WJ (1998a) Volume changes induced by osmotic stress in freshly isolated rat hippocampal neurons. Pflugers Arch. 436:991-8.

Aitken PG, Tombaugh GC, Turner DA, Somjen GG (1998b) Similar propagation of spreading depression and hypoxic spreading depression-like depolarization in rat hippocampus recorded optically and electrically. J Neurophysiol. 80:1514-21.

Albe-Fessard D, Condes-Lara M, Sanderson P (1983) The focal tonic cortical control of intralaminar thalamic neurons may involve a cortico-thalamic loop. Acta Morphol Hung. 31:9-26

Albe-Fessard D, Sanderson P, Condes-Lara M, Delandsheer E, Giuffrida R, Cesaro P (1984) [Leão's spreading depression in the study of the relationship of central structures]. An Acad Bras Cienc. 56:371-383.

Albe-Fessard D, Sanderson P, Mavoungou R (1990) The influence of striatum on the substantia nigra: a study using the spreading depression technique. Brain Res Bull. 24:213-219.

Alexis NE, Back T, Zhao W, Dietrich WD, Watson BD, Ginsberg MD (1996) Neurobehavioral consequences of induced spreading depression following photothrombotic middle cerebral artery occlusion. Brain Res. 706:273-282.

Amemori T, Bures J (1986) Terminal anoxic depolarization proceeds more slowly in the olfactory bulb than in the cerebral cortex of rats. Neurosci Lett. 71:323-328.

Amemori T, Bures J (1988) Functional ablation of the olfactory bulb by spreading depression: unit activity changes and transient anosmia. Brain Res Bull. 20:421-427.

Amemori T, Bures J (1990) Ketamine blockade of spreading depression: rapid development of tolerance. Brain Res. 519:351-354.

Amemori T, Gorelova NA, Bures J (1987) Spreading depression in the olfactory bulb of rats: reliable initiation and boundaries of propagation. Neuroscience. 22:29-36.

Amorim LF, Guedes RC, Medeiros MC, da Silva AT, Cabral-Filho JE (1988) Apomorphine does not mimic the effects of REM-sleep deprivation on cortical spreading depression. Braz J Med Biol Res. 21:611-614.

Andersen BJ, Marmarou A (1992) Functional compartmentalization of energy production in neural tissue. Brain Res. 585:190-195.

Andersson G (1995) Cortico-cortical mediation of short-latency (lemniscal) sensory input to the motor cortex in deeply pentobarbitone anaesthetized cats. Acta Physiol Scand. 153:381-392.

Andrade AF, Guedes RC, Teodosio NR (1990) Enhanced rate of cortical spreading depression due to malnutrition: prevention by dietary protein supplementation. Braz J Med Biol Res. 23:889-893.

Aquino-Cias J, Aneiros-Riba R, Hernandez-Mesa N (1976) Cortical afterdischarges during Leão's cortical spreading depression. Physiol Bohemoslov. 25:66-69.

Aquino-Cias J, Bures J (1967) Seizure irradiation during functional elimination of the thalamus by spreading depression in the rat. Epilepsia. 8:47-57.

Aquino Cias J, Bures J, Fifkova E, Popova NS (1966a) The effect of thalamic spreading depression on electric activity in the caudate nucleus and the hippocampus in rats. Physiol Bohemoslov. 15:195-200.

Aquino-Cias J, Belceva S, Bures J, Fifkova E (1966b) The influence of thalamic spreading depression on cortical and reticular unit activity in the rat. Brain Res. 1:77-85.

Arakawa S, Nakamura S, Kawashima N, Nishiike S, Fujii Y (1997) Antidromic burst activity of locus coeruleus neurons during cortical spreading depression. Neuroscience. 78:1147-1158.

Ashcroft NW, Mermin ND (1976) Solid State Physics. Holt, Rinehart, and Winston, New York.

Ashton D, Willems R, Marrannes R, Janssen PA (1990) Extracellular ions during veratridine-induced neurotoxicity in hippocampal slices: neuroprotective effects of flunarizine and tetrodotoxin. Brain Res. 528:212-222.

Ashton D, Willems R, Wynants J, Van Reempts J, Marrannes R, Clincke G (1997) Altered Na(+)-channel function as an in vitro model of the ischemic penumbra: action of lubeluzole and other neuroprotective drugs. Brain Res. 745:210-221.

Atri A (1996) Mathematical modeling and analysis of intracellular calcium dynamics: oscillations and wave propagation. Ph.D. Dissertation (Biomathematics). University of California, Los Angeles.

Atri A, Admundson J, Clapham D, Sneyd J (1993) A single pool model for intracellular calcium oscillations and waves in the xenopus laevis oocyte. Biophys J. 65:1727-1739.

Aurora SK, Ahmad BK, Welch KM, Bhardhwaj P, Ramadan NM (1998) Transcranial magnetic stimulation confirms hyperexcitability of occipital cortex in migraine. Neurology. 50:1111-1114.

Avis HH, Carlton PL (1968) Retrograde amnesia produced by hippocampal spreading depression. Science. 161:73-75.

Avoli M, Drapeau C, Louvel J, Pumain R, Olivier A, Villemure JG (1991) Epileptiform activity induced by low extracellular magnesium in the human cortex maintained in vitro. Ann Neurol. 30:589-596.

Avoli M, Louvel J, Drapeau C, Pumain R, Kurcewicz I (1995) GABAA-mediated inhibition and in vitro epileptogenesis in the human neocortex. J Neurophysiol. 73:468-484.

Avoli M, Nagao T, Kohling R, Lucke A, Mattia D (1996) Synchronization of rat hippocampal neurons in the absence of excitatory amino acid-mediated transmission. Brain Res. 735:188-196.

Back T, Ginsberg MD, Dietrich WD, Watson BD (1996) Induction of spreading depression in the ischemic hemisphere following experimental middle cerebral artery occlusion: effect on infarct morphology. J Cereb Blood Flow Metab. 16:202-213.

Balestrino M, Somjen GG (1986) Chlorpromazine protects brain tissue in hypoxia by delaying spreading depression-mediated calcium influx. Brain Res. 385:219-226.

Balestrino M, Aitken PG, Somjen GG (1989) Spreading depression-like hypoxic depolarization in CA1 and fascia dentata of hippocampal slices: relationship to selective vulnerability. Brain Res. 497:102-107.

Balinska H, Buresová O, Fifkova E (1967) The influence of cortical and thalamic spreading depression on feeding behavior of rats with lateral hypothalamic lesions. Acta Biol Exp (Warsz). 27:355-363.

Barchas JF, Faull KF, Wuinn B, Elliott GR (1994) Biochemical aspects of the psychotic disorders. In: Basic Neurochemistry: Molecular, cellular and Medical

Aspects. Fifth Edition. (ed. Siegel GJ, Agranoff BW, Albers RW, Molinoff PB) pp. 959-971. New York: Raven.

Barkley GL, Tepley N, Nagel-Leiby S, Moran JE, Simkins RT, Welch KM (1990) Magnetoencephalographic studies of migraine. Headache. 30:428-434.

Basarsky TA, Duffy SN, Andrew RD, MacVicar BA (1998) Imaging spreading depression and associated intracellular calcium waves in brain slices. J Neurosci. 18:7189-7199.

Bayer VE, Pickel VM (1990) Ultrastructural localization of tyrosine hydroxylase in the rat ventral tegmental area: relationship between immunolabeling density and neuronal associations. J Neurosci. 10:2996-3013.

Berridge, MJ 1993) Inositol trisphosphate and calcium signaling. Nature. 361:315-325.

Berridge MJ (1994) The biology and medicine of calcium signaling. Mol Cell Endocrinol. 98:119-124.

Best PJ, Orr J, Pointer JE (1975) Differential effects of cortical ablation and spreading depression on sensitivity to footshock: implications for the role of the cortex in learning. Physiol Behav. 14:801-807.

Bianki VL, Murik SE, Filippova EB (1989) Interhemispheric asymmetry of positive emotional reactions in rats. Int J Neurosci. 47:193-201.

Blank WF Jr, Kirshner HS (1977) The kinetics of extracellular potassium changes during hypoxia and anoxia in the cat cerebral cortex. Brain Res. 123:113-124.

Blatz AL, Magleby KL (1987) Calcium-activated potassium channels. TINS. 10:463-467.

Blau JN (1992) Classical migraine: symptoms between visual aura and headache onset. Lancet. 340:355-356.

Boiko VP, Buresh Ia (1981) [Reverberations of spreading depression in the pigeon forebrain]. Zh Vyssh Nerv Deiat. 31:871-873.

Bonthius DJ, Steward O (1993) Induction of cortical spreading depression with potassium chloride upregulates levels of messenger RNA for glial fibrillary acidic protein in cortex and hippocampus: inhibition by MK-801. Brain Res. 618:83-94.

Bonthius DJ, Stringer JL, Lothman EW, Steward O (1994) Spreading depression and reverberatory seizures induce the upregulation of mRNA for glial fibrillary acidic protein. Brain Res. 645:215-224.

Bonthius DJ, Lothman EW, Steward O (1995) The role of extracellular ionic changes in upregulating the mRNA for glial fibrillary acidic protein following spreading depression. Brain Res. 674:314-328.

Bosakowski T, Levin AA (1987) Comparative acute toxicity of chlorocitrate aand fluorocitrate in dogs. Toxicol Appl Pharmacol. 89:97-104.

Bozhilova-Pastirova A, Ovtscharoff W (1995) Structure of the synaptic junctions in the rat sensorimotor cortex: freeze-etching study of neuronal gap junctions. Neurosci Lett. 201:265-7.

Brand S, Fernandes de Lima VM, Hanke W (1998) Pharmacological modulation of the refractory period of retinal spreading depression. Naunyn Schmiedebergs Arch Pharmacol. 357:419-425.

Brian JE Jr, Faraci FM, Heistad DD (1996) Recent insights into the regulation of cerebral circulation. Clin Exp Pharmacol Physiol. 23:449-457.

Bures J (1956) Some metabolic aspects of Leão’s spreading depression. J Neurochem 1:153-158.

Bures J, Buresová O (1981) Cerebral [K+]e increase as an index of the differential susceptibility of brain structures to terminal anoxia and electroconvulsive shock. J Neurobiol. 12:211-220.

Bures J, Buresová O, Krívánèk J (1974) The Mechanism and Applications of Leão’s Spreading Depression of Electroencephalographic Activity. New York Academic Press.

Bures J, Buresová O, Krívánèk J (1984) The meaning and significance of Leão's spreading depression. An Acad Bras Cienc. 56:385-400.

Bures J, Hartman G (1967) Conduction block in capsula interna fibres caused by striatal spreading depression in rats. Experientia. 23:736-737.

Bures J, Hartmann G, Lukyanova LD (1967) Blockade of thalamocortical and pyramidal pathways by striatal spreading depression in rats. Exp Neurol. 18:404-415.

Bures J, Von Schwarzenfeld I, Borzek G (1975) Blockage of cortical spreading depression by picrotoxin foci of paroxysmal activity. Epilepsia. 16:111-118.

Buresová O, Fifkova E, Bures J (1966) Pupillary paralysis evoked by thalamic spreading depression in rats. Exp Brain Res. 2:168-175.

Buresová O, Bures J (1975) Functional decortication by cortical spreading depression does not prevent forced extinction of conditioned saccharin aversion in rats. J Comp Physiol Psychol. 88:47-52.

Buresová O, Bures J (1976) Piracetam-induced facilitation of interhemispheric transfer of visual information in rats. Psychopharmacologia. 46:93-102.

Buresová O, Bures J (1985) Unilateral and bilateral cortical spreading depression interferes with radial maze performance in rats. Brain Res. 344:365-368.

Burton FL, Hunter OF (1990) Sensitivity to flow of intrinsic gating in inwardly rectifying potassium channel from mammalian skeletal muscle. J Physiol (Lond) 424:253-61.

Busch E, Hoehn-Berlage M, Eis M, Gyngell ML, Hossmann KA (1995) Simultaneous recording of EEG, DC potential and diffusion-weighted NMR imaging during potassium induced cortical spreading depression in rats. NMR Biomed. 8:59-64.

Busch E, Gyngell ML, Eis M, Hoehn-Berlage M, Hossmann KA (1996) Potassium-induced cortical spreading depressions during focal cerebral ischemia in rats: contribution to lesion growth assessed by diffusion-weighted NMR and biochemical imaging. J Cereb Blood Flow Metab. 16:1090-1099.

Busija DW, Meng W (1993) Retention of cerebrovascular dilation after cortical spreading depression in anesthetized rabbits. Stroke. 24:1740-1744; discussion 1744-1745.

Cabral-Filho JE, Trindade-Filho EM, Guedes RC (1995) Effect of d-fenfluramine on cortical spreading depression in rats. Braz J Med Biol Res. 28:347-350.

Caggiano AO, Breder CD, Kraig RP (1996) Long-term elevation of cyclooxygenase-2, but not lipoxygenase, in regions synaptically distant from spreading depression. J Comp Neurol. 376:447-462.

Caggiano AO, Kraig RP (1996) Eicosanoids and nitric oxide influence induction of reactive gliosis from spreading depression in microglia but not astrocytes. J Comp Neurol. 369:93-108.

Caggiano AO, Kraig RP (1998) Neuronal nitric oxide synthase expression is induced in neocortical astrocytes after spreading depression. J Cereb Blood Flow Metab. 18:75-87.

Cammack J, Ghasemzadeh B, Adams RN (1992) Electrochemical monitoring of brain ascorbic acid changes associated with hypoxia, spreading depression, and seizure activity. Neurochem Res. 17:23-27.

Castillo J, Martinez F, Leira R, Prieto JM, Lema M, Noya M (1994) [Changes in neuroexcitatory amino acids during and between migraine attacks]. Neurologia. 9:42-45.

Chebabo SR, Do-Carmo RJ, Martins-Ferreira H (1988) The effect of diphenylhydantoin on spreading depression. Braz J Med Biol Res. 21:603-605.

Chebabo SR, Do Carmo RJ (1991) Phenytoin and retinal spreading depression. Brain Res. 551:16-19.

Chebabo SR, do Carmo RJ, Martins-Ferreira H (1993) Effects of local anaesthetics on retinal spreading depression. Exp Brain Res. 96:363-364.

Chebabo SR, Hester MA, Aitken PG, Somjen GG (1995) Hypotonic exposure enhances synaptic transmission and triggers spreading depression in rat hippocampal tissue slices. Brain Res. 695:203-216.

Chebabo SR, Hester MA, Jing J, Aitken PG, Somjen GG (1995) Interstitial space, electrical resistance and ion concentrations during hypotonia of rat hippocampal slices. J Physiol (Lond). 487 ( Pt 3):685-697.

Chen FF (1974) Introduction to Plasma Physics. Plenum Press, New York.

Chen Q, Chopp M, Chen H, Tepley N (1992) Magnetoencephalography of focal cerebral ischemia in rats. Stroke. 23:1299-1303.

Cherkin A, Van Harreveld A (1978) L-Proline and related compounds: correlation of structure, amnesic potency and anti-spreading depression potency. Brain Res. 156:265-273.

Chesler M, Kraig RP (1989) Intracellular pH transients of mammalian astrocytes. J Neurosci. 9:2011-2019.

Christie B, Eliot L, Kto K, Miyakawa H, Johnston D (1995) Different Ca++ channels in soma and dendrites of hippocampal pyramidal neurons mediate spike-induced Ca++ influx. J. Neurophysiol. 73:2553-2557.

Chu B, Treistman SN (1997) Modulation of two cloned potassium channels by 1-alkanols demonstrates different cutoffs. Alcohol Clin Exp Res. 21:1103-1107.

Clark RM, Collins GG (1976) The release of endogenous amino acids from the rat visual cortex. J Physiol (Lond). 262:383-400.

Colbert CM, Johnston D (1996) Axonal action-potential initiation and the Na+ channel densities in the soma and axon initial segment of subicular pyramidal neurons. J Neurosci. 16:6676-6686.

Colonna DM, Meng W, Deal DD, Busija DW (1994a) Calcitonin gene-related peptide promotes cerebrovascular dilation during cortical spreading depression in rabbits. Am J Physiol. 266:H1095-1102.

Colonna DM, Meng W, Deal DD, Busija DW (1994b) Nitric oxide promotes arteriolar dilation during cortical spreading depression in rabbits. Stroke. 25:2463-2470.

Colonna DM, Meng W, Deal DD, Gowda M, Busija DW (1997) Neuronal NO promotes cerebral cortical hyperemia during cortical spreading depression in rabbits. Am J Physiol. 272:H1315-1322.

Condes-Lara M, Leon-Olea M, Sanchez-Alvarez M, Omana-Zapata I (1989) Double cortical control acting upon activities of intralaminar thalamic cells. Bol Estud Med Biol. 37:63-68.

Condes-Lara M, Omana-Zapata I, Talavera E (1991) Facilitating action of medial prefrontal cortex upon the noxious thermally-evoked responses in thalamic centralis lateralis nucleus. J Physiol (Paris). 85:188-194.

Condes-Lara M, Sanchez-Moreno RM, Omana-Zapata I (1996) Cortical facilitatory action on centralis lateralis thalamic activity during the development of carrageenin-produced inflammation. Arch Med Res. 27:265-273.

Condes-Lara M, Zapata IO (1988) Suppression of noxious thermal evoked responses in thalamic central lateral nucleus by cortical spreading depression. Pain. 35:199-204.

Contreras D, Destexhe A, Steriade M (1997) Spindle oscillations during cortical spreading depression in naturally sleeping cats. Neuroscience. 77:933-936.

Coronodo R, Morrissette J, Sukhareva M, Vaughan DM (1994) Structure and function of ryanodine receptors. Am J Physiol. 266:C1485-C1504.

Crowe W, Mayevsky A, Mela L (1981) Ion transport and energy metabolism in brain. Neurol Res. 3:107-123.

Csiba L, Paschen W, Mies G (1985) Regional changes in tissue pH and glucose content during cortical spreading depression in rat brain. Brain Res. 336:167-170.

Curtis DR, Phillis J W, Watkins JC (1960) The chemical excitation of spinal neurons by certain amino acids. J Physiol 150:656-682.

Curtis DR, Watkins JC (1963) Acidic amino acids with strong excitatory actions on mammalian neurons. J Physiol. 166:1-14.

Czeh G, Aitken PG, Somjen GG (1992) Whole-cell membrane current and membrane resistance during hypoxic spreading depression. Neuroreport. 3:197-200.

Czeh G, Aitken PG, Somjen GG (1993) Membrane currents in CA1 pyramidal cells during spreading depression (SD) and SD-like hypoxic depolarization. Brain Res. 632:195-208.

Czeh G, Somjen GG (1990) Hypoxic failure of synaptic transmission in the isolated spinal cord, and the effects of divalent cations. Brain Res. 527:224-233.

Daffertshofer M, Hennerici M (1995) Cerebrovascular regulation and vasoneuronal coupling. J Clin Ultrasound. 23:125-138.

Dahlem MA, Muller SC (1997) Self-induced splitting of spiral-shaped spreading depression waves in chicken retina. Exp Brain Res. 115:319-324.

Davies JA, Annels SJ, Dickie BG, Ellis Y, Knott NJ (1995) A comparison between the stimulated and paroxysmal release of endogenous amino acids from rat cerebellar, striatal and hippocampal slices: a manifestation of spreading depression? J Neurol Sci. 131:8-14.

Davis AK, Janigro D, Schwartzkroin PA (1986) Effects of tissue preincubation and hypoxia on CA3 hippocampal neurons in the in vitro slice preparation. Brain Res. 370:44-53.

Davis JL, Buresová O, Bures J (1983) Cortical spreading depression and conditioned taste aversion: an attempt to resolve a controversy. Behav Neural Biol. 37:338-343.

De Arajo-Pinheiro RS, Marins-Ferreira H (1984) Spreading depression and the blood-brain barrier. Braz J Med Biol Res 17:265-270.

De Azeredo FA (1991) Transient changes in energy metabolites and intracellular pH during spreading depression in the chick retina. Metab Brain Dis. 6:75-82.

De Azeredo FA, Martins-Ferreira H (1979) Changes in fluid compartments and ionic composition in the isolated chick retina during SD. Neurochem Res. 4:99-107.

De Azeredo FA, Perret ML (1992) Cortical slow potential changes during convulsions induced by maximal electroshock or penicillin focus. Metab Brain Dis. 7:101-113.

De Azeredo FA, Ribeiro MF (1992) A simple biological way to screen dopaminergic agonists. Metab Brain Dis. 7:211-221.

De Crespigny A, Rother J, Van Bruggen N, Beaulieu C, Moseley ME (1998) Magnetic resonance imaging assessment of cerebral hemodynamics during spreading depression in rats. J Cereb Blood Flow Metab. 18:1008-1017.

De Lorey TM, Olsen RW (1992) Gamma-aminobutyric acid-A receptor structure and function. J Biol Chem. 267:16747-50.

De Luca B, Bures J (1977) Development of cortical spreading depression and of its transition to the caudate nucleus in rats. Dev Psychobiol. 10:289-297.

De Luca B, Cerciello A, Monda M (1982) Cortical control of neurally-mediated arrhythmogenic properties of desacetyl lanatoside C: the role of the posterior hypothalamus. Neuropharmacology. 21:1211-1214.

De Oliveria Castro G, Martins-Ferreira H (1970) Deformations and thickness variations accompanying spreading depression in the retina. J Neurophysiol. 33:891-900.

De Oliveira Castro G, Martins-Ferreira H, Gardino PF (1985) Dual nature of the peaks of light scattered during spreading depression in chick retina. An Acad Bras Cienc. 57:95-103.

De Schutter W (1998) Detailed model of ryanodine receptor mediated calcium release in Purkinje cells. In Computational Neuroscience (ed. Bower J) pp 161-1667. New York: Plenum.

De Schutter E, Bower J (1994) An active membrane model of the cerebellar Purkinje cell. I. Simulation of current clamps in slice. J Neurophysiol. 71:375-400.

De Schutter E, Smolen P (1998) Calcium dynamics in large neuronal networks. In Methods in neuronal modeling. From ions to networks. Second edition. (ed. Koch C, Segev I), pp 211-250. Cambridge, MA:MIT Press.

Destexhe A, Mainen ZF, Sejnowski TJ (1998) Kinetic models of synaptic transmission. In Methods in neuronal modeling. From ions to networks. Second ddition. (ed. Koch C, Segev I), pp 1-26. Cambridge, MA:MIT Press.

Diener HC, Gendolla A, Juptner M, Kaube H, Limmroth V (1997) Emerging treatments in headache. Eur Neurol. 38:167-174.

Dietrich WD, Feng ZC, Leistra H, Watson BD, Rosenthal M (1994) Photothrombotic infarction triggers multiple episodes of cortical spreading depression in distant brain regions. J Cereb Blood Flow Metab. 14:20-28.

Di Francesco D, Noble D (1985) A model of cardiac electrical activity incorporating ionic pumps and concentration changes. Tran Roy Soc Lond B307:353-398.

Dingledine R, McBain CJ (1994) Excitatory amino acid transmitters. In: Basic Neurochemistry: Molecular, cellular and Medical Aspects. Fifth Edition. (ed. Siegel GJ, Agranoff BW, Albers RW, Molinoff PB) pp. 367-387. New York: Raven.

DiPolo R, Beaugé L (1979) Physiological role of ATP-driven calcium pump in squid axon. Nature. 278:271-273.

DiPolo R, Beaugé L (1983) The calcium pump and sodium-calcium exchange in squid axons. Annual Reviews of Physiology. 45:313-324.

Do Carmo RJ, Martins-Ferreira H (1984) Spreading depression of Leão probed with ion-selective microelectrodes in isolated chick retina. An Acad Bras Cienc. 56:401-421.

Do Carmo RJ, Martins-Ferreira H (1988) Extracellular Ca2+ and retinal spreading depression. Braz J Med Biol Res. 21:607-610.

Donnet A, Bartolomei F (1997) Migraine with visual aura and photosensitive epileptic seizures. Epilepsia. 38:1032-1034.

Dragunow M, Goulding M, Faull RL, Ralph R, Mee E, Frith R (1990) Induction of c-fos mRNA and protein in neurons and glia after traumatic brain injury: pharmacological characterization. Exp Neurol. 107:236-248.

Dreier JP, Korner K, Ebert N, Gorner A, Rubin I, Back T, Lindauer U, Wolf T, Villringer A, Einhaupl KM, Lauritzen M, Dirnagl U (1998) Nitric oxide scavenging by hemoglobin or nitric oxide synthase inhibition by N-nitro-L-arginine induces cortical spreading ischemia when K+ is increased in the subarachnoid space. J Cereb Blood Flow Metab. 18:978-990.

Drejer J, Sheardown M, Nielsen EO, Honore T (1989) Glycine reverses the effect of HA-966 on NMDA responses in cultured rat cortical neurons and in chick retina. Neurosci Lett. 98:333-338.

Duckrow RB (1993) A brief hypoperfusion precedes spreading depression if nitric oxide synthesis is inhibited. Brain Res. 618:190-195.

Els T, Rother J, Beaulieu C, de Crespigny A, Moseley M (1997) Hyperglycemia delays terminal depolarization and enhances repolarization after peri-infarct spreading depression as measured by serial diffusion MR mapping. J Cereb Blood Flow Metab. 17:591-595.

Engeln-Müllges G, Uhlig F (1996) Numerical Algorithms with Fortran with CD-ROM. Berlin: Springer-Verlag.

Erxleben C (1991) Potassium channels in crustacean glial cells. Glia 4:285-92.

Evans D, Smith JC (1987) Seizure activity and cortical spreading depression monitored by an extrinsic potential-sensitive molecular probe. Brain Res. 409:350-357.

Fabricius M, Akgoren N, Dirnagl U, Lauritzen M (1997) Laminar analysis of cerebral blood flow in cortex of rats by laser-Doppler flowmetry: a pilot study. J Cereb Blood Flow Metab. 17:1326-1336.

Fabricius M, Akgoren N, Lauritzen M (1995) Arginine-nitric oxide pathway and cerebrovascular regulation in cortical spreading depression. Am J Physiol. 269:H23-29.

Fabricius M, Jensen LH, Lauritzen M (1993) Microdialysis of interstitial amino acids during spreading depression and anoxic depolarization in rat neocortex. Brain Res. 612:61-69.

Fabricius M, Lauritzen M (1993) Transient hyperemia succeeds oligemia in the wake of cortical spreading depression. Brain Res. 602:350-353.

Fabricius M, Lauritzen M (1996) Laser-Doppler evaluation of rat brain microcirculation: comparison with the [14C]-iodoantipyrine method suggests discordance during cerebral blood flow increases. J Cereb Blood Flow Metab. 16:156-161.

Fan J, Walsh KB (1999) Mechanical stimulation regulates voltage-gated potassium currents in cardiac microvascular endothelial cells. Circ Res 84:451-7.

Farley J, Rudy B (1988) Multiple types of voltage-dependent $Ca^{2+}$-activated $K^{+}$ channels of large conductance in rat brain synaptosomal membranes. Biophys J 53:919-934.

Felix JA, Woodruff, ML, Dirksen ER (1996) Stretch increases inositol 1,4,5 trisphosphate concentration in airway epithelial Cells. Am J Respir Cell Mol Biol 14:296-301.

Fernandes de Lima VM, Goldermann M, Hanke WR (1994) Calcium waves in gray matter are due to voltage-sensitive glial membrane channels. Brain Res. 663:77-83.

Fernandes de Lima VM, Hanke WR (1996) Observations of non-stationarities in extracellular potassium dynamics within the gray matter neuropil during self-sustained spreading depressions. J Hirnforsch. 37:505-518.

Fernandes de Lima VM, Scheller D, Tegtmeier F, Hanke W, Schlue WR (1993) Self-sustained spreading depressions in the chicken retina and short-term neuronal-glial interactions within the gray matter neuropil. Brain Res. 614:45-51.

Ferrari MD, Odink J, Bos KD, Malessy MJ, Bruyn GW (1990) Neuroexcitatory plasma amino acids are elevated in migraine. Neurology. 40:1582-1586.

Ferreira-Filho CR, Martins-Ferreira H (1982) Electrical impedance of isolated retina and its changes during spreading depression. Neuroscience. 7:3231-3239.

Fiero L, Llano I (1996) High endogenous calcium buffering in Purkinje cells from rat cerebellar slices. J Physiol. 496:617-625.

Fitzhugh R (1961) Impulses and physiological states in theoretical models of nerve membrane. Biophys J 1:445-466.

Florence G, Bonvento G, Charbonne R, Seylaz J (1994) Spreading depression reversibly impairs autoregulation of cortical blood flow. Am J Physiol. 266:R1136-1140.

Footitt DR, Newberry NR (1998) Cortical spreading depression induces an LTP-like effect in rat neocortex in vitro. Brain Res. 781:339-342.

Freedman NL, Pote R (1969) Activity impairment with circumscribed frontal spreading depression and ablation. Psychol Rep. 24:623-625.

Friberg L, Olesen J, Olsen TS, Karle A, Ekman R, Fahrenkrug J (1994) Absence of vasoactive peptide release from brain cerebral circulation during onset of migraine with aura. Cephalalgia. 14:47-54.

Friel DD (1995) [Ca2+]i oscillations in sympathetic neurons: an experimental test of a theoretical model. Biophys J 68:1752-66.

Fujii Y, Nakamura S, Ito H (1997) Developmental changes in the electrical activity of locus coeruleus neurons during cortical spreading depression. Brain Res Dev Brain Res. 104:91-100.

Fujimoto M, Tomita T (1986) The spreading depression potential and the ERG B-wave in retinas of the frog and chick. Neurosci Res Suppl. 4:S197-208.

Fujimoto M, Yanase H (1994) Properties of the 'neutral zone' explain polarity of retinal spreading depression. Neurosci Res (19:195-200.

Gabso M, Neher E, Spira ME (1997) Low modility of the Ca++ buffers in axons of cultured aplysia neurons. Neuron. 18:473-481.

Garaschuk O, Schneggenburger R, Schirra C, Tempia F, Konnerth A (1996) Fractional Ca2+ currents through somatic dendritic glutamate receptor channels of rat hippocampal CA1 pyramidal neurons. J Physiol. 471:757-772.

Gardino PF, do Carmo RJ (1983) Glutamate and spreading depression in chick retina. An Acad Bras Cienc. 55:297-307.

Gardner-Medwin AR (1981) Possible roles of vertebrate neuroglia in potassium dynamics, spreading depression and migraine. J Exp Biol. 95:111-127.

Gardner-Medwin AR, Tepley N, Barkley GL, Moran J, Nagel-Leiby S, Simkins RT, Welch KM (1991) Magnetic fields associated with spreading depression in anaesthetized rabbits. Brain Res. 540:153-158.

Gardner-Medwin AR, van Bruggen N, Williams SR, Ahier RG (1994) Magnetic resonance imaging of propagating waves of spreading depression in the anaesthetized rat. J Cereb Blood Flow Metab. 14:7-11.

Gass P, Spranger M, Herdegen T, Bravo R, Kock P, Hacke W, Kiessling M (1992) Induction of FOS and JUN proteins after focal ischemia in the rat: differential effect of the N-methyl-D-aspartate receptor antagonist MK-801. Acta Neuropathol (Berl). 84:545-553.

Gehrmann J, Mies G, Bonnekoh P, Banati R, Iijima T, Kreutzberg GW, Hossmann KA (1993) Microglial reaction in the rat cerebral cortex induced by cortical spreading depression. Brain Pathol. 3:11-17.

Gido G, Katsura K, Kristian T, Siesjo BK (1993) Influence of plasma glucose concentration on rat brain extracellular calcium transients during spreading depression. J Cereb Blood Flow Metab. 13:179-182.

Gido G, Kristian T, Siesjo BK (1994) Induced spreading depressions in energy-compromised neocortical tissue: calcium transients and histopathological correlates. Neurobiol Dis. 1:31-41.

Gill R, Andine P, Hillered L, Persson L, Hagberg H (1992) The effect of MK-801 on cortical spreading depression in the penumbral zone following focal ischemia in the rat. J Cereb Blood Flow Metab. 12:371-379.

Gillessen T, Alzheimer C (1997) Amplification of EPSPs by low Ni2+-and amiloride-sensitive Ca2+ channels in apical dendrites of rat CA1 pyramidal neurons. J Neurophysiol. 77:1639-1643.

Gjedde A, Hansen AJ, Quistorff B (1981) Blood-brain glucose transfer in spreading depression. J Neurochem. 37:807-812.

Goadsby PJ (1992) The oligemic phase of cortical spreading depression is not blocked by tirilazad mesylate (U-74006F). Brain Res. 588:140-143.

Goadsby PJ, Adner M, Edvinsson L (1996) Characterization of endothelin receptors in the cerebral vasculature and their lack of effect on spreading depression. J Cereb Blood Flow Metab. 16:698-704.

Goadsby PJ, Kaube H, Hoskin KL (1992) Nitric oxide synthesis couples cerebral blood flow and metabolism. Brain Res. 595:167-170.

Goldbeter A (1996) Biochemical Oscillations and Cellular Rhythms. Cambridge: Cambridge Univ Press.

Goldensohn E, Escueta A, Runk L (1967) Unit membrane shifts and firing patterns during spreading depression. Electroencephalogr Clin Neurophysiol. 23:84.

Gorczyca MG, Wu CF (1991) Single channel K+ currents in Drosophila muscle and their pharmacological block. J Membr Biol 121:237-48.

Gorelova NA, Bures J (1983) Spiral waves of spreading depression in the isolated chicken retina. J Neurobiol. 14:353-363.

Gorelova NA, Koroleva VI, Amemori T, Pavlik V, Bures J (1987) Ketamine blockade of cortical spreading depression in rats. Electroencephalogr Clin Neurophysiol. 66:440-447.

Gowers WR (1907) The border-land of epilepsy: faints, vagal attacks, vertigo, migraine, sleep symptoms and their treatment. London: London and Churchill.

Grafstein B (1956a) Mechanism of spreading cortical depression. J Neurophysiol (19:154-171.

Grafstein B (1956b) Locus of propagation of spreading cortical depression. J Neurophysiol (19:308-316.

Gruol DL, Jacquin T, Yool L (1991) Single channel $K^+$ currents recorded from the somatic and dendritic regions of cerebellar Purkinje neurons in culture. J Neurosci 11:1002-1015.

Guedes RC, Amorim LF, Teodosio NR (1996) Effect of aging on cortical spreading depression. Braz J Med Biol Res. 29:1407-1412.

Guedes RC, Andrade AF, Cabral-Filho JE (1987) Propagation of cortical spreading depression in malnourished rats: facilitatory effect of dietary protein deficiency. Braz J Med Biol Res. 20:639-642.

Guedes RC, Barreto JM (1992) Effect of anesthesia on the propagation of cortical spreading depression in rats. Braz J Med Biol Res. 25:393-397.

Guedes RC, Cavalheiro EA (1997) Blockade of spreading depression in chronic epileptic rats: reversion by diazepam. Epilepsy Res. 27:33-40.

Guedes RC, do Carmo RJ (1980) Influence of ionic disturbances produced by gastric washing on cortical spreading depression. Exp Brain Res. 39:341-349.

Guedes RC, Frade SF (1993) Effect of ethanol on cortical spreading depression. Braz J Med Biol Res. 26:1241-1244.

Guedes RC, Pereira-da-Silva MS (1993) Effect of pre- and postnatal propylthiouracil administration on the propagation of cortical spreading depression of adult rats. Braz J Med Biol Res. 26:1123-1128.

Hablitz JJ, Heinemann U (1989) Alterations in the microenvironment during spreading depression associated with epileptiform activity in the immature neocortex. Brain Res Dev Brain Res. 46:243-252.

Hada J, Kaku T, Morimoto K, Hayashi Y, Nagai K (1996) Adenosine transport inhibitors enhance high K(+)-evoked taurine release from rat hippocampus. Eur J Pharmacol. 305:101-107.

Haglund MM, Schwartzkroin PA (1984) Seizure-like spreading depression in immature rabbit hippocampus in vitro. Brain Res. 316:51-59.

Haglund MM, Schwartzkroin PA (1990) Role of Na-K pump potassium regulation and IPSPs in seizures and spreading depression in immature rabbit hippocampal slices. J Neurophysiol. 63:225-239.

Hansen AJ, Quistorff B, Gjedde A (1980) Relationship between local changes in cortical blood flow and extracellular K+ during spreading depression. Acta Physiol Scand. 109:1-6.

Hansen AJ, Olsen CE (1980) Brain extracellular space during spreading depression and ischemia. Acta Physiol Scand. 108:355-365.

Hansen AJ (1985) Effect of anoxia on ion distribution in the brain. Physiol Rev 65:101-148.

Hansen AJ, Nedergaard M (1988) Brain ion homeostasis in cerebral ischemia. Neurochem Pathol. 9:195-209.

Harada S, Kamiya K, Masago A, Iwata A, Yamada K (1997) Subarachnoid hemorrhage induces c-fos, c-jun and hsp70 mRNA expression in rat brain. Neuroreport. 8:3399-3404.

Harris RJ, Wieloch T, Symon L, Siesjo BK (1984) Cerebral extracellular calcium activity in severe hypoglycemia: relation to extracellular potassium and energy state. J Cereb Blood Flow Metab. 4:187-193.

Hasegawa Y, Latour LL, Formato JE, Sotak CH, Fisher M (1995) Spreading waves of a reduced diffusion coefficient of water in normal and ischemic rat brain. J Cereb Blood Flow Metab. 15:179-187.

Haselgrove JC, Bashford CL, Barlow CH, Quistorff B, Chance B, Mayevsky A (1990) Time resolved 3-dimensional recording of redox ratio during spreading depression in gerbil brain. Brain Res. 506:109-114.

Herdegen T, Sandkuhler J, Gass P, Kiessling M, Bravo R, Zimmermann M (1993) JUN, FOS, KROX, and CREB transcription factor proteins in the rat cortex: basal expression and induction by spreading depression and epileptic seizures. J Comp Neurol. 333:271-288.

Hernandez-Caceres J, Macias-Gonzalez R, Brozek G, Bures J (1987) Systemic ketamine blocks cortical spreading depression but does not delay the onset of terminal anoxic depolarization in rats. Brain Res. 437:360-364.

Herrera DG, Cuello AC (1992) MK-801 affects the potassium-induced increase of glial fibrillary acidic protein immunoreactivity in rat brain. Brain Res. 598:286-293.

Herrera DG, Maysinger D, Almazan G, Funnel R, Cuello AC (1998) Analysis of c-Fos and glial fibrillary acidic protein (GFAP) expression following topical application of potassium chloride (KCl) to the brain surface. Brain Res. 784:71-81.

Herrera DG, Maysinger D, Gadient R, Boeckh C, Otten U, Cuello AC (1993) Spreading depression induces c-fos-like immunoreactivity and NGF mRNA in the rat cerebral cortex. Brain Res. 602:99-103.

Herrera DG, Robertson HA (1990) Application of potassium chloride to the brain surface induces the c-fos proto-oncogene: reversal by MK-801. Brain Res. 510:166-170.

Herrera DG, Robertson HA (1996) Activation of c-fos in the brain. Prog Neurobiol. 50:83-107.

Herreras O, Largo C, Ibarz JM, Somjen GG, Martin del Rio R (1994) Role of neuronal synchronizing mechanisms in the propagation of spreading depression in the in vivo hippocampus. J Neurosci. 14:7087-7098.

Herreras O, Somjen GG (1993a) Analysis of potential shifts associated with recurrent spreading depression and prolonged unstable spreading depression induced by microdialysis of elevated K+ in hippocampus of anesthetized rats. Brain Res. 610:283-294.

Herreras O, Somjen GG (1993b) Effects of prolonged elevation of potassium on hippocampus of anesthetized rats. Brain Res. 617:194-204.

Herreras O, Somjen GG (1993c) Propagation of spreading depression among dendrites and somata of the same cell population. Brain Res. 610:276-282.

Hershkowitz N, Katchman AN, Veregge S (1993) Site of synaptic depression during hypoxia: a patch-clamp analysis. J Neurophysiol. 69:432-441.

Higashida H, Mitarai G, Watanabe S (1974) A comparative study of membrane potential changes in neurons and neuroglial cells during spreading depression in the rabbit. Brain Res. 65:411-425.

Higashida H, Miyake A, Tarao M, Watanabe S (1971) Membrane potential changes of neuroglial cells during spreading depression in the rabbit. Brain Res. 32:207-211.

Higashida H, Sakakibara M, Mitarai G (1977) Spreading depression in isolated carp retina. Brain Res. 120:67-83.

Hille B (1992) Ionic Channels of Excitable Membranes. Second Edition. Sunderland, MA: Sinauer.

Hodgkin AL, Huxley AF (1952) A quantitative description of membrane current and its application to conduction and excitation in nerve. J Physiol. 117:500-544.

Hofer AM, Machen TJ (1993) Technique for an in situ measurement of calcium in intracellular inositol 1,4,5-trisphosphate sensitive stores using the fluorescent indicator mag-fura-2. Proc Nat Acad Sci, USA. 90:2598-2602.

Hoffman DA, Magee JC, Colbert CM, Johnston D (1997) K+ channel regulation of signal propagation in dendrites of hippocampal pyramidal neurons. Nature. 387:869-875.

Holder DS (1992) Detection of cortical spreading depression in the anaesthetized rat by impedance measurement with scalp electrodes: implications for non-invasive imaging of the brain with electrical impedance tomography. Clin Phys Physiol Meas. 13:77-86.

Holder DS, Gardner-Medwin AR (1988) Some possible neurological applications of applied potential tomography. Clin Phys Physiol Meas. 9 Suppl A:111-119.

Holmes WR (1995) Modeling the effect of glutamate diffusion and uptake on NMDA and non-NMDA receptor saturation. Biophys J. 69:1734-1737.

Honkaniemi J, States BA, Weinstein PR, Espinoza J, Sharp FR (1997) Expression of zinc finger immediate early genes in rat brain after permanent middle cerebral artery occlusion. J Cereb Blood Flow Metab. 17:636-646.

Ikeda J, Nakajima T, Osborne OC, Mies G, Nowak TS Jr (1994) Coexpression of c-fos and hsp70 mRNAs in gerbil brain after ischemia: induction threshold, distribution and time course evaluated by in situ hybridization. Brain Res Mol Brain Res. 26:249-258.

Irwin DA, Kakolewski JW, Criswell HE, Popov A (1975) An injury-induced diffuse slow potential from brain. Electroencephalogr Clin Neurophysiol. 38:367-377.

Islam S, Buresová O (1975) The effect of cortical spreading depression on motor performance and depth avoidance in rats. Act Nerv Super (Praha). 17:8-14.

Islas L, Pasantes-Morales H, Sanchez JA (1993) Characterization of stretch-activated ion channels in cultured astrocytes. Glia 8:87-96.

Ives HE, Verkman AS (1985) Effects of membrane fluidizing agents on renal brush border proton permeability. Am J Physiol. 249:F933-F940.

Jakobson E (1980) Interactions of cell volume, membrane potential, and membrane transport parameters. Am. J. Physiol. 238:C196-206.

Ji S, John SA, Lu Y, Weiss JN (1998) Mechanosensitivity of the cardiac muscarinic potassium channel. A novel property conferred by the Kir3.4 subunit. J Biol Chem 273:1324-8.

Jing J, Aitken PG, Somjen GG (1991) Lasting neuron depression induced by high potassium and its prevention by low calcium and NMDA receptor blockade. Brain Res. 557:177-183.

Jing J, Aitken PG, Somjen GG (1993) Role of calcium channels in spreading depression in rat hippocampal slices. Brain Res. 604:251-259.

Jing J, Aitken PG, Somjen GG (1994) Interstitial volume changes during spreading depression (SD) and SD-like hypoxic depolarization in hippocampal tissue slices. J Neurophysiol. 71:2548-2551.

Johnston D, Wu SM (1995) Foundations of Cellular Neurophysiology. Cambridge, MA: Bradford Books.

Kaku T, Hada J, Hayashi Y (1994) Endogenous adenosine exerts inhibitory effects upon the development of spreading depression and glutamate release induced by microdialysis with high K+ in rat hippocampus. Brain Res. 658:39-48.

Kandel ER, Schwartz JH, Jessell T (1991) Principles of Neural Science. Norwalk, CN: Appleton and Lange.

Kandler K, Katz LC (1995) Relationship between dye coupling and spontaneous activity in developing ferret visual cortex. Dev Neurosci 20:59-64

Kapp BS, Schneider AM (1971) Selective recovery from retrograde amnesia produced by hippocampal spreading depression. Science. 173:1149-1151.

Kasser RJ, Renner KJ, Feng JX, Brazell MP, Adams RN (1988) Spreading depression induced by 100 mM KCl in caudate is blocked by local anesthesia of the substantia nigra. Brain Res. 475:333-344.

Kaube H, Goadsby PJ (1994) Anti-migraine compounds fail to modulate the propagation of cortical spreading depression in the cat. Eur Neurol. 34:30-35.

Kavalali ET, Zhuo M, Bito H, Tsien RW (1997) Dendritic Ca2+ channels characterized by recordings from isolated hippocampal dendritic segments. Neuron 18:651-663.

Kawahara K (1990) A stretch activated K+ channel in the basolateral membrane of Xenopus kidney proximal tubule cells. Pflugers Archiv 415:629-629.

Kawahara K (1993) [Stretch-activated channels in renal tubule.] Nippon Rinsho. Jap J Clin Med 51:2201-8 (in Japanese).

Kawahara N, Croll SD, Wiegand SJ, Klatzo I (1997) Cortical spreading depression induces long-term alterations of BDNF levels in cortex and hippocampus distinct from lesion effects: implications for ischemic tolerance. Neurosci Res. 29:37-47.

Kawahara N, Ruetzler CA, Klatzo I (1995) Protective effect of spreading depression against neuronal damage following cardiac arrest cerebral ischemia. Neurol Res. 17:9-16.

Kawasaki K, Traynelis SF, Dingledine R (1990) Different responses of CA1 and CA3 regions to hypoxia in rat hippocampal slice. J Neurophysiol. 63:385-394.

Keizer J, Levine L (1996) Ryanodine Receptor Adaptation and Ca2+-Induced Ca2+ Release-Dependent Ca2+ Oscillations. Biophysical Journal. 71:3477-3487.

Keener J, Sneyd J (1998) Mathematical Physiology. New York: Springer-Verlag.

Kelley MS, Steward O (1996a) The process of reinnervation in the dentate gyrus of adult rats: physiological events at the time of the lesion and during the early postlesion period. Exp Neurol. 139:73-82.

Kelley MS, Steward O (1996b) The role of postlesion seizures and spreading depression in the upregulation of glial fibrillary acidic protein mRNA after entorhinal cortex lesions. Exp Neurol. 139:83-94.

Kelley MS, Steward O (1997) Injury-induced physiological events that may modulate gene expression in neurons and glia. Rev Neurosci. 8:147-177.

Kelly ME, McIntyre DC (1996) Perirhinal cortex involvement in limbic kindled seizures. Epilepsy Res. 26:233-243.

Kendal JM, Dormer RL, Campbell AK (1992) Target aquerin to the endoplasmic reticulum of living cells. Biochem Biophys Res Commun (1989:1008-1016.

Kim D, Sladek CD, Aguado-Velasco C, Mathiasen JR (1995) Arachidonic acid activation of a new family of K+ channels in cultured rat neuronal cells. J Physiol (Lond) 484:643-60.

Kim YK, Lee SH, Goldinger JM, Hong SK (1986) Effect of ethanol on organic ion transport in rabbit kidney. Toxicol Appl Pharmacol. 86:411-420.

Klee CB (1988) Interaction of calmodulin with Ca++ and target proteins. In: Calmodulin (ed. Cohen P, Clee CB) pp 35-46. Amsterdam: Elsevier.

Klosterhalfen W, Klosterhalfen S (1985) Habituation of heart rate in functionally decorticate rats. Behav Neurosci. 99:555-563.

Kobayashi S, Harris VA, Welsh FA (1995) Spreading depression induces tolerance of cortical neurons to ischemia in rat brain. J Cereb Blood Flow Metab. 15:721-727.

Koch C (1998) Biophysics of computation. New York: Oxford.

Kocher M (1990) Metabolic and hemodynamic activation of postischemic rat brain by cortical spreading depression. J Cereb Blood Flow Metab. 10:564-571.

Koenig H, Patel A (1970) Biochemical basis for fluorouracil neurotoxicity. The role of Krebs cycle inhibition by fluoroacetate. Arch Neurol. 23:155-160.

Kokaia Z, Gido G, Ringstedt T, Bengzon J, Kokaia M, Siesjo BK, Persson H, Lindvall O (1993) Rapid increase of BDNF mRNA levels in cortical neurons following spreading depression: regulation by glutamatergic mechanisms independent of seizure activity. Brain Res Mol Brain Res (19:277-286.

Komaromi I, Malkinson TJ, Veale WL, Rosenbaum G, Cooper KE, Pittman QJ (1994) Effect of potassium-induced cortical spreading depression on prostaglandin-induced fever in conscious and urethane-anesthetized rats. Can J Physiol Pharmacol. 72:716-721.

Koroleva VI, Bures J (1979) Circulation of cortical spreading depression around electrically stimulated areas and epileptic foci in the neocortex of rats. Brain Res. 173:209-215.

Koroleva VI, Bures J (1980) Blockade of cortical spreading depression in electrically and chemically stimulated areas of cerebral cortex in rats. Electroencephalogr Clin Neurophysiol. 48:1-15.

Koroleva VI, Bures J (1982) Stimulation induced recurrent epileptiform discharges block cortical and subcortical spreading depression in rats. Physiol Bohemoslov. 31:385-400.

Koroleva VI, Bures J (1983) Cortical penicillin focus as a generator of repetitive spike-triggered waves of spreading depression in rats. Exp Brain Res. 51:291-297.

Koroleva VI, Oitzl MS, Bures J (1985) Threshold of synaptically elicited cortical spreading depression: drug-induced changes in rats. Electroencephalogr Clin Neurophysiol. 60:55-64.

Koroleva VI, Vinogradova LV, Bures J (1993) Reduced incidence of cortical spreading depression in the course of pentylenetetrazol kindling in rats. Brain Res. 608:107-114.

Koroleva VI, Bures J (1993) Rats do not experience cortical or hippocampal spreading depression as aversive. Neurosci Lett. 149:153-156.

Koroleva VI, Korolev OS, Loseva E, Bures J (1998) The effect of MK-801 and of brain-derived polypeptides on the development of ischemic lesion induced by photothrombotic occlusion of the distal middle cerebral artery in rats. Brain Res. 786:104-114.

Kostyuk PG, Verkhratsky AN (1995) Calcium signaling in the nervous system. Chichester: Wiley.

Kraig RP, Cooper AJ (1987) Bicarbonate and ammonia changes in brain during spreading depression. Can J Physiol Pharmacol. 65:1099-1104.

Kraig RP, Dong LM, Thisted R, Jaeger CB (1991) Spreading depression increases immunohistochemical staining of glial fibrillary acidic protein. J Neurosci. 11:2187-2198.

Kraig RP, Ferreira-Filho CR, Nicholson C (1983) Alkaline and acid transients in cerebellar microenvironment. J Neurophysiol. 49:831-850.

Kraig RP, Jaeger CB (1990) Ionic concomitants of astroglial transformation to reactive species. Stroke. 21:III184-187.

Kraig RP, Kunkler PE (1997) Calcium waves precede potential changes of spreading depression in hippocampal organ cultures. Soc Neurosci Abs 23:546.

Kraig RP, Nicholson C (1978) Extracellular ionic variations during spreading depression. Neuroscience. 3:1045-1059.

Kríváněk J (1977) Brain cyclic adenosine 3',5'-monophosphate during depolarization of the cerebral cortical cells in vivo. Brain Res. 120:493-505.

Kríváněk J (1980) May K+ ions stimulate the formation of cyclic AMP in the brain independently on their depolarizing action? Experientia. 36:1185-1186.

Kríváněk J, Koroleva VI (1996) Protein kinase C in the rat cerebral cortex during spreading depression. Neurosci Lett. 210:79-82.

Kruger H, Luhmann HJ, Heinemann U (1996) Repetitive spreading depression causes selective suppression of GABAergic function. Neuroreport. 7:2733-2736.

Kubota M, Nakamura T, Sunami K, Ozawa Y, Namba H, Yamaura A, Makino H (1989) Changes of local cerebral glucose utilization, DC potential and extracellular potassium concentration in experimental head injury of varying severity. Neurosurg Rev. 12 Suppl 1:393-399.

Kuffler SW, Nicholls JG (1976) From neuron to brain: a cellular approach to the function of the nervous system. Sunderland, Mass.:Sinauer Associates.

Kunkler PE, Kraig RP (1998) Calcium waves precede electrophysiological changes of spreading depression in hippocampal organ cultures. J Neurosci. 18:3416-3425.

Kurata Y, Marszalec W, Yeh JZ, Narahashi T (1999) Agonist and potentiation actions of n-octanol on gamma-aminobutyric acid type A receptors. Mol Pharmacol. 55:1011-1019.

Lacombe P, Sercombe R, Correze JL, Springhetti V, Seylaz J (1992) Spreading depression induces prolonged reduction of cortical blood flow reactivity in the rat. Exp Neurol. 117:278-286.

Lambert GA, Michalicek J (1994) Cortical spreading depression reduces dural blood flow--a possible mechanism for migraine pain? Cephalalgia. 14:430-436; discussion 393-434.

Lance JW (1991) Solved and unsolved headache problems. Headache. 31:439-45.

Lance JW (1993) Current concepts of migraine pathogenesis. Neurology. 43:S11-15.

Largo C, Cuevas P, Herreras O (1996) Is glia dysfunction the initial cause of neuronal death in ischemic penumbra? Neurol Res. 18:445-448.

Largo C, Cuevas P, Somjen GG, Martin del Rio R, Herreras O (1996) The effect of depressing glial function in rat brain in situ on ion homeostasis, synaptic transmission, and neuron survival. J Neurosci. 16:1219-1229.

Largo C, Ibarz JM, Herreras O (1997) Effects of the gliotoxin fluorocitrate on spreading depression and glial membrane potential in rat brain in situ. J Neurophysiol. 78:295-307.

Largo C, Tombaugh GC, Aitken PG, Herreras O, Somjen GG (1997) Heptanol but not fluoroacetate prevents the propagation of spreading depression in rat hippocampal slices. J Neurophysiol. 77:9-16.

Lashley KS (1941) Patterns of Cerebral Integration Indicated by the Scotomas of Migraine. Arch. Neurol Psychiat. 46:331-339.

Latour LL, Hasegawa Y, Formato JE, Fisher M, Sotak CH (1994) Spreading waves of decreased diffusion coefficient after cortical stimulation in the rat brain. Magn Reson Med. 32:189-198.

Lauritzen M (1984) Long-lasting reduction of cortical blood flow of the brain after spreading depression with preserved autoregulation and impaired CO2 response. J Cereb Blood Flow Metab. 4:546-554.

Lauritzen M (1985) On the possible relation of spreading cortical depression to classical migraine. Cephalalgia. 5 Suppl 2:47-51.

Lauritzen M (1987) Cerebral blood flow in migraine and cortical spreading depression. Acta Neurol Scand Suppl. 113:1-40.

Lauritzen M (1987) Regional cerebral blood flow during cortical spreading depression in rat brain: increased reactive hyperperfusion in low-flow states. Acta Neurol Scand. 75:1-8.

Lauritzen M (1992) Spreading depression and migraine. Pathol Biol (Paris). 40:332-337.

Lauritzen M (1994) Pathophysiology of the migraine aura. The spreading depression theory. Brain. 117 ( Pt 1):199-210.

Lauritzen M, Fabricius M (1995) Real time laser-Doppler perfusion imaging of cortical spreading depression in rat neocortex. Neuroreport. 6:1271-1273.

Lauritzen M, Hansen AJ (1992) The effect of glutamate receptor blockade on anoxic depolarization and cortical spreading depression. J Cereb Blood Flow Metab. 12:223-229.

Lauritzen M, Hansen AJ, Kronborg D, Wieloch T (1990) Cortical spreading depression is associated with arachidonic acid accumulation and preservation of energy charge. J Cereb Blood Flow Metab. 10:115-122.

Lauritzen M, Jorgensen MB, Diemer NH, Gjedde A, Hansen AJ (1982) Persistent oligemia of rat cerebral cortex in the wake of spreading depression. Ann Neurol. 12:469-474.

Lauritzen M, Olesen J (1984) Regional cerebral blood flow during migraine attacks by Xenon-133 inhalation and emission tomography. Brain. 107 ( Pt 2):447-461.

Lauritzen M, Rice ME, Okada Y, Nicholson C (1988) Quisqualate, kainate and NMDA can initiate spreading depression in the turtle cerebellum. Brain Res. 475:317-327.

Lauritzen M, Skyhoj Olsen T, Lassen NA, Paulson OB (1983) Changes in regional cerebral blood flow during the course of classic migraine attacks. Ann Neurol. 13:633-641.

Leão AAP (1944a). Spreading depression of activity in the cerebral cortex. J Neurophysiol. 7:359-390.

Leão AAP (1944b). Pial circulation and spreading depression of activity in cerebral cortex. J Neurophysiol. 7:391-396.

Leão AAP (1944c). Spreading depression of activity in the cerebral cortex. Ph. D. Dissertation (Physiology). Harvard University.

Leão AAP (1947) Further observations on the spreading depression of activity in the cerebral cortex. J Neurophysiol. 10:409-419.

Leão AAP (1951) The slow voltage variation of cortical spreading depression of activity. EEG Clin Neurophysiol. 3:315-321.

Leão AAP (1972) Spreading Depression. In: Experimental Models of Epilepsy – A Manual for the Laboratory Worker. (ed. Purpura DP, Penry JK, Woodbury DM, Tower DB, Walter RD). New York: Raven.

Leão AAP, Morrison RS (1945) Propagation of spreading cortical depression. J Neurophysiol. 8:33-45.

Leibowitz DH (1992) The glial spike theory. I. On an active role of neuroglia in spreading depression and migraine. Proc R Soc Lond B Biol Sci. 250:287-295.

Lemieux DR, Roberge FA, Joly D (1992) Modeling the dynamic features of the electrogenic Na, K pump of cardiac cells. J Theor Biol. 154:335-358.

Lemieux G, Baverel G, Vinay P, Gougoux A (1979) Effect of fluoroacetate on the inhibitory action of ketone bodies and fatty acids on renal ammoniagenesis. Am J Physiol. 237:F7-F13.

Lendvai D, Monteleone F, Melpignano G, Turri E, Verdecchia P, Cantani A (1996) Familial hemiplegic migraine in developmental age: report of two cases. Riv Eur Sci Med Farmacol. 18:143-147.

Llano I, Di Polo R, Marty A (1994) Calcium induced calcium release in cerebellar Purkinje cells. Neuron. 12:663-673.

Magee JC, Johnston D (1995a) Characterization of single voltage-gated Na+ and Ca++ channels in apical dendrites of rat CA2 pyramidal neurons. J Physiol. 487:67-90.

Magee JC, Johnston D (1995b) Synaptic activation of voltage gated channels in dendrites of hippocampal pyramidal neurons. Science. 268:301-304.

Mainen ZF, Sejnowski TJ (1998) Modeling active dendritic processes in pyramidal neurons. In: Methods in Neuronal Modeling: From Ions to Networks (ed. Koch C, Segev I) pp. 171-210. Cambridge MA: MIT Press.

Manalan AS, Klee CB (1984) Calmodulin. Adv Cyclic Nucleotide Protein Phosphorylation Res. 18:27-278.

Maranhao-Filho PA, Martins-Ferreira H, Vincent MB, Ribeiro LJ, Novis SA (1997) Sumatriptan blocks spreading depression in isolated chick retina. Cephalalgia. 17:822-825.

Maranhao-Filho P de A, Leão AA (1991) A note on the action of glutamine on cortical spreading depression. Cephalalgia. 11:201-204.

Marrannes R, Willems R, De Prins E, Wauquier A (1988) Evidence for a role of the N-methyl-D-aspartate (NMDA) receptor in cortical spreading depression in the rat. Brain Res. 457:226-240.

Marrocos MA, Martins-Ferreira H (1990) Effect of Na+ and Cl- on the velocity of propagation of the spreading depression in chick retina. Braz J Med Biol Res. 23:473-476.

Marshall W (1950) Relation of dehydration of brain to spreading depression of Leão. EEG Clin Neurophysiol. 2:177-185.

Marshall WH (1959) Spreading Cortical Depression of Leão. Physiological Reviews. 39:239-279.

Martin DL (1995) The role of glia in the inactivation of neurotransmitters. In: Neuroglia (ed. Kettenmann H, Ransom BR) New York: Oxford, pp. 732-745.

Martin H, Warner DS, Todd MM (1994) Effects of glycine receptor antagonism on spreading depression in the rat. Neurosci Lett. 180:285-289.

Martina M, Mozrzmas JW, Vittur F (1997) Membrane stretch activates a potassium channel in pig articular chondrocytes. Biochim Biophys Acta 1329:205-210.

Martins-Ferreira H,  Leão AAP.  1958)  [Note on the study of spreading depression in reptiles]. Anais acad brasil cienc. 30:1.

Martins-Ferreira H, De Oliveria Castro (1966) Light-scattering changes accompanying spreading depression in isolated retina. J Neurophysiol. 29:715-726.

Martins-Ferreira H, De Oliveira Castro G (1971) Spreading depression in isolated chick retina. Vision Res. Suppl 3:171-184.

Martins-Ferreira H, De Oliveira Castro G, Struchiner CJ, Rodrigues PS (1974) Circling spreading depression in isolated chick retina. J Neurophysiol. 37:773-784.

Martins-Ferreira H, Do Carmo RJ (1987) Retinal spreading depression and the extracellular milieu. Can J Physiol Pharmacol. 65:1092-1098.

Martins-Ferreira H, Ribeiro LJ, Do Carmo RJ (1993) Threshold determination of spreading depression evoking substances in the retina in vitro. Braz J Med Biol Res. 26:875-877.

Martins-Ferreira H, Ribeiro LJ (1995) Biphasic effects of gap junctional uncoupling agents on the propagation of retinal spreading depression. Braz J Med Biol Res. 28:991-994.

Matsushima K, Hogan MJ, Hakim AM (1996) Cortical spreading depression protects against subsequent focal cerebral ischemia in rats. J Cereb Blood Flow Metab. 16:221-226.

Mayer ML, Westbrook GL (1987) Permeation and block of n-methyl-d-aspartic acid receptor channels by divalent cations in mouse cultured central neurons. J Physiol. 394:501-527.

Mayevsky A (1978) Pyridine nucleotide oxidation-reduction state of the cerebral cortex in the awake gerbil. J Neurosci Res. 3:369-374.

Mayevsky A, Chance B (1975) Metabolic responses of the awake cerebral cortex to anoxia hypoxia spreading depression and epileptiform activity. Brain Res. 98:149-165.

Mayevsky A, Crowe W, Mela L (1980) The interrelation between brain oxidative metabolism and extracellular potassium in the unanesthetized gerbil. Neurol Res. 1:213-225.

Mayevsky A, Doron A, Manor T, Meilin S, Zarchin N, Ouaknine GE (1996) Cortical spreading depression recorded from the human brain using a multiparametric monitoring system. Brain Res. 740:268-274.

Mayevsky A, Frank K, Muck M, Nioka S, Kessler M, Chance B (1992) Multiparametric evaluation of brain functions in the Mongolian gerbil in vivo. J Basic Clin Physiol Pharmacol. 3:323-342.

Mayevsky A, Lebourdais S, Chance B (1980) The interrelation between brain PO2 and NADH oxidation-reduction state in the gerbil. J Neurosci Res. 5:173-182.

Mayevsky A, Weiss HR (1991) Cerebral blood flow and oxygen consumption in cortical spreading depression. J Cereb Blood Flow Metab. 11:829-836.

Mayevsky A, Zarchin N, Friedli CM (1982) Factors affecting the oxygen balance in the awake cerebral cortex exposed to spreading depression. Brain Res. 236:93-105.

Mayevsky A, Ziv I (1991) Oscillations of cortical oxidative metabolism and microcirculation in the ischaemic brain. Neurol Res. 13:39-47.

McCarty MF (1996) Magnesium taurate and fish oil for prevention of migraine. Med Hypotheses. 47:461-466.

McLachlan RS (1992) Suppression of spreading depression of Leão in neocortex by an N-methyl-D-aspartate receptor antagonist. Can J Neurol Sci (19:487-491.

McLachlan RS, Girvin JP (1994) Spreading depression of Leão in rodent and human cortex. Brain Res. 666:133-136.

McCown TJ, Breese GR (1990) Effects of apamin and nicotinic acetylcholine receptor antagonists on inferior collicular seizures. Eur J Pharmacol. 187:1 49-58.

McQuarrie DA (1976) Statistical Mechanics. New York: Harper & Row.

Megirian D, Bures J (1970) Unilateral cortical spreading depression and conditioned eyeblink responses in the rabbit. Exp Neurol. 27:34-45.

Meilin S, Sonn J, Zarchin N, Rogatsky G, Guggenheimer-Furman E, Mayevsky A (1998) Responses of rat brain to induced spreading depression following exposure to carbon monoxide. Brain Res. 780:323-328.

Meng W, Colonna DM, Tobin JR, Busija DW (1995) Nitric oxide and prostaglandins interact to mediate arteriolar dilation during cortical spreading depression. Am J Physiol. 269:H176-181.

Mienville JM, Barker JL, Lange GD (1996) Mechanosensitive properties of BK channels from embryonic rat neuroepithelium. J Membrane Biol 153: 211-216.

Mies G (1993) Inhibition of protein synthesis during repetitive cortical spreading depression. J Neurochem. 60:360-363.

Mies G, Paschen W (1984) Regional changes of blood flow, glucose, and ATP content determined on brain sections during a single passage of spreading depression in rat brain cortex. Exp Neurol. 84:249-258.

Miettinen S, Fusco FR, Yrjanheikki J, Keinanen R, Hirvonen T, Roivainen R, Narhi M, Hokfelt T, Koistinaho J (1997) Spreading depression and focal brain ischemia induce cyclooxygenase-2 in cortical neurons through n-methyl-d-aspartic acid-receptors and phospholipase A2. Proc Nat Acad Sci U S A. 94:6500-6505.

Mihic SJ, Harris RA (1996) Inhibition of rho1 receptor GABAergic currents by alcohols and volatile anesthetics. J Pharmacol Exp Ther. 277:411-416.

Mody I, Lambert JD, Heinemann U (1987) Low extracellular magnesium induces epileptiform activity and spreading depression in rat hippocampal slices. J Neurophysiol. 57:869-888.

Moghaddam B, Gruen RJ, Roth RH, Bunney BS, Adams RN (1990) Effect of L-glutamate on the release of striatal dopamine: in vivo dialysis and electrochemical studies. Brain Res. 518:55-60.

Moghaddam B, Schenk JO, Stewart WB, Hansen AJ (1987) Temporal relationship between neurotransmitter release and ion flux during spreading depression and anoxia. Can J Physiol Pharmacol. 65:1105-1110.

Monda M, Pittman QJ (1993) Cortical spreading depression blocks prostaglandin E1 and endotoxin fever in rats. Am J Physiol. 264:R456-459.

Mori S, Miller WH, Tomita T (1976) Muller cell function during spreading depression in frog retina. Proc Nat Acad Sci U S A. 73:1351-1354.

Morris C, Lecar H (1981) Voltage oscillation in the barnacle giant muscle fiber. Biophys J. 35:193-213.

Morrison DP (1990) Abnormal perceptual experiences in migraine. Cephalalgia. 10:273-277.

Morton KW, Mayers DF (1994) Numerical solution of partial differential equations: an introduction. Cambridge: Cambridge University Press.

Moskowitz MA, Nozaki K, Kraig RP (1993) Neocortical spreading depression provokes the expression of c-fos protein-like immunoreactivity within trigeminal nucleus caudalis via trigeminovascular mechanisms. J Neurosci. 13:1167-1177.

Mraovitch S, Calando Y, Goadsby PJ, Seylaz J (1992) Subcortical cerebral blood flow and metabolic changes elicited by cortical spreading depression in rat. Cephalalgia. 12:137-141; discussion 127.

Mutch WA, Hansen AJ (1984) Extracellular pH changes during spreading depression and cerebral ischemia: mechanisms of brain pH regulation. J Cereb Blood Flow Metab. 4:17-27.

Nagumo J, Arimoto S, Yoshizawa S (1964) An active pulse transmission line simulating nerve axon. Proc IRE. 50:2061-2070.

Nedergaard M, Cooper AJ, Goldman SA (1995) Gap junctions are required for the propagation of spreading depression. J Neurobiol. 28:433-444.

Nedergaard M, Hansen AJ (1988) Spreading depression is not associated with neuronal injury in the normal brain. Brain Res. 449:395-398.

Nedergaard M, Hansen AJ (1993) Characterization of cortical depolarizations evoked in focal cerebral ischemia. J Cereb Blood Flow Metab. 13:568-574.

Neher E (1995) The use of fura-2 for estimating Ca buffers and Ca fluxes. Neuropharmacol. 34:1423-1442.

Nellgard B, Wieloch T (1992) NMDA-receptor blockers but not NBQX, an AMPA-receptor antagonist, inhibit spreading depression in the rat brain. Acta Physiol Scand. 146:497-503.

Newman, EA (1995) Glial cell regulation of extracellular potassium. In: Neuroglia (ed. Kettenmann H, Ransom BR) New York: Oxford, pp. 717-731.

Nichelli P, Menabue R (1988) Can association between transient global amnesia and migraine tell us something about the pathophysiology of transient global amnesia? Ital J Neurol Sci. Suppl 9:41-43.

Nicholson C, Bruggencate GT, Steinberg R, Stockle H (1977) Calcium modulation in brain extracellular microenvironment demonstrated with ion-selective micropipette. Proc Nat Acad Sci U S A. 74:1287-1290.

Nicholson C, Ten Bruggencate G, Stockle H, Steinberg R (1978) Calcium and potassium changes in extracellular microenvironment of cat cerebellar cortex. J Neurophysiol. 41:1026-1039.

Noma A, Tsuboi N (1987) Dependence of junctional Conductance on Proton, Calcium and Magnesium Ions in Cardiac Paired Cells of Guinea-Pig. Journal of Physiology. 382:193-211.

Obrenovitch TP, Richards DA (1995) Extracellular neurotransmitter changes in cerebral ischemia. Cerebrovasc Brain Metab Rev. 7:1-54.

Obrenovitch TP, Zilkha E (1996) Inhibition of cortical spreading depression by L-701,324, a novel antagonist at the glycine site of the N-methyl-D-aspartate receptor complex. Br J Pharmacol. 117:931-937.

Obrenovitch TP, Zilkha E, Urenjak J (1996) Evidence against high extracellular glutamate promoting the elicitation of spreading depression by potassium. J Cereb Blood Flow Metab. 16:923-931.

Ochs S (1962) The Nature of Spreading Depression in Neural Networks. In: International Review of Neurobiology, Volume 4. (ed. Pfeiffer CC, Smythies JR). pp. 2-69. New York: Academic Press.

Oitzl MS, Huston JP (1984) Electroencephalographic spreading depression and concomitant behavioral changes induced by intrahippocampal injections of ACTH1-24 and d-ala-2-met-enkephalinamide in the rat. Brain Res. 308:33-42.

Oitzl MS, Koroleva VI, Bures J (1985) D-ala2-Metenkephalinamide blocks the synaptically elicited cortical spreading depression in rats. Experientia. 41:625-627.

Oka H, Kako M, Matsushima M, Ando K (1977) Traumatic spreading depression syndrome. Review of a particular type of head injury in 37 patients. Brain. 100:287-298.

Okada YC, Lauritzen M, Nicholson C (1988) Magnetic field associated with spreading depression: a model for the detection of migraine. Brain Res. 442:185-190.

Olesen J, Jorgensen MB (1986) Leão's spreading depression in the hippocampus explains transient global amnesia. A hypothesis. Acta Neurol Scand. 73:219-220.

Ookawa T, Bures J (1969) Spreading depression in the striatum and optic lobes of the chicken. Brain Res. 13:119-128.

Osten P, Hrabetova S, Sacktor TC (1996) Differential downregulation of protein kinase C isoforms in spreading depression. Neurosci Lett. 221:37-40.

Ottman R, Lipton RB (1994) Comorbidity of migraine and epilepsy. Neurology. 44:2105-2110.

Paternostre M, Pichon Y (1987) Effects of N-alcohols on potassium conductance in squid giant axons. Eur Biophys J. 14:279-288.

Pavlasek J, Haburcak M, Masanova C, Orlicky J (1993) Increase of catecholamine content in the extracellular space of the rat's brain cortex during spreading depression wave as determined by voltammetry. Brain Res. 628:145-148.

Peinado A, Yuste R, Katz LC (1993) Gap junctional communication and the development of local circuits in neocortex. Cereb Cortex 3:488-98.

Pieri L, Bartholini G, Keller HH, Pletscher A (1973) Effect of spreading depression on electrical activity and dopamine turnover in the striatum of rats. Experientia. 29:452-455.

Piper RD, Edvinsson L, Ekman R, Lambert GA (1993) Cortical spreading depression does not result in the release of calcitonin gene-related peptide into the external jugular vein of the cat: relevance to human migraine. Cephalalgia. 13:180-183; discussion 149.

Piper RD, Lambert GA (1996) Inhalational anesthetics inhibit spreading depression: relevance to migraine. Cephalalgia. 16:87-92.

Pleumsamran A, Kim D (1995) Membrane stretch augments the cardiac muscarinic K+ channel activity. J Membr Biol 148:287-97.

Plumier JC, David JC, Robertson HA, Currie RW (1997) Cortical application of potassium chloride induces the low-molecular weight heat shock protein (Hsp27) in astrocytes. J Cereb Blood Flow Metab. 17:781-790.

Protopapas AD, Vanier M, Bower JA (1998) Simulating large networks of neurons. In: Methods in neuronal modeling. From ions to networks. Second edition (ed. Koch C, Segev I) pp. 461-498. Cambridge MA:MIT Press.

Psarropoulou C, Avoli M (1993) 4-aminopyridine-induced spreading depression episodes in immature hippocampus: developmental and pharmacological characteristics. Neuroscience. 55:57-68.

Qian N, Sejnowski TJ (1989) An Electro-Diffusion Model for Computing Membrane Potentials and Ionic Concentrations in Branching Dendrites, Spines and Axons. Biological Cybernetics. 62:1-15.

Ramos JG (1975) Ionic movements in the isolated chicken retina during spreading depression. Acta Physiol Lat Am. 25:112-119.

Rampin O, Morain P (1987) Cortical involvement in dorsal horn cell hyperactivity and abnormal behavior in rats with dorsal root section. Somatosens Res. 4:237-251.

Ransom BR (1995) Gap Junctions. In: Neuroglia (ed. Kettenmann H, Ransom BR) New York: Oxford, pp. 299-318.

Rashidy-Pour A, Motaghed-Larijani Z, Bures J (1995) Tolerance to ketamine-induced blockade of cortical spreading depression transfers to MK-801 but not to AP5 in rats. Brain Res. 693:64-69.

Rawanduzy A, Hansen A, Hansen TW, Nedergaard M (1997) Effective reduction of infarct volume by gap junction blockade in a rodent model of stroke. J Neurosurg. 87:916-920.

Rebert CS (1970) Spreading depression in squirrel monkey lissencephalic cortex. Physiol Behav. 5:239-241.

Reddy MM, Bures J (1980) Cortical (K+)e and the stimulation induced blockade of spreading depression in the rat cerebral cortex. Neurosci Lett. 17:243-247.

Reggia JA, Montgomery D (1994) Modeling cortical spreading depression. Proc Annu Symp Comput Appl Med Care:873-877.

Reggia JA, Montgomery D (1996) A computational model of visual hallucinations in migraine. Comput Biol Med. 26:133-141.

Reigart JR, Brueggeman JL, Keil JE (1975) Sodium fluoroacetate poisoning. Am J Dis Child. 129:1224-1226.

Reinhart PH, Shung S, Levitan IB (1989) A family of calcium-dependent potassium channels from rat brain. Neuron 2:1031-1041.

Reshodko LV, Bures J (1975) Computer simulation of reverberating spreading depression in a network of cell automata. Biol Cybernetics. 18:181-189.

Revett K, Ruppin E, Goodall S, Reggia JA (1998) Spreading depression in focal ischemia: a computational study. J Cereb Blood Flow Metab. 18:998-1007.

Rex EE, Cannestra AF, Toga AW (1997) Optical intrinsic signal imaging of neurovascular response during cortical spreading depression. Soc Neurosci Abs. 23:1578.

Reynolds IJ, Rush EA (1990) Role of lipid solubility in th einteraction of drugs with the N-methyl-D-aspartate receptor. Synapse. 5:71-76.

Ribeiro LJ, Martins-Ferreira H (1994) Elicitation of retinal spreading depression by barium ions. Braz J Med Biol Res. 27:2457-2460.

Rice ME, Nicholson C (1987) Interstitial ascorbate in turtle brain is modulated by release and extracellular volume change. J Neurochem. 49:1096-1104.

Rice ME, Nicholson C (1988) Behavior of extracellular K+ and pH in skate (Raja erinacea) cerebellum. Brain Res. 461:328-334.

Riexinger KG, Petit TL, Dudek FE (1986) The effects of lead exposure on field potentials of CA3 pyramidal cells from mossy fiber stimulation in rat hippocampus. Neurotoxicology. 7:35-45.

Rist RJ, Romero IA, Chan MW, Abbott NJ (1996) Effects of energy deprivation induced by fluorocitrate in immortalised rat brain microvessel endothelial cells. Brain Res. 730:87-94.

Rocha-de-Melo AP, Guedes RC (1997) Spreading depression is facilitated in adult rats previously submitted to short episodes of malnutrition during the lactation period. Braz J Med Biol Res. 30:663-669.

Rodrigues PS, Guimaraes AP, de Azeredo FA, Martins-Ferreira H (1988) Involvement of GABA and ACh in retinal spreading depression: effects of "low calcium-high magnesium" solutions. Exp Brain Res. 73:659-664.

Rodrigues PS, Martins-Ferreira H (1980) Cholinergic neurotransmission in retinal spreading depression. Exp Brain Res. 38:229-236.

Rogatsky G, Mayevsky A, Zarchin N, Doron A (1996) Continuous multiparametric monitoring of brain activities following fluid-percussion injury in rats: preliminary results. J Basic Clin Physiol Pharmacol. 7:23-43.

Rörig B, Klausa G, Sutor B (1995) Dye coupling between pyramidal neurons in developing rat prefrontal and frontal cortex is reduced by protein kinase A activation and dopamine. J Neurosci 15:7386-400.

Roth BJ, Yagodin SV, Holzclaw L, Russel JT (1995) A mathematical model of agonist induced propagation of calcium waves in astrocytes. Cell Calcium 17:53.64.

Rother J, de Crespigny AJ, DqArceuil H, Mosley ME (1996b) MR detection of cortical spreading depression immediately after focal ischemia in the rat. J Cereb Blood Flow Metab. 16:214-220.

Rounds HD (1967) KC1-induced 'spreading depression' in the cockroach. J Insect Physiol. 13:869-872.

Rounds HD (1968) KC-1-induced "spreading depression" and ventilation in the cockroach. Comp Biochem Physiol. 24:653-655.

Ruknudin A, Sachs F, Bustamante JO (1993) Stretch activated ion channels in tissue cultured chick heart. Am J Physiol 264:H960-72.

Ruppin E, Ofer E, Reggia JA, Revett K, Goodall S (1999) Pathogenic mechanisms in ischemic damage: a computational study. Computers in Biol and Med 29:39-59.

Saavedra de Camargo B, Brust-Carmona H, Roig JA (1981) Effects of general anesthesia, neodecortication and spreading depression upon somatic evoked responses in caudate and entopeduncular nuclei, and their electrophysiological correlates in cats. Brain Res Bull. 6:219-225.

Sackin H (1987) Stretch activated potassium channels in renal proximal tissue. Am J Physiol 253:F1253-62.

Sah P (1996) $Ca^{2+}$-activated $K^{+}$ currents in neurones: types, physiological roles and modulation. TINS 19:150-154.

Sah P, Bekkers JM (1996) Apical dendritic location of slow afterhyperpolarization current in hippocampal pyramidal neurons: implications for the integration of long-term potentiation. J Neurosci. 16: 4537-4542.

Saito R, Graf R, Hubel K, Taguchi J, Rosner G, Fujita T, Heiss WD (1995) Halothane, but not alpha-chloralose, blocks potassium-evoked cortical spreading depression in cats. Brain Res. 699:109-115.

Saito R, Graf R, Hubel K, Fujita T, Rosner G, Heiss WD (1997) Reduction of infarct volume by halothane: effect on cerebral blood flow or perifocal spreading depression-like depolarizations. J Cereb Blood Flow Metab. 17:857-864.

Sand T (1991) EEG in migraine: a review of the literature. Funct Neurol. 6:7-22.

Sasaki N, Mitsuiye T, Noma A (1992) Effects of mechanical stretch on membrane currents of single ventricular myocytes of guinea pig hearts. Jap J of Physiol 42:957-70.

Scheller D, Tegtmeier F, Schlue WR (1998) Dose-dependent effects of tetraethylammonium on circling spreading depressions in chicken retina. J Neurosci Res. 51:85-89.

Schilling L, Wahl M (1989) Cerebrovascular effects of nimodipine in cats. Miner Electrolyte Metab. 15:178-184.

Schmidtke K, Ehmsen L (1998) Transient global amnesia and migraine. A case control study. Eur Neurol. 40:9-14.

Schneggenburger R (1996) Simultaneous measurement of the Ca++ influx and reversal potentials in recombinant n-methyl-d-aspartate receptor channels. Biophys J. 70:2165-2174.

Sheardown MJ (1993) The triggering of spreading depression in the chicken retina: a pharmacological study. Brain Res. 607:189-194.

Sheardown MJ (1997) The triggering of spreading depression in the chick retina by nicotinic receptor agonists. Eur J Pharmacol. 337:209-212.

Shibata M, Bures J (1975) Techniques for termination of reverberating spreading depression in rats. J Neurophysiol. 38:158-166.

Shibata M, Leffler CW, Busija DW (1991a) Evidence against parenchymal metabolites directly promoting pial arteriolar dilation during cortical spreading depression in rabbits. Brain Res Bull. 26:753-758.

Shibata M, Leffler CW, Busija DW (1991b) Prostanoids attenuate pial arteriolar dilation induced by cortical spreading depression in rabbits. Am J Physiol. 261:R828-834.

Shibata M, Leffler CW, Busija DW (1992) Pial arteriolar constriction following cortical spreading depression is mediated by prostanoids. Brain Res. 572:190-197.

Shimazawa M, Hara H, Watano T, Sukamoto T (1995) Effects of Ca2+ channel blockers on cortical hypoperfusion and expression of c-Fos-like immunoreactivity after cortical spreading depression in rats. Br J Pharmacol. 115:1359-1368.

Shimazawa M, Hara H (1996) An experimental model of migraine with aura: cortical hypoperfusion following spreading depression in the awake and freely moving rat. Clin Exp Pharmacol Physiol. 23:890-892.

Simbürger E, Stang A, Kremer M, Dermietzel R (1997)Expression of connexin43 mRNA in adult rodent brain. Histochem Cell Biol 107:127-37

Siniatchkin M, Gerber WD, Vein A (1998) Clinical efficacy and central mechanisms of cyclandelate in migraine: a double-blind placebo-controlled study. Funct Neurol. 13:47-56.

Sloper JJ, Powell TP (1978) Gap junctions between dendrites and somata of neurons in the primate sensori-motor cortex. Proc R Soc Lond B Biol Sci 203:39-47

Sneyd J, Wetton BTR, Charles AC, Sanderson MJ (1995) Intercellular calcium waves mediated by diffusion of inositol trisphosphate: a two dimensional model. AM J Physiol. 268:C1547-C1545.

Snow RW, Taylor CP, Dudek FE (1983) Electrophysiological and optical changes in slices of rat hippocampus during spreading depression. J Neurophysiol. 50:561-572.

Somjen GG (1984) Acidification of interstitial fluid in hippocampal formation caused by seizures and by spreading depression. Brain Res. 311:186-188.

Somjen GG, Aitken PG, Balestrino M, Herreras O, Kawasaki K (1990) Spreading depression-like depolarization and selective vulnerability of neurons. A brief review. Stroke. 21:III179-183.

Somjen GG, Aitken PG, Czeh GL, Herreras O, Jing J, Young JN (1992) Mechanism of spreading depression: a review of recent findings and a hypothesis. Can J Physiol Pharmacol. 70 Suppl:S248-254.

Somjen GG, Czeh G (1989) Pathophysiology of the spinal cord studied in vitro. J Neurosci Methods. 28:35-46.

Spector GJ, Carr CD (1976) Fluorocitrate ototoxicity. A morphologic and cytochemical model for primary neural degeneration in the guinea pig cochlea. Ann Otol Rhinol Laryngol. 85:185-97.

Sprick U, Oitzl MS, Ornstein K, Huston JP (1981) Spreading depression induced by microinjection of enkephalins into the hippocampus and neocortex. Brain Res. 210:243-252.

Stockbridge LL, French AS (1988) Stretch activated cation channels in human fibroblasts. Biophys J 54:187-90.

Sramka M, Brozek G, Bures J, Nadvornik P (1977) Functional ablation by spreading depression: possible use in human stereotactic neurosurgery. Appl Neurophysiol. 40:48-61.

Storozeva ZI, Pletnicov MV (1994) Habituation of acoustic startle in rats--a functional ablation study. Neuroreport. 5:2065-2068.

Streit DS, Ferreira Filho CR, Martins-Ferreira H (1995) Spreading depression in isolated spinal cord. J Neurophysiol. 74:888-890.

Strupp M, Bruning R, Wu RH, Deimling M, Reiser M, Brandt T (1998) Diffusion-weighted MRI in transient global amnesia: elevated signal intensity in the left mesial temporal lobe in 7 of 10 patients. Ann Neurol. 43:164-170.

Stuart G, Sakmann B (1994) Active propagation of somatic action potentials into neocortical pyramidal cell dendrites. Nature. 367:69-72.

Sugaya E, Takato M, Noda Y (1975) Neuronal and glial activity during spreading depression in cerebral cortex of cat. J Neurophysiol. 38:822-841.

Sutor B, Hablitz JJ (1989) Cholinergic modulation of epileptiform activity in the developing rat neocortex. Brain Res Dev Brain Res. 46:155-160.

Svensson L, Zhang J, Johannessen K, Engel JA (1994) Effect of local infusion of glutamate analogues into the nucleus accumbens of rats: an electrochemical and behavioural study. Brain Res. 643:155-161.

Sze SM (1969) Physics of Semiconductor Devices. New York: Wiley.

Taga K, Patel PM, Drummond JC, Cole DJ, Kelly PJ (1997) Transient neuronal depolarization induces tolerance to subsequent forebrain ischemia in rats. Anesthesiology. 87:918-925.

Takano K, Latour LL, Formato JE, Carano RA, Helmer KG, Hasegawa Y, Sotak CH, Fisher M (1996) The role of spreading depression in focal ischemia evaluated by diffusion mapping. Ann Neurol. 39:308-318.

Tas PWI, Massa PT, Koschel K (1986) Preliminary characterization of an Na+, K+, Cl- co-transport activity in cultured human astrocytes. Neurosci Lett. 70:369-377.

Tas PWI, Massa PT, Kress HG, Koschel K (1987) Characterization of a Na+, K+, Cl- cotransport in primary cultures of rat astrocytes. Biochim Biophys Acta. 903:411-416.

Tassoni G, Bucherelli C, Bures J (1992) Lateralized contributions of the cerebral cortex, parabrachial nucleus, and amygdala to acquisition and retrieval of passive avoidance reaction in rats: a functional ablation study. Behav Neurosci. 106:933-939.

Taylor WM, D'Costa M, Angel A, Halperin ML (1977) Insulin-like effects of fluoroacetate on lipolysis and lipogenesis in adipose tissue. Can J Biochem. 55:982-987.

Tepley N, Wijesinghe RS (1996) A dipole model for spreading cortical depression. Brain Topography. 8:345-353.

Tobiasz C, Nicholson C (1982) Tetrodotoxin resistant propagation and extracellular sodium changes during spreading depression in rat cerebellum. Brain Res. 241:329-333.

Traub RD, Jefferys JGR, Miles R, Whittington M, Toth K (1994) A branching dendritic model of a rodent CA3 pyramidal neurone. J Physiol. 481:79-95.

Traynelis SF, Dingledine R (1989) Role of extracellular space in hyperosmotic suppression of potassium-induced electrographic seizures. J Neurophysiol. 61:927-938.

Tuckwell HC (1980) Predictions and properties of a model of potassium and calcium ion movements during spreading cortical depression. Int J Neurosci. 10:145-164.

Tuckwell HC (1981) Simplified reaction-diffusion equations for potassium and calcium ion concentrations during spreading cortical depression. Int J Neurosci. 12:95-107.

Tuckwell HC, Hermansen CL (1981) Ion and transmitter movements during spreading cortical depression. Int J Neurosci. 12:109-135.

Tuckwell HC, Miura RM (1978) A mathematical model for spreading cortical depression. Biophys J. 23:257-276.

Turner DA, Aitken PG, Somjen GG (1995) Optical mapping of translucence changes in rat hippocampal slices during hypoxia. Neurosci Lett (195:209-213.

Ueda M, Bures J (1977) Differential effects of cortical spreading depression on epileptic foci induced by various convulsants. Electroencephalogr Clin Neurophysiol. 43:666-674.

Ueda M, Bures J, Fischer J (1977) Spreading depression elicited by thermal effects of ultrasonic irradiation of cerebral cortex in rats. J Neurobiol. 8:381-393.

Ulmer HJ, de Lima VM, Hanke W (1995) Effects of nitric oxide on the retinal spreading depression. Brain Res. 691:239-242.

Van Harreveld A (1959) Compounds in brain extracts causing spreading depression of cerebral cortical activity and contraction of crustacean muscle. J Neurochem. 3:300-315.

Van Harreveld A (1984) The nature of the chick's magnesium-sensitive retinal spreading depression. J Neurobiol. 15:333-343.

Van Harreveld A, Cherkin A, Davis JL (1980) Amnestic potency of proline analogs correlates with anti-spreading depression potency. Pharmacol Biochem Behav. 12:533-541.

Van Harreveld A, Khattab FI (1967) Changes in cortical extracellular space during spreading depression investigated with the electron microscope. J Neurophysiol. 30:911-929.

Van Harreveld A, Reuter JH (1981) The dual effect of L-proline on spreading depression in the chicken retina. Neurosci Lett. 23:329-332.

Van Harreveld A, Stamm JS (1953) Spreading cortical convulsions and depressions. J Neurophysiol. 16:352-366.

Van Harreveld A, Stamm JS (1954) Consequences of cortical convulsive activity in rabbit. J Neurophysiol. 17:505-520.

Van Harrevald A, Stamm JS, Christensen E (1956) Spreading depression in rabbit, cat and monkey. Am J Physiol. 184:312-320.

Vergara C, Latorre R, Marrion NV, Adelman JP (1998) Calcium-activated potassium channels. Curr Opin Neurobiol 8:321-329.

Verhaegen M, Todd MM, Warner DS (1992) The influence of different concentrations of volatile anesthetics on the threshold for cortical spreading depression in rats. Brain Res. 581:153-155.

Vinogradova LV, Koroleva VI, Bures J (1991) Re-entry waves of Leão's spreading depression between neocortex and caudate nucleus. Brain Res. 538:161-164.

Voets T, Droogmans G, Raskin G, Eggermont J, Nilius B (1999) Reduced intracellular ionic strength as the initial trigger for activation of endothelial volume-regulated anion channels. Proc Natl Acad Sci USA 96:5298 - 5303.

Vogel R, Weingart R (1998) Mathematical model of vertebrate gap junctions derived from electrical measurements on homotypic and heterotypic channels. J Physiol. 510:177-189.

Wahl M, Schilling L, Parsons AA, Kaumann A (1994) Involvement of calcitonin gene-related peptide (CGRP) and nitric oxide (NO) in the pial artery dilatation elicited by cortical spreading depression. Brain Res. 637:204-210.

Watanabe SI, Tanizaka M, Kaneko A (1997) Two types of stretch-activated channels coexist in the rabbit corneal epithelial cell. Exp Eye Res 64:1027-35.

Watz W (1995) Distribution and transport of chloride and bicarbonate ions across membranes. In: Neuroglia (ed. Kettenmann H, Ransom B) New York: Oxford.

Wauquier A, Ashton D, Marrannes R (1985) The effects of flunarizine in experimental models related to the pathogenesis of migraine. Cephalalgia. 5 Suppl 2:119-123.

Wiedemann M, Fernandes de Lima VM, Hanke W (1996) Effects of antimigraine drugs on retinal spreading depression. Naunyn Schmiedebergs Arch Pharmacol. 353:552-556.

Winn FJ Jr, Kent MA, Libkuman TM (1975) Learned taste aversion induced by cortical spreading depression. Physiol Behav. 15:21-24.

Wolfe LS, Horrocks LA (1994) Eicosanoids. In: Basic neurochemistry: molecular, cellular and medical aspects. Fifth edition. (ed. Siegel GJ, Agranoff BW, Albers RW, Molinoff PB) pp. 475-490. New York: Raven.

Wood SC, Tonner PH, de Armendi AJ, Bugge B, Miller KW (1995) Channel inhibition by alkanols occurs at a binding site on the nicotinic acetylcholine receptor. Mol Pharmacol. 47:121-130.

Woods RP, Iacoboni M, Mazziotta JC (1994) Bilateral spreading cerebral hypoperfusion during spontaneous migraine headache. New Eng J Med. 331:1689-92.

Yamada WM, Koch C, Adams PR (1998) Multiple channels and calcium dynamics. In: Methods in neuronal modeling. From ions to networks. Second edition. (ed. Koch C, Segev I). Cambridge, MA: MIT Press.

Yanamoto H, Hashimoto N, Nagata I, Kikuchi H (1998) Infarct tolerance against temporary focal ischemia following spreading depression in rat brain. Brain Res. 784:239-249.

Yang XC, Sachs F (1990) Characterization of stretch-activated ion channels in Xenopus oocytes. J Physiol (Lond) 431:103-22.

Yeh TH, Tsai MC, Lee SY, Hsu MM, Tran Ba Huy P (1997) Stretch activated nonselective cation, Cl- and K+ channels in apical membrane of epithelial c ells of Reissner's membrane. Hearing Res 109:1-10.

Yoon RS, Tsang PW, Lenz FA, Kwan HC (1996) Characterization of cortical spreading depression by imaging of intrinsic optical signals. Neuroreport. 7:2671-2674.

Young W (1980) Spreading depression in elasmobranch cerebellum. Brain Res (199:113-126.

Young JN, Aitken PG, Somjen GG (1991) Calcium, magnesium, and long-term recovery from hypoxia in hippocampal tissue slices. Brain Res. 548:343-345.

Young JN, Somjen GG (1992) Suppression of presynaptic calcium currents by hypoxia in hippocampal tissue slices. Brain Res. 573:70-76.

Zachar J, Zacharova D (1961) Subthreshold changes at the site of initiation of spreading cortical depression by mechanical stimuli. EEG Clin. Neurophysiol. 13:896-904.

Zhang ZG, Chopp M, Maynard KI, Moskowitz MA (1994) Cerebral blood flow changes during cortical spreading depression are not altered by inhibition of nitric oxide synthesis. J Cereb Blood Flow Metab. 14:939-943.

Zorzon M, Longo R, Mase G, Biasutti E, Vitrani B, Cazzato G (1998) Proton magnetic resonance spectroscopy during transient global amnesia. J Neurol Sci. 156:78-82.